The Dissertation Committee for Reynaldy Fifariz Certifies that this is the approved version of the following Dissertation:

Controls on Oligocene-Miocene Carbonate Shelf Evolution, Offshore East Java, Indonesia: Insights from Architecture, Facies, and Seismic Geomorphology

Committee:

Xavier Janson, Co-Supervisor

Charles Kerans, Co-Supervisor

Benyamin Sapiie

Craig Fulthorpe

Mark Cloos

Ronald Steel

Controls on Oligocene-Miocene Carbonate Shelf Evolution, Offshore East Java, Indonesia: Insights from Architecture, Facies, and Seismic Geomorphology

by

Reynaldy Fifariz

Dissertation

Presented to the Faculty of the Graduate School of

The University of Texas at Austin

in Partial Fulfillment

of the Requirements

for the Degree of

Doctor of Philosophy

The University of Texas at Austin

December 2018

Dedication

To my dearest wife—Desi Maulani Rosadi,

To my precious daughter—Syalabiyyah Naura Fifariz,

To my beloved parents—Afifah and Basrizal.

Acknowledgements

Al-hamdu lillahi rabbil ‘aalamiin. Praise be to Allah, the Cherisher and Sustainer of the worlds.

First, I would like to acknowledge that this work would not have been possible without help and support from many wonderful people I have met during this rewarding journey. As an aspiring scientist, I am truly humbled by this experience. It will help me to become a better person in the future, in both my personal life and professional career.

My sincere gratitude goes to my co-supervisors—Dr. Xavier Janson and Dr. Charles Kerans, for their guidance, patience, and continued support for me in navigating this complicated carbonate research. Xav has constantly challenged my critical thinking regarding carbonate research, yet he always had my back. Thank you, Xav! I am tremendously grateful for all the carbonate classes and mentorship from Charlie. It has truly improved my comprehensive understanding of the subject. My heartfelt thanks to my dissertation committee—Dr. Craig Fulthorpe, Dr. Ron Steel, Dr. Mark Cloos, and Dr. Benyamin Sapiie, for their time, flexibility, review, and feedback toward this work. Dr. Fulthorpe is one of the nicest person I have ever met. I have benefited a lot from discussions with Dr. Steel regarding siliciclastic aspects of my research. Encouragement from Dr. Cloos helped give me momentum to finish. Dr. Sapiie is very much appreciated and thanked for his continued support; despite his unbelievably busy schedule, he attended my defense via a tele-conference from Indonesia, at 1–4 a.m. local time. Dr. William L. Fisher and Dr. Scott W. Tinker are thanked very much, as they were my first points of contact when I was applying to UT. I appreciate kindness and support from Dr. Fisher throughout my time at UT, until the very end. I had been very fortunate to have served twice as a TA

for Dr. Fisher's and Charlie's sequence stratigraphy class, where I learned a lot about both siliciclastic and carbonate sequence stratigraphy.

I thank all the institutions that have provided me with financial support—The Fulbright Program for my Fulbright Presidential Ph.D. Scholarship; RCRL, GCCC, and their sponsors for my GRA positions; DGS for my TA positions, and DeFord Family for my Ronald K. DeFord Field Scholarship. I would like to also thank Trey Cortez for giving me the opportunity to do a couple of part-time summer internships at ENXP.

I am forever thankful for being a part of RCRL, as it is the best place I could ever hope to learn about carbonate rocks and to interact with world-class carbonate experts, such as Bob Loucks, Jerry Lucia, Chris and Laura Zahm, Steve Bachtel, Shawn Fullmer, Bill Morgan, Jean Hsieh, and many more.

I would like to thank PHE-WMO for providing the data, for encouraging and expressing permission to publish the work, and for welcoming me during my dissertation research trips to Indonesia. Mukhlis Setiawan, Pak Dwi Mandhri, Pak Ary Iriawan, Pak Shofiyuddin, Mas Bintoro Wibowo, Pak Oma Sulaeman, Hade Maulin, Priyo Herlambang, Tomi Miarso, and other PHE-WMO colleagues are thanked very much for their kindness and support. Mukhlis contributed significantly to the work in Chapter 4. Dr. Benyamin Sapiie from ITB is greatly appreciated for accommodating my research permission at PHE-WMO. I also thank PUDC for accommodating me during my time describing core samples. Mas Warta, Pak Gun, Pak Wawan, Mas Agus, Mas Lamijan, and the rest of the PUDC crew are thanked for their hospitality. Friends and colleagues at PHE-WMO and PUDC are thanked for having me in their fun Futsal matches.

I would like to sincerely thank GCCC, especially Dr. Tip Meckel, Mr. Ramon Treviño, and Dr. Sue Hovorka for having me as their GRA and for their support. It has

provided me with a positive work environment where I felt very much appreciated, in which I could contribute scientifically in my side-research related to CO_2 sequestration.

I thank Amanda Masterson, whose editorial review has tremendously improved the quality of this dissertation. Bob Penman is also thanked for checking the format of this dissertation and giving the final approval.

I appreciate my mentors at ITB—Dr. Dardji Noeradi, Dr. Benyamin Sapiie, Dr. Eddy A. Subroto, Dr. Dwiharso Nugroho, Dr. Sonny Winardhi, Dr. Wahyu Triyoso, Dr. Fatkhan, Dr. Tutuka Ariadji, Dr. Taufan Marhaendrajana, and many others, are all thanked for their great influence on my early career as a geologist. Dr. Noeradi was my supervisor for both my Bachelor's and Master's degrees and I learned a lot from him. He provided me with the opportunity to work in projects dealing with subsurface data.

Staff at AMINEF, IIE, the UT International Office, RCRL, and DGS are very much appreciated—Mbak Adeline, Mbak Mita, Mbak Tia, Zach Alger, Claire Thornton, Liz Smith, Tina Fiet, Stephaine Lane, and Philip Guerrero, are all thanked for their administrative support.

All of the 2012 Indonesian Fulbrighters, 'Monterey' Fulbrighters, and pre-academic training instructors are also thanked for their friendship and kindness. They have all been successful in their own journeys in pursuing higher education in the United States. Education really is a slow-moving but powerful force.

Classmates, RCRL-mates, and GCCC-mates—Suzan Ergene, Max Pommer, Menal Gupta, Khushboo Arora, Chris Liu, Logan West, Jinyu Zhang, Jah Fong-ngern, Maren Mathisen, Sam Hiebert, Alex Parker, Gordon Smith, Ahmed Hassan, Ozen Gurbuz, Greg Hurd, Ben Smith, Josh Lambert, Yawen He, Peter Soto-Kerans, Yaser AlZayer, Kris Voorhees, Nate Tinker, Taylor Canada, Scarlette Hsia, Izaak Ruiz, Emily Beckham, and all my friends who cannot be mentioned here one-by-one, have comforted me with their

friendship and fruitful discussions during my time at UT, and all are thanked for their kindness and support. They are all wonderful people.

I would also like to thank the Indonesian community in Austin—our family away from home, especially the Austin Halaqah group, for making us feel closer to home.

I offer my apology for my shortcomings if there is any missing acknowledgement that should have been given.

Finally, I wholeheartedly and infinitely thank and appreciate my dearest wife—Desi Maulani Rosadi, my precious daughter—Syalabiyyah Naura Fifariz (Sasya), my beloved parents—Afifah and Basrizal, and my family for their unconditional love and endless support, from the beginning until the completion of my Ph.D. program, which I consider to be one of the most important episodes of my life.

Abstract

Controls on Oligocene-Miocene Carbonate Shelf Evolution, Offshore East Java, Indonesia: Insights from Architecture, Facies, and Seismic Geomorphology

Reynaldy Fifariz, Ph.D.

The University of Texas at Austin, 2018

Co-Supervisor: Xavier Janson

Co-Supervisor: Charles Kerans

Carbonates were extensively deposited in the Oligocene–Miocene and are now prolific hydrocarbon reservoirs in the Southeast Asia region. Hydrocarbon exploration and production activities have resulted in extensive availability of subsurface data from this stratigraphic interval. During the Oligocene–Miocene, carbonate shelves in this region have evolved and show spatial-temporal variations in term of architecture and facies. Despite the economic importance, data availability, and complexity of the region, little effort has been made to decipher the dominant controls on carbonate shelves evolution.

This research utilized 24 wells and 1,300 km^2 of 3D seismic data from offshore East Java, Indonesia to study the Oligocene–Early Miocene Kujung Formation and the Late Miocene Wonocolo Formation. Depositional settings of the Kujung Formation have evolved from mixed-siliciclastic-carbonate shelf in the Oligocene (Rupelian–Chattian) to

carbonate-buildups shelf in the Early Miocene (Aquitanian). The change happened at around the Oligocene-Miocene boundary (23 Ma). Three-dimensional seismic geomorphology techniques were utilized to further characterize the Early Miocene Kujung and Late Miocene Wonocolo Formations. Carbonate shelves in the study area have evolved from having west-southwest – east-northeast elongated, circular-ovoid, to polygonal carbonate buildups in the Early Miocene to being dominated by north-south elongated flat-topped carbonate platforms in the Late Miocene. Hydrocarbons have been produced mainly from the Kujung Formation buildup-core. On the basis of well data, off-buildup carbonate-dominated strata are considered as an upside potential with indications of gas accumulation. Volumetric calculations demonstrated encouraging results for this interval, which could be developed as part of an integrated field development strategy.

Tectonically inherited antecedent topography, siliciclastic sediment routing, and localized differential tectonic subsidence are the dominant controls on platform-, basin-, to regional-scale spatial variation in distribution of siliciclastic and carbonate sediments, and the resulting architecture and facies on carbonate shelves during the Oligocene–Early Miocene. Change in the global sea-level fluctuation patterns seems to have caused the temporal variation represented in extensive carbonate buildups development starting in the Early Miocene. These controls could even override the influence of regional climatic change around the Oligocene-Miocene boundary. In the Late Miocene, intensifying compressional tectonic events have resulted in decreased accommodation on the carbonate shelves. Development of Indonesian through-flow during this period have strongly

influenced the oceanic circulation resulted in extensive development of north-south elongated flat-topped carbonate platforms. Ultimately, this research aims to provide valuable insights to better explain controls on Oligocene-Miocene carbonate shelf evolution and to better predict architecture, facies, geometry, and distribution of carbonate reservoirs situated in a tectonically active region.

Table of Contents

Abbreviations and Acronyms

^{87}Sr—strontium isotope
2D—two-dimensional
3D—three-dimensional
AI—acoustic impedance
AMINEF—American Indonesian Exchange Foundation
BEG—Bureau of Economic Geology
Bg—formation volume factor for gas
CBS—carbonate-buildups shelf
F#—assigned number for facies
FA-#—assigned number for facies association
FWWB—fair-weather wave base
GCCC—Gulf Coast Carbon Center
GR—gamma-ray
GRA—Graduate Research Assistant
GRV—gross rock volume
GWC—gas-water contact
IIE—Institute of International Education
IL—inline
ITB—Institut Teknologi Bandung
ITF—Indonesian through-flow
JS-1—Java Sea #1, based on an exploration well
Kujung-UP—the Kujung Formation upside potential
LBF—large benthic foraminifer
LKW—lowest-known water
MD—measured depth
MSCS—mixed-carbonate-siliciclastic shelf
NTG—net-to-gross
OGIP—original gas in-place
Por—porosity
PHE-WMO—Pertamina Hulu Energi – West Madura Offshore
PUDC—Pertamina Upstream Data Center
RCRL—Reservoir Characterization Research Laboratory
RF—recovery factor
SF-#—assigned number for seismic facies
Sw—water saturation
SWWB—stormy-weather wave base
TA—Teaching Assistant
TD—total depth
TVD—true vertical depth
TWT—two-way time
UT—The University of Texas at Austin
XL—crossline

Units of Measurement

%—percent
µm—micrometer or micron
BCF—billion cubic feet
cm—centimeter
ft—feet
k.y.—kilo-year, thousand-year in duration
km—kilometer
m.y.—million-year in duration
Ma—mega-annum, million-year of age
mD—millidarcy
mm—millimeter
MMSCF—million standard cubic feet
ms—millisecond
MSCF—thousand standard cubic feet
RB—reservoir barrel

List of Tables

List of Figures

Chapter 1: Introduction and Geologic Background

INTRODUCTION

Carbonate sediments were produced and deposited extensively during the Cenozoic in southeastern Asia, from Sumatra on the west to New Guinea on the east, and from the Philippines on the north to Java and Bali on the south (Wilson, 2002). Carbonates were also deposited further south, to the northwest shelf of Australia, during this period (Rosleff-Soerensen et al., 2012). These carbonates were deposited under various and complex tectonic settings such as continental passive margins, convergent plate boundaries, and obliquely convergent plate boundaries (Fulthorpe & Schlanger, 1989; Hall, 2002; Wilson, 2002). Cenozoic carbonates in this region have long been proven as prolific hydrocarbon reservoirs including the Oligocene–Miocene carbonates of the East Java Basin with estimated hydrocarbon reserves of as much as several billion-barrels-of-oil-equivalent (Doust & Noble, 2008). Significant amount of subsurface data have become available through hydrocarbon exploration and production activity. Previous studies based on these subsurface data demonstrated variations in distribution of siliciclastic sediments as well as architecture and facies of carbonate formations in the East Java Basin (Kenyon, 1977; Mudjiono & Pireno, 2002; Welker-Haddock et al., 2002; Johansen, 2003; Adhyaksawan, 2003; Carter et al., 2005; Maynard & Morgan, 2005; Ruf et al., 2008; Posamentier et al., 2010). Despite its economic importance and subsurface data availability, little effort has been made to study dominant controls on carbonate shelf evolution in this region.

This study utilizes a comprehensive subsurface data set of almost continuous Oligocene–Miocene stratigraphic section that shows carbonate shelf evolution, from the

earliest Oligocene to the end of the Miocene (33–5 Ma). Subsurface data include well logs, cuttings lithology, core samples, thin sections, strontium isotopes dating, and 3D seismic. Carbonate shelf architecture, facies, and seismic geomorphology were described and interpreted in detail. By comparing the results regionally and referring to the literature, controls on carbonate shelf evolution were deciphered.

Controls on carbonate shelf development and evolution include eustasy, tectonics, climate, oceanography, trophic resources, and temperature (Figure 1.1; Lukasik & Simo, 2008). The interplay of these controls are often hard to entangle and subsequently interpreted as though one control dominates the other. This study acknowledges the dynamic nature of spatial and temporal controls on carbonate shelf evolution and highlights the significance of controls such as tectonically inherited antecedent topography, siliciclastic sediment routing, global sea-level fluctuation patterns, localized differential subsidence, regional oceanic circulation, and compressional tectonic events in a tectonically active region. Furthermore, the upside potential of under-explored and under-developed off-buildup carbonate-dominated strata was investigated.

This dissertation includes five chapters, of which three of them are written as self-contained journal-style papers. Chapter 1 includes mutual geologic background for the following three chapters. Chapter 2 discusses controls on carbonate shelf evolution during Oligocene to Early Miocene time based on architecture and facies of the Kujung Formation and its comparison to equivalent formations in the southeastern Sundaland region. Chapter 3 discusses possible influences of regional oceanic circulation and compressional tectonic events on the resulting architecture of the carbonate buildups and platforms during

Miocene time, as observed in seismic geomorphology. Chapter 4 investigates the upside potential of an Early Miocene off-buildup carbonate strata. Manuscripts from Chapter 2 and Chapter 3 will be submitted to international peer-reviewed journals (i.e., Journal of Sedimentary Research and Marine & Petroleum Geology). Work from Chapter 3 and Chapter 4 have been published in AAPG conferences abstracts (Fifariz et al., 2017, Fifariz et al.; 2018). Finally, Chapter 5 concludes this dissertation by listing significant findings of this study.

GEOLOGIC BACKGROUND

The study area is situated in southeastern Sundaland (Figure 1.2), which is a convergence zone between Eurasian and Indo-Australian plates (Manur & Barraclough, 1994; Hall, 2002; Hall et al., 2008). This is region characterized by dissected pattern of sets of NE-SW to E-W-trending paleo-highs and paleo-lows and several broad stable highs considered as platforms (Figure 1.3; Kenyon, 1977; Ardhana, 1993; Manur & Barraclough, 1994; Matthews & Bransden, 1995; Mudjiono & Pireno, 2002; Kupecz et al., 2013; Pubellier & Morley, 2014). This tectonically inherited structural trend is the result of a pre-Cenozoic to early Cenozoic subduction zone at the southeastern Sundaland margin that extends from the Meratus Ridge in South Borneo southwest to the Java Sea (Mudjiono & Pireno, 2002).

The study area is located offshore of East Java Island, northwest of present-day Madura Island, Indonesia, within an area regionally known as the East Java Basin. This region is characterized by sets of mostly northeast-southwest oriented structural highs and lows in the Paleogene (Figure 1.3). The study area is situated over one of the paleo-highs,

regionally known as the JS-1 Ridge (Kenyon, 1977, Maulin et al., 2016). Two grabens bounded the JS-1 Ridge on both sides, namely the East Bawean Trough to the west and the Central Deep to the east (Figure 1.4). Other paleo-highs that are nearby are the Bawean Arch to the west and the North Madura Platform to the east. The JS-1 Ridge was initially transgressed by marine conditions in the Early Oligocene (Manur & Barraclough, 1994). During the Oligocene to Miocene, in the adjacent platform to the east, the North Madura Platform, the Oligocene–Miocene successions have a widespread distribution that marks the post-rift tectonic quiescence episode of the region (Johansen, 2003). Thus, it is inferred that the JS-1 Ridge was already considered a submerged faulted block platform (paleo-high) situated on a highly irregular shelf in the Oligocene marked a post-rift episode of the basin filling history (Pubellier & Morley, 2014).

Four main tectonic episodes can be recognized in the study area (Johansen, 2003), which fit into the broader context of basin evolution wihtin the southeastern Sundaland region (Pubellier & Morley, 2014). These tectonic episodes are: 1) the pre-Cenozoic to Paleogene rifting (syn-rift); 2) the Oligocene sag phase and tectonic quiescence (post-rift); 3) the Miocene initial, early, to intense compression (inversion) that peaked at the Miocene-Pliocene boundary (5 Ma); and 4) the Pliocene to recent post-inversion, modern East Java back arc setting. The inversion began in the east and progressively migrated west, away from the convergence zone between the Eurasian and Australian plates.

The East Java Basin regional stratigraphy is based on geologic age and lithology from outcrop and subsurface (Mudjiono & Pireno, 2002; Johansen, 2003; Sharaf et al., 2005; Carter et al., 2005). It is commonly divided between the southern area (onshore East

Java, Madura Strait, and Madura Island) and the northern area (offshore East Java) (Mudjiono & Pireno, 2002; Johansen, 2003). The stratigraphy is subdivided from older to younger into: 1) the Pre-Cenozoic basement, 2) the Middle Eocene – Early Oligocene Ngimbang & CD Formations, 3) the Late Oligocene – lower Early Miocene Kujung Formation, 4) the upper Early Miocene Tuban & Rancak Formations, 5) the Middle Miocene Ngrayong Formation, 6) the Late Miocene Wonocolo Formation, and 7) other younger formations that include the Ledok Member, the Kalibeng Formation, and other locally recognized formations (Figure 1.5).

The basement is pre-Cenozoic in age and has lithology that includes igneous, metamorphic, volcanic rocks that underlie the Cenozoic formations (Mudjiono & Pireno, 2002). The Cenozoic formations started with the Middle Eocene – Early Oligocene Ngimbang Formation, consisting mostly of siliciclastic lacustrine shale and coarse-grained siliciclastic rocks near the basement-highs mostly distributed in the southern area. The lithology changed laterally into marine limestones of the CD Formation in the northern area.

The Ngimbang Formation is overlain by the Late Oligocene to Early Miocene Kujung Formation, which consisted of minor siliciclastic rock components around the local highs in the Oligocene, and laterally change into marine shale and limestones in the basin, which are the dominant lithology of the Kujung Formation toward the Early Miocene. The Kujung Formation is subdivided into three units based on its subsurface depth, Kujung-1, Kujung-2, and Kujung-3, from shallowest (youngest) to deepest (oldest).

The Kujung Formation is overlain by a set of formations of late Early Miocene to Late Miocene age, with varying lithologies. The Tuban Formation, which is mostly marine shale with minor carbonates component in the southern area, laterally changed into the Rancak Formation, which consists of marine shale, sands, and limestones in the northern area. These formations are overlain by the Ngrayong Formation of Middle Miocene age. The lithology of the Ngrayong Formation is dominated by sandstones in the northern area, which marked the renewed siliciclastic deposition in the region (Mudjiono & Pireno, 2002), and shale in the southern area. The Ngrayong Formation is overlain by the Wonocolo Formation of Late Miocene age. In the study area, this formation is also known as the OK Reef (Carter et al., 2005). This formation lithology is dominated by carbonates in the northern area, and they changed laterally to shale and volcaniclastic and sandstones in the southern area. The shift of the siliciclastic distribution from the northern area in Middle Miocene (the Ngrayong Formation) to the southern area in Late Miocene (the Wonocolo Formation), is a result of the inversion tectonics that started in the Late Miocene (Mudjiono & Pireno, 2002).

From the Pliocene to recent, other formations were deposited with varying lithology that include marls, reworked sandstones, planktonic foraminifer rich deposits, and volcaniclastic sandstones from the volcanic arc in the south.

Throughout the Cenozoic, major sources of siliciclastic sediments in the southeastern Sundaland region are major deltas in eastern–southeastern parts of Borneo (Hall & Nichols, 2002) and the Karimunjawa Arch in the Java Sea (Smyth et al., 2008). In

the Paleogene, localized basement highs in the region could as well be the sources of siliciclastic sediments for their surrounding area.

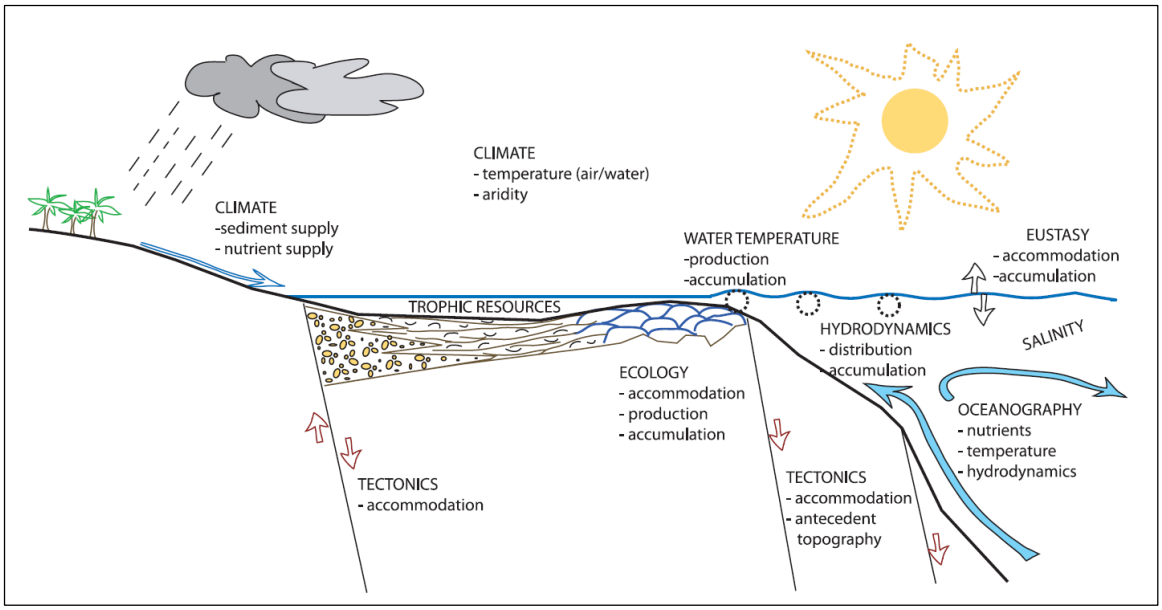

Figure 1.1. Schematic diagram of contemporaneous controls on the development and evolution of carbonate shelf, including reefs and platforms (Lukasik & Simo, 2008).

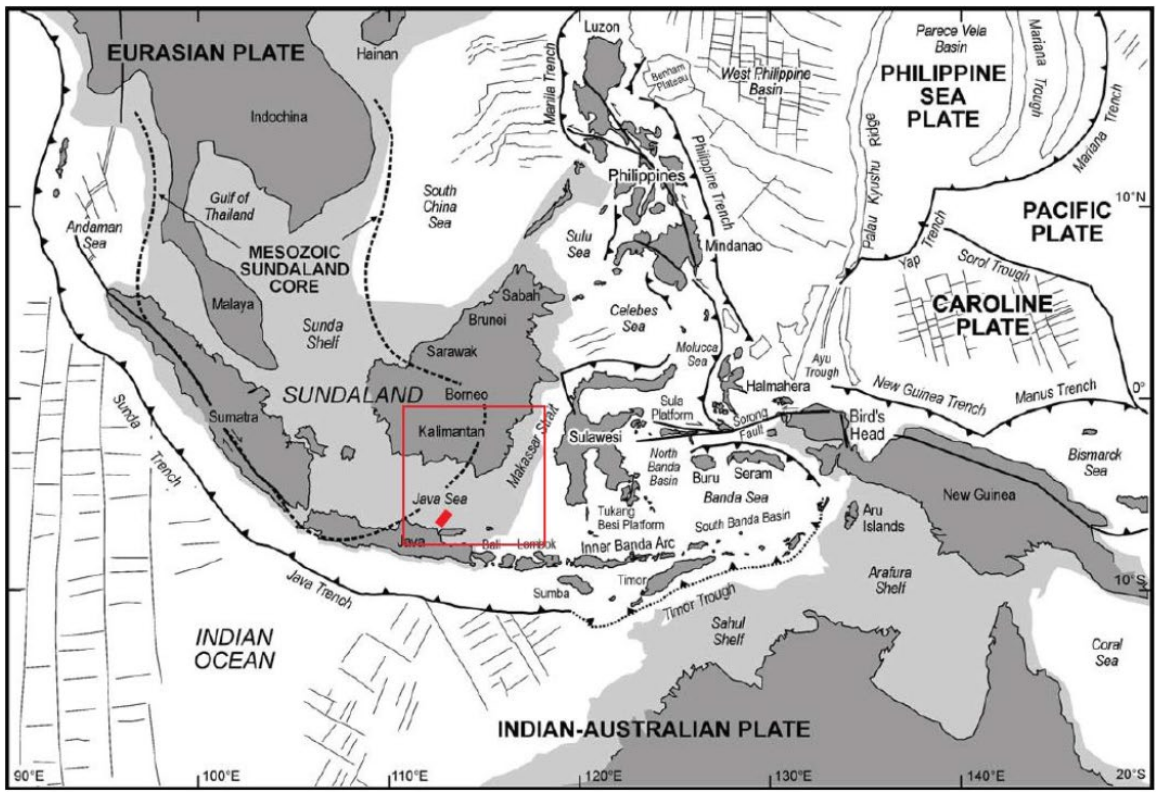

Figure 1.2. Regional tectonic setting of the southeast Asian region (Hall, 2002). The study area is located offshore East Java area, northwest of Madura Island (red box).

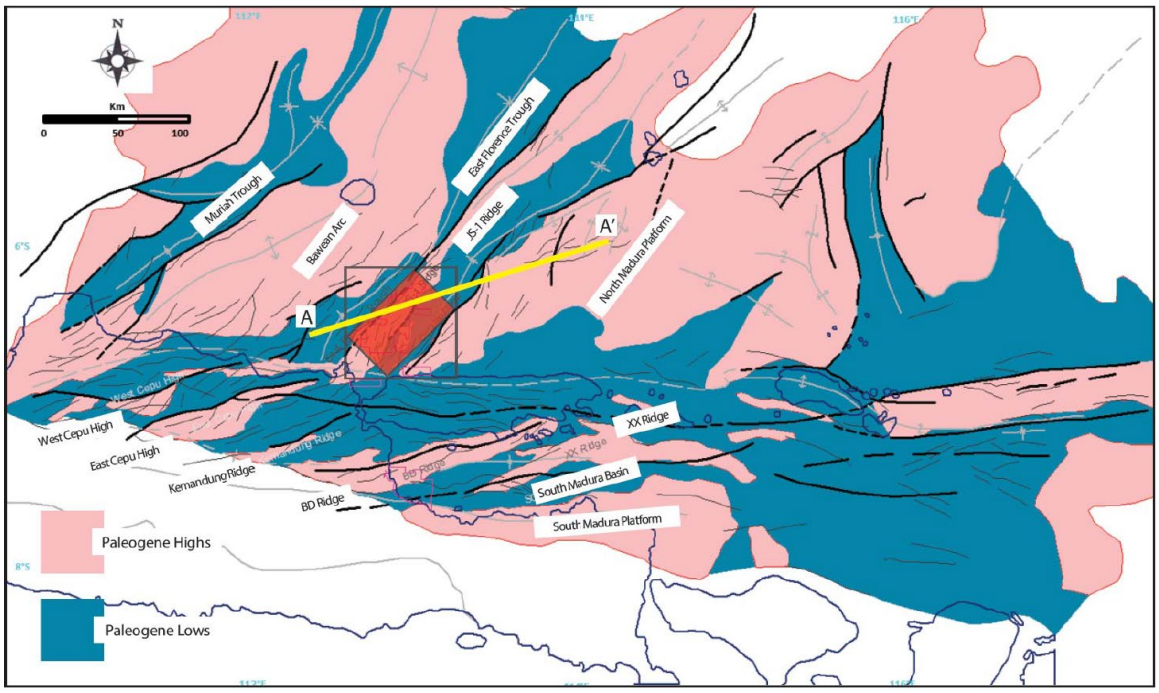

Figure 1.3. Distribution of northeast-southwest to east-west-trending structural highs and lows represented in the Paleogene (modified after Maulin et al., 2016). The study area is marked by transparent red box situated over a paleo-high regionally known as the JS-1 Ridge. A-A′ is a regional 2D seismic line shown in Figure 1.4.

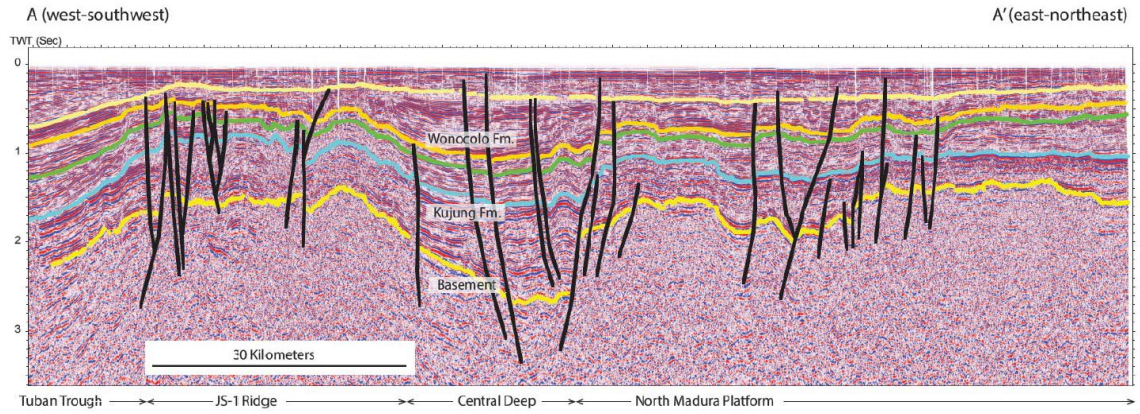

Figure 1.4. The JS-1 Ridge and the North Madura Platform as paleo-highs, separated by the Central Deep as paleo-low in between, shown by a west-southwest to east-northeast regional 2D seismic section. Another paleo-low, the Tuban Trough, is located west of the JS-1 Ridge. The Kujung Formation is marked by the blue seismic horizon, and the Wonocolo Formation is marked by the light brown seismic horizon (above the green seismic horizon).

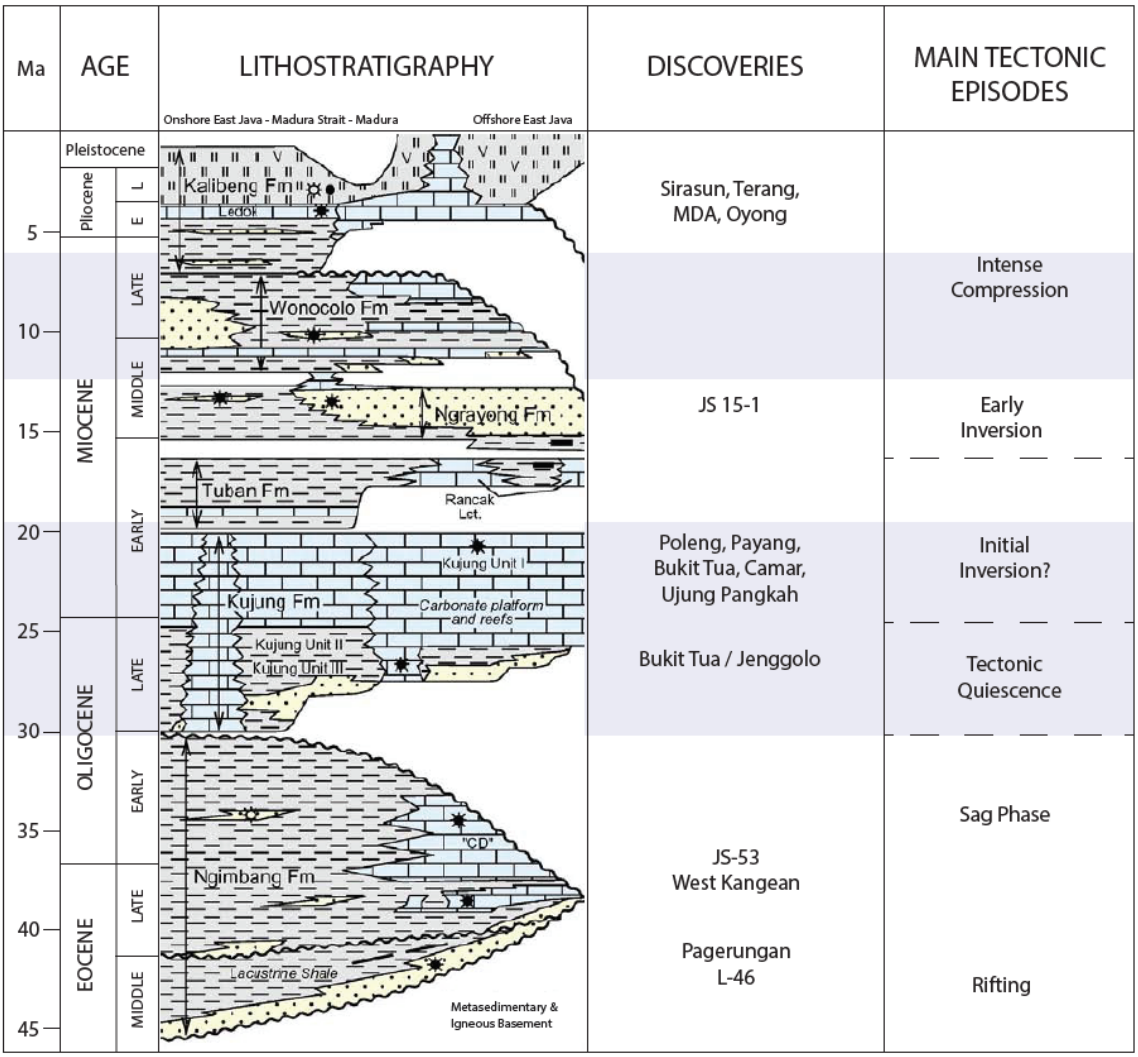

Figure 1.5. Regional stratigraphy of East Java Basin. The Early Miocene Kujung Formation and the Late Miocene Wonocolo Formation are both highlighted by pale blue background. The two carbonate formations were deposited under transition from tectonic quiescence in the Oligocene to initial inversion in the Early Miocene through intense compression in the Late Miocene (modified after Johansen 2003).

Chapter 2: Antecedent Topography and Siliciclastic Sediment Routing Controls on Carbonate Shelf Evolution during Oligocene to Early Miocene: Insights from Architecture and Facies of the Kujung Formation, Offshore East Java, Indonesia

ABSTRACT

Oligocene–Miocene carbonates are proven and prolific hydrocarbon reservoirs in the Southeast Asia region. Hydrocarbon exploration and production activities have resulted in extensive availability of subsurface data from this stratigraphic interval. Carbonate shelves in this region demonstrated spatial and temporal variations in distribution of siliciclastic sediments as well as architecture and facies of carbonate formations. Despite the economic importance, data availability, and complexity of the region, little effort has been made to decipher the dominant controls on carbonate shelves evolution.

This study utilized subsurface data from 19 wells and 1,300 km^2 of 3D seismic data from the offshore East Java area to study the Oligocene–Early Miocene Kujung Formation. Seismic sections clearly show an architecture of shoal-water complexes and numerous flat-topped to pinnacle-shaped carbonate buildups with high depositional-angle margins or flanks. Seismic slices laterally show depositional geometries such as east-west elongated buildups, circular-ovoid buildups, polygonal buildups, as well as shoal-water complexes that are a few hundred meters to a few kilometers wide. Well data include gamma-ray logs, cuttings, cores, thin sections, and $^{87}Sr/^{86}Sr$ measurements. Approximately 750 m (2,500 ft) of continuous stratigraphic section of the Kujung Formation were analyzed. Constrained by numerical ages from $^{87}Sr/^{86}Sr$ analysis, this interval covers a duration of approximately 13.5 m.y. from Rupelian, Chattian, and Aquitanian age. Ten facies were identified and

described from 789 feet of core samples and were qualitatively constrained by several thin sections. Dominant faunal constituents of the carbonate sediments include large benthic foraminifera, corals, and red algae. Skeletal fragments of echinoids and mollusks were also commonly found.

After integrating architecture, facies, and numerical age constraints, a stratigraphic framework was built to subdivide the Kujung Formation interval based on its depositional settings into mixed-siliciclastic-carbonate shelf in the Rupelian–Chattian and carbonate-buildups shelf in the Aquitanian. The change happened at around the Oligocene-Miocene boundary at 23 Ma. Accumulation rates, for both siliciclastic and carbonate sediments, in the Aquitanian interval are as much as three times higher than those in the Rupelian–Chattian.

These results were then compared to other Oligocene–Miocene carbonate shelves from selected areas within the southeastern Sundaland region. Using regional comparisons, I interpreted that tectonically inherited antecedent topography, siliciclastic sediment routing, and localized differential tectonic subsidence are the dominant controls on the platform-, basin-, to regional-scale spatial variation in distribution of siliciclastic and carbonate sediments, and the resulting architecture and facies on carbonate shelves during the Oligocene–Early Miocene. Change in the global sea-level fluctuation patterns seems to have caused the temporal variation represented in extensive carbonate buildups development starting in the Early Miocene. These controls could even override the influence of regional climatic change around the Oligocene-Miocene boundary.

INTRODUCTION

In the Southeast Asia region, equatorial carbonate sediments were produced extensively during the Cenozoic, from Sumatra to the west to New Guinea to the east, and from the Philippines to the north to Java and Bali to the south (Wilson, 2002). Carbonates were also deposited further south in the northwest shelf of Australia during this period (Rosleff-Soerensen et al., 2012). These Southeast Asia carbonates were deposited within continental passive margins, convergent plate boundaries, and obliquely convergent plate boundaries (Fulthorpe & Schlanger, 1989). Dominant faunal constituents of these carbonates changed from large benthic foraminifers (LBF) to corals at around the same time as the Oligocene–Miocene boundary (Wilson, 2008). Carbonate systems are very sensitive to changes in the conditions of its depositional environments and therefore carbonate rock records may be used to investigate large-scale changes such as the globally significant Oligocene–Miocene climatic transition (Mutti et al., 2011).

The Oligocene-Miocene carbonates in southeast Asia have long been known to be prolific hydrocarbon reservoirs. Significant amounts of subsurface data have become available as a result of hydrocarbon exploration and production activity. Despite its economic importance and subsurface data availability, its architecture, facies, and depositional model remain understudied. Questions regarding which controls are dominant on its deposition and implication to regional shelf evolution remain unanswered.

In the offshore East Java area, Indonesia, the Oligocene-Miocene carbonates are represented by the Kujung Formation. Previous studies based on subsurface data show a wide range of spatio-temporal variation of the architecture and facies of the Kujung

Formation (Kenyon, 1977; Johansen, 2003; Carter et al., 2005; Maynard & Morgan, 2005; Posamentier et al., 2010). Not observed in the offshore East Java area, the Kujung Formation changed from a carbonate-dominated system to a mixed-siliciclastic-carbonate system, from the lower to upper part, according to an outcrop study in the onshore East Java area (Sharaf et al., 2005). This shows a localized variation in siliciclastic sediment influence over relatively short distance (≤ 100 km).

This chapter of the dissertation presents an integrated analysis of the Kujung Formation based on 3D seismic and well logs, core, cuttings, and $^{87}Sr/^{86}Sr$ measurements from 19 wells. Approximately 750 m (2,500 ft) of a continuous stratigraphic section that covers approximately 13.5 m.y. from the Rupelian and Chattian, through the Aquitanian (Early Oligocene to Early Miocene) was analyzed in this research.

By analyzing subsurface data, this study describes and interprets architecture, facies, and depositional model of the Oligocene–Miocene Kujung Formation. The depositional settings were subdivided into the Rupelian–Chattian mixed-siliciclastic-carbonate shelf (MSCS) and the Aquitanian carbonate-buildups shelf (CBS). Results were then compared to other Oligocene–Miocene carbonate shelves in the southeastern Sundaland region, which includes onshore–offshore East Java, East Java sea to the east, and southeastern Borneo to the north. Finally, based on the regional comparison, possible dominant controls on regional carbonate shelves evolution are discussed.

DATA AND METHODS

This study utilized a subsurface data set that consists of 3D seismic and 19 wells from an active block operated by Pertamina Hulu Energi – West Madura Offshore or PHE-

WMO (Figure 2.1). The 3D seismic data were acquired in 1999 and cover an approximately 1,300 km^2 area and have a dominant frequency content of 25–35 Hz (Carter et al., 2005). Well data include gamma-ray logs from 17 wells, cuttings lithology from 3 wells, 789 ft of core samples from 11 wells, and several representative thin sections. In 2006 and 2007, CSIRO Petroleum collected the $^{87}Sr/^{86}Sr$ measurements used in this study. The numerical ages of the $^{87}Sr/^{86}Sr$ were analyzed using the look-up table from McArthur et al. (2001). Fifty-two samples of $^{87}Sr/^{86}Sr$ measurement are available from 10 wells (Table 2.1). Samples for $^{87}Sr/^{86}Sr$ measurement are distributed mostly in the lower part of the Kujung Formation (Kujung-2 & Kujung-3).

Four regional seismic horizons were picked and interpreted within the 3D seismic volume. The seismic horizons were tied to well data using synthetic seismogram based on previous work on KE 7-1 (Well-G, this study) from Carter et al. (2005). Vertical seismic sections were used to describe the seismic facies that include seismic amplitude, frequency, continuity, and geometry of the Kujung Formation and underlying formations. Depositional morphology of the Kujung Formation was also interpreted. Semblance seismic attribute was extracted from the 3D seismic volume, and horizon slicing on the Top Kujung horizon was performed to describe the carbonate buildups based on lateral event's continuity such as the carbonate buildups shape outline.

Three terms were used to describe the characteristics of any given stratigraphic intervals based on well data: 1) *Electrofacies*, 2) *Lithofacies*, and 3) *Facies*. The term *Electrofacies* was defined as a distinguishable set of log responses that characterizes the sediment within a stratigraphic interval (Serra & Abbott, 1980). Gamma-ray log responses

were described as cylindrical, bell, funnel, or serrated shapes that indicate the interval's clay mineral content in the form of *shale* or *claystones* (Rider, 1990). *Lithofacies,* which was tied to Electrofacies, was defined as the interval's generalized lithology based on cuttings description. *Facies* was defined as the specific depositional characteristics of carbonate rock based on core samples using the Dunham (1962) and Embry & Klovan (1971) classification schemes. *Facies* discussed here also includes additional siliciclastic rock such as *shale*, *siltstone*, and *sandstone*.

Electrofacies and *Lithofacies* were described and utilized to perform well-to-well correlation. *Facies* were identified and described based on approximately 789 feet of core samples from 11 wells that were qualitatively constrained by several representative thin sections for carbonate grains and matrix identification. All facies were then grouped into two main facies associations corresponding to their depositional systems. Well-E was chosen as the reference well due to its broad coverage of numerical age constraint with 20 samples of $^{87}Sr/^{86}Sr$ measurements within the Kujung Formation. Results were constrained by numerical ages from the $^{87}Sr/^{86}Sr$ analysis. Geologic age boundaries from the 2012 edition of the GSA Geologic Time Scale were used (Gradstein et al., 2012 and Cohen et al., 2013).

RESULTS

Using architecture and facies described from seismic and well data, this study subdivides the depositional settings of the Oligocene–Miocene Kujung Formation into the Rupelian–Chattian mixed-siliciclastic-carbonate shelf (MSCS) and the Aquitanian

carbonate-buildups shelf (CBS). The stratigraphic framework is constrained by numerical ages from $^{87}Sr/^{86}Sr$ analysis.

Seismic Facies and Horizons Interpretation

Seismic facies were described based on the amplitude, frequency, continuity, and geometry of the seismic reflectors (Figure 2.2; Fontaine et al., 1987; Janson et al., 2011). Based on the seismic facies definition, four seismic horizons were picked and interpreted within the 1,300 km^2 of 3D seismic data (Figure 2.3). They are, from older to younger, 1) Top Basement horizon (top pre-Cenozoic interval), 2) Top Pre-MSCS horizon (top Eocene interval, top Ngimbang Formation), 3) Top MSCS horizon (top Oligocene interval, top Kujung-2), and 4) Top CBS horizon (top early Miocene interval, top Kujung-1). The Oligocene–Miocene interval consists mainly of carbonates and shale.

The pre-Cenozoic interval (SF-8), capped by the Top Basement horizon, has low to moderate amplitude and low-frequency seismic reflectors. They show discontinuous and chaotic to sub-parallel geometry as representative of the mixed basement lithology of igneous, metamorphic, and volcanic rock. The basement structure forms a northeast-southwest trending fault block gently dipping southeastward and bounded by set of normal faults northwestward (Figure 2.3). Sets of southeastward-dipping normal faults were also observed in the eastern flank of the JS-1 Ridge throughout the northwest-southeast seismic sections.

The Eocene interval (SF-7) is characterized by low to moderate amplitude and moderate-frequency seismic reflectors. They show discontinuous to semi-continuous and chaotic to sub-parallel geometry. This interval is capped by the Top Pre-MSCS horizon

(SF-6) that is characterized by a high positive amplitude and a low-frequency seismic reflector. The seismic reflector shows continuous to semi-continuous and parallel to sub-parallel geometry.

The Oligocene interval (SF-5) is as much as approximately 300 ms TWT thick and is characterized by low to moderate amplitude and moderate-frequency seismic reflectors. They show a discontinuous to semi-continuous and chaotic to sub-parallel seismic reflector geometry. This interval is capped by a high negative amplitude, low-frequency seismic reflector of Top MSCS horizon (SF-4) that is mostly continuous and shows parallel to sub-parallel seismic reflector geometry. A relatively continuous moderate negative amplitude and low frequency seismic reflector representing widespread strata with lower impedance in the middle of this interval were also observed.

The Early Miocene interval is as much as approximately 200 ms TWT thick and its seismic characteristic varies greatly depending on the architecture of the Early Miocene carbonate buildups. In term of architecture, the carbonate buildups were subdivided laterally based on their depositional profile into buildup-core, buildup-flank, and inter-buildups, from the shallowest part of the buildups into the deeper part of the open shelf. This subdivision will be discussed in more detail in the architecture interpretation in a later section. Within buildup-core (SF-2), the interval is characterized by moderate amplitude, moderate frequency seismic reflectors. They show semi-continuous to discontinuous and mounded-chaotic to sub-parallel geometry. In contrast, within the buildup-flank and inter-buildups area (SF-3), the interval is characterized by moderate to low-amplitude and moderate-frequency seismic reflectors. They show semi-continuous to discontinuous and

sub-parallel to chaotic seismic reflectors geometry. The Early Miocene interval is capped by the Top CBS horizon (SF-1) which shows a high positive amplitude and a low-frequency seismic reflector. The horizon is mostly continuous and has a parallel to mounded geometry.

Electrofacies and Lithofacies

Four electrofacies were identified and described based on gamma-ray log responses. They are cylindrical, bell, funnel, and serrated shapes. Gamma-ray log responses indicate the interval's clay mineral content in the form of *shale* or *claystones* (Rider, 1990). Each electrofacies is characterized by a distinguishable gamma-ray log pattern within an interval. First, cylindrical shape is characterized by a consistent low gamma-ray log value within the interval. The bell shape is characterized by an increasing upward gamma-ray log value within the interval. In contrast, the funnel shape shows a decreasing upward gamma-ray log value within the interval (Rider, 1990). Finally, the serrated shape is characterized by an interval dominated by high gamma-ray log values with spikes of thin intervals of medium to low gamma-ray log value.

Based on electrofacies description in Well-E, the lower part of the Kujung Formation comprises two intervals of alternating bell and funnel shape electrofacies separated in the middle by an interval dominated by serrated shape electrofacies with a total thickness of slightly over 315 m (1,033 ft). Based on this electrofacies differentiation, the lower part of the Kujung Formation is subdivided into Lower MSCS, Middle MSCS, and Upper MSCS, from older to younger. The upper part of the Kujung Formation contains an interval of cylindrical shape electrofacies with a total thickness reaching approximately

287 m (940 ft) (Figure 2.4). Well tops are then picked at the top of each interval. The following are seven well tops that were picked in each well in the study area: 1) Top Basement, 2) top Pre-MSCS, 3) top Lower MSCS, 4) top Middle MSCS, 5) top MSCS – equivalent to top Upper MSCS, the MSCS-CBS boundary, 6) top Lower CBS, and 7) top CBS – equivalent to top Upper CBS (Figure 2.4).

High-gamma ray log values correspond to shale that contains radioactive clay minerals and low gamma-ray log values correspond to mostly carbonates and a few thin beds of siltstone and sandstone found in the lower part of the Kujung Formation. When trying to distinguish siltstone and sandstone beds from the carbonates, they usually have a lower bulk density log value compared to the carbonates. Thin beds of siltstone and sandstone are present in the Lower MSCS interval, as described in core samples of Well-A (Figure 2.7).

Four lithofacies groups were described based on cuttings lithology. They are 1) limestone, 2) shale-limestone interbeds (shaly-limestone/limey-shale), 3) shale, and 4) igneous-metamorphic-volcanic basement rocks. Other siliciclastic rocks such as siltstone, sandstone, and coal are occasionally present as thin beds in the lower part of the Kujung Formation. Basement rocks have varying lithology of igneous, metamorphic, and volcanic rocks (Figure 2.5).

This study benefits from having data from wells that penetrate buildup-flanks or inter-buildups off the buildups, such as Well-K, Well-N, and Well-O. They show different electrofacies and lithofacies characteristics of the CBS interval. The CBS interval in these wells is subdivided into two intervals: a lower part that is characterized by the presence of

cylindrical shape that subsequently changed into bell shape electrofacies and an upper part that is dominated by serrated shape and alternating bell and funnel shape electrofacies. These two intervals subdivided the CBS into the Lower CBS and Upper CBS with a somewhat gradational boundary. In term of lithology, carbonates dominated the Lower CBS, whereas carbonate and shale interbeds characterized the Upper CBS. Figure 2.5 shows the correlation between Well-J and Well-K, two wells that are 1.5 km separate from each other and that represent the change in the CBS interval characteristics from buildup-core to buildup-flank and inter-buildups.

Facies

Core samples were acquired and annotated in imperial units (feet). There are 282 ft (86 m) of core samples from the MSCS interval and 613 ft (187 m) from the CBS interval distributed in eleven wells. The longest continuous core samples with 240 ft (73 m) were available in the MSCS interval (Table 2.1, Table 2.2, and Figure 2.6).

Ten facies were identified and described. Classification scheme from Dunham (1962) and Embry & Klovan (1971) was used for carbonate rocks. Two siliciclastic facies are *shale* (F1) and *siltstone – sandstone* (F2). The rest of the facies are: *silty-mudstone* (F3), *LBF wackestone – mud-dominated packstone* (F4), *LBF-echinoid-coral – grain-dominated packstone – grainstone* (F5), *LBF floatstone – rudstone* (F6), *Coral floatstone – rudstone* (F7), *Coral-algal framestone* (F8), *Coral-algal bindstone* (F9), and *Rhodolith floatstone – rudstone* (F10). The depositional textures that indicate that the sediments were bound together during deposition (framestone and bindstone) represent the capability of the carbonate sediments to form a carbonate buildup. Main faunal constituents of the carbonate

grains are large benthic foraminifers (LBF), corals, red algae, echinoids, and mollusks. LBF include *Lepidocyclina*, *Eulepidina*, *Amphistegina*, *Operculina*, *Miogypsina, Sphaerogypsina*, and *Heterostegina*. Other types of foraminifera include *Miliolids*, *Soritidae*, *Austrotrillina*, *Victoriella*, encrusting foraminifera, and planktonic foraminifera. Corals are *Scleractinian* corals of several forms that include branching/finger, head, and platy corals. Red algae are present in encrusting and branching forms. Mollusks include bivalves and gastropods. Another carbonate grain that was observed in minor amounts is *Bryozoan*. One of the core samples in Well-S (42 ft) that is situated over the southwestern margin of the North Madura Platform consists entirely of *Rhodolith floatstone - rudstone* (F10). Figure 2.8 shows representative photographs of each facies, and Figure 2.9 shows representative microfacies photographs from selected thin sections.

Detailed description of each facies, as summarized in Table 2.2, are as follows:

Shale (F1) has dark gray to greenish gray colors, breaks in fissile structure representing the abundance of clay mineral content. Rare carbonate grains include planktonic foraminifera and thin-shelled mollusks. Thickness varies from few centimeters to several meters.

Siltstone – sandstone (F2) has light gray to whitish colors, grain size ranging from silt to medium sand (up to 0.2–0.5 mm), mostly composed of quartz grains, thinly bedded sometimes with ripples and cross-laminations. It is bioturbated and glauconitic, and thickness varies from a few feet to less than 10 ft.

Silty-mudstone (F3) is dark gray, mostly massive but sometimes laminated. It is composed mostly of fine-grained carbonates with silt-sized quartz grains, matrix-supported

depositional texture. Occasional carbonate grains include planktonic foraminifera and thin-shelled mollusks.

LBF wackestone – mud-dominated packstone (F4) is gray and shows faint laminations and grains orientation, matrix-supported depositional texture. Carbonate grains include LBF (≤ 1 cm wide) and planktonic foraminifera.

LBF-echinoid-coral – grain-dominated packstone – grainstone (F5) has creamish- to yellowish-white colors, shows laminations and tens-of-centimeters-thick beddings. It has grain-supported depositional texture and well-sorted grains. Carbonate grains consist of coarse sand-sized (≤ 2 mm wide) spherical-form LBF, echinoid plates, coral, and mollusk fragments.

LBF floatstone – rudstone (F6) is light gray, shows moderate laminations and grain orientations, and matrix- to grain-supported depositional texture. Carbonate grains consist exclusively of LBF ≤ 5 cm wide. It is dominated by *Eulipidina* and *Lepidocyclina* in the MSCS interval. LBF grains were observed to become smaller and rounder (spherical-form) in the CBS interval *Miogypsina* and *Amphistegina*.

Coral floatstone – rudstone (F7) has light gray to cream colors, shows no laminations, and is massive. It has matrix- to grain-supported depositional texture. Carbonate grains consist mostly of coral fragments with a size of 1–2 cm wide.

Coral-algal framestone (F8) is whitish-cream to white, shows no laminations, and is massive in texture. Carbonate grains consist of head and branching corals as framework builder and encrusting and branching red algae.

Coral-algal bindstone (F9) has whitish cream to white colors, shows no laminations, and is massive. Carbonate grains consist of platy corals as framework builder and encrusting red algae as binder.

Rhodolith floatstone – rudstone (F10) has gray, whitish, and greenish colors, shows weak laminations, and has a matrix- to grain-supported depositional texture, with poorly to moderately sorted grains. Carbonate grains consist of almost entirely *Rhodolith* (mostly 1–2 cm wide, ≤ 5 cm). Matrix is silty and argillaceous sediments.

Numerical Ages Based on $^{87}Sr/^{86}Sr$ Data

Numerical ages derived from $^{87}Sr/^{86}Sr$ analysis of 52 samples taken from 10 wells within the Kujung Formation yielded $^{87}Sr/^{86}Sr$ values ranging from 0.70778–0.708415 and resulting in an age range of 34.4–20.5 Ma (Table 2.3). This covers the entire 13.5 m.y. duration (33.9–20.4 Ma) from the Rupelian, Chattian, and Aquitanian ages (Early Oligocene–Early Miocene). The look-up table from McArthur et al. (2001) were used in the analysis. This analysis has range of errors of about ± 0.1–0.3 Ma depending on the ages: ± 0.2 Ma for Rupelian, ± 0.1 for Chattian, and ± 0.3 Ma for Aquitanian.

The samples covered all intervals within the Kujung Formation but are mostly distributed in the Lower MSCS interval. There are 39 samples within the Lower MSCS interval, with numerical ages ranging from 33.5–28.1 Ma (Rupelian, Early Oligocene), two samples are anomalous and yield numerical ages of 34.4 Ma and 34.1 Ma (Priabonian, Eocene), respectively. In the Middle MSCS interval, there is one sample with an age of 27.2 Ma (Chattian, Late Oligocene). There are two samples within the Upper MSCS interval with ages ranging from 26.1–24.9 Ma (Chattian, Late Oligocene). In the CBS,

almost all samples belong to the Upper CBS interval, where the main producing reservoir intervals are located. In the Lower CBS interval, there is one sample with a numerical age of 22.1 Ma (Aquitanian, Early Miocene). There are nine samples plotted within the Upper CBS interval with numerical ages ranging from 21.9–20.5 Ma (Aquitanian, Early Miocene). Figure 2.10 shows the schematic distribution of all samples plotted within the intervals used for well correlation in Well-E.

All samples were plotted within the framework of well-tops interpretation. Three well-tops, which are top Pre-MSCS, top MSCS, and top CBS, were considered as important stratigraphic boundaries with inferred numerical ages that coincide with important event in the stratigraphy (Figure 2.4). Those stratigraphic boundaries are, from older to younger, the Eocene-Oligocene boundary (33.9 Ma), the Oligocene-Miocene boundary (23 Ma), and the end of Aquitanian in the Early Miocene (20.4 Ma).

The distribution of numerical ages from all 52 samples was interpreted to be in agreement with the stratigraphic framework used for well correlation in the study area. This validates the stratigraphic framework of the Kujung Formation for other interpretations such as architecture, facies, and depositional model. The stratigraphic framework of the Kujung Formation was used in a broader context for regional comparison to other Oligocene–Miocene carbonate shelves.

Architecture

The architectural elements of the Kujung Formation were interpreted based on seismic scale observations. The JS-1 Ridge was subdivided based on structural configuration of the basement into two areas, horst and graben. Horst represents the

basement high oriented northeast–southwest. The Eocene Ngimbang Formation (Pre-MSCS interval) thickens to the graben and thins to the horst. This formation is interpreted as syn-rift deposits that onlaps onto the basement high. Main lithology in this interval includes carbonates, marine shale, and other coarse-grained siliciclastics in the lower part whose distribution were controlled by the proximity to local paleo-highs that were still sub-aerially exposed during Paleogene time.

The overlying Oligocene–Miocene Kujung Formation (MSCS and CBS interval) was distributed with relatively similar thicknesses in both horst and graben areas. This formation is interpreted as post-rift deposits over the transgressed basement high, mainly consisting of carbonates and shale lithology (Figure 2.3).

The MSCS interval is characterized by low to moderate amplitude of seismic reflectors with moderate frequency. These reflectors show a discontinuous to semi-discontinuous, chaotic to sub-parallel geometry. Seismic architecture in this interval could not be used with a high confidence level due to pull-up effects from the overlying CBS interval. However, vertical subdivision of the Lower, Middle, and Upper MSCS intervals could still be observed. Based on well logs and cuttings lithology, these intervals characterized by bell- and funnel shape electrofacies correspond to alternating carbonate and shale beds lithofacies in the Lower and Upper MSCS intervals. Serrated electrofacies are representative of widespread shale characterized the Middle MSCS interval. *LBF floatstone – rudstone* (F6) dominated the carbonate beds in the MSCS interval. *Coral-algal framestone* (F8) and *Coral-algal bindstone* (F9) were present in limited distribution. *Shale* (F1), *silty-mudstone* (F3), and *LBF wackestone – mud-dominated packstone* (F4)

characterized the finer-grained facies. *Siltstone* and *sandstone* as coarser-grained siliciclastic facies were present as thin beds in the Lower MSCS interval.

Horizon slicing at the Top CBS level was performed to the semblance seismic attribute volume in order to characterize the carbonate buildups lateral geometry and distribution. Based on the horizon slice, the CBS carbonate buildups were subdivided into east-west elongated flat-topped buildups in the southern area, circular-ovoid pinnacle buildups in the central area, and polygonal flat-topped buildups in the northern area. Shallow-water shoal complexes are present in both southern and northern areas. The size of the buildups varies from 500 m to 2 km wide. The elongated buildups are up to 8 km long (Figure 2.11).

Furthermore, a set of distinctive architectural elements was observed within the CBS based on the carbonate buildups morphology and geometry interpreted at the Top CBS (Top Kujung Formation, Early Miocene/Aquitanian). Interpreted seismic sections clearly show the depositional geometries of the carbonate buildups, which were further subdivided into buildup-core, buildup-flank, and inter-buildups. Buildup-core is interpreted as the shallowest parts of the carbonate buildups characterized by flat-topped to pinnacle-like geometry. Buildup-flank is interpreted as the inclined slope surrounding the buildup-core. Buildup-core and inter-buildups have a relatively low depositional angle compared to the high depositional angle of the buildup-flank. Buildup-flank is bounded by inflection points of the slope to buildup-core up-dip and to inter-buildups down-dip. Inter-buildups is interpreted as the area in between carbonate buildups that can be characterized as an open shelf with varying depth. The overlying Tuban Formation was observed to onlap

onto the Top CBS seismic horizon (Figure 2.3 and Figure 2.12). Most of the wells in the study area penetrated buildup-core, except for Well-K, Well-N, and Well-O. These wells penetrated the buildup-flank or inter-buildups area and are characterized by alternating carbonate and shale beds (Figure 2.1, Figure 2.5, and Figure 2.13).

Seismic facies of the CBS interval varies relative to the architecture of the Early Miocene carbonate buildups. Seismic reflectors with moderate amplitude and frequency characterized the buildup-core. Seismic reflectors within the buildup-core show semi-continuous to discontinuous, mounded-chaotic to sub-parallel geometry. In contrast, seismic facies of the buildup-flank and inter-buildups is characterized by seismic reflectors with moderate to low amplitude and moderate frequency. Seismic reflectors of the buildup-flank and inter-buildups show semi-continuous to discontinuous, sub-parallel to chaotic geometry. Lateral variation between seismic characteristics within the buildup-core and buildup-flank to inter-buildups is also observed in lateral variation of electrofacies and lithofacies. Cylindrical electrofacies and massive carbonates lithofacies characterize the buildup-core, whereas bell- and funnel shape electrofacies representative of interbedded carbonate and shale lithofacies characterize the buildup-flank and inter-buildups. *Coral floatstone – rudstone* (F7)*, Coral-algal framestone* (F8)*,* and *Coral-algal bindstone* (F9) characterized the buildup-core of the CBS interval*. LBF-echinoid-coral grain-dominated packstone – grainstone* (F5) was present in the buildup-core to buildup-flank. *Shale* (F1) and *LBF wackestone – mud-dominated packstone* (F4) were interpreted as finer-grained facies in the buildup-flank to inter-buildups.

Well Correlation, Unit Thicknesses, and Accumulation Rates

By analyzing the electrofacies and lithofacies, seven well tops were picked and correlated throughout the study area. Those well tops, from older to younger, are top Basement, top Pre-MSCS, top Lower MSCS, top Middle MSCS, top MSCS, top Lower CBS and top CBS. Well correlations were performed regionally using 13 selected wells along (northeast-southwest) and across (northwest-southeast) the JS-1 Ridge to show the distribution of Pre-MSCS, MSCS, and CBS successions. The Pre-MSCS successions, interpreted as syn-rift deposits, were diachronously deposited and show thinning and onlaps toward the basement high. In contrast, the MSCS and the CBS successions, interpreted as post-rift deposits, were widely distributed over the JS-1 Ridge with relatively consistent thickness (Figure 2.13).

In term of lithofacies and electrofacies, three distinct intervals were observed within the MSCS interval, which are Lower, Middle, and Upper MSCS. Shale with serrated electrofacies of the Middle MSCS are sandwiched between two intervals with relatively similar characteristics, interbedded carbonate-shale with bell-funnel shape electrofacies of the Lower and Upper MSCS. In some areas in the southern part of the JS-1 Ridge, Well-H shows a less shaly Middle MSCS interval. In the Lower CBS interval, carbonates with cylindrical to bell shape electrofacies, were widely distributed over the study area even in the area described as inter-buildups, marking a period of widespread platformal carbonate deposition. In contrast, massive carbonates lithofacies with cylindrical shape electrofacies characterize buildup-core that changes somewhat abruptly laterally into interbedded

carbonate-shale with bell-funnel-serrated shape electrofacies of buildup-flank and inter-buildups in the Upper CBS interval (Figure 2.13).

By utilizing well correlation, the total thickness from the Kujung Formation was then calculated by subtracting the depth of top CBS and top Pre-MSCS of each well. It ranges from approximately 1,900 ft (~580 m) to more than 2,500 ft (~760 m). The MSCS interval has thicknesses ranging from less than 1,000 ft (~300 m) to more than 1,500 ft (~460 m) and the CBS interval has thickness ranging from less than 700 ft (~210 m) to more than 1,100 ft (~335 m) (Table 2.4).

Well-I, Well-O, and Well-R have the thickest MSCS interval of over 1,500 ft (~450 m). Well-I and Well-O are both interpreted to be situated in the graben of the JS-1 Ridge and Well-R is situated over the southern edge of the North Madura Platform. In contrast, the thinnest MSCS intervals were observed in Well-A, Well-B, and Well-D, with thickness less than 1,000 ft (~300 m). All those three wells are interpreted to be situated over the horst of the JS-1 Ridge.

The thickest CBS intervals were observed in Well-C and Well-J with thicknesses of more than 1,100 ft (~330 m). Both wells are interpreted as buildup-core in the central area. Well-O has the thinnest CBS interval with a thickness of slightly less than 700 ft (~210 m) and is interpreted as inter-buildups deposits.

Numerical ages for top Pre-MSCS, top MSCS, and top CBS were inferred by plotting the results of $^{87}Sr/^{86}Sr$ analysis within the intervals of correlated well-tops. These well-tops are considered significant as they are close to, if not coincident with, important stratigraphic boundaries such as Top Eocene (Priabonian) at 33.9 Ma for top Pre-MSCS,

Oligocene-Miocene boundary at 23 Ma for top MSCS (MSCS-CBS boundary), and top Aquitanian (early Miocene) at 20.4 Ma for top CBS.

This interpretation is based on the distribution of samples for $^{87}Sr/^{86}Sr$ measurement around the three well tops mentioned above. The closest sample from Well-E, ~30 ft above the top Pre-MSCS, has a numerical age of 33.5 Ma. For the top MSCS, the closest sample also from Well-E, ~100 ft below the well-top, has a numerical age of 24.9 Ma. For the top CBS, the closest samples, ~15–100 ft below the well-top, have numerical ages of 20.5 Ma (Well-D) and 20.9 Ma (Well-E), respectively (Figure 2.10).

Accumulation rates for the MSCS and CBS intervals were then estimated by dividing the interval thickness over the interval's inferred depositional duration, 10.9 m.y. for the MSCS (Rupelian – Chattian) and 2.6 m.y. for the CBS (Aquitanian). Accumulation rates are estimated in centimeter per thousand-year unit (cm/k.y.). The thickness of the MSCS and CBS intervals in Well-E as reference well are 1,033 ft (314.86 m) and 940 ft (286.51 m), respectively. Accumulation rates were estimated to be approximately 2.89 cm/k.y. and 11.02 cm/k.y. for the MSCS and CBS intervals, respectively. These accumulation rates vary between wells depending on the interval thicknesses. The accumulation rate for the MSCS interval is ranging from 2.62–4.41 cm/k.y. with an average of 3.49 cm/k.y. In contrast, the accumulation rate for the CBS interval ranges from 8.07–13.29 cm/k.y. with an average of 10.85 cm/k.y. (Table 2.4).

Facies Association

During the deposition of the Oligocene–Early Miocene Kujung Formation, the JS-1 Ridge was a middle to outer shelf with localized shallow areas development (Wilson &

Vescei, 2005). The distribution of architectural elements of the Kujung Formation was put into general depositional settings such as basin, open shelf, slope (foreslope to toe of slope), ecologic reefal buildup, and open platform (Wilson, 1975).

Six associations of one or more facies correspond to their depositional environments were interpreted based on faunal assemblages, depositional textures, and inferred depositional settings (Wilson, 1975; Hallock & Glenn, 1986). They are clay-rich planktonic foraminifer deep open shelf to basin deposits (FA-1), larger-flat foraminifer open shelf to toe of slope deposits (FA-2), coral-algal reefal buildup to foreslope deposits (FA-3), smaller-robust foraminifer open platform deposits (FA-4), coarser-grained siliciclastic shallow open shelf deposits (FA-5), and rhodolithic drowned shelf margin deposits (FA-6). Facies included in each facies associations are *shale* (F1) and *silty-mudstone* (F3) in FA-1, *LBF wackestone – mud-dominated packstone* (F4), *LBF floatstone – rudstone* (F6), and *Coral-algal floatstone - rudstone* (F7) in FA-2, *Coral-algal floatstone – rudstone* (F7), *Coral-algal framestone* (F8), and *Coral-algal bindstone* (F9) in FA-3, *LBF-echinoid-coral grain-dominated packstone – grainstone* (F5) and *Coral-algal floatstone – rudstone* (F7) in FA-4, *siltstone – sandstone* (F2) in FA-5, *rhodolith floatstone – rudstone* (F10) in FA-6 (Table 2.2).

F1 is interpreted to be the background clay-rich facies as hemipelagic deposits with the lowest depositional energy. F1 is also interpreted to be deposited whenever the conditions were unfavorable for carbonates sedimentation. F1 is in association with F2 as the carbonate-rich fine-grained facies. Together, F1 and F2 characterize the sediments in the deep open shelf and the basin (FA-1).

F4 and F6 characterize the facies in the open carbonate shelf to toe-of-slope settings (FA-2). F7 is interpreted to be present close to the buildups. The large and flat shape of the LBF tests in this setting represent a deeper environment with relatively low to moderate energy and light penetration.

F8 and F9 characterize the dominant facies in the ecologic reefal buildups setting, while F7 characterizes the foreslope setting (FA-3). This depositional setting developed under constant high-energy and high-light penetration conditions. Corals are the main faunal constituent and act as framework builders for the carbonate buildups. Fine-grained siliciclastic sediments were constantly being winnowed away from this setting.

F5 and F7 characterize the facies in the open platform setting (FA-4). These facies were distributed in the shallow-water part of the buildup-core and also possible to be found in the shoal complexes. The small and spherical shapes of the LBF tests in this setting represent shallower environment with high energy and light penetration.

The distribution of F2 in a shallow open shelf setting (FA-5) is limited within the Lower MSCS interval. The coarse-grained siliciclastic sediments were sourced from the localized basement highs over the JS-1 Ridge that were still exposed during Early Oligocene time (Figure 2.17). This facies was deposited during low sea-level under moderate to high energy conditions over the shelf.

F10 characterizes the facies in a drowned shelf margin setting (FA-6). This facies is dominated by red algae (both encrusting and branching forms) and skeletal grains (echinoids and mollusk). The sediments in this settings were constantly influenced by

moderate energy that resulting in *rhodolith* grains. These *rhodolith* assemblages in the Cepu area were described as drowning facies (Hakiki et al., 2012).

Depositional Model

The depositional model was built with consideration of analogues from the literatures (Kenyon, 1977; Longman et al., 1992; Bassant, 1999; Bassant et al., 2005; Wilson & Vescei, 2005). One analogue was used from a modern carbonate shelf of the Seribu Platform that resembles architecture and facies of the Kujung Formation (Jordan Jr, 1998; Park et al., 2010). Mud banks or mud mounds were used to describe depositional systems rich in micrites (Kenyon, 1977; Longman et al., 1992). This type of carbonate-mud rich buildups may also be present in the study area in the Early Miocene (Kenyon, 1977). The depositional model proposed by this study was not addressed to explain this carbonate-mud rich carbonate buildups. By integrating architectural elements and facies associations, the depositional model of the Kujung Formation is proposed (Figure 2.14).

The water depth of the open shelf is interpreted to vary from 30–100 m (Bassant, 1999; Bassant et al., 2005; Park et al., 2010). The fair-weather wave base (FWWB) was placed at around 10–15 m of water depth and the stormy-weather wave base (SWWB) was placed at around 20–30 m. Water depth is interpreted to be gradually decreasing, from 30–10 m along the buildup-flank. Within the buildup-core, the water depth is interpreted to be shallower than 10 m above the FWWB. In the present-day Seribu Islands, up to 85% siliciclastic mud were found in depths around 30–50 m in the inter-island channels or shelf (Park et al., 2010), which is analogous to deep open shelf to basin deposits (FA-1) of inter-buildups area in this study that is dominated by *shale*.

Based on results from this study, several key observations were taken into consideration when building the depositional model for the Kujung Formation:

- Fine-grained siliciclastic sediments were present within the whole section of Oligocene to Early Miocene (outside the buildup-core area) and were deposited as *shale*.
- Based on core sample in Well-A, coral-dominated facies such as *Coral-algal framestone* and *Coral-algal bindstone* were present within the Kujung Formation since the Early Oligocene (Lower MSCS). This facies is interpreted to have formed 100–200-meter-wide small patch reefs with thicknesses ≤ 30 ft. These patch reefs were subsequently terminated and overlain by *shale* deposits.
- In the Early Miocene, coral-dominated facies were accumulated massively in the buildup-core with a total thickness of as much as 1,100 ft (~335 m). This was not the case in the previously mentioned Oligocene interval. This condition suggests that there were set of depositional conditions, unique to the buildup-core during Early Miocene time, that allowed the corals to have thrived, kept-up with sea-level fluctuations, and been deposited as massive carbonate buildups with very minor, if not almost zero, amounts of *shale*.

Furthermore, should more data become available, detailed identification and description of types of foraminifer present in the sediments can be used to interpret depositional environments (Hallock & Glenn, 1986). Planktonic foraminifer characterized the basin and deep shelf in water depths of more than 100 m. Large and flat *Rotaliines* foraminifer such *Lepidocyclina, Eulepidina, Cycloclypeus, Heterostegina,* and *Operculina*

characterized the open shelf to toe-of-slope environments within a wide range of water depth of 20–100 m. In the shallower environments of less than 20 m of water depth, the size of foraminifer is smaller, and the shape of the tests is more robust such as *Amphistegina* and *Miogypsina.* The faunal diversity increases as the water depth decreases in the shallower part of the platform, such as foreslope, ecologic reef, and shoals in the open platform. *Miliolids*, *peneroplids*, *soritids*, *alveolinids,* and other small *Rotaliines* characterized depositional environments in restricted platform and lagoon settings.

The distribution of the facies belt is interpreted mainly based on facies associations in photic zone subdivision and depositional energy level of the carbonate sediment producer. Corals were inferred to inhabit the euphotic zone, whereas LBF inhabits the oligophotic zone. In the Oligocene, within the MSCS interval, alternating LBF-dominated facies and shale of FA-1 and FA-2 respectively, characterized the deposits. Coral-dominated facies of FA-3 were found as smaller patch reefs with low topographic relief before it subsequently terminated and were overlain by shale. Coarse-grained siliciclastic facies of FA-5 were found in the Lower MSCS as thin beds when there were still localized and exposed basement highs. In the Early Miocene, within the CBS interval, coral-dominated facies of FA-3 were able to form massive carbonate buildups that can reach more than 1,000 ft of thickness over the Aquitanian time. These carbonate buildups were characterized by very minor shale content. Depending on the architecture, grainy facies of FA-4 can be found in the open platform and the shoal complex area. Away from the shallow-water carbonate buildups and shoal complexes, similar alternation of the LBF-dominated facies and shale to that of the MSCS interval were found (Figure 2.14).

DISCUSSION

Regional Comparison of Oligocene–Miocene Carbonate Shelves in the Southeastern Sundaland Region

Widespread carbonates deposition was taking place during the Oligocene–Miocene in Southeast Asia (Wilson, 2002). Miocene carbonates were more widely distributed compared to their Oligocene counterparts due to the regional Neogene transgressive phase (Fulthorpe & Schlanger, 1989; Wilson, 2002; Wilson & Hall, 2010). These carbonates include the Kujung Formation in the offshore East Java area and other equivalent formations from several selected areas within the southeastern Sundaland region (Figure 2.15).

Figure 2.16 shows regional distribution of tectonically inherited paleo-highs and paleo-lows in the southeastern Sundaland region and is based on regional map from Pubellier & Morley (2014), with considering additional details in the offshore East Java area from Mudjiono & Pireno (2002), and the Makassar Strait and SE Borneo area from Courel et al. (2011). For regional comparison purposes, six comparative areas were selected and compared to the study area: the study area (red-filled box), onshore East Java area (box-1), offshore East Java area (box-2, and box-3), East Java Sea area (box-4), Makassar Strait area (box-5), and SE Borneo area (box-6).

In order to decipher controls of the Oligocene–Early Miocene carbonate shelf evolution in this region, the above-mentioned areas were compared in term of their regional setting, age range, architecture, and facies. The discussion will start with a brief summary of the study area and then other comparative areas will be discussed, from south to north, counter-clockwise along the southeastern Sundaland margin.

The Study Area

The study area is situated over the JS-1 Ridge, a northeast-southwest trending paleo-high, northward of the Oligocene–Miocene shelf edge, westward of another stable paleo-high to the east, the North Madura Platform (Figure 2.16, red-filled box). The Oligocene–Miocene carbonates in the study area, namely the Kujung Formation, has an age range of Rupelian–Aquitanian (Early Oligocene–Early Miocene) based on numerical ages from $^{87}Sr/^{86}Sr$ analysis.

Based on results from this study, the depositional setting of the Kujung Formation was changing from a mixed-siliciclastic-carbonate shelf (MSCS) to a carbonate-buildups shelf (CBS), from the older interval of Rupelian–Chattian (Oligocene) age to the younger interval of Aquitanian (Early Miocene) age, respectively. The MSCS is characterized by alternating shale and carbonate beds. The carbonate beds can be distinguished by two main faunal constituents, corals-dominated and LBF-dominated. Although corals have been found as main faunal constituent since the Early Oligocene, their depositional geometry could only considered as patch reefs with thickness not exceeding tens of feet (few tens of meters) and width of 100–200 m. In contrast, during Aquitanian time, within the CBS, carbonate buildups up to 1,100 ft in total thickness were deposited with very minor amount argillaceous shale deposits. The accumulation rate for the MSCS interval ranges from 2.62–4.41 cm/k.y., with an average of 3.49 cm/k.y. In contrast, the accumulation rate for the CBS interval ranges from 8.07–13.29 cm/k.y. with an average of 10.85 cm/k.y. These numbers suggest that the accumulation rate in the CBS is up to two or three times higher if compared to the MSCS.

The above-mentioned accumulation rates are much lower in comparison to the Eocene–Miocene Tonasa Formation foraminiferal estimated carbonates production rates of up to 20–30 cm/k.y. (Wilson et al., 2000, Wilson, 2000) and the modern reefal-carbonates production rates of up to 1,000 cm/k.y. (Jones & Desrochers, 1992). The significant difference in those numbers is interpreted as the result of limitation of methods used in this study. The accumulation rates have not been calibrated to decompaction correction and hiatuses, time missing during a non-depositional period.

However, the ratio between the accumulation rates of MSCS and the CBS is still important. This significant increase in accumulation rate in the Early Miocene compared to the Oligocene may have been caused by the combination of 1) higher production and sedimentation rates of both carbonate and siliciclastic sediments, and 2) higher accommodation due to increase in subsidence rate after influences from of sea-level fluctuations. This suggests a possible combination of events around the Oligocene–Miocene boundary, at 23 Ma, that may have caused the significant increase in the sediment thickness of the Early Miocene interval.

The Oligocene–Early Miocene carbonate shelf in the study area demonstrated a shift from an open shelf dominated by alternating LBF-dominated carbonate and fine-grained siliciclastic shale facies with occasional deposition of patch reefs up to few tens of meters thick and few hundreds of meters wide in the MSCS, to a shelf with numerous carbonate buildups distribution, that show coral-algal dominated facies in the buildup-core and alternating LBF-dominated carbonate and shale facies in the buildup-flank and inter-buildups in the CBS. Carbonate buildups in the CBS show varying geometries, elongated

W-E trending flat-topped carbonate buildups and shoal complexes in the southern area, circular-ovoid pinnacle buildups in the central area, and polygonal flat-topped carbonate buildups and shoal complexes in the northern area.

Assemblages similar to the MSCS were described as the oligophotic foramol facies in the area around the Makassar Strait. This facies represents the depositional condition of the shelf with limited light penetration due to high nutrients, siliciclastic influx, and murky water caused by suspended fine-grained siliciclastic sediments (Wilson & Vescei, 2005).

Onshore East Java Area

The onshore East Java area discussed in this study includes the Cepu block and the Rembang region. The Cepu block (Figure 2.16, SW part of box-1**)** has been extensively discussed in previous work based on subsurface data (Cahyono & Burgess, 2007; Simo et al., 2011, 2012; Sekti et al., 2011; van Simaeys et al., 2011). This area consists of several isolated platforms that are located south of the Oligocene-Miocene continental Borneo shelf edge position (Figure 2.16; Ardhana, 1993; Satyana, 2005). These isolated platforms, west of the BD Ridge, are situated over the East Cepu High, a northeast–southwest trending Paleogene structural high of the southeastern Sundaland region (Figure 1.2). The age range of the Oligocene–Miocene Kujung Formation in this area is Rupelian to Burdigalian (Early Oligocene to Early Miocene) that can reach a total thickness of approximately 3,000 ft (Simo et al., 2011). The thickness of the Kujung Formation in the Cepu block is slightly higher but comparable to the total thickness of the MSCS and the CBS in the study area of around 2,500 ft in total. Carbonate sedimentation that extended through the Burdigalian most likely contributed to the higher thickness of the Kujung Formation in this area.

The morphology of the isolated platforms in this area, namely Cendana, Banyu Urip, Jambaran, and Alas Tua, follows their corresponding normal fault trend on the 3D seismic. Cendana and Jambaran show a pinnacle geometry compared to Alas Tua's flatter geometry (Cahyono & Burgess, 2007). These isolated carbonate platforms have developed in different age ranges similar to those in the study area: Cendana (Chattian), Jambaran (Rupelian–Chattian), and Banyu Urip (Chattian, Aquitanian, Burdigalian) (Simo et al., 2012).

The facies in Banyu Urip range from shallow-water boundstone and rudstone to deeper-marine planktonic foraminifera wackestone and packstone that are mostly carbonates and are lacking siliciclastic content (Sekti et al., 2011). Main faunal constituents of coral, red-algae, LBF, echinoids, and mollusk are similar to those observed in the study area. In Jambaran field, shale and carbonate composition varies because of the well trajectory relative to the carbonate buildup's position. The J-1 well, which penetrated the buildup-core, consists of mostly carbonates and thicker Chattian interval (~1000 ft MD) compared to the J-2 well, which penetrated the buildup-flank, that has interbedded shale-carbonate and thinner Chattian interval (~340 ft MD) (van Simaeys et al., 2011). This variation resembles a similar lithofacies variation of the buildup-core to buildup-flank and inter-buildups in the study area.

The outcrop study in the Rembang region is located in the present-day Rembang zone and the northern part of the Randublatung zone that are a series of up to 500 m tall, east-west oriented hills (Sharaf et al., 2005) (Figure 2.16, NE part of box-1). In the Oligocene–Miocene times, the Rembang region is situated over the northeastern part of the

East Cepu High (Figure 1.2). The Oligocene–Miocene carbonate in the Rembang area is also named the Kujung Formation and has an age range of Chattian to Aquitanian (Late Oligocene to Early Miocene) based on combination of strontium isotope dating and biostratigraphic data (Sharaf et al., 2014).

Based on its architecture and facies, as also observed in the study area, the Kujung Formation in this area is generally subdivided into mound and off-mound. Three distinct units characterized the formation, reefal in the lower Kujung, alternating shale and chalk in the middle Kujung, and alternating shale, chalk, and carbonate turbidites in the upper Kujung. Shallow-water carbonates are widely distributed in the lower Kujung and deeper-water carbonates became more dominant in the middle-upper Kujung. Although, based on subsurface data in other locations, the middle and upper Kujung change laterally into reefal carbonates (Sharaf et al., 2005). The change from a shallow-water into a relatively deeper-water setting in the upper part of the Kujung Formation seems to be the opposite trend of the MSCS to the CBS observed in the study area.

As in the study area, the main faunal constituent of the shallow-water carbonates facies of the Kujung Formation in this area include corals, red algae, large benthic foraminifer, echinoids, and mollusk. In the deeper-water carbonates facies, it consists of skeletal fragments, large clasts, planktonic foraminifera, chert nodules, and shale that may contains glauconite and pyrite grains (Sharaf et al., 2005).

Offshore East Java and East Java Sea Area

The Offshore East Java area includes the southwestern and northeastern part of the North Madura Platform (Figure 2.16, box-2 and box-3). The East Java Sea area includes the area near the Kangean Island (Figure 2.16, box-4).

The southwestern part of the North Madura Platform discussed in this study is mainly located in the Ketapang block (Mudjiono & Pireno, 2002; Maynard & Morgan, 2005). The Oligocene–Miocene carbonates in this area, also known as the Kujung Formation, have an age range of Late Oligocene to Early Miocene (Mudjiono & Pireno, 2002). The Kujung Formation was interpreted as a product of marine sedimentation due to subsidence and gradual transgression from Early Oligocene through Early Miocene, approximately 33.5–21.5 Ma. Based on 3D seismic data, smaller patch reefs, few hundreds of meters wide, characterized the lower part of the Kujung Formation and larger carbonate buildups, a few kilometers wide, characterized the upper part of the Kujung Formation (Maynard & Morgan, 2005). The depositional geometries of the Kujung Formation in this area, especially for the better image of the lower part of the formation, is similar and comparable to the study area.

East-west-trending, high-energy bank-edge foram-algal shoals extended from the southern margin of the North Madura Platform to the southern area of the JS-1 Ridge in Ujung Pangkah field during Early Miocene time. These areas contain encrusting red-algae, fragments of branching red-algae, and *Lepidocyclina – Sphaerogypsina* foraminiferal debris, but lack of framework builders (Kenyon, 1977). This assemblage is probably

similar to that of the Well-S (Figure 2.7), that being dominated by encrusting red-algae that deposited under moderate – high energy setting as *Rhodolith* (Figure 2.8).

In the northeastern part of the North Madura Platform, analysis of 3D seismic data shows depositional geometries of the Oligocene–Miocene carbonate buildups such as circular to elongated, ≤ 2-km-wide buildups within a buildups complex with north–south trending intersecting inter-buildups channels, with vertical relief of 200–300 m (Johansen, 2003; Posamentier et al., 2010). The interpreted vertical relief is considerably higher compared to our interpretation in the study area of around 100 m. It is inferred that these carbonate buildups in the NE North Madura area were deposited in a deeper oceanic basin compared to the study area. However, the carbonate buildups seem to have the aggradation capacity to keep up with increasing accommodation due to a combination of subsidence and sea-level rise.

Deposition of the Oligocene–Miocene carbonates of the Kangean area is situated between the Sibaru Platform and the Southern High. This area comprises northeast–southwest to east–west trending paleo-highs with a northeast-southwest trending paleo-low in between. The Oligocene–Miocene carbonates in this area are known as the Kujung Formation and have an age range of Oligocene to Early Miocene (Siemers et al., 1992; Matthews & Bransden, 1995; Shimazu et al., 2017). Although the architecture and the facies of the Oligocene–Miocene carbonates were not discussed in detail, the strata of the underlying formation, the Eocene Ngimbang Formation, represent a marine transgressive sequence with fluvio-deltaic and shallow marine clastics in the lower part and shallow-marine carbonates in the upper part. This formation is overlain by the Kujung Formation,

which primarily consists of deep-marine shale that grade upward to siltstone to moderately deep to shallow-marine carbonates (Siemers et al., 1992). This gradation represents a shallowing upward trend that might be similar to the trend observed in the study area, where the CBS carbonate buildups developed in the Early Miocene represent shallower water environment overlying the MSCS in the Oligocene. Furthermore, the transition from shallow-water carbonates of the Ngimbang Formation to deeper-water shale and marls of the Kujung Formation in this area also represents a regional trend that was also observed in the transition from Pre-MSCS to MSCS in the study area. The Kangean area is interpreted to be a deeper distal basin of the southeastern Sundaland region, where the open marine transgression started relatively earlier compared to the study area to the west.

Makassar Strait and SE Borneo Area

The Makassar Strait area includes the Paternoster Platform area and is located approximately in the middle between present-day Borneo and Sulawesi Islands (Figure 2.16, box-5). The SE Borneo area includes the Barito Shelf and Basin around the present-day shoreline in the south-southeastern part of Borneo (Figure 2.16, box-6).

The Paternoster Platform area includes the Pangkat Graben as the normal faults bounded paleolow surrounded by broad and stable paleohigh of the Paternoster Platform. The area also includes the South Makassar Basin to the southeast. The Oligocene–Miocene carbonates of this area is known as the Berai Formation. This formation has an age range that is similar to that of this study, which is Rupelian, Chattian, and Aquitanian (Early Oligocene to Early Miocene). Over the paleohigh, the shelf is dominated by shallow-water platformal carbonates in the Rupelian and Chattian through Aquitanian ages, and

subsequently overlain by deep marine shale in the Burdigalian. In contrast, grainy carbonates and debris flow deposits characterized the area around the margin of the Paternoster Platform and the Pangkat Graben and gradually change into deeper-water shale and marls in the South Makassar Basin. Over that period, carbonate buildups few kilometers wide are distributed in the basin, off the platform (Kupecz et al., 2013). Significant exposure events that have resulted in debris flows deposits and platform exposures were recorded around 28 Ma and 20 Ma, respectively (Kupecz et al., 2013).

The transition from the Aquitanian shallow-water carbonates to the Burdigalian deep-water shale is similar to the transition from the Kujung Formation to the overlying Tuban Formation in the study area. During the Rupelian through Aquitanian, shale, as an indicator of the mixed-siliciclastic-carbonate shelf, were not present over the platform. Shale were observed in this period only in the deeper-part of the Pangkat Graben, based on data from the Pangkat-1 well (Kupecz et al., 2013).

The Barito Shelf is located offshore of the present-day SE Borneo coastline, and the Barito Basin is located onshore, west of the Meratus Mountains. The Oligocene–Miocene carbonates in this area are known as the Berai Formation carbonates that laterally changes into the Montalat Formation fluvio-deltaic deposits in the northern part of the Barito Basin. The age range of the Berai Formation is Late Oligocene to Early Miocene. The depositional environments and the age were determined based on foraminiferal assemblages (Witts et al., 2001).

Similar to that of the Kujung Formation, the transition from a clay-rich to carbonate-rich lithology including foraminifer, corals, and red-algae in the Berai Formation

is observed based on bioclasts described from cuttings data (Pelton, 1974). Based on regional 2D seismic lines, the Berai Formation is dominated by lagoonal to grainy platform interior deposits with patch reef development in the southern part of the Barito Basin and the Barito Shelf. Based on the seismic mapping, patch reef dimension is a few kilometers wide (Werdaya et al., 2013). This is comparable to the carbonate buildups within the CBS in the study area.

Synthesis

The Oligocene–Early Miocene carbonate shelves in the region developed in several settings of tectonically inherited antecedent topographic highs that include platform or shelf attached to the Borneo landmass (Barito Basin & Barito Shelf), detached broad and stable platform (the Paternoster Platform and the North Madura Platform), narrow faulted block/ ridge (the JS-1 Ridge), shelf around the platform (Kangean area), and isolated platform and shelf over a paleo-high beyond the shelf edge (Cepu and Rembang areas). Carbonate deposition started during a renewed transgression period in the Early Oligocene, developed through the Early Miocene, and ended in the Aquitanian–Burdigalian age. The underlying and overlying formations consist of mostly marine deposits with coarse-grained siliciclastic distributed locally, close to the sources. The architecture and facies of the carbonate shelves were characterized by reefal carbonate buildups, shallow-water platformal carbonates, and shale as fine-grained siliciclastic deposits. Figure 2.15 shows a composite regional stratigraphic column for the areas discussed in this study.

The Oligocene–Miocene carbonate shelves in the southeastern Sundaland show spatial and temporal trends and variations in regional tectonic setting as tectonically

inherited antecedent topography, age range of the carbonate formations, the underlying and overlying formations, and architecture and facies within the carbonate shelves. This study demonstrates that these trends and variations can be observed across almost all geographic scale; intra- and inter-platform, basin, and regional scale. Careful consideration is required in order to decipher the dominant controls on the carbonate shelf evolution.

Controls on Carbonate Shelf Evolution

Controls on carbonate shelf evolution include factors that may influence accommodation for and accumulation of the carbonate sediment producers. The accumulation is defined as combination of carbonate sediment production rate and distribution pattern (Lukasik & Simo, 2008). These controls are generally classified into six categories; eustasy, tectonics, climate, oceanography, trophic resources, and temperature. These controls influence the initiation, growth, and demise of carbonate platforms and reefs. The influences of these controls can also be distinguished based on their geographical scale of dominance; platform-, basin-, regional-, and global-scale (Lukasik & Simo, 2008).

This study presents an investigation to better understand the complex relationship between the controls on carbonate shelf evolution to their influences on spatial and temporal variation of the resulting architecture and facies. Controls on the Oligocene–Miocene carbonate shelf evolution are discussed in this study based on architecture and facies of the Kujung Formation and its comparison to other Oligocene–Miocene carbonate formations within the southeastern Sundaland region. In this study, the controls are grouped into five main categories: 1) antecedent topography, 2) siliciclastic sediment

routing, 3) global sea-level fluctuation patterns, 4) tectonic activity, 5) regional climatic change, and 6) volcanism.

Antecedent Topography

The southeastern Sundaland region is characterized by tectonically inherited northeast-southwest to east-west trending topographic highs and lows (Mudjiono & Pireno, 2002, Pubellier & Morley, 2014). These antecedent topographic features include platforms, ridges, shelves, troughs, and basins, from structurally highest to lowest respectively (Figure 2.16). These antecedent topographic features were formed by the underlying formations of Eocene age deposited throughout the region as the representation of the pre-Cenozoic basement structural configuration. The continental Borneo shelf edge during Oligocene–Miocene time is interpreted to be located along the lineation of the southern margin of the JS-1 Ridge and the North Madura Platform, following an east-west orientation (Ardhana, 1993; Satyana, 2005).

In a larger geographic scale, this study shows that the tectonically inherited antecedent topography in the southeastern Sundaland region strongly controls the distribution of shallow-water carbonates deposition as well as their deeper-water shale and marls counterparts. The example of this is shown by the distribution of shallow-water platformal carbonates in the Paternoster Platform compared to deeper-water shale and marls within the Pangkat Graben and South Makassar Basin area of the surrounding Paternoster Platform (Figure 2.16).

On a smaller geographic scale, the distribution of the isolated carbonate platforms in Cepu area follows their corresponding normal fault trend (Cahyono & Burgess, 2007).

In the study area, the topographic relief within the JS-1 Ridge, possibly enhanced by differential subsidence syn-depositionally, controls the resulting carbonate shelf architecture as shown by the distribution of the carbonate buildups and shoal complexes (Figure 2.11 and Figure 2.12).

The southern margin of the JS-1 Ridge and the North Madura Platform were dominated by carbonates contemporaneous with the deposition of fine-grained siliciclastic of the MSCS over most area of the JS-1 Ridge in the Oligocene. This situation suggests that the topographic relief of the southern margin of the JS-1 Ridge and the North Madura platform resulting in a shallow-water and high-energy setting that has hindered the shale deposition by constant winnowing of the fine-grained siliciclastic sediments (Figure 2.13, Well-R).

In the study area, thin siltstone-sandstone beds were observed in the lower MSCS of the Early Oligocene interval (Figure 2.7). The coarse-grained siliciclastic sediments were interpreted to be sourced locally from a nearby basement high in the northern area of the JS-1 Ridge (Figure 2.17). This demonstrates siliciclastic facies distribution that was locally controlled by antecedent topographic feature. The localized basement high was fully transgressed by marine conditions in Middle Oligocene time and was overlain by alternating carbonate-shale beds of the Upper MSCS in the Late Oligocene.

There were significant differences in the vertical relief of the carbonate buildups measured from their corresponding open shelf area (inter-buildups) between the study area and that of the northeastern North Madura Platform area. The vertical relief of the carbonate buildups is approximately 50–100 m and 200–300 m (Posamentier et al., 2010),

respectively. These differences may be due to variation in the paleo-topographic relief of the shelf or variation of the subsidence over the area.

Siliciclastic Sediment Routing

Discussion of siliciclastic sediment routing includes the siliciclastic sediment sources, the mechanism of siliciclastic sediment transport, and the route of siliciclastic sediment transport over the southeastern Sundaland region.

The siliciclastic influx is interpreted to be sourcing from major deltas in the southeastern Borneo basins; Barito, Kutai, and Asem-Asem (Figure 2.16). These deltaic systems have Cenozoic sediment thicknesses of 8 km (Hall & Nichols, 2002). The provenance of the siliciclastic sediments in this area during the Cenozoic is believed to have mostly originated from the Central Kalimantan Range and the Schwarner Complex of the mainland Borneo (Hall & Nichols, 2002; Witts et al., 2011). In addition to the Borneo deltas, during the Late Eocene to Late Miocene period, the Karimunjawa Arch in the Java Sea, northwest of the study area, have been uplifted and might have been supplying sediments to the East and West Java Basins (Smyth et al., 2008).

From the sources, influxes of coarse-grained and fine-grained siliciclastic sediments were transported through different routes. Coarse-grained siliciclastic sediments were transported by bed load mechanism following the route of antecedent topographic lows. Coarse-grained siliciclastic sediments were not deposited over antecedent topographic highs. Its transport pathway was blocked and re-routed by the antecedent topographic highs as observed in the Paternoster Platform. No sandstones were found in the Paternoster and Pangkat Graben area (Kupecz et al., 2013) although it is very close to

a major deltaic system in the Kutai Basin with the largest sediment volume in the SE Borneo region (Hall & Nichols, 2002).

In contrast, fine-grained siliciclastic sediments, that constitutes most of the siliciclastic portion in the Oligocene-Miocene carbonate shelves of the southeastern Sundaland region as shale deposits, were transported by suspended load mechanism, following the southward dispersal pattern influenced by the main oceanic circulation pattern in the region (Figure 2.16, Figure 2.19, Kuhnt et al., 2004). Fine-grained sediments can be transported by shelf currents as far as 10,000 km (Gao & Collins, 2014). An example from Holocene deposits over the eastern China Sea region shows that mud deposits can be found more than 500 km away from the nearby river delta systems (Gao & Collins, 2014). Based on the distribution of shale found in the formations during Oligocene–Miocene time, the fine-grained siliciclastic sediments in southeastern Sundaland region were dispersed as far as more than 500 km from its sources to the Cepu, Rembang, and Kangean areas (Figure 2.16).

The oceanic circulation pattern shows south- to southwestward oceanic circulation from the Pacific Ocean to the Indian Ocean through the north through Makassar Strait area (Kuhnt et al., 2004; Figure 2.16, Figure 2.19). Based on the carbonate buildups geometry, the oceanic circulation pattern is inferred to have shifted from north–south to nearly east–west near the Oligocene–Miocene shelf edge (Figure 2.16, Figure 2.19). This interpretation is supported by the presence of north-south trending inter-buildups channels and buildups complex in the northeastern part of the North Madura Platform (Posamentier et al., 2010)

and east-west trending elongated carbonate buildups in the southern area of the JS-1 Ridge in the Early Miocene time (Carter et al., 2005).

Global Sea-level Fluctuation Patterns

Global sea-level (eustasy) influences the carbonate shelves globally, including the Oligocene–Miocene carbonate shelves of southeastern Sundaland. This global sea-level control works on large geographic scale to govern global and regional trends in temporal sense. It may not be used to explain spatial variation such as the presence of carbonate-dominated interval in Well-R (Figure 2.13) related to mixed-siliciclastic-carbonate interval in other wells in the study area during Oligocene time.

The global sea-level curve from Haq et al. (1987) is widely used and has a single event of sea-level fall in the Middle Oligocene with a magnitude of around 150 m. This event was adopted as the Mid-Oligocene unconformity that was represented as a major hiatus in stratigraphic columns around the Mid-Oligocene time according to previous work in the region with no convincing evidence (Mudjiono & Pireno, 2002; Johansen, 2003; Carter et al., 2005). According to the results of this study, such a high magnitude of sea-level fall in the Mid-Oligocene is unlikely and is not represented by any stratigraphic records. Any evidences of unconformity, such as large-scale exposure surface, an abrupt shift in shallower-water/siliciclastic facies and depositional systems, para- or disconformity related to non-depositional period, and/or supporting seismic signatures, were not found. Furthermore, around the Middle Oligocene, the study area was characterized by widespread shale deposition in the Middle MSCS. An event of sea-level

fall with 150 m in magnitude would have completely exposed most of the the JS-1 Ridge shelf.

In contrast, the global sea-level curve from Miller et al. (2005) is interpreted to be a better fit for discussion in this study. The selection was mainly due to consideration of the magnitude of sea-level fluctuations during the Oligocene–Miocene times. The magnitude is within 50 m in a single event of sea-level fall or rise. This magnitude is reasonable to be applied to the study area where the deepest part of the JS-1 Ridge shelf is interpreted not exceeding 100 m, hence no major hiatuses will be recorded.

During Oligocene–Miocene time, variation of sea-level fluctuation trends can be observed in the sea-level curve (Miller et al., 2005). There were periods of rapid rise – rapid fall with higher magnitude of more than 50 m in the Oligocene and rapid rise – slow fall with lower magnitude of around 30 m that started in the Early Miocene. Longer-term trends of Oligocene regression and Miocene transgression were also observed (Figure 2.18). The slower rate of sea-level fall in the Early Miocene represents the warmer period of transitional condition to Mid-Miocene climatic optimum, shifting from the Oligocene icehouse condition (Zachos et al., 2001). The variation in sea-level fluctuation patterns is interpreted to have contributed to the shift in the carbonate shelf in the study area, from MSCS to CBS (Figure 2.18). It is interpreted that if the event of sea-level fall happens slowly over a longer period with a lower magnitude, there would be a relatively prolonged period of available accommodation for the carbonate buildups with coral-dominated facies to be developed, compared to that of the event of rapid sea-level fall with higher magnitude.

The depositional model presented in this study represents the localized shallow interiors within siliciclastic-influenced, more than 30 meters deep, shelf (Wilson & Vescei, 2005). Distribution of carbonates and shale with regard to the sea-level fluctuation can be inferred. It is interpreted that carbonates were deposited during sea-level rise and the shale were deposited during sea-level fall.

During periods of sea-level fall, an increase of siliciclastic sediments influx and increase dispersal radius due deltas progradation in the Borneo area are interpreted to have caused an increase of water turbidity and decrease in water clarity on the shelf. Suspended fine-grained siliciclastic sediments were proven to have existed during the whole stratigraphic interval of the Early Oligocene to Early Miocene. They are mainly distributed on the shelf where the depositional energy is low, allowing the suspended sediments to be deposited as shale in either times of sea-level fall or sea-level rise.

During periods of sea-level rise, accommodation was available for the deposition of carbonates. This includes corals as framework builders for the extensive carbonate buildups development in the Aquitanian. Deltas were pushed landward, contemporaneously decreasing the fine-grained siliciclastic sediment influx to the system. In the Aquitanian, the absence of shale beds over the buildup-core suggests that the magnitude and the rate of sea-level rise did not exceed the limit in depositional conditions of which, the corals could still keep up.

Tectonic Activity

The southeastern Sundaland region was greatly influenced by the tectonic convergence of Eurasian (Sundaland) and Australian plates throughout the Cenozoic. This

tectonic activity mainly governs the regional tectono-stratigraphic evolution from syn-rift to post-rift episodes that were observed during Oligocene–Miocene within this region. Subsequently, the Miocene compressional regime in the region has initiated in the Early Miocene and intensified toward the Miocene-Pliocene boundary around 5 Ma (Figure 2.19; Hall, 1997, 1998, 2002, 2012; Johansen, 2003; Pubellier & Morley, 2014).

Tectonic activity has widely been known to cause vertical movements of the earth's crust, manifested as uplift and subsidence. The initiation of a compressional regime in the region at around the Early Miocene time may have had indirect regional influences on the development of the carbonate shelf, especially on accommodation. This tectonic activity influenced the region by increasing the regional subsidence rate and in turn may have created accommodation for the carbonate shelf to develop thicker carbonate buildup deposit over relatively short period of time during Aquitanian age.

When discussing antecedent topographic control in the Oligocene–Miocene carbonate shelf evolution, it should be considered as a pre-depositional control from tectonically inherited pre-existing topographic features. However, I observed that syn-depositional control such as tectonic subsidence that varies locally within a platform could also contributed to the resulting architecture. The pinnacle buildups in the central area of the JS-1 Ridge have thicker carbonate buildups, up to approximately 200 ft thicker than the buildups that have flat-topped geometry in the southern and northern area (Figure 2.12). Further study with a more detailed analysis is needed to carefully investigate the effect of syn-depositional subsidence.

Regional Climatic Change

Climate is a regional control that affects the environmental condition of the sub-aerial as well as sub-aqueous environments. Climate influences sediment and nutrient supply to the basin (Lukasik & Simo, 2008). Regional climatic change in the region were inferred based on palynological records in the terrestrial area of the Sundaland. The climate was changing from a seasonal condition in the Oligocene to an everwet-superwet condition in the Miocene (Figure 2.19; Morley, 2012). Much wetter climate in the Miocene resulting in higher rainfall. Thus, one can expect a higher rate of weathering, higher freshwater flux, and ultimately higher siliciclastic sediments influx to the basin from the Borneo fluvio-deltaic systems. This situation would have caused elevated trophic resources and decreased light penetration in a murkier water condition. This condition is generally detrimental to the corals that would require a clear-water with good light penetration in their living condition. The fact that corals were thriving in the Early Miocene compared to the Oligocene, as shown by up to 1,100 ft thick massive carbonate buildups, is contradictory to the regional climatic change in the region. This is in agreement with a previous study that shows the extensive distribution of coral-dominated facies during the Early Miocene (Wilson, 2008). However, based on core samples from Well-A (Figure 2.7), this study shows that the coral-dominated patch reefs have existed and started to develop since the Oligocene with limited capacity (≤ 30 ft thick). This suggests conditions of limited accommodation, interpreted to be mainly caused by the rapid rise–rapid fall of sea-level fluctuation pattern.

Volcanism

Throughout the Cenozoic, there are two recognizable magmatic belts related to volcanisms in the region. They are both east-west trending and parallel to each other. The southern magmatic belt, also known as the "Old Andesite", is related to Paleogene subduction, whereas the northern magmatic belt is related to Neogene subduction (Soeria-Atmadja et al., 1994). Arc loading by volcanism has been influencing the basins around the Java volcanic arc throughout the Cenozoic (Waltham et al., 2008; Pubellier & Morley, 2014). The effect includes increased subsidence in the area near the arc position. However, arc loading is not relevant to basins that relatively far, more than 100 km, away from the arc (Waltham et al., 2008). The Cepu and Rembang regions that are discussed in this study are within the 100 km radius. The southern margin of the JS-1 Ridge is approximately 100 km away from the Java volcanic arc and the northern limit of the study area is within 200 km radius. Thus, arc loading should have a considerable effect of the increase in subsidence, not only in Cepu and Rembang, but also in the JS-1 Ridge area.

Synthesis

This study suggests that the shift from MSCS to CBS around the Oligocene-Miocene boundary is in agreement with the regional trend observed of change in main carbonate constituents from LBF to Coral in SE Asia (Wilson, 2008). However, this study shows that coral-dominated facies had existed since the earliest Oligocene with limited capacity to form only up to 30-ft-thick patch reefs in the MSCS (Figure 2.7, Well-A). This study also shows spatial variations in the distribution of shale-rich mixed-siliciclastic-carbonate shelf in the Oligocene time. In the southern margin of the JS-1 Ridge and the

North Madura Platform, carbonate-dominated sediments with very minor shale content were deposited in the Oligocene (Figure 2.12, Well-R). This area was interpreted as an east-west trending belt of high-energy bank edge foram-algal shoals and coral reefs along the shelf margin (Kenyon, 1977). In Cepu area and the Paternoster Platform, clean carbonates have also been deposited with minor shale content throughout Early Oligocene to Early Miocene. The broad and stable, shallow water platform of the Paternoster Platform is interpreted to act as a barrier for the siliciclastic sediment influx from the north, suggesting a combination of antecedent topography and siliciclastic sediment routing controls. High-energy setting over the shallow-water platform is interpreted to have constantly winnowed the fine-grained siliciclastic sediments suspended in the water column. Isolated platforms in Cepu area were situated far offshore southward of the Oligocene-Miocene shelf edge, approximately 500 km away from the Borneo deltaic systems (Figure 2.16). The spatial distribution of dispersed fine-grained siliciclastic sediments might have been diminishing.

A change in sea-level fluctuation patterns, from rapid rise–rapid fall in the Oligocene to rapid rise–slow fall in the Miocene (Miller et al., 2005), is interpreted to have contributed to the temporal change represented in the study area as the shift from MSCS to CBS. A slower rate of sea-level fall in the Early Miocene is interpreted to have preserved the accommodation for thicker carbonate buildups to be deposited. Furthermore, long-term trends show transgression phase in the Early Miocene compared to regression phase in the Oligocene (Figure 2.18). The accumulation rate of the CBS, which is up to three times higher than that of the MSCS, suggests that there was an increase in accommodation in the

Early Miocene. The increase in accommodation is interpreted to have also caused by subsidence due to tectonic and volcanism. A regional climatic change, from a seasonal climate in the Oligocene to an everwet–superwet climate in the Miocene, was inferred based on palynological data in the region (Morley, 2012). A wetter climate in the Miocene would have caused higher rates of rainfall and weathering in the Borneo mainland that in turn would have caused increased freshwater flux to the system, decreased salinity, increased siliciclastic sediments supply, and increased trophic resources. These conditions would have promoted a murkier water and limited light penetration that would have been detrimental to corals. However, this study shows that corals were thriving in the Early Miocene.

Throughout the Cenozoic, the shelf of southeastern Sundaland has evolved from the early sediment fill of tectonically inherited antecedent topographic lows to a point where the entire shelf was transgressed by marine conditions. The evolution of the Oligocene–Miocene carbonate shelves represented the influence of the regional Neogene transgression. This study suggests that antecedent topography and siliciclastic sediment routing are dominant in controlling the spatial variations in architecture and facies of the Oligocene–Miocene carbonate shelves in the region. However, temporal changes in the carbonate shelves represented by shift from MSCS to CBS may have partly caused by the combination of regional and global controls that possess a temporal element such as change in sea-level fluctuation patterns and increased subsidence due to tectonic activity and volcanic arc loading in the Early Miocene. The influence of regional climatic change across the Oligocene-Miocene boundary in the region seems to have been overrode by the

previously-mentioned controls. Table 2.5 summarizes the interpreted controls on carbonate shelf evolution in the southeastern Sundaland region during Oligocene–Early Miocene time in term of their geographic scale of influence and their resulting spatial and temporal variations on the carbonate shelf architecture and facies.

CONCLUSIONS

By utilizing subsurface data such as 3D seismic, well-log, cuttings lithology, core samples, thin sections, and numerical ages from $^{87}Sr/^{86}Sr$ analysis, this study described and interpreted the architecture and facies of the Oligocene–Early Miocene Kujung Formation, offshore East Java, Indonesia. Depositional setting of the Kujung Formation in the study area was changing from a mixed-siliciclastic-carbonate shelf (MSCS) in the Rupelian–Chattian to a carbonate-buildups shelf (CBS) in the Aquitanian that covers a total duration of 13.5 million years. Accumulation rates within the CBS interval are as much as three times higher to those of the MSCS suggesting higher accommodation and sedimentation/production rate. Depositional models for the MSCS and CBS were built based on the architecture and facies of the Kujung Formation with inferred parameters from the literature.

By comparing the Kujung Formation to other Oligocene-Miocene carbonate formations in the southeastern Sundaland region, spatial variations and temporal trends in tectonically inherited antecedent topography, age range of the carbonate formations, underlying as well as overlying formations, architecture, and facies were observed across almost all geographic scales; platform-, basin-, and regional-scale.

This study advances the understanding of the interplay between controls on the Oligocene–Early Miocene carbonate shelf evolution within a complex tectonic setting. This study suggests that tectonically inherited antecedent topography and siliciclastic sediment routing are the most dominant controls for the spatial variations in architecture and facies of the carbonate shelves. Regional and global controls such as sea-level fluctuation patterns, and subsidence due to tectonic activity and volcanism might have partly contributed to the temporal change observed in the region, such as the extensive development of carbonate buildups in the Early Miocene. The influence of regional climatic change observed in the mainland Borneo, from seasonal to everwet–superwet condition, throughout Oligocene–Miocene appeared to be overrode by previously-mentioned controls.

Table 2.1. The availability of well-based data

Well name	Gamma-ray (GR) log	Cuttings lithology	Core samples in feet (Interval)	Number of $^{87}Sr/^{86}Sr$ measurements (Interval)
Well-A	Available	-	240 (MSCS)	-
Well-B	Available	-	-	-
Well-C	Available	-	-	1 (CBS), 6 (MSCS)
Well-D	Available	Available	18 (MSCS)	1 (CBS), 2 (MSCS)
Well-E	Available	Available	80 (CBS)	4 (CBS), 16 (MSCS)
Well-F	Available	-	-	7 (MSCS)
Well-G	Available	-	-	4 (MSCS)
Well-H	Available	-	24 (MSCS)	-
Well-I	Available	-	58 (CBS)	-
Well-J	Available	-	-	1 (MSCS)
Well-K	Available	-	-	3 (MSCS)
Well-L	Available	-	18.5 (CBS)	3 (MSCS)
Well-M	Available	-	60 (CBS)	1 (CBS)
Well-N	Available	-	119 (CBS)	-
Well-O	Available	-	-	-
Well-P	-	-	44 (CBS)	-
Well-Q	-	-	96 (CBS)	3 (CBS)
Well-R	Available	Available	-	-
Well-S	Available	-	31.5 (CBS)	-
Total	***17 wells***	***3 wells***	***789 (11 wells)***	***52 (10 wells)***

Table 2.2. Characteristics of facies and their associations observed in the core samples

F#	Facies	Texture/ Sed. Structure	Grain size (sorting)	Association	Depositional Energy
F1	*Shale*	Fissile	Clay, <4 µm	FA-1	Low
F2	*Siltstone – sandstone*	Bedded with ripple	Silt – very fine sand, 4-125 µm (well sorted)	FA-5	Moderate
F3	*Silty-mudstone*	Bedded	4-63 µm (moderately sorted)	FA-1	Low
F4	*LBF wackestone – mud-dominated packstone*	Bedded	Up to 5 cm (poorly sorted)	FA-2	Low–Moderate
F5	*LBF-echinoid-coral Grain-dominated packstone – grainstone*	Bedded	Up to 1 – 2 cm (well sorted)	FA-4	High
F6	*LBF floatstone – rudstone*	Bedded	Up to 5 cm (poorly sorted)	FA-2	Low–Moderate
F7	*Coral floatstone – rudstone*	Bedded–massive	Up to 2 – 3 cm of coral fragments (poorly sorted)	FA-2, FA-3	Moderate–High
F8	*Coral-algal framestone*	Massive with stylolites	Cm-scale corals (framework builder)	FA-3	High
F9	*Coral-algal bindstone*	Massive with stylolites	Cm-scale corals (red algae-platy corals)	FA-3	High
F10	*Rhodolith floatstone – rudstone*	Bedded	Up to 5 cm (moderately sorted)	FA-6	Moderate–High

Table 2.3. Numerical ages from $^{87}Sr/^{86}Sr$ analysis from 10 wells in the study area

Sample	$^{87}Sr/^{86}Sr$	Age in Ma (McArthur et al., 2001)	Uncertainty	Epoch	Age
L1 xx39'	0.708035	28.4	+/- 0.2 Ma	Oligocene	Rupelian
L2 xy06'	0.707976	29.9	+/- 0.2 Ma	Oligocene	Rupelian
L3 xy21'	0.707903	31.7	+/- 0.2 Ma	Oligocene	Rupelian
G1 xx38'	0.708045	28.1	+/- 0.2 Ma	Oligocene	Rupelian
G2 xy40'	0.708010	29	+/- 0.2 Ma	Oligocene	Rupelian
G3 xy63'	0.707967	30.1	+/- 0.2 Ma	Oligocene	Rupelian
G4 yx02'	0.707924	31.2	+/- 0.2 Ma	Oligocene	Rupelian
M1 xy43'	0.708340	21.9	+/- 0.2 Ma	Miocene	Aquitanian
J1 xy47'	0.707913	31.5	+/- 0.2 Ma	Oligocene	Rupelian
C1 xy44'	0.708328	22.1	+/- 0.3 Ma	Miocene	Aquitanian
C2 yx62'	0.707957	30.4	+/- 0.2 Ma	Oligocene	Rupelian
C3 yx45'	0.707889	32.1	+/- 0.2 Ma	Oligocene	Rupelian
C4 yx66'	*0.707787*	*34.1*	*N/A*	*Eocene*	*Priabonian*
C5 yy46'	0.708038	28.3	+/- 0.2 Ma	Oligocene	Rupelian
C6 yy42'	0.707913	31.5	+/- 0.2 Ma	Oligocene	Rupelian
C7 yy42' *	0.707960	30.3	+/- 0.2 Ma	Oligocene	Rupelian
D1 xx94'	0.708415	20.5	+/- 0.2 Ma	Miocene	Aquitanian
D2 yy92'	0.707999	29.3	+/- 0.2 Ma	Oligocene	Rupelian
D2 yy99'	0.707954	30.4	+/- 0.2 Ma	Oligocene	Rupelian
E1 xy46'	0.708373	21.2	+/- 0.2 Ma	Miocene	Aquitanian
E2 xy13'	0.708343	21.8	+/- 0.2 Ma	Miocene	Aquitanian
E3 yy12'	0.708122	26.1	+/- 0.2 Ma	Oligocene	Chattian
E4 zx06'	0.708026	28.6	+/- 0.2 Ma	Oligocene	Rupelian
E5 zx31'	0.707960	30.3	+/- 0.2 Ma	Oligocene	Rupelian
E6 zx50'	0.707911	31.6	+/- 0.2 Ma	Oligocene	Rupelian
E7 zx71'	0.707877	32.3	+/- 0.2 Ma	Oligocene	Rupelian
E8 zx92'	0.707954	30.4	+/- 0.2 Ma	Oligocene	Rupelian
E9 zy08'	0.707814	33.5	+/- 0.2 Ma	Oligocene	Rupelian
E10 zy56'	*0.707780*	*34.4*	*N/A*	*Eocene*	*Priabonian*
E11 xy62.13'	0.708386	20.9	+/- 0.2 Ma	Miocene	Aquitanian
E12 xy92.13'	0.708361	21.4	+/- 0.2 Ma	Miocene	Aquitanian
E13 yy34'	0.708184	24.9	+/- 0.2 Ma	Oligocene	Chattian
E14 zx15.35'	0.707943	30.7	+/- 0.2 Ma	Oligocene	Rupelian
E15 zx24.08'	0.707964	30.2	+/- 0.2 Ma	Oligocene	Rupelian
E16 zx47.92' *	0.707946	30.6	+/- 0.2 Ma	Oligocene	Rupelian

Table 2.3.—continued

Sample	$^{87}Sr/^{86}Sr$	Age in Ma (McArthur et al., 2001)	Uncertainty	Epoch	Age
E17 zx47.92' *	0.707971	30	+/- 0.2 Ma	Oligocene	Rupelian
E18 zx47.92' *	0.707923	31.3	+/- 0.2 Ma	Oligocene	Rupelian
E19 zy40' *	0.707822	33.3	+/- 0.2 Ma	Oligocene	Rupelian
E20 zy40'	0.707853	32.7	+/- 0.2 Ma	Oligocene	Rupelian
F1 zx72'	0.708073	27.2	+/- 0.3 Ma	Oligocene	Chattian
F2 zx97'	0.708023	28.6	+/- 0.2 Ma	Oligocene	Rupelian
F3 zx46'	0.708012	28.9	+/- 0.2 Ma	Oligocene	Rupelian
F4 zx10'	0.708020	28.7	+/- 0.2 Ma	Oligocene	Rupelian
F5 zy04'	0.707984	29.6	+/- 0.2 Ma	Oligocene	Rupelian
F6 zy70'	0.707955	30.4	+/- 0.2 Ma	Oligocene	Rupelian
F7 zy53'	0.707921	31.5	+/- 0.2 Ma	Oligocene	Rupelian
K1 zy25'	0.707961	30.2	+/- 0.2 Ma	Oligocene	Rupelian
K2 zy50.5'	0.707967	30.1	+/- 0.2 Ma	Oligocene	Rupelian
K3 zy74.5'	0.707971	29.9	+/- 0.2 Ma	Oligocene	Rupelian
Q1 xy46'	0.708343	21.5	+/- 0.2 Ma	Miocene	Aquitanian
Q2 yx00'	0.708333	21.6	+/- 0.2 Ma	Miocene	Aquitanian
Q3 yx64'	0.708330	21.6	+/- 0.2 Ma	Miocene	Aquitanian

Notes:

- Samples are annotated by well name, sample numbers, obfuscated depth in feet (x<y<z). Samples from each well are in order of depth, from shallowest to deepest. Well-E consists of two sets of measurements, E1-E9 (2006) and E10-E20 (2007).
- Upper CBS: 9 samples; 20.5 – 21.9 Ma
- Lower CBS: 1 sample; 22.1 Ma
- Upper MSCS: 2 samples; 24.9 – 26.1 Ma
- Middle MSCS: 1 sample; 27.2 Ma
- Lower MSCS: 37 samples; 28.1 – 33.5 Ma
- Two samples, C4 & E10, yield ages of 34.1 & 34.4 Ma, respectively.
- Rows highlighted blue: the closest samples to infer the numerical age of the top CBS
- Row highlighted orange: the closest sample to infer the numerical age of the top MSCS
- Row highlighted purple: the closest sample to infer the numerical age of the top Pre-MSCS

Table 2.4. Thickness distribution and accumulation rates of the mixed-siliciclastic-carbonate shelf (MSCS interval) and the carbonate-buildups shelf (CBS interval), based on well correlation

Well Name	Trajectory	Position (MSCS/ CBS)	MSCS Thickness (ft)	MSCS Acc. Rate (cm/k.y.)	MSCS Siliciclastic (%, est.)	CBS Thickness (ft)	CBS Siliciclastic (%, est.)	CBS Acc. Rate (cm/k.y.)
Well-A	Vertical	H/BC	986	2.76	>50%	922	<5%	10.81
Well-B	Vertical	H/BC	989	2.77	>50%	986	<5%	11.56
Well-C	Vertical	H/BC	1,095	3.06	>50%	1,134	<5%	13.29
Well-D	Vertical	H/BC	938	2.62	>50%	958	<5%	11.23
Well-E	Deviated	H/BC	1,033	2.89	>50%	940	<5%	11.02
Well-F	Vertical	H/BC	1,194	3.34	>50%	870	<5%	10.20
Well-G	Vertical	G/BC	1,341	3.75	~40%	876	<5%	10.27
Well-H	Vertical	G/BC	1,467	4.10	~30%	863	<5%	10.12
Well-I	Vertical	G/BC	1,545	4.32	~30%	1,014	<5%	11.89
Well-J	Vertical	H/BC	1,189	3.32	>50%	1,106	<5%	12.97
Well-K	Deviated	G/IB	1,225	3.43	>50%	748	>50%	8.77
Well-L	Vertical	G/BC	1,317	3.68	~40%	993	<5%	11.64
Well-O	Vertical	G/IB	1,576	4.41	>50%	688	~30%	8.07
Well-R	Vertical	SNMP	1,577	4.41	~20%	862	<5%	10.11
Average			*1,248*	*3.49*		*926*		*10.85*

Notes:

- Position: H = Horst, G = Graben, BC = Buildup-core, IB = Inter-buildups, SNMP = Southern North Madura Platform
- MSCS depositional duration is 10.9 m.y. (Rupelian–Chattian).; CBS depositional duration is 2.6 m.y. (Aquitanian)

Table 2.5. Controls on carbonate shelf evolution within the southeastern Sundaland region during the Oligocene to Early Miocene

Controls	Geographic Scale			Resulting Variations		*Notes*
	Local	**Regional**	**Global**	**Spatial**	**Temporal**	
Antecedent topography	o	o		o		*Tectonically inherited paleo-highs and -lows*
Siliciclastic sediment routing	o	o		o		*Influenced by sediment source, oceanographic circulation, and antecedent topography distribution*
Sea-level fluctuation patterns			o		x	*Change in sea-level fluctuation patterns as well as long-term regression-transgression trends*
Tectonic activity		o		x	x	*Major shift in tectonic regime towards Miocene compression*
Volcanism		o		x	x	*Subsidence due to arc loading in the Java island volcanoes*
Regional climatic change		o		-	-	*Major regional climatic change across Oligocene-Miocene boundary*
					o	*Dominant controls*
					x	*Partial controls*
					-	*Possibly overrode by other controls*

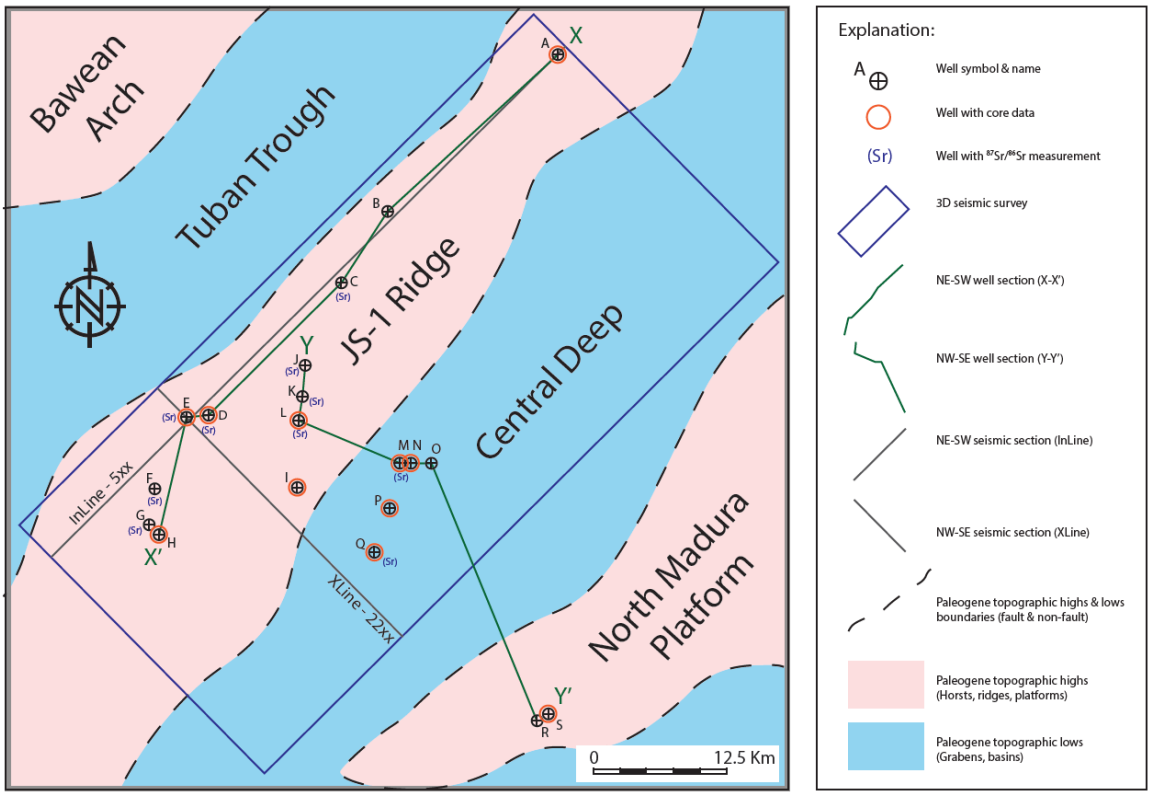

Figure 2.1. Base map of subsurface data used in this study that include 3D seismic, well logs, core samples, and strontium isotopes analysis.

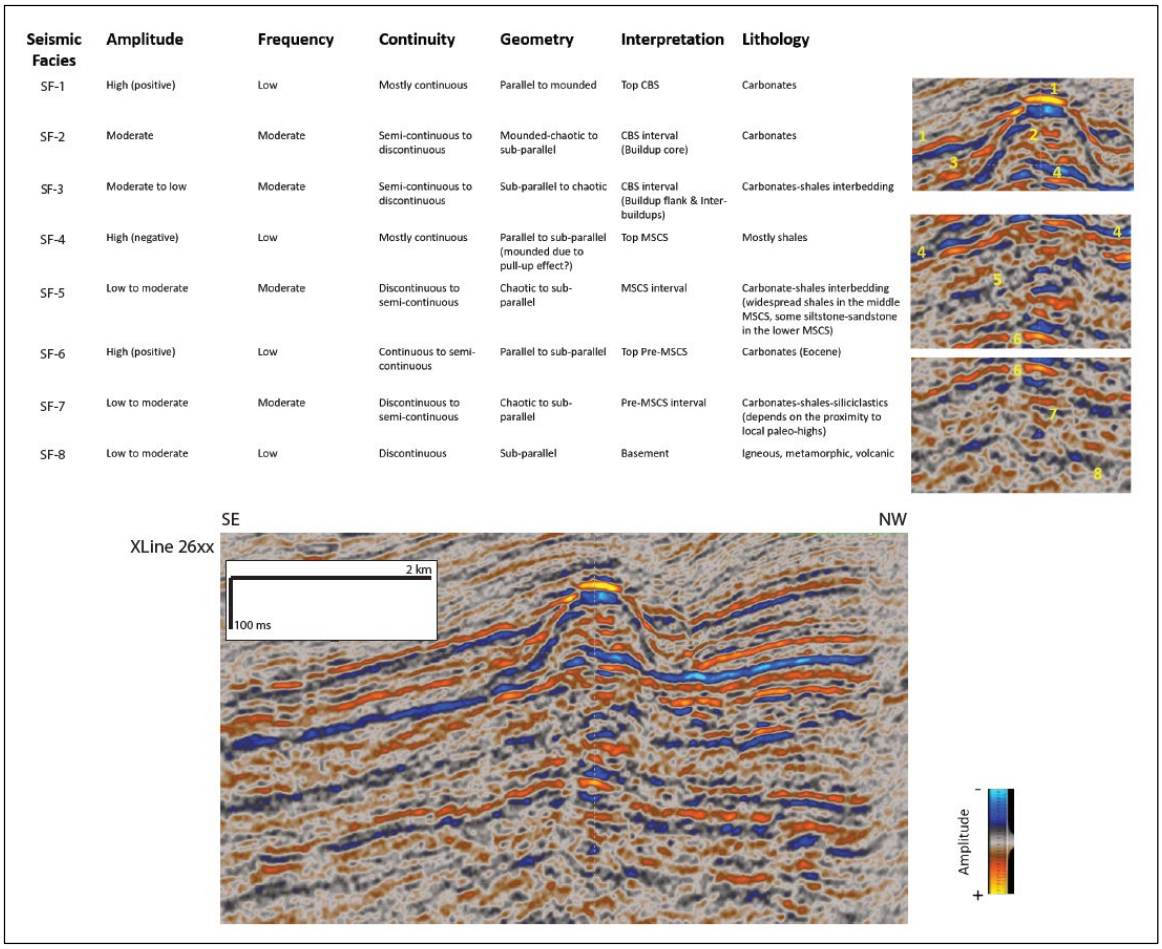

Figure 2.2. Definition of seismic facies based on seismic reflection amplitude, frequency, continuity, and geometry within MSCS and CBS intervals. Seismic horizon interpretation was performed using distinctive seismic facies within each interval.

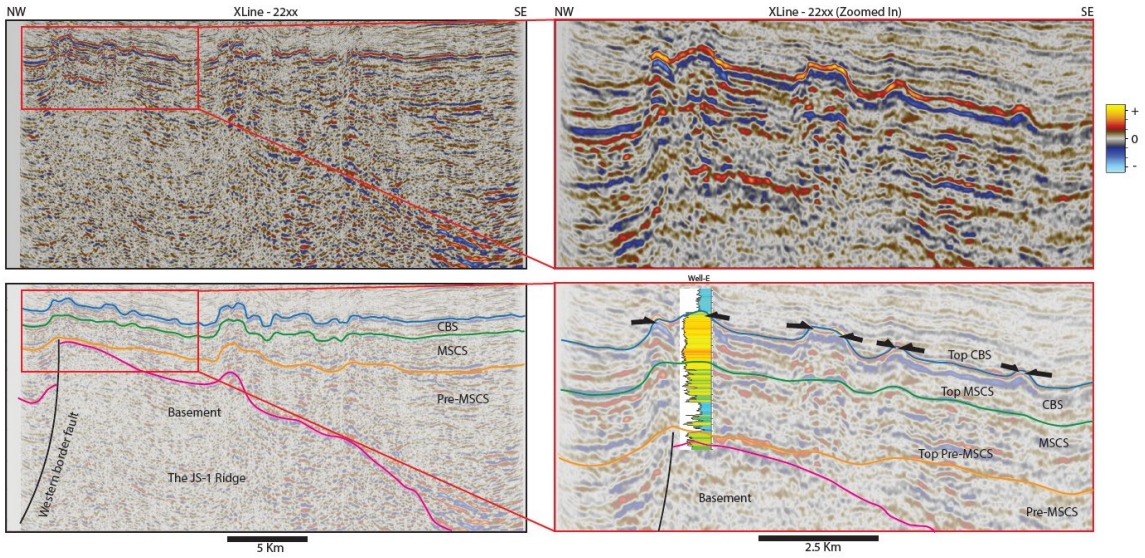

Figure 2.3. Uninterpreted (upper left and upper right figures) and interpreted (lower left and lower right figures) northwest-southeast seismic sections across the JS-1 Ridge intersected with Well-E location (lower right figure). Location of XLine-22xx seismic section is shown in Figure 5. Right figures are zoomed-in version of inserted orange boxes in left figures. Lower left figure clearly shows horst geometry of the JS-1 Ridge, and thickening of Pre-MSCS successions to the graben as syn-rift deposits. Both MSCS and CBS successions show a generally homogeneous thickness across the section as post-rift deposits. Lower right figure clearly shows the contrast between MSCS and CBS in term of seismic facies and depositional geometries. The subsequent Tuban/Rancak Formation shows onlaps to the top of CBS. This represents the depositional profile of CBS carbonate buildups near the end of the Aquitanian.

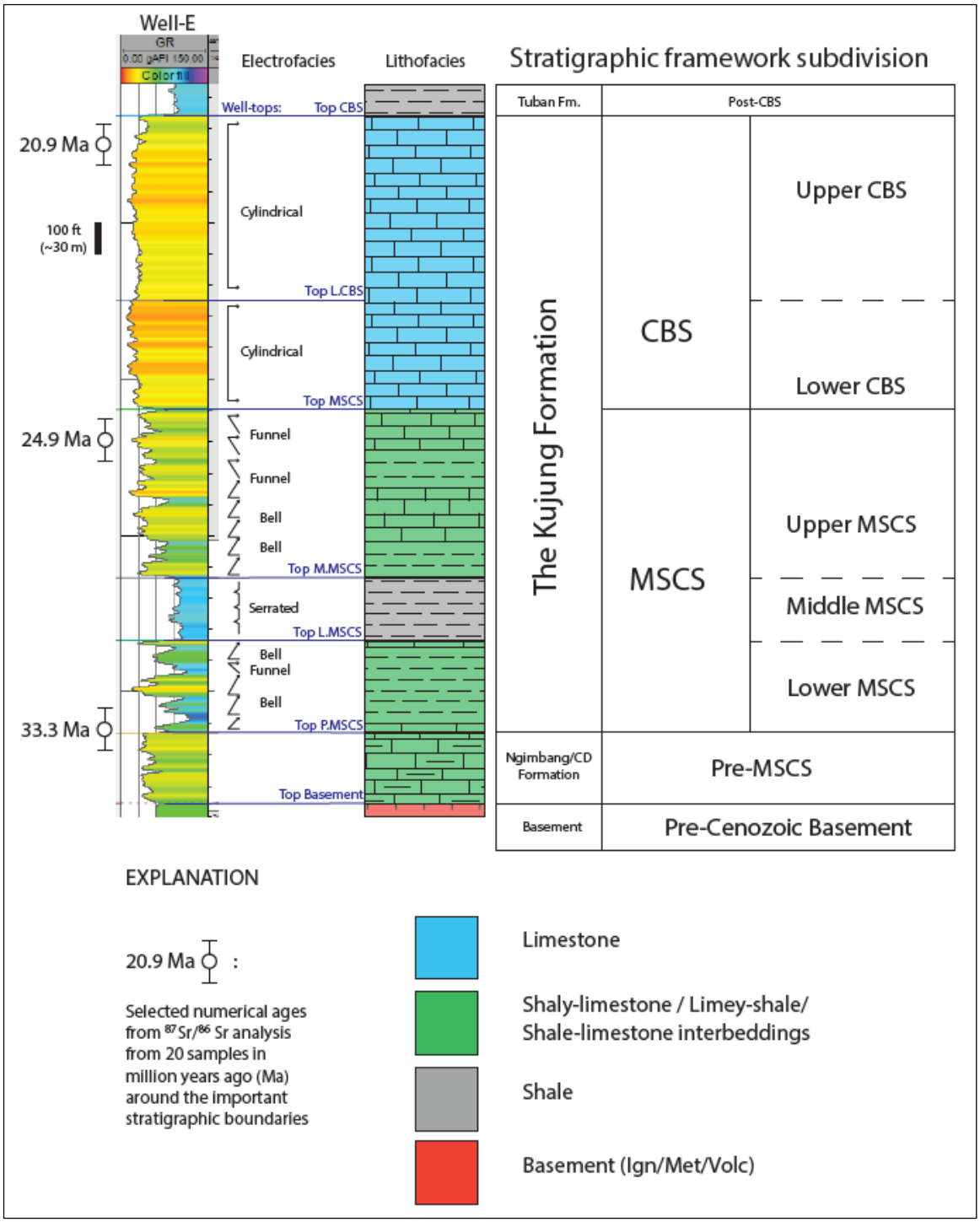

Figure 2.4. Gamma-ray type log, electrofacies, lithofacies, and stratigraphic framework subdivision used in this study, based on Well-E as the reference well.

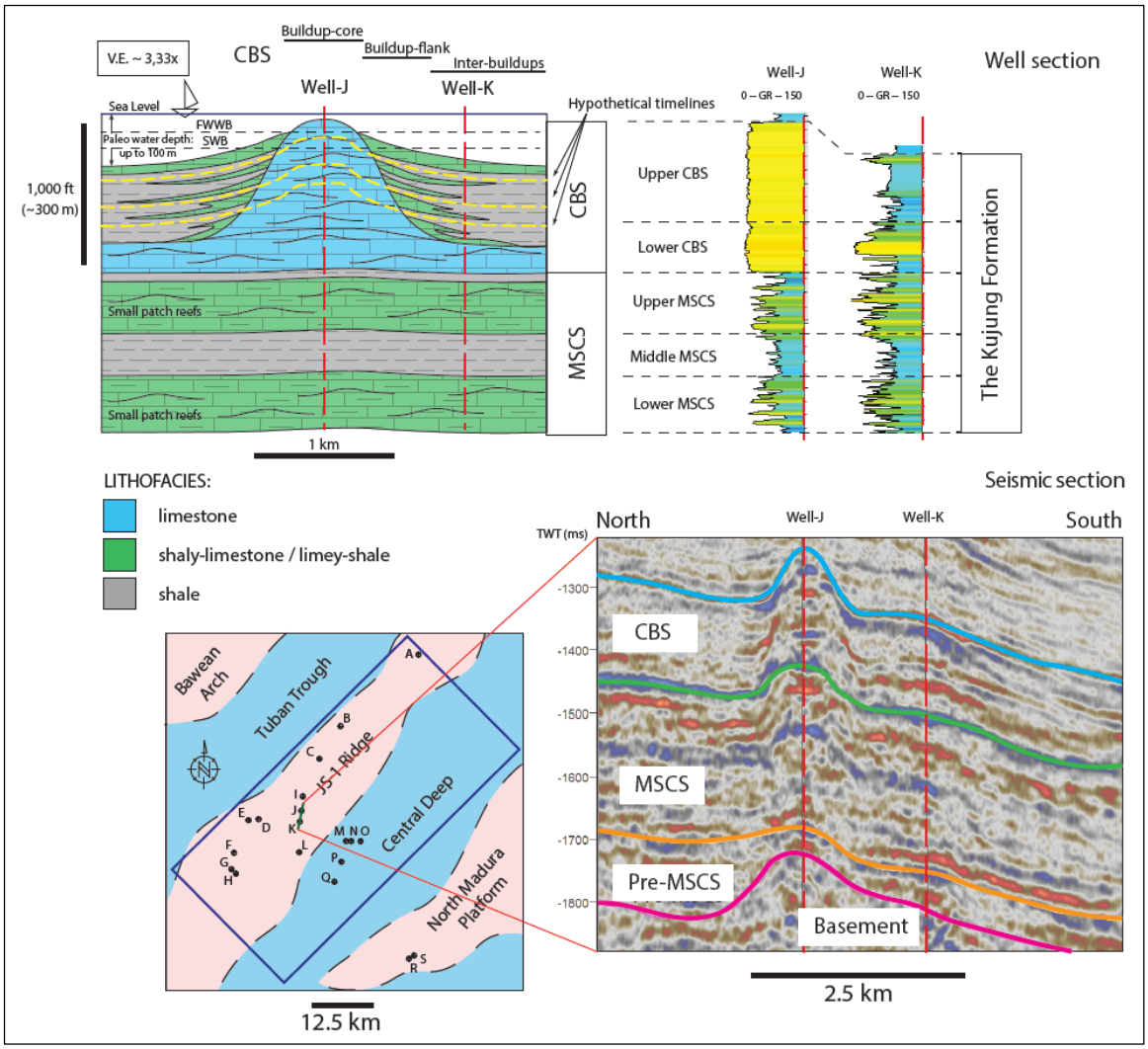

Figure 2.5. Conceptual lithofacies distribution, based on electrofacies and seismic characteristics of MSCS and CBS intervals. Both well and seismic sections show Well-J and Well-K, which are 1.5 km apart. Well section shows similar electrofacies between the two wells within MSCS interval. In the CBS interval, the electrofacies changes from cylindrical shape in Well-J as buildup-core deposits to alternating bell-, funnel-, and serrated shape in Well-K as inter-buildups deposits. Seismic section shows the depositional profile of CBS carbonate buildups penetrated by Well-J in its buildup-core, gradually changing into buildup-flank and inter-buildups profile toward Well-K. The positive feature of the top MSCS (green horizon) is interpreted to be due to seismic pull-up effect. MSCS successions do not have the capacity to form such buildups. Hypothetical timelines following the buildup topography in the Upper CBS interval are shown in yellow dashed-lines.

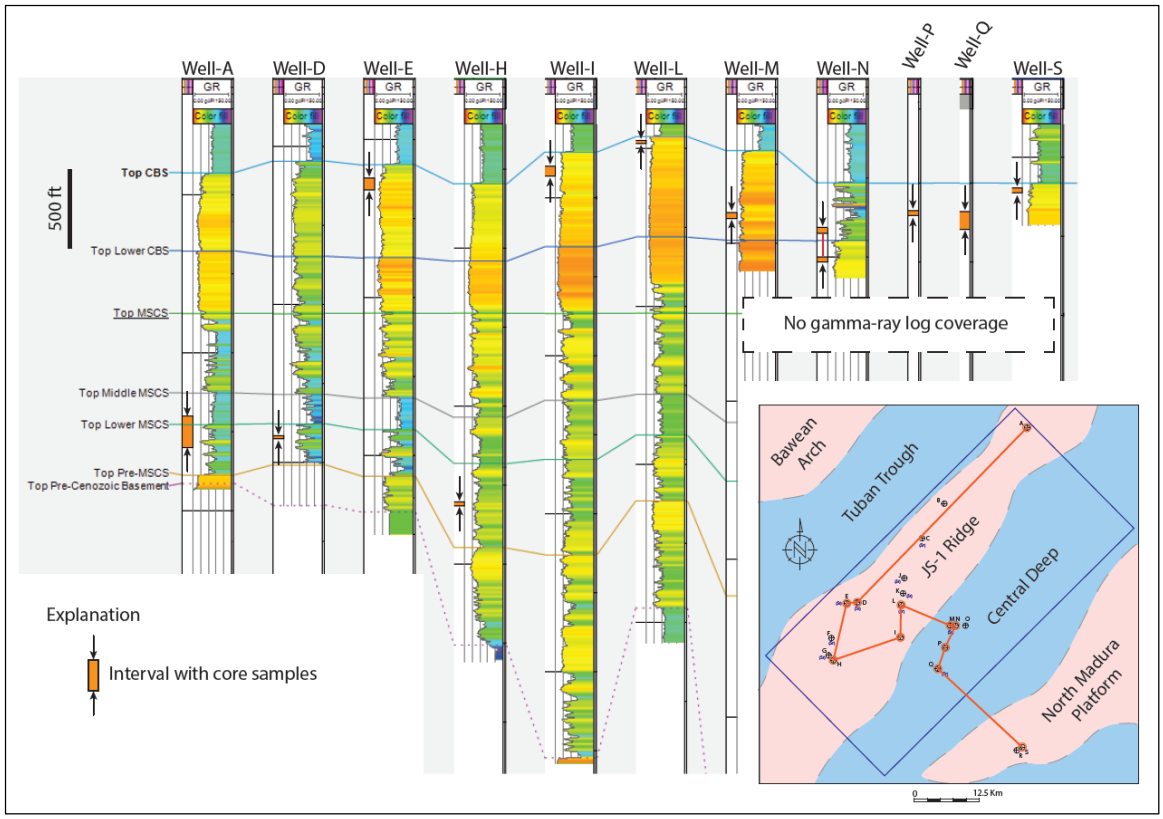

Figure 2.6. Correlation of wells with core samples that are sparsely distributed but that represent both intervals, MSCS and CBS. Orange boxes with pointing arrows in both upper and lower parts represent the cored interval.

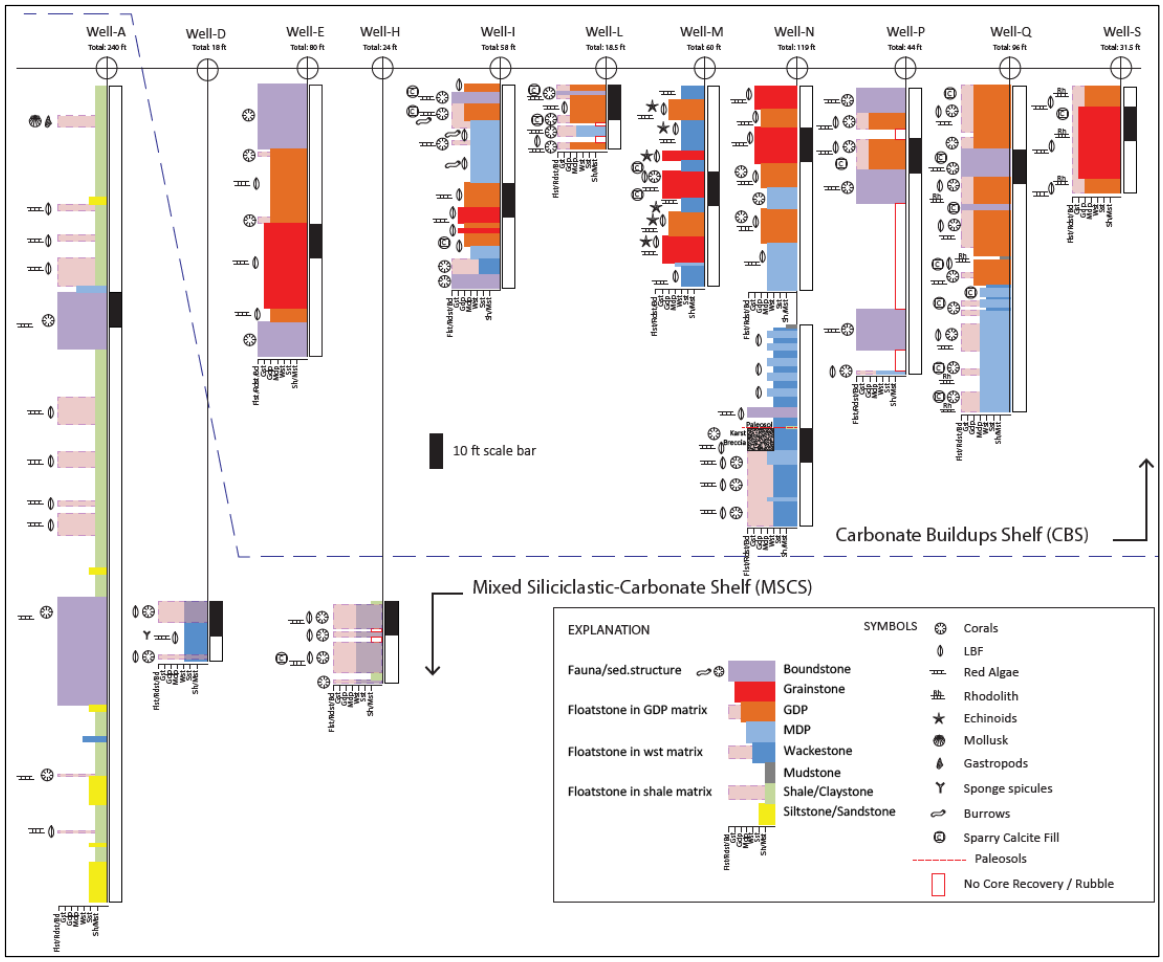

Figure 2.7. Facies description of 789 ft of core samples within MSCS and CBS intervals from 11 wells in the study area. The MSCS interval consists of LBF-dominated facies, shale, and siltstone-sandstone characterize the MSCS interval. The CBS interval contains coral-dominated facies.

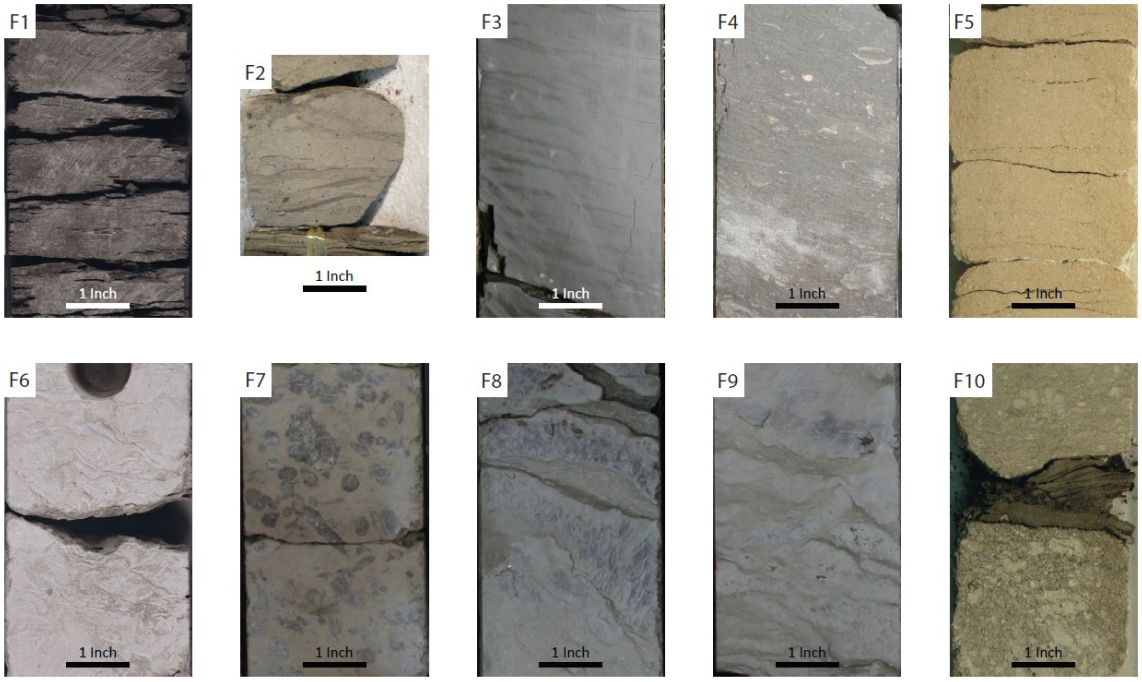

Figure 2.8. Representative core photographs of each facies: F1) shale, F2) *siltstone-sandstone*, F3) *silty-mudstone*, F4) LBF *wackestone – mud-dominated packstone*, F5) LBF-coral-echinoid *grain-dominated packstone – grainstone*, F6) LBF *floatstone – rudstone*, F7) Coral *floatstone – rudstone*, F8) Coral-algal *framestone*, F9) Coral-algal *bindstone*, F10) Rhodolith *floatstone – rudstone*. One inch equals approximately 2.5 cm.

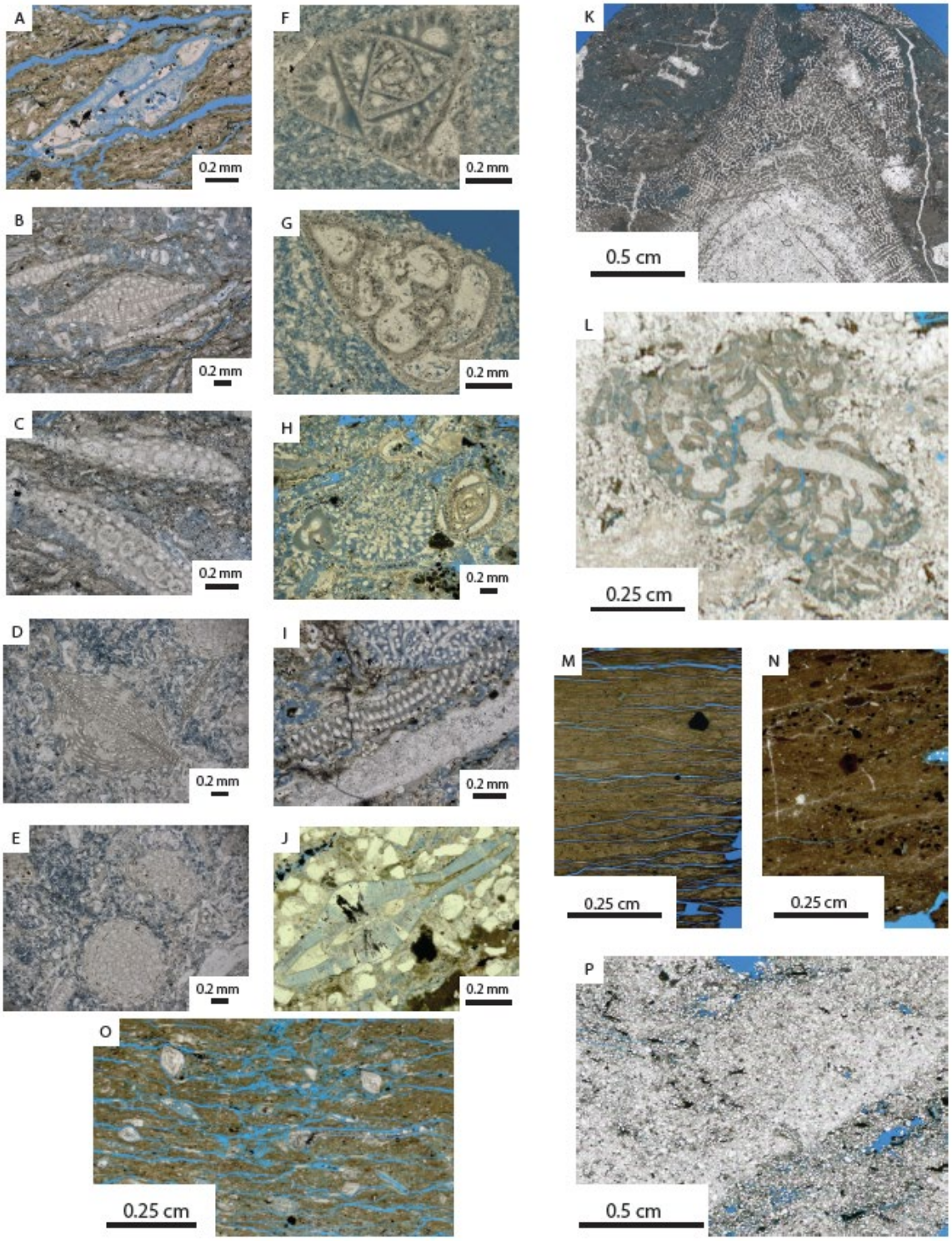
A
0.2 mm
F
0.2 mm
K
0.5 cm
B
0.2 mm
G
0.2 mm
L
0.25 cm
C
0.2 mm
H
0.2 mm
D
0.2 mm
I
0.2 mm
M
0.25 cm
N
0.25 cm
E
0.2 mm
J
0.2 mm
P
0.5 cm
O
0.25 cm

Figure 2.9.

Figure 2.9. Representative microphotographs of dominant faunal constituents and microfacies based on thin sections from Well-A: A) *Operculina*, B) & D) *Lepidocyclina*, C) *Miogypsinid*, E) *Sphaerogypsina*, F) *Austrotrillina*, G) *Victoriella*, H) *Miliolid*, I) *Soritidae*, J) *Heterostegina*, K) & L) Corals, M) shale, N) Claystone, O) *Amphistegina*, P) Siltstone – sandstone.

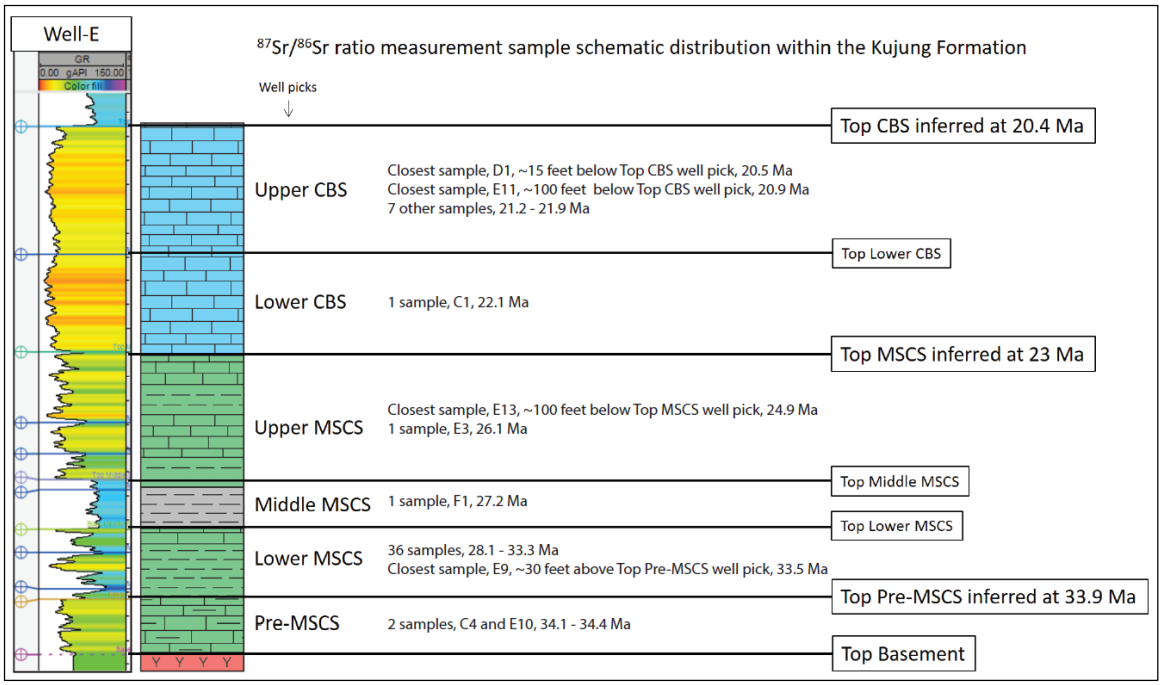

Figure 2.10. Inferred numerical ages of important stratigraphic boundaries inferred from distribution of the $^{87}Sr/^{86}Sr$ measurements within the MSCS and CBS intervals with regard to interpreted well-picks in well correlation. Top Pre-MSCS was inferred at 33.9 Ma (Eocene–Oligocene boundary), Top MSCS was inferred at 23 Ma (Oligocene–Miocene boundary), and Top CBS was inferred at 20.4 Ma (end of Aquitanian age).

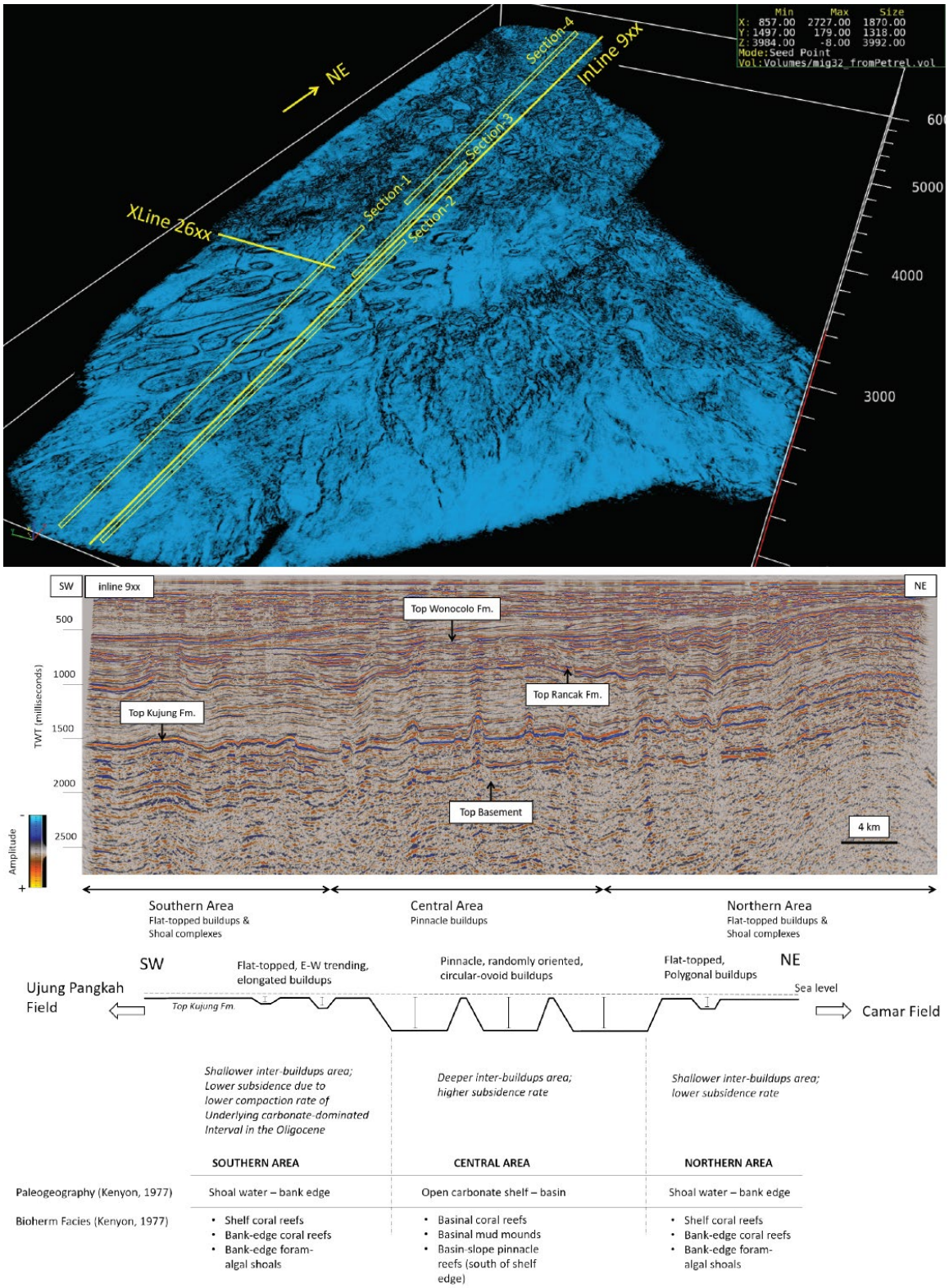
Min Max Size
X: 857.00 2727.00 1870.00
Y: 1497.00 179.00 1318.00
Z: 3984.00 -8.00 3992.00
Mode: Seed Point
Vol: Volumes/mig32_fromPetrel.vol
NE
InLine 9xx
XLine 26xx
Section-1
Section-2
Section-3
Section-4
5000
4000
3000
SW
inline 9xx
NE
Top Wonocolo Fm.
Top Rancak Fm.
Top Kujung Fm.
Top Basement
4 km
TWT (milliseconds)
500
1000
1500
2000
2500
Amplitude
Southern Area
Flat-topped buildups & Shoal complexes
Central Area
Pinnacle buildups
Northern Area
Flat-topped buildups & Shoal complexes
SW
Flat-topped, E-W trending, elongated buildups
Pinnacle, randomly oriented, circular-ovoid buildups
Flat-topped, Polygonal buildups
NE
Ujung Pangkah Field
Top Kujung Fm.
Sea level
Camar Field
Shallower inter-buildups area; Lower subsidence due to lower compaction rate of Underlying carbonate-dominated Interval in the Oligocene
Deeper inter-buildups area; higher subsidence rate
Shallower inter-buildups area; lower subsidence rate
SOUTHERN AREA
CENTRAL AREA
NORTHERN AREA
Paleogeography (Kenyon, 1977)
Shoal water – bank edge
Open carbonate shelf – basin
Shoal water – bank edge
Bioherm Facies (Kenyon, 1977)
• Shelf coral reefs
• Bank-edge coral reefs
• Bank-edge foram-algal shoals
• Basinal coral reefs
• Basinal mud mounds
• Basin-slope pinnacle reefs (south of shelf edge)
• Shelf coral reefs
• Bank-edge coral reefs
• Bank-edge foram-algal shoals

Figure 2.11.

Figure 2.11. Lateral and vertical architecture variations of the JS-1 Ridge carbonate shelf in the southern, central, and northern parts of the study area, based on semblance horizon slice around Top Kujung Fm (top figure). seismic horizon, interpreted SW-NE seismic section—inline-9xx (middle figure), and schematic architecture compared to the literature (bottom figure). Locations for Section-1 through Section-4 (Figure 2.12) are shown.

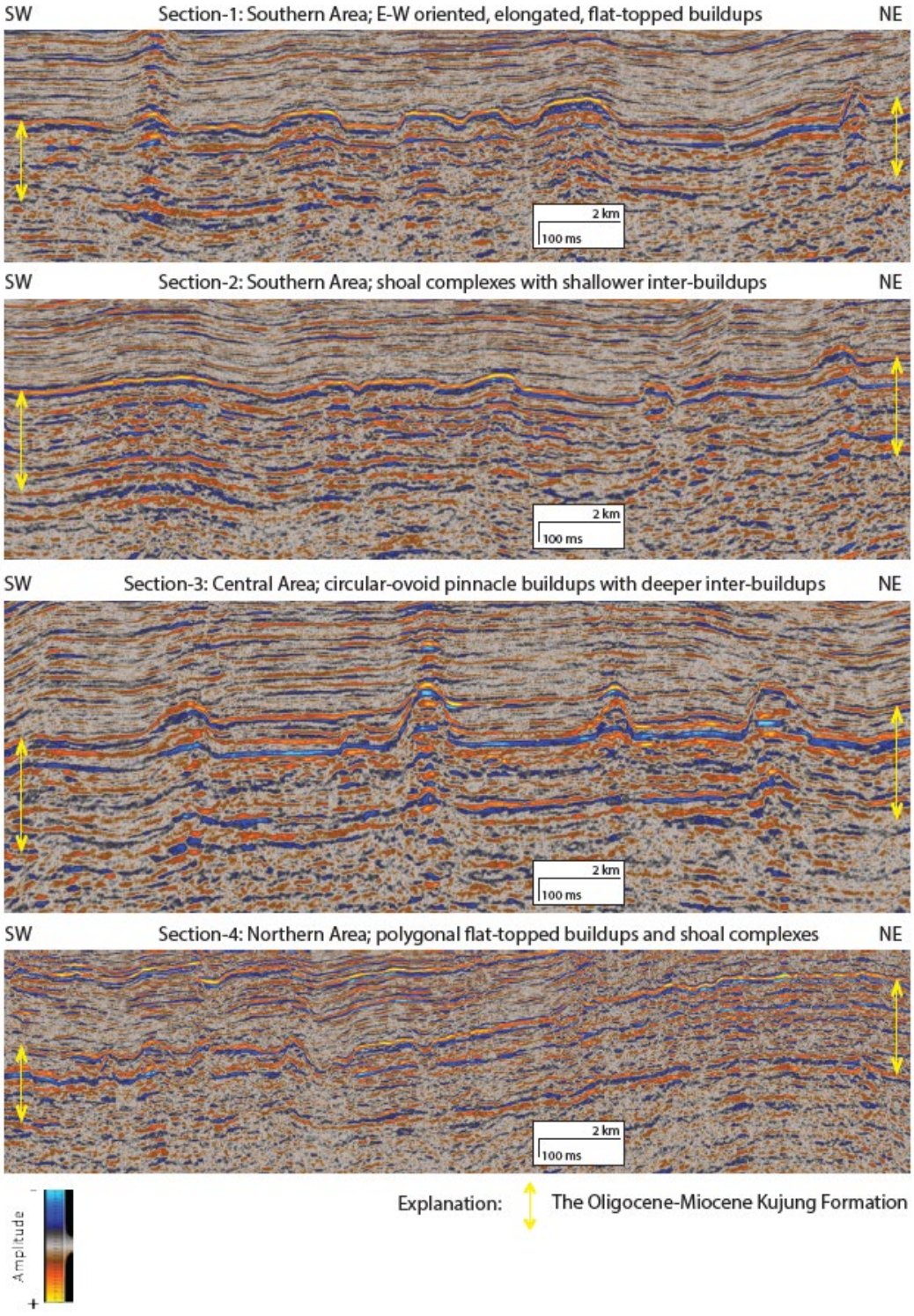

Figure 2.12. CBS vertical architecture interpreted from seismic sections (close-up) showing flat-toped buildups, pinnacle buildups, and shoal complexes.

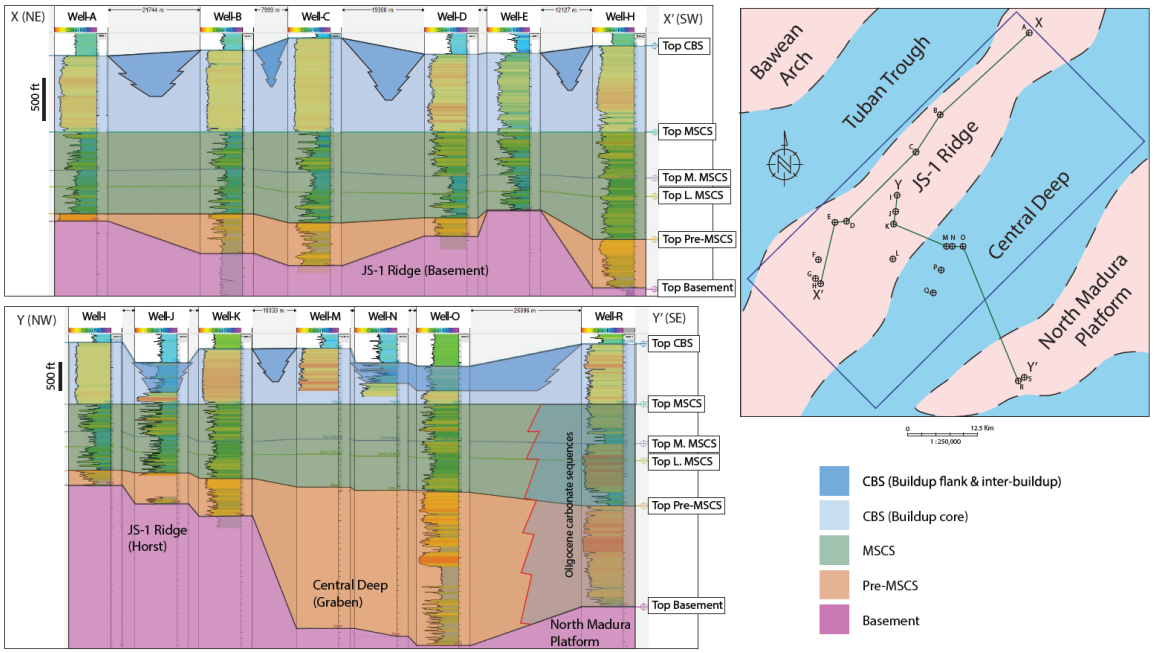

Figure 2.13. Northeast-southwest (X-X′) well correlation along the crest of the JS-1 Ridge and northwest-southeast (Y-Y′) well correlation across the JS-1 Ridge to the Central Deep. Pre-MSCS successions thicken to the Central Deep (graben). MSCS successions thicken somewhat gradually to the graben area. Thickness difference in CBS were observed between buildup-core and buildup-flank to inter-buildups. Electrofacies is noticeably different in MSCS (bell-, funnel-, and serrated shape) compared to CBS (cylindrical shape in the buildup-core, similar to MSCS in the buildup-flank and inter-buildups). Well-R in the southwestern margin of the North Madura Platform shows carbonate-dominated successions in the Oligocene, which is equivalent to the MSCS interval in the study area.

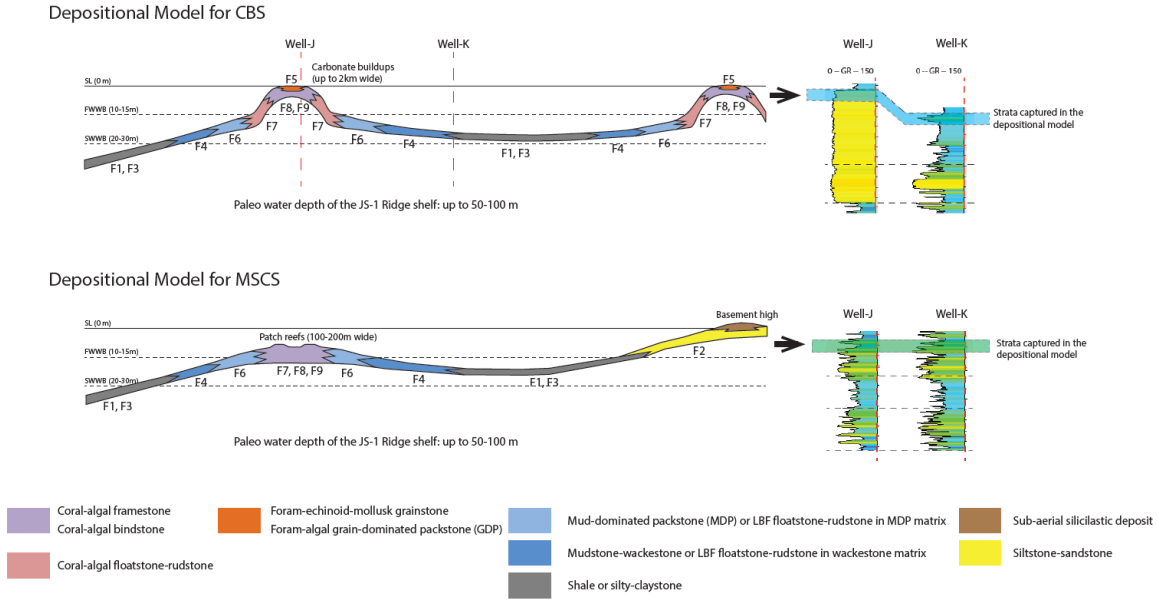

Figure 2.14. Depositional models of two intervals within the Kujung Formation, MSCS in the Oligocene (lower figure) and CBS in the Early Miocene (upper figure). Coral-dominated facies formed smaller patch reefs (100–200 m wide) in the MSCS and built larger carbonate buildups (1–2 km wide) in the CBS. In the Lower MSCS in particular, localized basement highs were exposed and became a source of coarse-grained siliciclastic sediments. In the CBS, the buildup-core as well as the shallow-water shoal complex area were characterized by the presence of smaller LBF with robust and spherical form (F5) deposited in an open platform setting. The different characteristics of buildup-core and buildup-flank to inter-buildups deposits in CBS were represented by the electrofacies variations shown in Well-J and Well-K. In the same wells, the MSCS interval shows negligible lateral variation. Facies definition refers to Table 2.2.

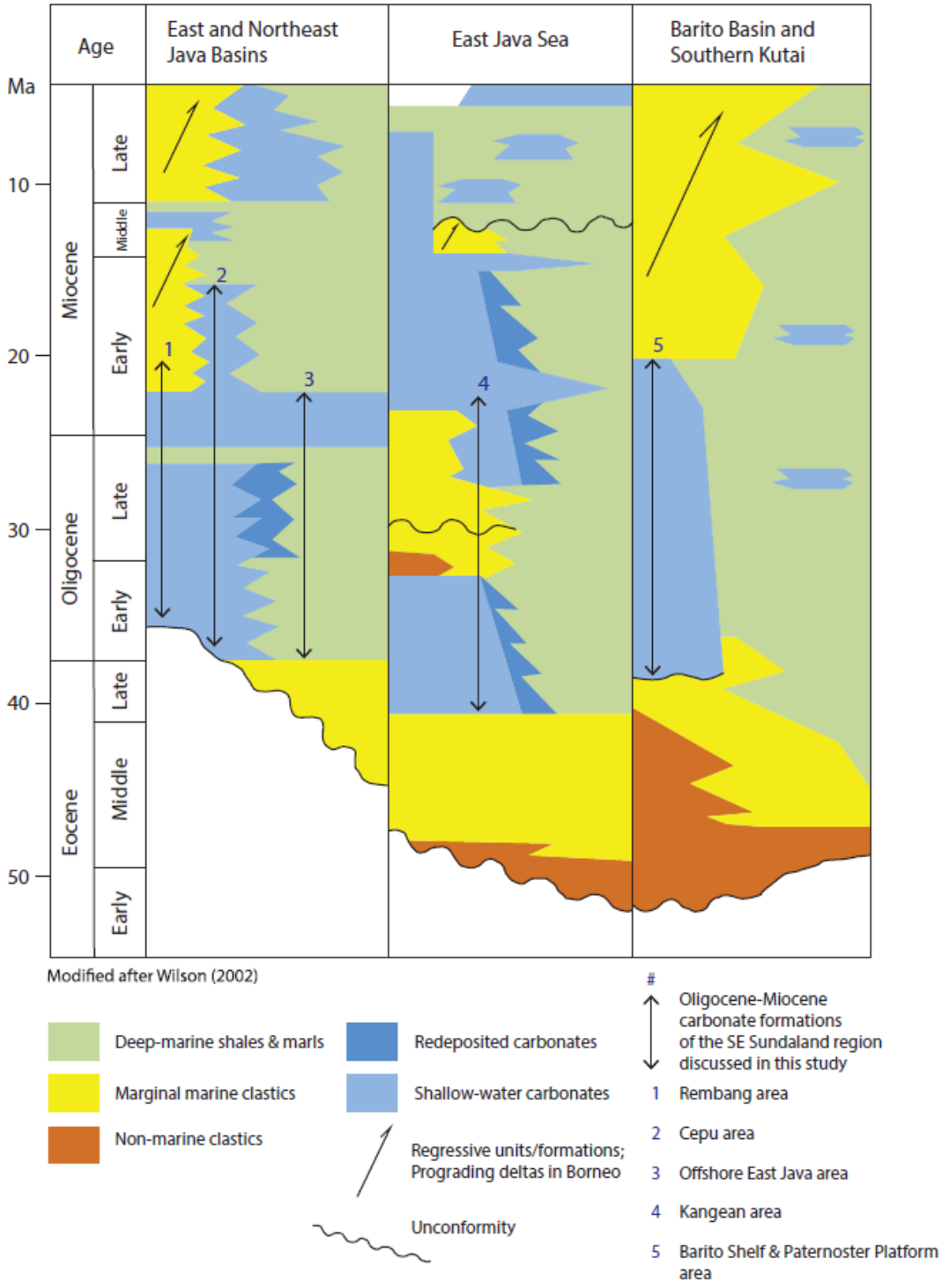

Figure 2.15. Regional composite stratigraphic column (modified after Wilson, 2002) of the selected comparative areas in the southeastern Sundaland region, as discussed in this study.

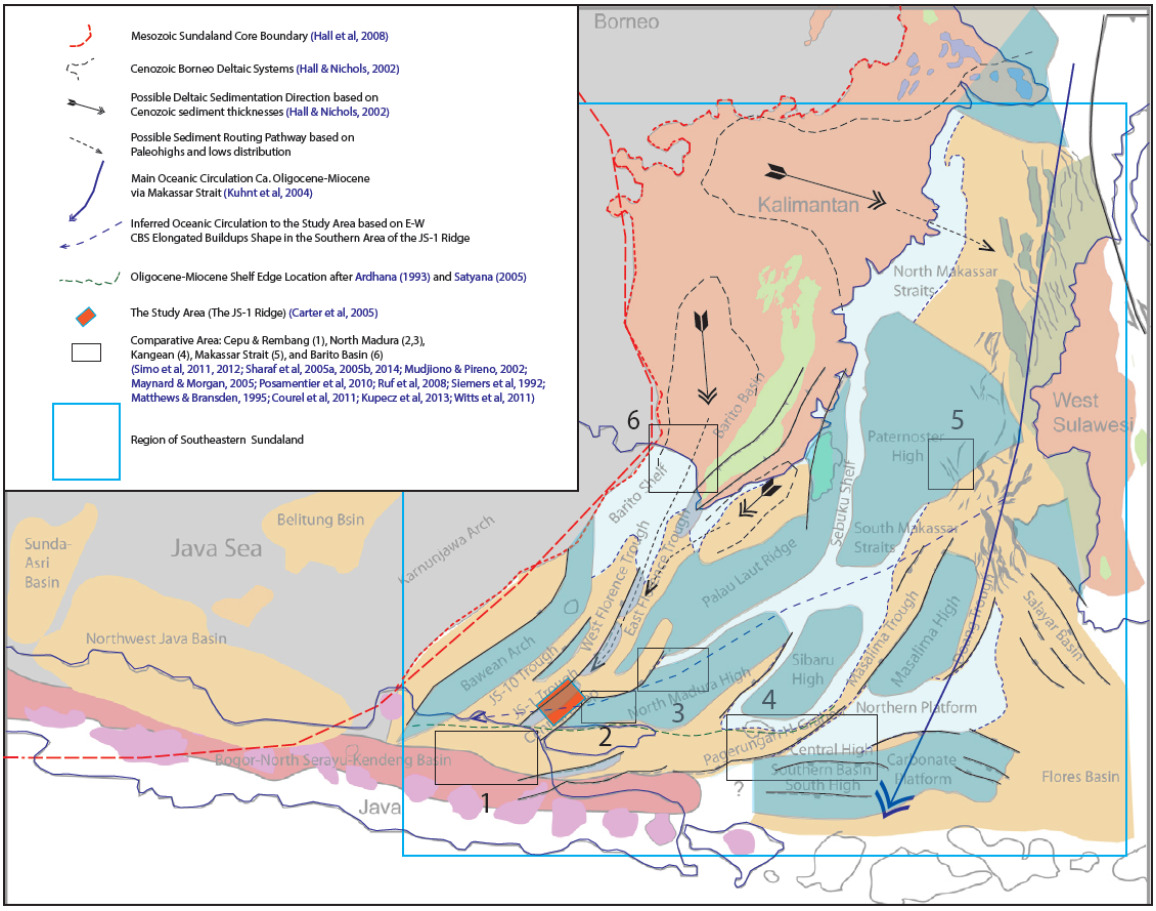

Figure 2.16. Regional distribution of paleo-highs and -lows in southeastern Sundaland region (modified after Pubellier & Morley, 2014) with synthesis of interpreted controls on carbonate shelves evolution during Oligocene to Early Miocene, as discussed in this study.

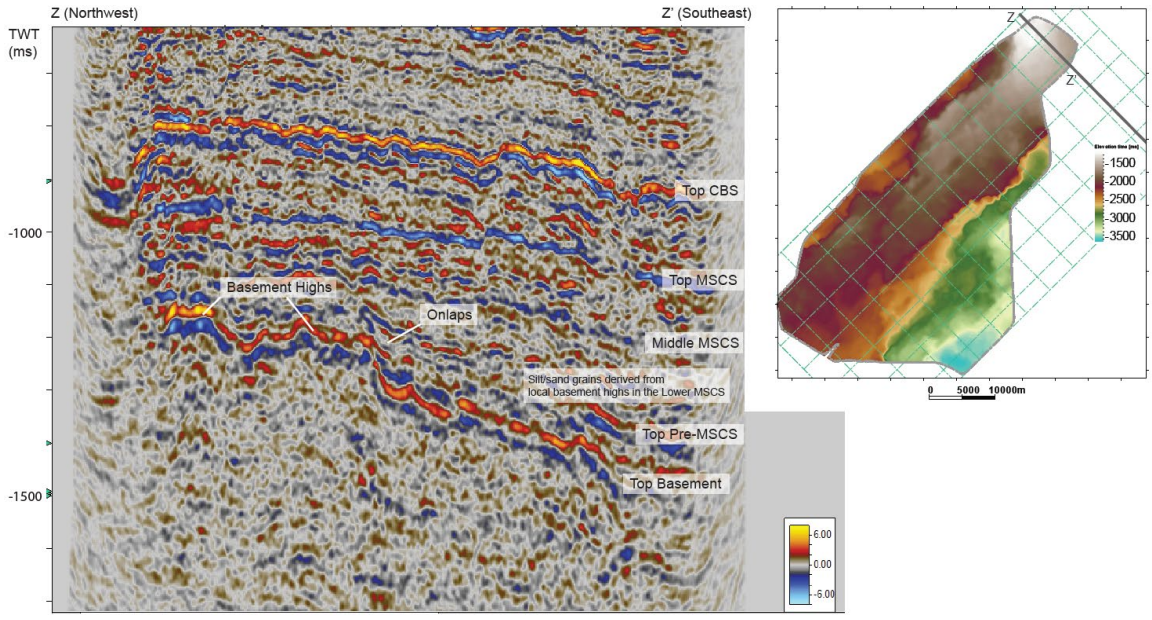

Figure 2.17. Localized basement highs in the northern area of the JS-1 Ridge, southwest of Well-A. These basement highs were the source for coarse-grained siliciclastic sediments that were deposited as siltstone-sandstone in the Lower MSCS interval, as observed in core samples of Well-A.

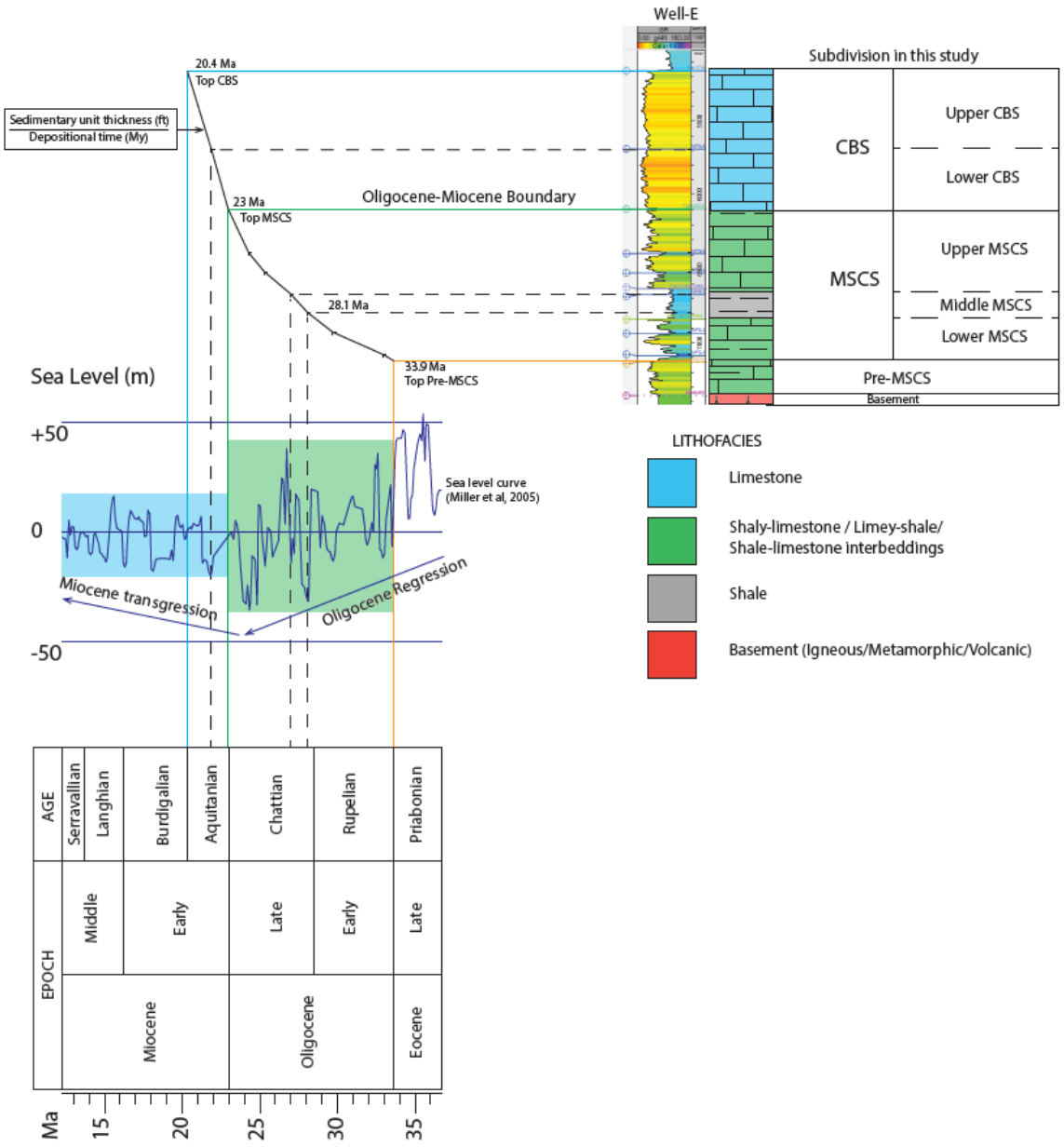

Figure 2.18. Tie between the Kujung Formation interval with sea-level curve (Miller et al., 2005). Two trends of sea-level fluctuations were observed; rapid rise – rapid fall with higher magnitude of 50 m in the Oligocene (highlighted green) and rapid rise – slow fall with lower magnitude of ~30 m starting in the Early Miocene (highlighted blue). Long-term trends of Oligocene regression and Miocene transgression were also observed (blue arrowed-lines). The gradient (slope) of the black curve shows the accumulation rates, which are up to three times higher in the CBS interval compared to the MSCS.

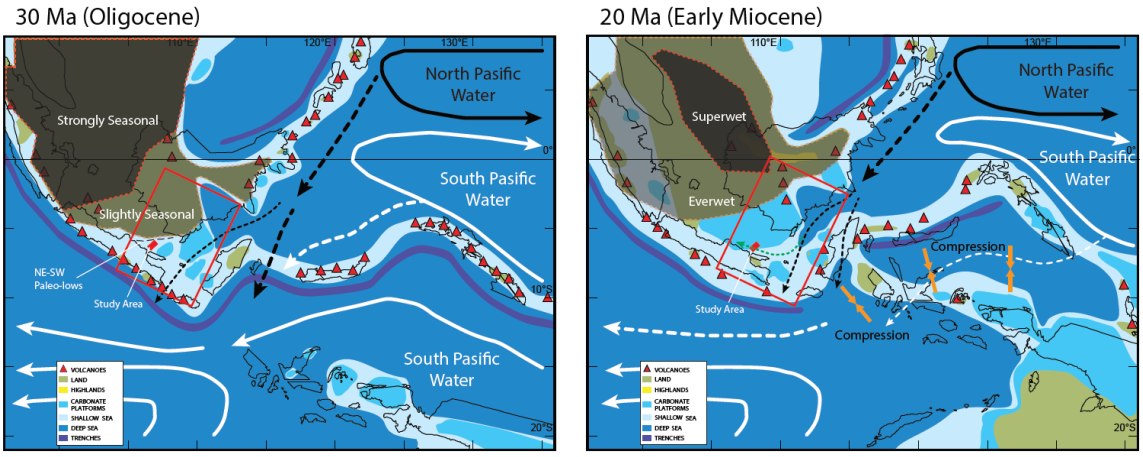

Figure 2.19. Distribution of land and sea in Oligocene ca. 30 Ma (left figure) and Early Miocene ca. 20 Ma (right figure) (Hall, 1998, 2009), paleo-oceanic circulation of the North and South Pacific water (Kuhnt et al., 2004), major change of climatic conditions on the Borneo mainland (Morley, 2012), and the initiation of compressional tectonics east of the study area (Hall, 1997, 2002, 2012; Johansen, 2003; Pubellier & Morley, 2014). The study area is represented by red-filled box, while the region of southeastern Sundaland discussed in this study is represented by red-outlined box. In the Oligocene, the study area is separated with the northwest Borneo mainland by a series of northeast-southwest trending paleo-lows (black dashed-line, see details on Figure 2.16) that is interpreted to have acted as a barrier that rerouted siliciclastic sediments. Green-dashed arrow represents inferred east-west oceanic circulation, based on elongated carbonate buildup geometry in the southern part of the study area.

Chapter 3: Influence of Compressional Tectonic Events and Paleo-Indonesian-Through-flow on the Morphology of Carbonate Platforms in the Miocene, Offshore East Java, Indonesia

ABSTRACT

Seismic geomorphology techniques were utilized to study the carbonate shelf in the Miocene using 1,300 km^2 of 3D seismic data from the West Madura Offshore (WMO) block, offshore East Java, Indonesia. The study area is situated along the back-arc zone of the Java subduction. This carbonate shelf shows distinctive characteristics in the Early and Late Miocene intervals in term of its depositional geometries, architecture, growth pattern, and geomorphic features. An interval dominated by marine siliciclastic deposits without development of carbonate buildups in the Middle Miocene separated the two intervals.

Carbonate shelves in the study area have evolved from a shelf characterized by west-southwest – east-northeast elongated, circular-ovoid, to polygonal carbonate buildups in the Early Miocene to a shelf dominated by north-south elongated flat-topped carbonate platforms in the Late Miocene. The Early Miocene carbonate buildups are 0.5–2 km wide and as much as 8 km long, whereas the Late Miocene carbonate platforms are as much as 5 km wide and more than 20 km long. Each of these carbonate-dominated intervals reaches a total thickness of approximately 335–365 m (1,100–1,200 ft).

On the basis of semblance horizon slices, 150 individual Early Miocene carbonate buildups and 8 Late Miocene carbonate platforms were delineated. Early Miocene carbonate buildups cover a total area of approximately 180 km^2, and Late Miocene carbonate platforms cover a total area of approximately 400 km^2. The Early Miocene carbonate buildups' distribution follows the northeast-southwest orientation of the

basement high structure of the JS-1 Ridge. In contrast, the distribution of the Late Miocene carbonate platforms does not indicate a major influence from the antecedent topography.

Depositional and geomorphic features such as a flat-topped carbonate platform architecture, a progradational platform margin, and sinuous channels developed on the upper part of the larger Late Miocene carbonate platforms strongly suggest a condition of decreasing accommodation. This condition is interpreted to have been caused by regional compression and tectonic inversion during a period of relatively low amplitude global sea-level fluctuation.

In the Late Miocene, intensifying compressional tectonic events have resulted in decreased accommodation on the carbonate shelves. Development of Indonesian through-flow during this period have strongly influenced the oceanic circulation resulted in extensive development of north-south elongated flat-topped carbonate platforms. Ultimately, this study aims to provide valuable insights to better determine the geometry, architecture, and distribution of the carbonate reservoirs situated in tectonically active regions.

INTRODUCTION

Carbonate sediments were produced extensively in the Southeastern Asia region during the Cenozoic (Wilson, 2002). Carbonates were deposited in a wide range of tectonic settings, including continental passive margins, convergent plate boundaries, and obliquely convergent plate boundaries (Fulthorpe & Schlanger, 1989). Cenozoic carbonates in the Southeast Asia region have long been known as proven and prolific hydrocarbon reservoirs with varying architectures. A significant amount of subsurface data has become available

as a result of hydrocarbon exploration and production activity. In the offshore East Java area, Indonesia, the Early Miocene Kujung Formation and the Late Miocene Wonocolo Formation constitute the carbonate formations in the Miocene. Previous studies based on subsurface data show a wide range of variations in the depositional geometries and architectures of these carbonate formations (Kenyon, 1977; Mudjiono & Pireno, 2002; Johansen, 2003; Adhyaksawan, 2003; Carter et al., 2005; Maynard & Morgan, 2005; Ruf et al., 2008; Posamentier et al., 2010). Despite its economic importance and subsurface data availability, its detailed seismically mapped geomorphic features have been understudied.

This study utilizes seismic geomorphology techniques in order to describe and interpret the depositional systems (Posamentier, 2004). By utilizing subsurface data, mainly the 3D seismic, this study aims to analyze in detail the three-dimensional seismic architecture and geomorphology of the Early and Late Miocene carbonate formations that were deposited in an active tectonic margin in the offshore East Java area, Indonesia.

Results of subsurface data description and interpretation of the carbonate formations, such as their depositional geometries, architecture, growth pattern, and geomorphic features, present possible controls on the development of the two distinct carbonate formations during the Miocene. This study shows the responses of carbonate shelves during the Miocene, recorded in its architecture and geomorphic features, as the compression intensifies within an active tectonic margin.

DATA AND METHODS

Regional stratigraphy served as a reference to define the general lithofacies and the age range of the Early Miocene Kujung Formation and Late Miocene Wonocolo Formation. This study utilized a subsurface data set that consists mainly of 3D seismic data from an active block operated by Pertamina Hulu Energi – West Madura Offshore, or PHE-WMO. The 3D seismic data were acquired in 1999 and cover an area of approximately 1,300 km^2. The seismic data have a dominant frequency content of 25–35 Hz (Carter et al., 2005). Well data include gamma-ray log and cuttings lithology from one reference well (Well-G) in the southern part of the study area (Figure 3.1). Cuttings from eight other wells were used to describe the lithofacies of the Early and Late Miocene intervals.

Seismic sections were used to describe and interpret seismic facies within the Miocene interval, including amplitude, frequency, continuity, and geometry of the seismic reflectors (Fontaine et al., 1987; Janson et al., 2011). Based on interval differentiation, five regional seismic horizons were picked and interpreted within the 3D seismic volume. The seismic horizons were tied to well data using a synthetic seismogram based on previous work on Well-G (Figure 3.1, Carter et al., 2005). Time structure maps were generated using the interpreted seismic horizons. Semblance seismic attributes were generated from the 3D seismic volume in order to analyze the lateral discontinuity of the carbonate buildups and platforms. Semblance horizon and time slices were utilized to delineate the outlines of the Early and Late Miocene carbonate buildups and platforms. Depositional geometries, architecture, growth pattern, and geomorphic features of the carbonate buildups and platforms were then described, analyzed, and interpreted. By analyzing and comparing the

results to the literature, controls on the carbonate shelf development during the Miocene were inferred.

RESULTS

Lithofacies of Early and Late Miocene Intervals

Lithofacies of the two intervals were described based on cuttings lithology. In the Early Miocene interval, buildup-core is characterized by massive carbonates with minor shale breaks. In contrast, buildup-flanks and inter-buildups are characterized by carbonate and shale interbeddings (Chapter 2). In the Late Miocene interval, similar characteristics were observed. Platform interior and margin are dominated by massive carbonates, while slope and open carbonate shelf consist interbeddings of carbonate and shale. On the basis of drilling data from four wells (Figure 2.1; Well-J, Well-D, and Well-E) that are located in the platform interior, the Late Miocene Wonocolo ("OK Reef") Formation contains interval of no return in drilling mud due to loss of circulation in a very porous limestone.

Seismic Facies and Horizons Interpretation

Seismic facies of the intervals of interest—the Pre-Cenozoic, the Early Miocene, and the Late Miocene intervals—were described based on the amplitude, frequency, continuity, and geometry of the seismic reflectors (Figure 3.2; Fontaine et al., 1987; Janson et al., 2011). Using the defined seismic facies within the Miocene interval and around the top of the basement, five seismic horizons were picked and interpreted from 1,300 km^2 of 3D seismic data. Those seismic horizons are 1) Top Basement horizon, 2) Base Early Miocene horizon, 3) Top Early Miocene horizon, 4) Base Late Miocene horizon, and 5)

Top Late Miocene horizon, from oldest to youngest (Figure 3.2). Based on regional stratigraphy of East Java Basin, the Early Miocene interval constitutes the Kujung Formation whereas the Late Miocene interval represents the Wonocolo Formation. Both formations are dominated by carbonates and marine shale, as indicated by cuttings from wells drilled in the region (Figure 1.5). The Pre-Cenozoic interval is capped by the Top Basement horizon and consists of a low- to moderate-amplitude and low-frequency seismic reflector. The seismic reflector shows a discontinuous and chaotic to sub-parallel geometry. These seismic facies represent the basement mixed lithology that is predominantly igneous and metamorphic rock (Carter et al., 2005).

The Early Miocene interval has an average thickness of around 140 ms TWT, and in some places can reach up to approximately 200 ms TWT. Its seismic characteristics vary greatly along the architecture of the Early Miocene carbonate shelf. The Early Miocene carbonate shelf architecture types were subdivided, mainly based on their depositional profile, into buildup-core, buildup-flank, and inter-buildups, from the shallowest part of the buildups into the deeper part of the open shelf. Shallow-water shoal complexes developed in the northern and southern area of the JS-1 Ridge. Subdivision of the Early Miocene carbonate shelf architecture will be discussed in detail a later section.

Within *Buildup-core*, the interval is dominated by moderate- to high-amplitude, moderate-frequency seismic reflectors. They show discontinuous to semi-continuous and mounded-chaotic to sub-parallel geometry. In contrast, along *Buildup-flanks*, the interval consists low- to moderate-amplitude and low- to moderate-frequency seismic reflectors. They show a semi-continuous to continuous, highly inclined seismic reflectors geometry.

Inter-buildups area contains low- to moderate-amplitude, low- to moderate-frequency seismic reflectors. Mostly, seismic reflectors appear to be most parallel and continuous in this area. However, in some areas, they can be somewhat inclined. Inter-buildups areas can also be considered as open carbonate shelf. *Shoal-Water Complexes* in the northern and southern areas are dominated by seismic facies similar to those of the buildup-core with distribution over a larger area and not limited or bounded by buildup-flanks. The Early Miocene interval is capped by the Top Early Miocene horizon that shows high-, positive-amplitude and low-frequency seismic reflector. The horizon is mostly continuous and shows a parallel to mounded geometry (Figure 3.2 and Figure 3.4).

The Late Miocene interval is thicker than the Early Miocene interval, with average thickness of around 290 ms TWT and a maximum of 330 ms TWT. Generally, the Late Miocene interval has a higher resolution of seismic data compared to the Early Miocene interval. Its seismic characteristics also vary along the architecture of the Late Miocene carbonate shelf. The Late Miocene carbonate shelf architectures were subdivided, based mainly on their depositional profile, into platform interior, platform margin, slope, and open carbonate shelf, from the shallowest part of the platform top into the deeper part of the open shelf. Subdivision of the Late Miocene carbonate shelf architecture will be discussed in detail later.

Within the *Platform Interior*, the interval is dominated by moderate- to high-amplitude, high-frequency seismic reflectors. They show mostly semi-continuous to continuous and sub-parallel to parallel geometry, but discontinuous-chaotic seismic reflectors are observed in some places. The *Platform Margin* is the starting point of inclined

seismic reflectors of the slope. Along the platform margin, the interval shows moderate- to high-amplitude, high-frequency seismic reflectors. They show truncated-discontinuous to semi-continuous and sub-parallel to mounded-chaotic geometry. Along *Slope*, the interval consists of low- to moderate-amplitude, moderate- to high-frequency seismic reflectors. They show a semi-continuous to continuous and highly inclined, concave-up, draped-to-the-platform-margin geometry. The *Open Carbonate Shelf* contains low-, moderate-, to high-amplitude and moderate- to high-frequency seismic reflectors. Seismic reflectors in this area appear to be mostly parallel and continuous, as observed in the inter-buildups area of the Early Miocene interval. The Late Miocene interval is capped by the Top Late Miocene horizon, which is characterized by mostly high-, positive-amplitude and moderate- high-frequency seismic reflectors. The horizon has a continuous and parallel geometry, except in the slope area, where it can be discontinuous and inclined (Figure 3.2 and Figure 3.5). The Top Late Miocene horizon represents a diachronous event that shows the time-transgressive nature of the end of the carbonate platforms deposition.

Time Structure Maps and Semblance Horizon Slices

Time structure maps were generated utilizing the interpreted seismic horizons. The Top Basement time structure map shows the structural configuration of the basement. The basement in the study area is a fault block with a northeast-southwest orientation, regionally known as the JS-1 Ridge. The fault block is dipping southeastward and is bounded by a normal border fault system to the northwest (Figure 3.3). The eastern flank of the JS-1 Ridge comprises sets of southeastward-dipping normal faults that can be clearly observed in seismic sections perpendicular to the ridge orientation (Figure 1.4).

Semblance seismic attributes were generated from the 3D seismic volume. In order to analyze the lateral discontinuity of within the intervals of interest, semblance horizon slices were generated using time structure maps of the Top Early Miocene and Base Late Miocene horizons (Figure 3.6). Intervals of interest are the Early Miocene Kujung Formation and the Late Miocene Wonocolo Formation, both of which are characterized by low gamma-ray log values in Well-G. Both intervals can reach total thickness of more than 1,000 ft (Figure 3.7). Geologic features, were delineated utilizing semblance horizon slices, include faults, carbonate buildups and platform boundaries, and geomorphic features such as channels. Adjusted semblance horizon slices (slicing-up and -down) within the Early and Late Miocene intervals have generated spectacular 3-D images in perspective views that represent the distribution of carbonate buildups and platforms in Miocene time (Figures 3.8 and 3.9).

Depositional Geometries of Carbonate Buildups and Platforms

Outlines of the Early Miocene carbonate buildups and the Late Miocene carbonate platform were delineated utilizing semblance horizon slices. These carbonate buildups and platform outlines were analyzed in order to describe and interpret depositional geometries of each carbonate formation (Figures 3.10 and 3.11).

In the Early Miocene carbonate shelf, approximately 150 individual carbonate buildups were identified. The dimension of these carbonate buildups ranges from 0.5–2 km wide and as much as 8 kilometers long. In the southern area, the carbonate buildups are elongated in the east-west direction. In the central area, the shape of the carbonate buildups is circular to ovoid. In the northern area, the carbonate buildups have a polygonal shape.

The Early Miocene carbonate buildups cover a total area of approximately 180 km^2. In the main ridge area of the JS-1 Ridge, 117 carbonate buildups with around 94% of the total carbonate buildups areal coverage are distributed. Shoal complexes in the southern area cover a total area of approximately 340 km^2 (Figures 3.8 and 3.10).

In the Late Miocene carbonate shelf, eight main carbonate platforms and one small carbonate buildup in the southeastern part of the study area were identified. Larger carbonate platforms are 5–8 km wide and more than 20 km long. Their dominant orientation is north-northwest – south-southeast to north – south. The Late Miocene carbonate platforms cover a total area of approximately 400 km^2. Six carbonate platforms with around 72% of the total carbonate platform areal coverage are distributed within the main ridge of the JS-1 Ridge (Figures 3.9 and 3.11).

Architecture of Carbonate Shelf in Early and Late Miocene

Using the interpreted seismic sections, the architecture of the Miocene carbonate buildups and platforms were described and interpreted in order to contextualize the depositional geometries and morphology observed in the seismic sections into carbonate depositional systems within an idealized facies belt (Wilson, 1975; Handford & Loucks, 1993).

Both of the Early Miocene and Late Miocene carbonate shelves described in this study were detached from the continental coastline and situated over a relatively deep shelf from more than 30 m up to few hundreds of meters as part of the middle to outer shelf. Smaller-scale slopes are found around the individual carbonate buildups and platforms. A

larger-scale continental slope related to basin-floor systems was located farther south of the Oligocene–Miocene shelf margin (Ardhana, 1993; Satyana, 2005).

The Early Miocene carbonate shelf architecture consists of buildup-core–shoal complex, buildup-flank, and inter-buildups, from shallowest to deepest settings. Inter-buildups is equivalent to open shelf. The southern area is dominated by east-west oriented, elongated, flat-topped buildups and shallow-water shoal complex with no inter-buildups area. The central area contains circular-ovoid, pinnacle buildups and a deeper inter-buildups area. The northern area consists of polygonal, flat-topped buildups and shallow-water shoal complexes with shallower inter-buildups areas (Figure 3.15).

The Late Miocene carbonate shelf architecture consists of platform interior, platform margin, slope, and open shelf, from shallowest to deepest settings. The platform interior has a flat-topped geometry formed where carbonate sediments were deposited in a very low angle dip at the platform top. The platform margin has an inflection point from the low-angle dip of the platform interior to the highly inclined slope. Rimmed platform margins may have formed by the framework builders. Escarpment-type margin were commonly observed. The slope comprises inclined and draped-to-margin strata. Some of these strata were disconnected in some degree from their corresponding platform margin, thus showing the escarpment characteristics. Open shelf is the deepest setting in the architecture, and it is characterized by mostly parallel, low-angle strata (Figure 3.16).

Growth Patterns: Initiation, Coalescence, and Amalgamation

Growth patterns of the Early Miocene carbonate buildups and the Late Miocene carbonate platforms were described based on lateral discontinuity of semblance horizon

slices and vertical seismic impressions of section sections. Both Early and Late Miocene carbonate buildups and platforms show three distinct stages of development: initiation, coalescence, and amalgamation (Figure 3.17).

Initiation is interpreted as the first stage, when associations of framework builders such as corals and red algae formed smaller patch reefs and started to colonize the favorable area of the open shelf over the JS-1 Ridge. These patch reefs, often found in clusters, then grew and coalesced to the nearby patch reefs in a cluster to form carbonate buildups or platforms (Figure 3.17).

The inter-buildups and inter-platforms area between the prograding margin of the carbonate buildups and platforms continually deposit sediments at a relatively higher rate compared to the open shelf. They then form a shallower inter-buildups and inter-platforms area, and finally, they were filled to form an amalgamated larger carbonate buildups or platforms (Figures 3.17 and 3.18).

This study shows a couple of differences in growth pattern between the Early Miocene carbonate buildups and Late Miocene carbonate platforms. The patch reefs in the Late Miocene initiation stage cover a much larger area compared to that of the Early Miocene', hence, larger, kilometer-scale carbonate platforms were formed. The amalgamation distance in the Late Miocene carbonate platforms are as much as 2 km compared to a few hundreds of meters in the Early Miocene carbonate buildups (Figures 3.17 and 3.18).

Depositional Sequences of Late Miocene Carbonate Platforms

Due to its higher resolution, depositional sequences were described and interpreted in the Late Miocene interval based on its seismic stratal pattern configuration. This was done for analyzing the development of carbonate platforms during Late Miocene time. An interpreted seismic section on one of the larger Late Miocene carbonate platforms shows at least four depositional sequences of the Late Miocene carbonate platform (Figure 3.19). Depositional sequence definition is based on seismic stratal configuration and idealized platform margin characteristics. The depositional sequence is bounded by sequence boundaries (SB) at its top and bottom, where a negative amplitude reflector overlies the bottom SB, followed by a retrograding or backstepping package that onlaps to the margin. The sequence is capped by a prograding package that shows toplaps to the top SB (Figure 3.20).

In sequence-1, the carbonate platform started to form with the initiation of smaller early platforms separated by parallel, high amplitude inter-platform deposits. These smaller platforms coalesced, forming the larger platform started in sequence-2. Development of a pinnacle carbonate buildup was observed near the end of sequence-3. Wedge-shaped deposits were observed off the eastern platform margin in sequence-3 and -4. In sequence-4, a two-way dipping deposit was observed near the toe-of-slope, 2 km off the platform margin (Figure 3.19). Channels that appear to be sinuous in plan view were observed in sequence-4 (Figure 3.22).

Contemporaneous Variation in Platform Margin Style

Within a single Late Miocene north-south oriented carbonate platform, contemporaneous development of two types of platform margin were observed (Figure 3.21). In the northern part of the platform, highly progradational platform margins were observed on both of its western and eastern margins (Section-1). Highly aggradational platform margins were also observed in the southern part of the platform, also on both the western and eastern margins (Section-2). In terms of Late Miocene interval thicknesses, there is no significant difference between the two areas. The Late Miocene interval thicknesses in both areas are approximately 300–325 ms TWT.

Geomorphic Features: Sinuous Channels

Semblance horizon and time slices show sinuous channels developed near the top of Late Miocene interval (Figure 3.22). These sinuous channels developed only on the larger, north-south oriented, elongated carbonate platforms. Smaller isolated platforms do not appear to have these channels (Figure 3.9).

Based on semblance time slices, these sinuous channels are progressively wider in younger strata, from 150–175 m wide on the 680 ms time slice to 225–335 m on the time slice 40 ms above (640 ms). Channels are also relatively wider going northward, away from the channel mouth. The channel mouth is located on the western margin of the platform and is slightly wider than the rest of the channel body. Deposits around the channel mouth appear to have originated from reworking of the sediments around the platform margin where the channel initially intruded (Figure 3.22).

DISCUSSION

Evolution of Carbonate Shelf during Miocene Times

The Miocene covers a period of more than 18 million years, from 23 to 5.3 Ma (Gradstein et al., 2012), which is part of the extensive history of Cenozoic carbonate sedimentation in the Southeast Asia region (Wilson, 2002). The study area is situated in an active tectonic margin of southeastern Sundaland, a convergence margin between the Eurasian and Indo-Australian plates influenced by multiple subductions and eastward collisional tectonics (Hall, 2002; Johansen, 2003). Depositional sequences of the Early and Late Miocene carbonate formations and the siliciclastic-dominated formation in the Middle Miocene constitute the East Java depositional cycles (Kenyon, 1977) and the regional Neogene transgressive cycle in convergent plate boundaries of the Southeast Asia region (Fulthorpe & Schlanger, 1989).

This study shows that the carbonate shelf in the study area has evolved from the Early Miocene carbonate shelf of the Kujung Formation dominated by smaller-scale carbonate buildups development to the Late Miocene carbonate shelf of the Wonocolo Formation consists of larger-scale carbonate platforms. An interval in the Middle Miocene, regionally known as the Tuban-Rancak and Ngrayong Formation, dominated by marine siliciclastic deposits, separates the two formations.

The Early Miocene carbonate formation age range, based on strontium isotopes dating from Chapter 2, is 23–20.4 Ma (Aquitanian), or approximately 2.6 m.y. in duration. This formation is equivalent to the Kujung unit-1 carbonate in the East Java area (Kenyon, 1977; Carter et al., 2005; Maynard & Morgan, 2005; Posamentier et al., 2010). This

excludes the Kujung unit-2 that was described as and included in the Miocene buildups in the North Madura Platform area (Posamentier et al., 2010). The age range of the Wonocolo Formation (based on limited data) is 12–6 Ma, or approximately 6 million years in duration (Mudjiono & Pireno, 2002), equivalent to Tortonian–Messinian age. This study demonstrates that the main differences between the two formations are their depositional geometries (size and orientation) and architectures. For the Late Miocene, the term "carbonate platform" was used instead of "carbonate buildup" because of its distinctive flat-topped geometry with kilometer-scale dimension compared to the Early Miocene carbonate buildups.

Carbonate shelves in the study area have evolved from a shelf characterized by west-southwest – east-northeast elongated to circular isolated carbonate buildups in the Early Miocene to a shelf dominated by north-south elongated flat-topped carbonate platforms in the Late Miocene. The Early Miocene carbonate buildups are 500 m to 2 km wide and ≤ 8 km long, whereas the Late Miocene carbonate platforms are as much as more than 5 kilometers wide and more than 20 km long. Each of these carbonate formations can reach a total thickness of 1,100–1,200 ft. The size, circular nature of the buildups, and elongated buildups pattern influenced by oceanic circulation of the Early Miocene carbonate buildups in the JS-1 Ridge appear to be similar and comparable to those of the North Madura Platform (Figure 3.12; Maynard & Morgan, 2005; Ruf et al., 2008; Posamentier et al., 2010). The north-south orientation of the Late Miocene carbonate platforms was observed even farther regionally, stretching more than 1,000 km, from offshore West Java to the East Java Sea (Figure 3.13). These Late Miocene formations

include the Parigi Formation of West Java (Burbury, 1977; Carter & Hutabarat, 1994) and the Wonocolo Formation of the North Madura Platform area (Mudjiono& Pireno, 2002; Adhyaksawan, 2003; Posamentier et al., 2010).

In terms of areal coverage, the Late Miocene carbonate platforms were deposited over approximately 400 km^2, more than twice the areal coverage of the Early Miocene carbonate buildups that cover a total area of approximately 180 km^2, if the southern area shoal complexes are excluded (Figure 3.10 and Figure 3.11). Similar comparison was described in the North Madura Platform area between Kujung-1 and Wonocolo carbonate buildups (Posamentier et al., 2010). The Early Miocene carbonate buildups were distributed following the northeast-southwest orientation of the basement high structure of the JS-1 Ridge. The Late Miocene carbonate platforms, in contrast, do not indicate a major influence from the antecedent topography (Figure 3.14).

The architecture of the Early Miocene carbonate shelf is relatively more complex than that of the Late Miocene carbonate shelf. Geometries of the carbonate buildups seem to have a strong influence from the antecedent topography or even differential subsidence along the open shelf of the JS-1 Ridge. The central area resembles a saddle zone, where the inter-buildups area appears to be deeper and carbonate buildups develop in pinnacle shape. Carbonate buildups in the northern and southern areas developed a flat-topped geometry with the presence of shallow-water shoal complexes with relatively shallow inter-buildups areas. In the southern area, the shoal complex that covers approximately 340 km^2 of area (Figures 3.8 and 3.10) is interpreted to be the back-reef area associated with the barrier-reef system that extends from the Ujung Pangkah area to the southern margin

of the North Madura Platform. In the northern area, shoal complexes are interpreted to be associated with the interior of the large polygonal buildups (Figure 3.10). In the Late Miocene carbonate shelf, several kilometers-scale, north-south elongated carbonate platforms developed over the open shelf. Its architecture, from shallowest to deepest, consists of platform interior, platform margin, slope, and open shelf (Figures 3.15 and 3.16).

Despite the differences in depositional geometries and architectural elements between the two formations, they demonstrate a similar growth pattern in their development of initiation, coalescence, and amalgamation stages, as was previously described in the Early Miocene carbonate buildups of the northeast area of the North Madura Platform (Ruf et al., 2008; Posamentier et al., 2010). The depositional sequences of the Late Miocene carbonate buildups are also similar to that demonstrated in the growth phases of Wonocolo platforms in the North Madura Platform (Adhyaksawan, 2003). Geomorphic features described as tidal creeks with smaller dimensions (less than 100 meters wide) were also developed on the top of Wonocolo platforms in the northeastern North Madura Platform (Posamentier et al., 2010). The Late Miocene carbonate platforms were terminated and then overlain by southward-prograding sequences of mixed shale, sandstones, and carbonates (Carter et al., 2005). This termination of the Late Miocene carbonate platforms is interpreted to be a regional event, similar to that shown in the Segitiga Platform, Natuna Sea, several thousand kilometers northwest of the study area (Bachtel et al., 2004).

Morphological Comparison with Modern and Ancient Carbonate Platforms

The size of the Early and Late Miocene carbonate buildups in the study area ranges from few hundreds of meters to few tens of kilometers in width or length. The shape of the buildups and platforms varies from circular-ovoid, polygonal, to highly-elongated platforms. Figure 3.24 shows the comparison between carbonate buildups and platforms in the study area with the well-known Modern Bahamian Platform, the Permian Central Basin Platform, and the Carboniferous Tengiz Buildups Complex (Collins et al., 2006). It is clear that these modern and ancient carbonate platforms are much different in term of size and shapes, which in turn suggest different controls on their development.

However, when other Miocene carbonate buildups and platforms are plotted with those of the study area (Figure 3.25), they show comparable size and shapes. Outlines of carbonate buildups and platforms from Segitiga Platform and Luconia Platform in NW Borneo (Bachtel et al., 2004; Koša et al., 2015), Browse Basin in NW Shelf of Australia (Bachtel et al., 2011; van Tuyl et al., 2018), and Zincir Kaya and Pirinc Platform in Mut Basin, Turkey (Bassant et al., 2004), demonstrated hundreds-of-meters to tens-of-kilometers, circular-ovoid, polygonal, to elongated shapes. Unlike the buildups and platforms of Segitiga Platform and Luconia Platform in the north and Browse Basin in the south, Late Miocene carbonate platforms in the study area show strong evidence of consistent north-south elongation of the platforms over wide area, from offshore West Java to offshore East Java and further eastward in the East Java Sea. Carbonate platforms in NW Borneo (Segitiga and Luconia Platforms) are strongly controlled by structural grains of the basement (Bachtel et al., 2004; Koša et al., 2015). Carbonate buildups in the Browse Basin, NW Shelf of Australia seem to develop in radial pattern over a tectonically less-active region (Bachtel et al., 2011; van Tuyl et al., 2018).

Figure 3.26 shows satellite images of modern carbonate shelf that are influenced by different controls. Five kilometers scale bars are posted on each figures. Torres Reefs that are situated in the Torres Strait (Figure 3.6 A), between northern part of Australia and southern part of Papua New Guinea, are characterized by convex-shaped, highly-elongated in west-east direction, coral reefs and shoals. Morphology of Torres Reefs is highly influenced by strong tidal flows (Jones, 1995). The Belize shelf (Figure 3.26 B) consists of rhomboid-shaped shoal and reef complexes, which are influenced by paleo-fluvial systems drainage patterns (Esker et al., 1998). The shelf in Red Sea (Figure 3.26 C), north of Jeddah, consists of fault-controlled, north-south oriented, carbonate shoal and reef complexes. Reef complexes to the east of Selayar Islands, northeast of the Flores Sea (Figure 3.26 D), shows carbonate shoal and reef complexes that are intersected by numerous north-south to northeast-southwest intra-platform channels. These channels are interpreted to be the conduit of sea water circulation influenced by tidal and oceanic current from the surrounding oceans.

Influence of Compressional Tectonic Events and Paleo-Indonesian-Through-flow

Controls on the development of carbonate buildups and platforms can be subdivided on the basis of their geographic scale of influence (Lukasik & Simo, 2008). Comparing the results of the study to previous studies in the region, it appears that the evolution of the Early to Late Miocene carbonate shelf may have had a strong regional influence. Five main controls on the development of carbonate shelf during Miocene times in the study area were identified and inferred, based on interpretation of the depositional geometries, architecture, growth pattern, depositional sequences, and geomorphic features of the carbonate buildups and platforms. Dominant controls on the carbonate shelf development include regional compressional tectonism in the Miocene, oceanic circulation

pattern influenced by the development of the Indonesian Through-flow (ITF), third- to fourth-order global sea-level fluctuations, antecedent topography, and differential subsidence.

Tectonic events is one of the dominant controls in carbonate shelf development that have regional geographic scale (Lukasik & Simo, 2008). The East Java region underwent compressional tectonic during the Miocene, from initial inversion in the Early Miocene to intense compression toward the Miocene-Pliocene boundary (Figure 3.28, Figure 3.29, Johansen, 2003; Pubellier & Morley, 2014). The change in orientation of Miocene carbonate buildups and platforms, from west-east to north-south, may have been influenced by Borneo's counter-clockwise rotation prior to Late Miocene (Hall, 1997).

Toward the end of the Miocene, depositional and geomorphic features such as flat-topped carbonate platforms, progradational platform margins, and sinuous channels, strongly suggest a condition of decreasing accommodation. The fact that the Early and Late Miocene intervals have a relatively similar thickness of approximately 335–365 meters (1,100–1,200 feet), despite the latter's depositional duration being more than double the former's (6 m.y. in the Late Miocene, 2.6 m.y. in the Early Miocene), supports this interpretation. Assuming the accommodation was filled by carbonate buildups and platforms, accumulation rates can represent the rate of accommodation creation. The approximate accumulation rates are 14 cm/k.y. in the Early Miocene and 6 cm/k.y. in the Late Miocene. The condition of decreasing accommodation is interpreted to have been caused by regional compression and tectonic inversion during a period of relatively low amplitude global sea-level fluctuation.

The development of sinuous channels in the younger sequences of the Late Miocene carbonate platform is interpreted to be analogous to that of the Late Cretaceous Top Natih Formation in Oman (Figure 3.23; Grélaud et al., 2010). These sinuous channels are interpreted to be tidal channels based on their size when compared to the incised valley fills. They were formed when the carbonate platforms were periodically emergent, and they have ravinement surfaces, as demonstrated by widening channels on younger strata (Figure 3.22). In the North Madura Platform area, top of the Wonocolo carbonate platforms were influenced by subaerial exposure and meteoric diagenesis during later phases of their growth history (Adhyaksawan, 2003). The Late Miocene's intensified compression that decreased accommodation, because of a gradual decrease on subsidence rate, or even uplift in some areas, happened over a relatively several million years' period in the Late Miocene, possibly within a third-order sequence. In the slope to open shelf area, in an interval younger than sequence-4, a mounded feature that downlaps in both directions was observed (Figure 3.19). This might be related to a lowstand event that ultimately followed the decreasing accommodation period in the Late Miocene.

The regional trend of north-south-trending elongated carbonate platforms that was observed over a wide area for hundreds of kilometers (from western to eastern, offshore of present-day Java Island). This suggests that the morphology Late Miocene carbonate platforms were influenced by a regional control (Figures 3.13 and 3.14). The development of the Indonesian through-flow (ITF) because of the formation of the Makassar Strait might have generated a strong north-south oceanic circulation pattern from the Pacific Ocean in

the north to the Indian Ocean in the south (Kuhnt et al., 2004), which could act as the regional control on the Late Miocene carbonate platform morphology.

In sequence-3 and sequence-4 of the Late Miocene carbonate platforms, wedge-shaped seismic features were observed (Figure 3.19). These features are interpreted to have formed during periods of falling sea-level as forced-regressive deposits and were strongly influenced by global sea-level fluctuations in the Late Miocene (Haq et al., 1987; Miller et al., 2005), which was happening within a higher-order (shorter durations) compared to regional tectonic subsidence or uplift.

The Early Miocene carbonate buildups were distributed following the northeast-southwest orientation of the basement high structure of the JS-1 Ridge. In contrast, the distribution of the Late Miocene carbonate platforms does not reflect major influence from the antecedent topography (Figure 3.14). Carbonate buildups with pinnacle geometry in the central area that are comparably thicker (100–200 ft thicker) suggest that subsidence rate might have been higher in the central area compared to that of the northern and southern areas of the JS-1 Ridge.

The contemporaneous development of significantly different platform margin styles, aggradational in the south and progradational to both direction, west and east, in the north (Figure 3.21), can be explained by two scenarios: 1) differential subsidence, where the southern part has undergone a higher subsidence rate than that in the northern part of the platform, and 2) as the result of sediment-dispersal patterns due to windward-leeward margin asymmetry (Handford & Loucks, 1993).

The challenge in explaining the first scenario is that there is no significant thickness difference in the carbonate platforms between the aggradational southern part and the progradational northern part. The interval thickness in both areas of the platform is approximately 325 ms TWT. Ideally, the aggradational southern part of the platform, if it has undergone a much higher subsidence rate, and yet still maintained its flat-topped morphology, should have deposited thicker interval due to higher accommodation. The challenge in explaining the situation by using the second scenario is that the windward-leeward directions are usually perpendicular to the long axis of the carbonate platform, not parallel, as was observed in the study area (Figure 3.21). Thus, there might be a combination of differential subsidence and sediment-dispersal patterns due to current reworking that influenced the contemporaneous development of an aggradational margin in the southern part and a progradational margin in the northern part of the carbonate platform.

CONCLUSIONS

In the study area, two distinctive carbonate formations can be described and interpreted in detail in term of their depositional geometries, architecture, growth pattern, depositional sequences, and geomorphic features. By utilizing 3D seismic geomorphology techniques, spectacular three-dimensional images of the carbonate buildups and platforms were generated.

Based on seismic geomorphology, the Early Miocene carbonate shelf is characterized by circular, E-W elongated to polygonal buildups, 0.5–2 km wide and ≤ 8 km long. The Late Miocene carbonate shelf is characterized by N-S elongated to oval

shaped, flat-topped-like carbonate platforms, 5–8 km wide and ≤ 20 km long. Both intervals can attain thickness of 1,100–1,200 ft, and both demonstrated development in three stages: 1) initiation, 2) coalescence, and 3) amalgamation. Early Miocene carbonate buildup distribution follows the basement structure, but Late Miocene carbonate platform distribution does not.

Sinuous tidal channels developed over larger platforms near the end of the Miocene. These tidal channels were not observed in the smaller platforms. Variation in margin style on a single platform, prograding in the north, aggrading in the south, may suggests higher subsidence rates southward. This indicates the syn-depositional tectonic deformation of the shelf during the intense compressional regime in the Late Miocene. Growth faults were also observed on the inter-platform area. The details observed in the Late Miocene carbonate platforms suggest that, toward the end of Miocene time, the shelf underwent decreasing accommodation marked by development of sinuous tidal channels and wedge-shaped deposits of forced-regression strata, mainly caused by the regional tectonic inversion during the Miocene compressional regime. The regional trends in north-south elongated platforms also suggest control of regional oceanic circulation. Geometrically, the Late Miocene carbonate platforms are potential reservoirs with significant capacity if the reservoirs are supported by a good source and seal.

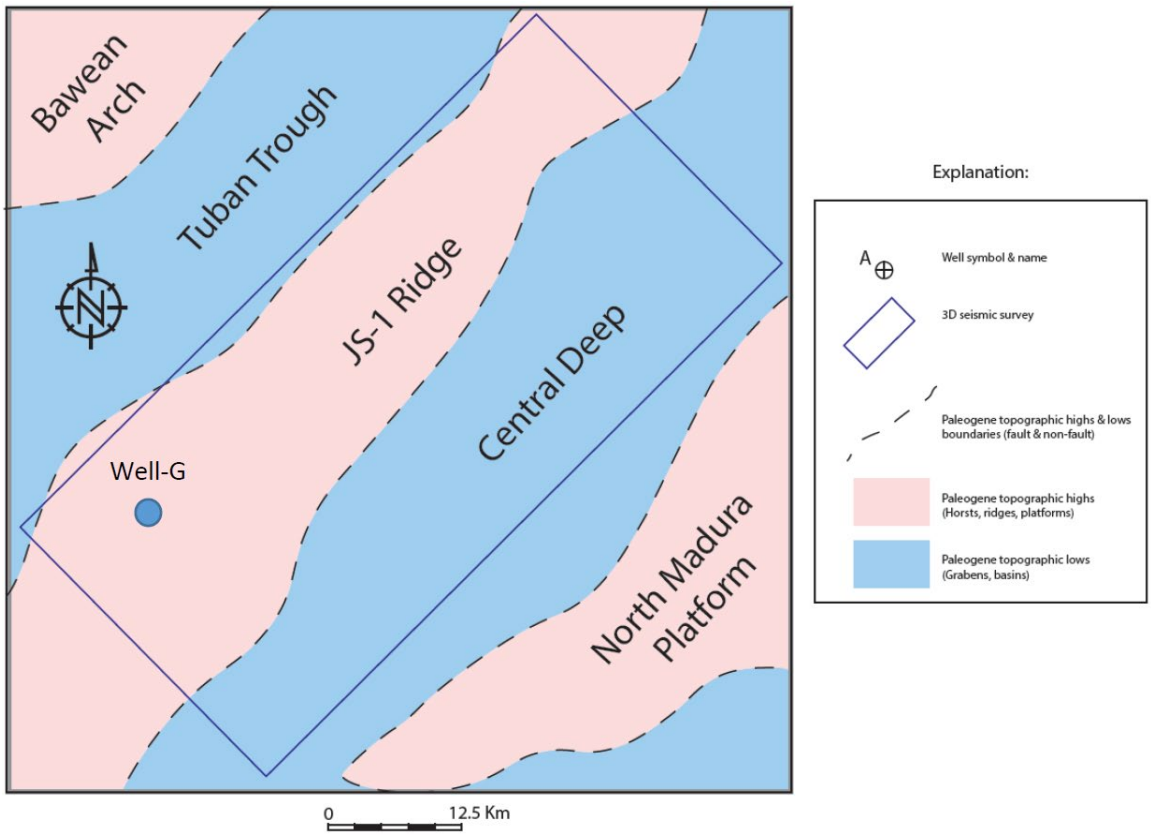

Figure 3.1. Base map of the 3D seismic data used in this study. The seismic data cover both the JS-1 Ridge as a paleo-high and the Central Deep as a paleo-low in the study area.

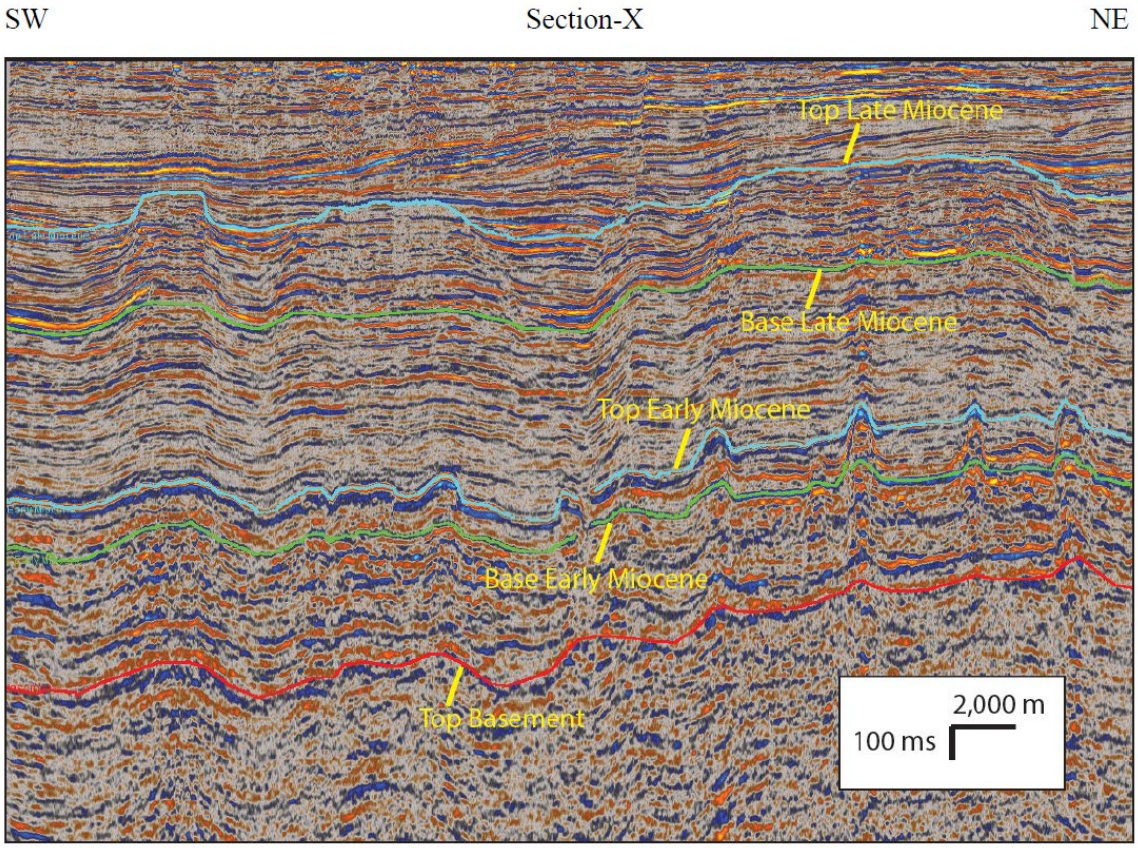

Figure 3.2. Five seismic horizons interpreted in this study shown in a southwest-to-northeast seismic section (Section X). They are, from oldest to youngest, Top Basement, Base Early Miocene, Top Early Miocene, Base Late Miocene, and Top Late Miocene seismic horizons. Well-to-seismic tie was based on a previous study (Carter et al., 2005). Top Early Miocene and Top Late Miocene seismic horizons represent the two carbonate formations present during the Miocene. Location of section refer to Figure 3.8 and Figure 3.9.

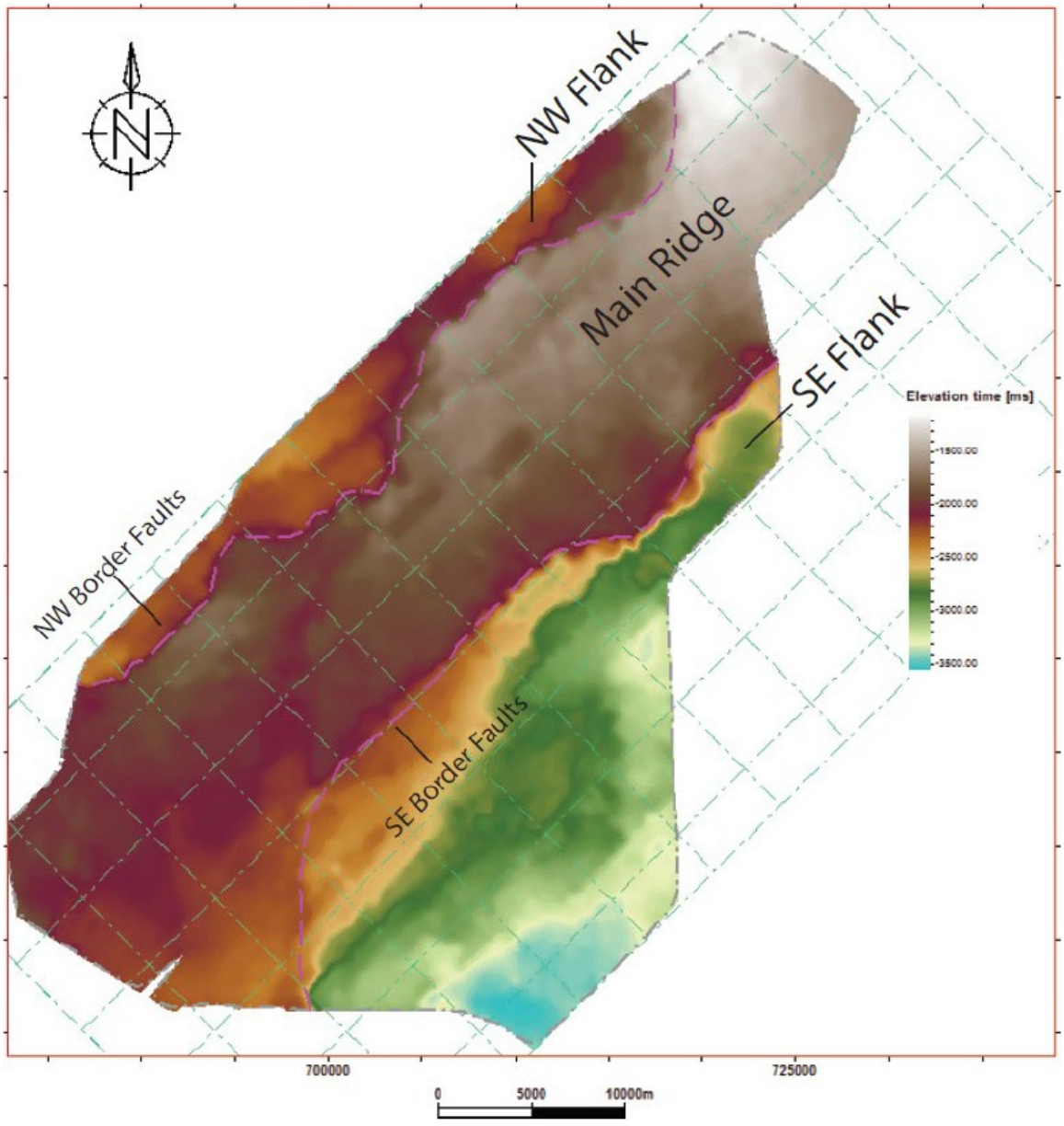

Figure 3.3. Basement structural configuration of the study area shown in a time structure map of the Top Basement. The JS-1 Ridge is subdivided into three main areas, the northwest-southeast trending main ridge, and the northwest and southeast flanks on both sides. Border faults system (normal faults) separate the main ridge from the flanks on both sides.

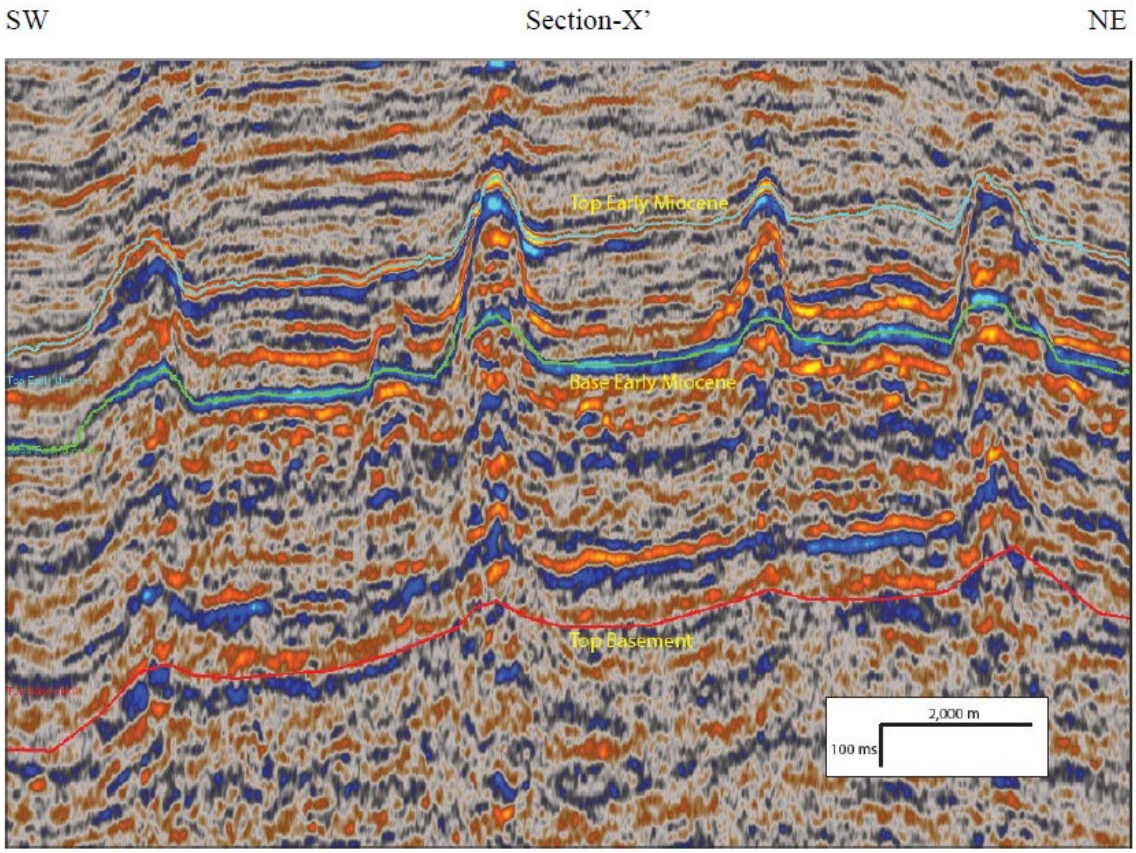

Figure 3.4. Close-up view of the Early Miocene carbonate-dominated interval shown in the southwest-to-northeast seismic section (Section X′, zoomed-in version of Section X). Four pinnacle carbonate buildups, more than a kilometer wide, are laterally distributed somewhat evenly within the Early Miocene interval across the seismic section. Location of section refer to Figure 3.8 and Figure 3.9.

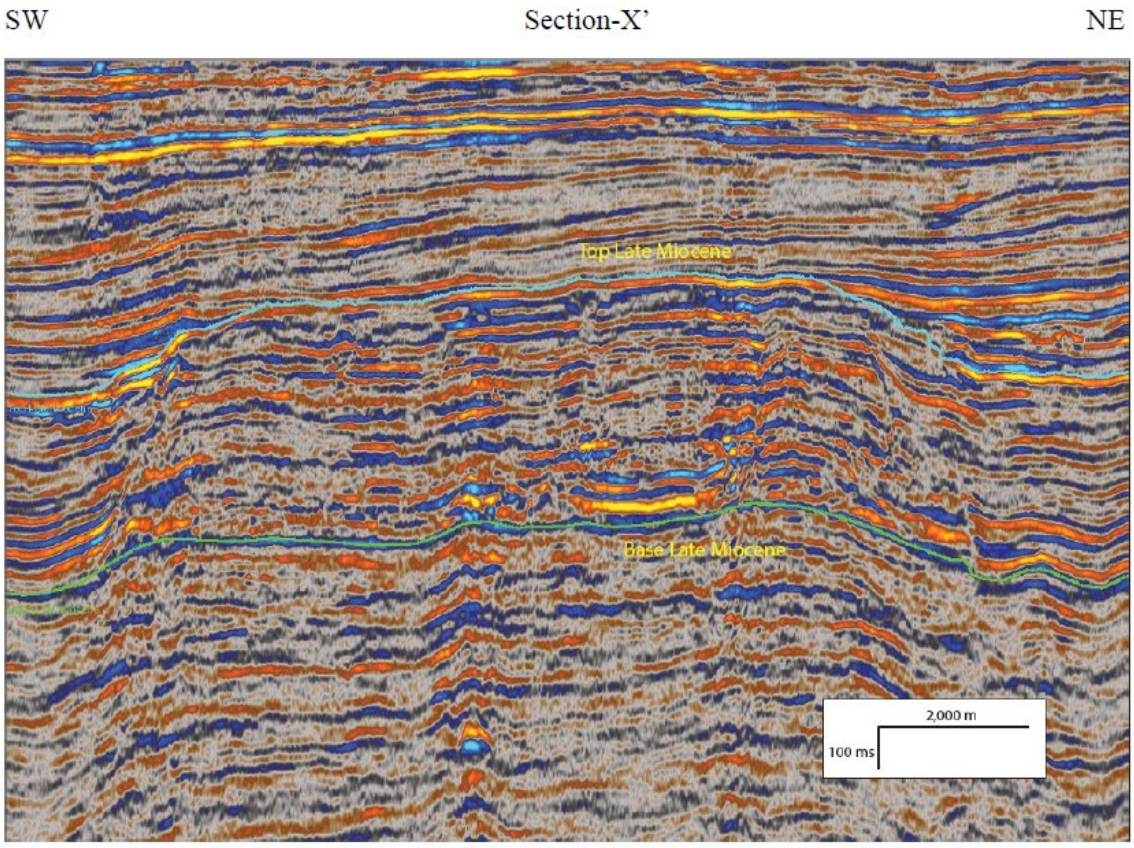

Figure 3.5. Close-up view of seismic characteristics of the Late Miocene carbonate-dominated interval shown in a southwest-to-northeast seismic section (Section X′, zoomed-in version of Section X). One large carbonate platform, more than 5 km wide, can be clearly observed within the Late Miocene interval in this seismic section. Location of section refer to Figure 3.8 and Figure 3.9.

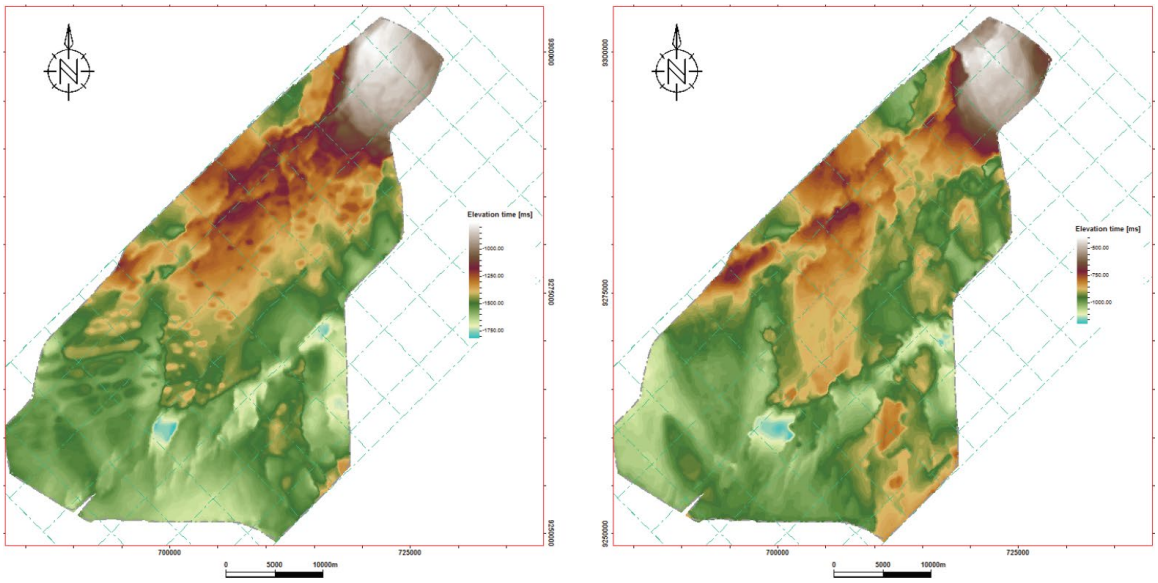

Figure 3.6. Time structure maps of the Top Early Miocene or top of the Kujung Formation (left) and Base Late Miocene or base of the Wonocolo Formation (right). The full scale bar is 10 km. The color scale was adjusted for each of the maps, white being the shallowest, blue being the deepest subsurface depth in milliseconds two-way time (TWT) domain. These time structure maps were used in horizon slicing of the semblance seismic attribute volume. Top Late Miocene or top of the Wonocolo Formation is a diachronous event and therefore was not used in regional horizon slicing.

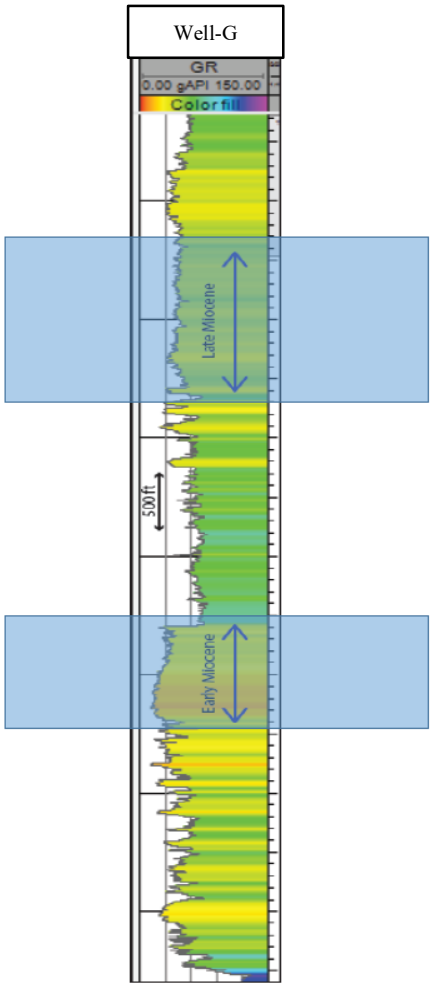

Figure 3.7. Carbonate sequences of the Early Miocene (lower blue box) and Late Miocene (upper blue box) intervals characterized by low gamma-ray log values in Well-G. Both intervals can reach total thickness of more than 1,000 ft.

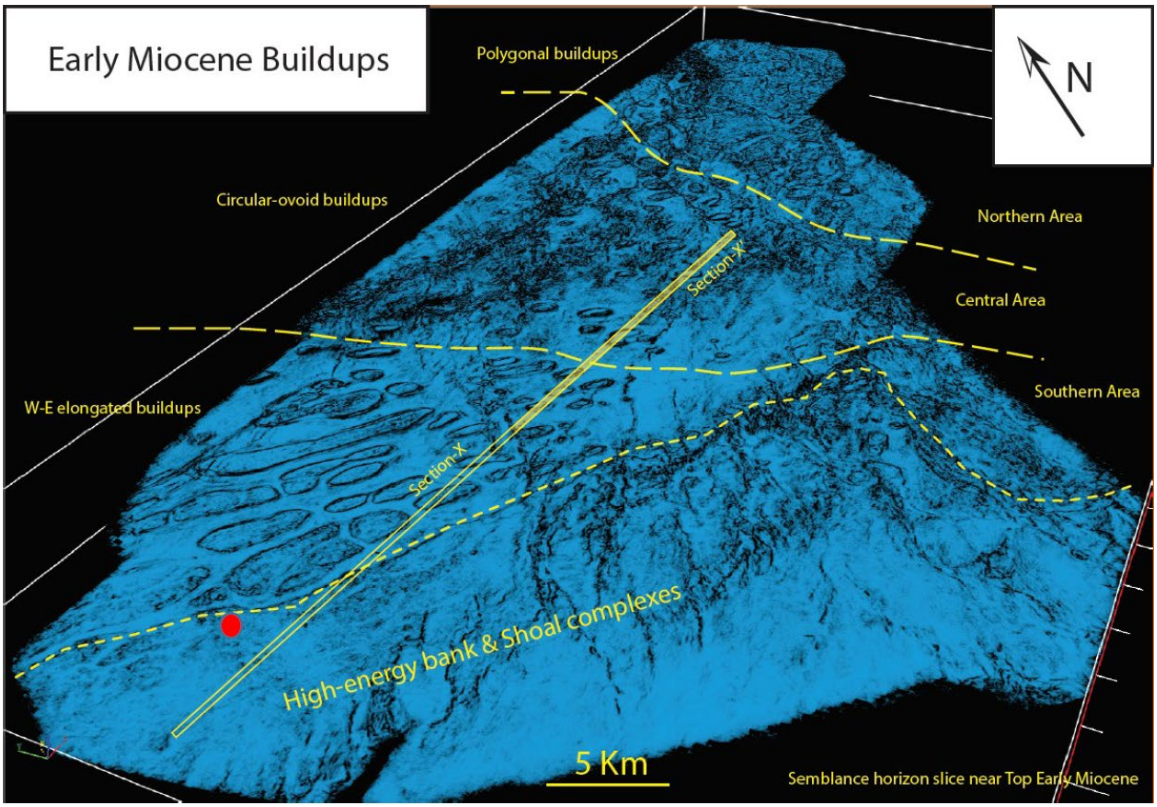

Figure 3.8. Distribution of smaller carbonate buildups in the Early Miocene carbonate shelf shown in perspective view of a horizon slice near the Top Early Miocene of the semblance seismic attribute. Well-G location is marked by a red circle.

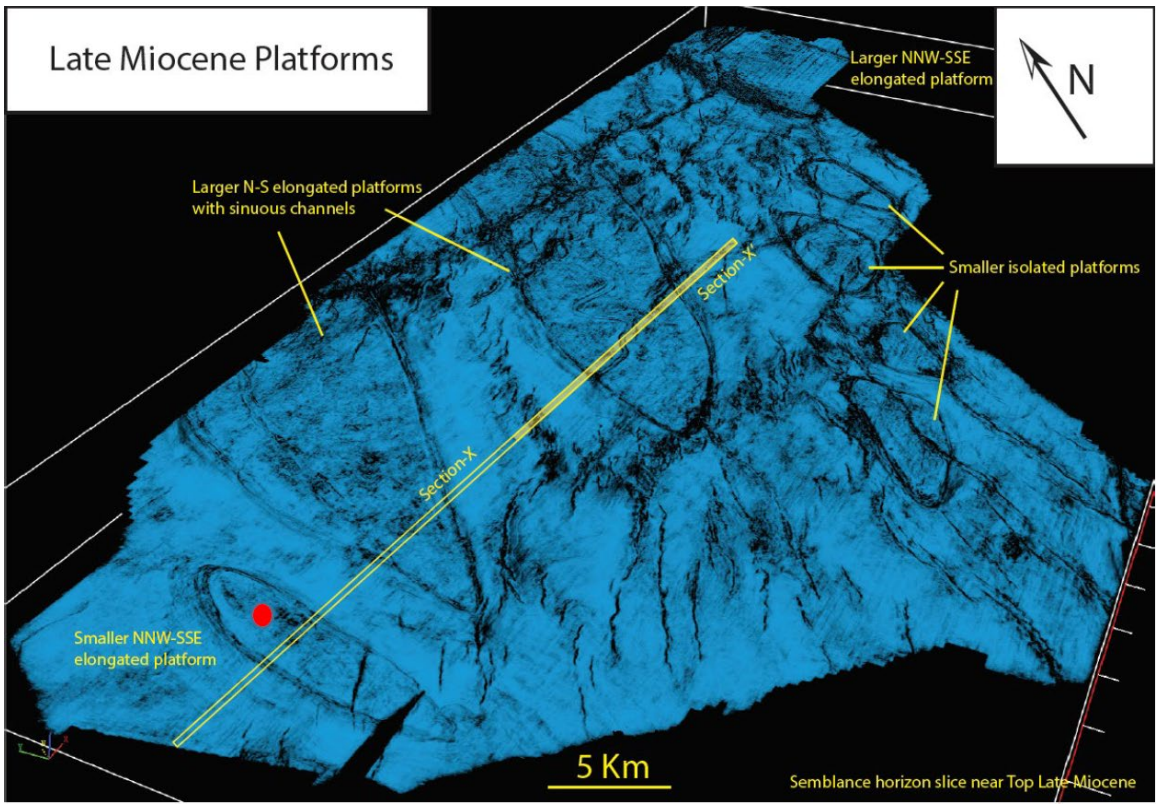

Figure 3.9. Distribution of larger carbonate platforms in the Late Miocene carbonate shelf shown in perspective view of a horizon slice near the Top Late Miocene of the semblance seismic attribute. Well-G location is marked by a red circle.

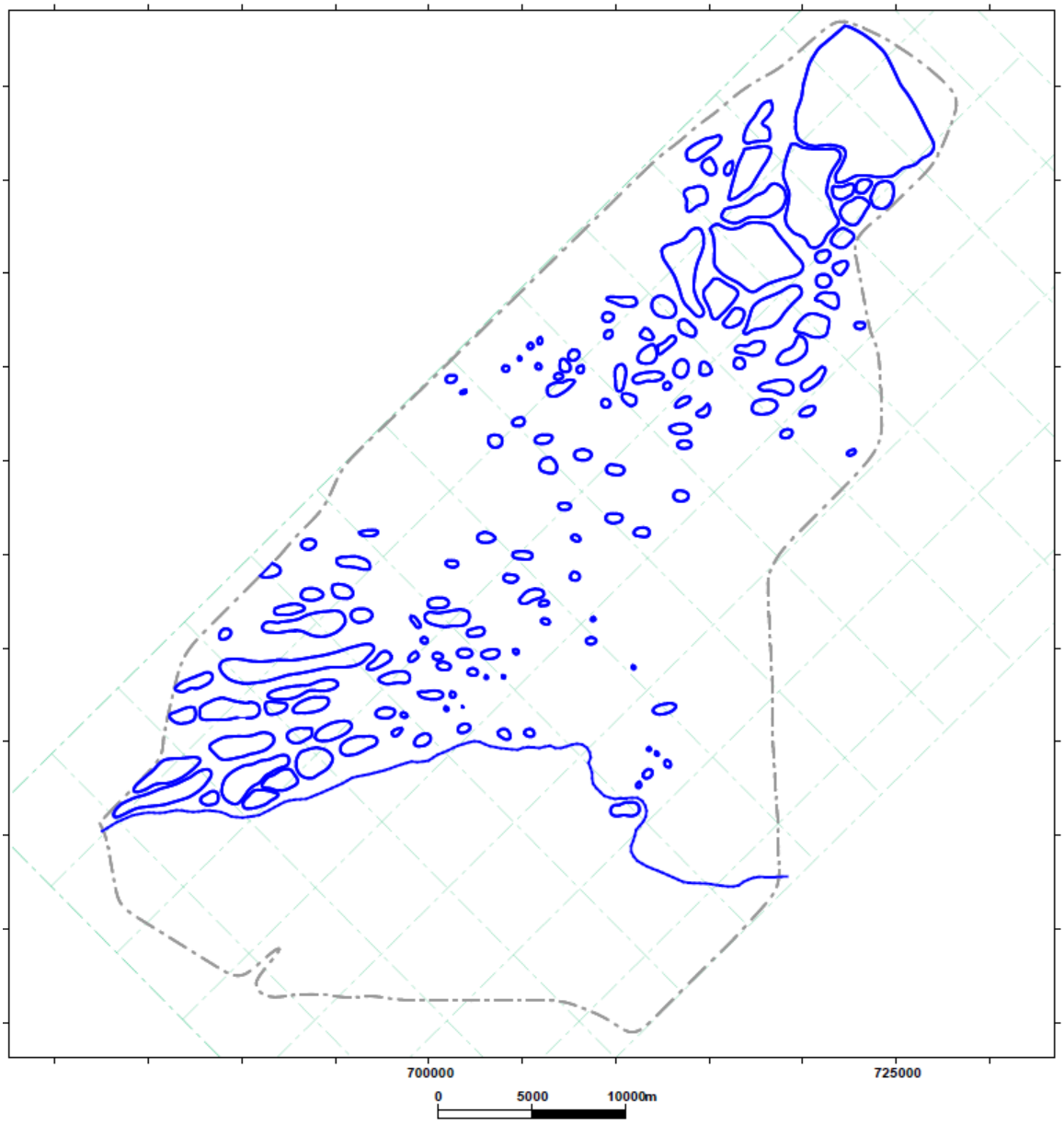

Figure 3.10. Outlines of the Early Miocene carbonate buildups delineated based on horizon slicing of the semblance seismic attribute. About 150 individual carbonate buildups ≤ 2 km wide were delineated. Blue line in the southern area marked the limit of the area containing possible shoal complexes.

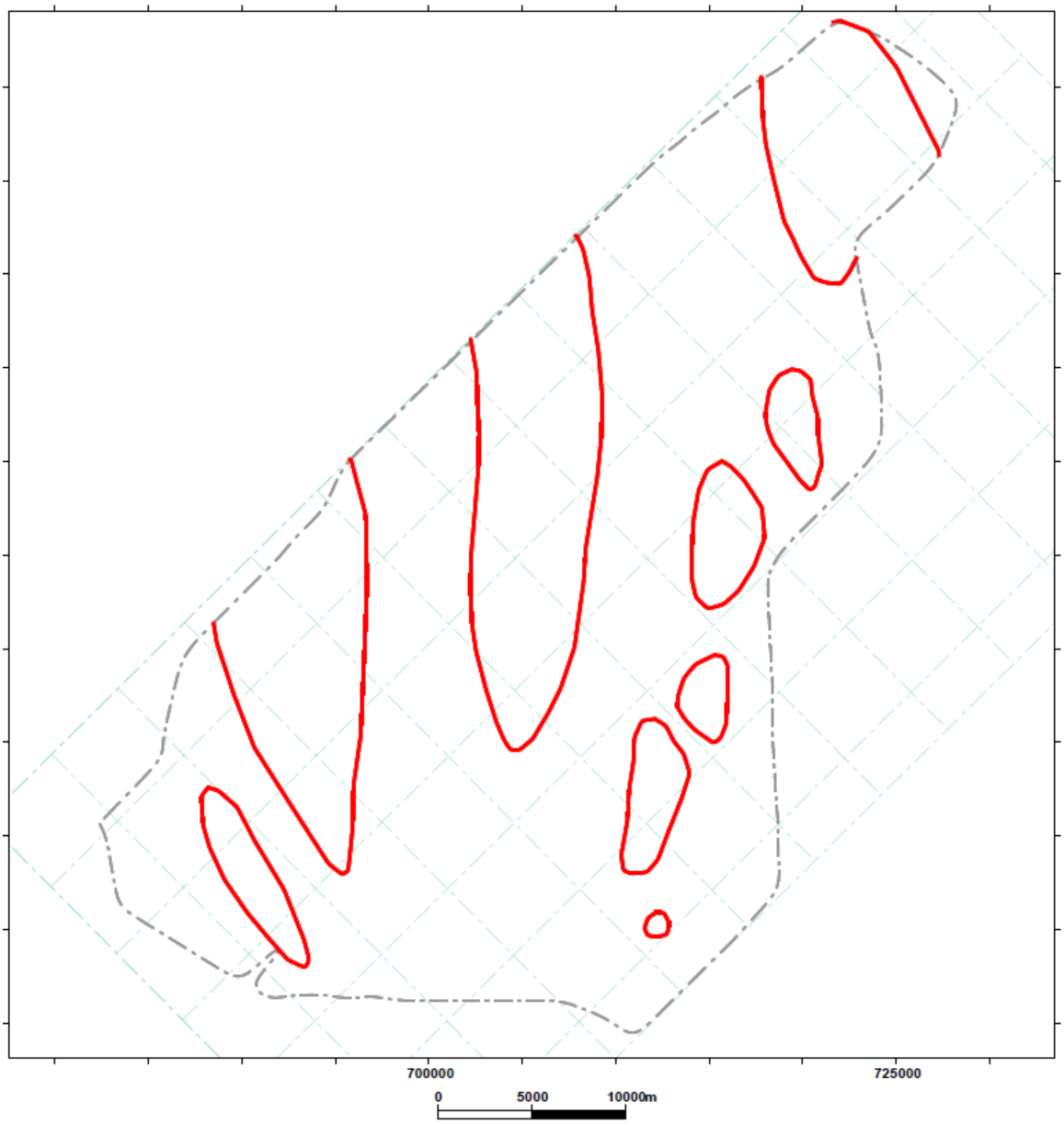

Figure 3.11. Outlines of the Late Miocene carbonate platforms delineated based on horizon slicing of the semblance seismic attribute. Nine individual carbonate platforms ≤ 8 km wide were delineated.

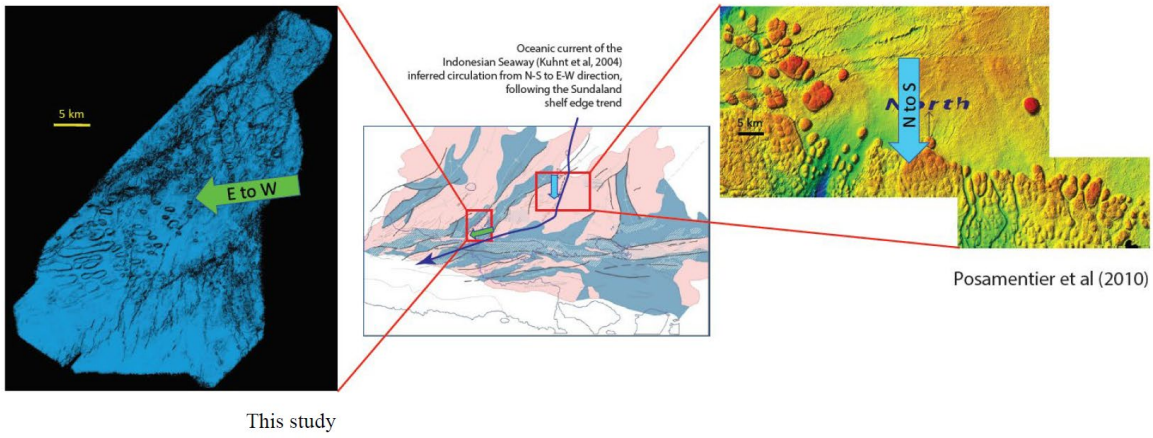

Figure 3.12. Depositional geometries of the Early Miocene carbonate buildups in the northeast area of the North Madura Platform (right; Posamentier et al., 2010) and the JS-1 Ridge (left; this study) based on seismic interpretation. The orientation of elongated carbonate buildups is interpreted to be strongly influenced by the oceanic current of the Indonesian Seaway (Kuhnt et al., 2004). Oceanic circulation (blue line) is inferred to have switched from north-south in the northeast area of the North Madura Platform to east-west in the southern area of the JS-1 Ridge, possibly following the Sundaland shelf edge orientation in the Early Miocene.

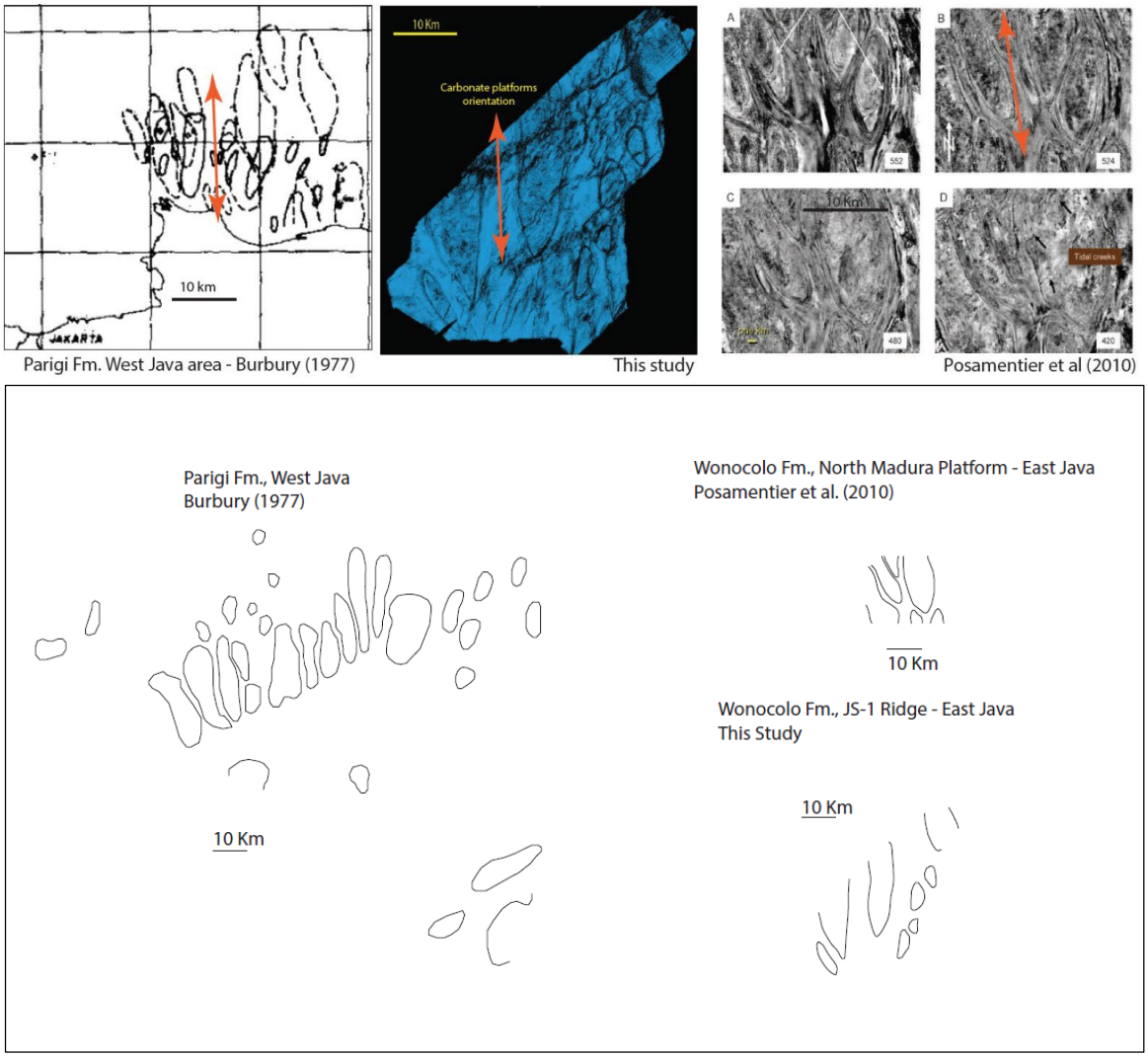

Figure 3.13. Depositional geometries of the Late Miocene carbonate platforms in the northeast area of the North Madura Platform (right; Posamentier et al., 2010), the JS-1 Ridge area (middle; this study), and offshore West Java area near Jakarta (left; Burbury, 1977) based on seismic interpretation. Lower figure shows platform outlines plotted in the same scale. The north-south orientation of carbonate platforms is a regional trend and is interpreted to be strongly influenced by the oceanic current of the Indonesian Through-flow (ITF) caused by the formation of the Makassar Strait in the Late Miocene (Kuhnt et al., 2004).

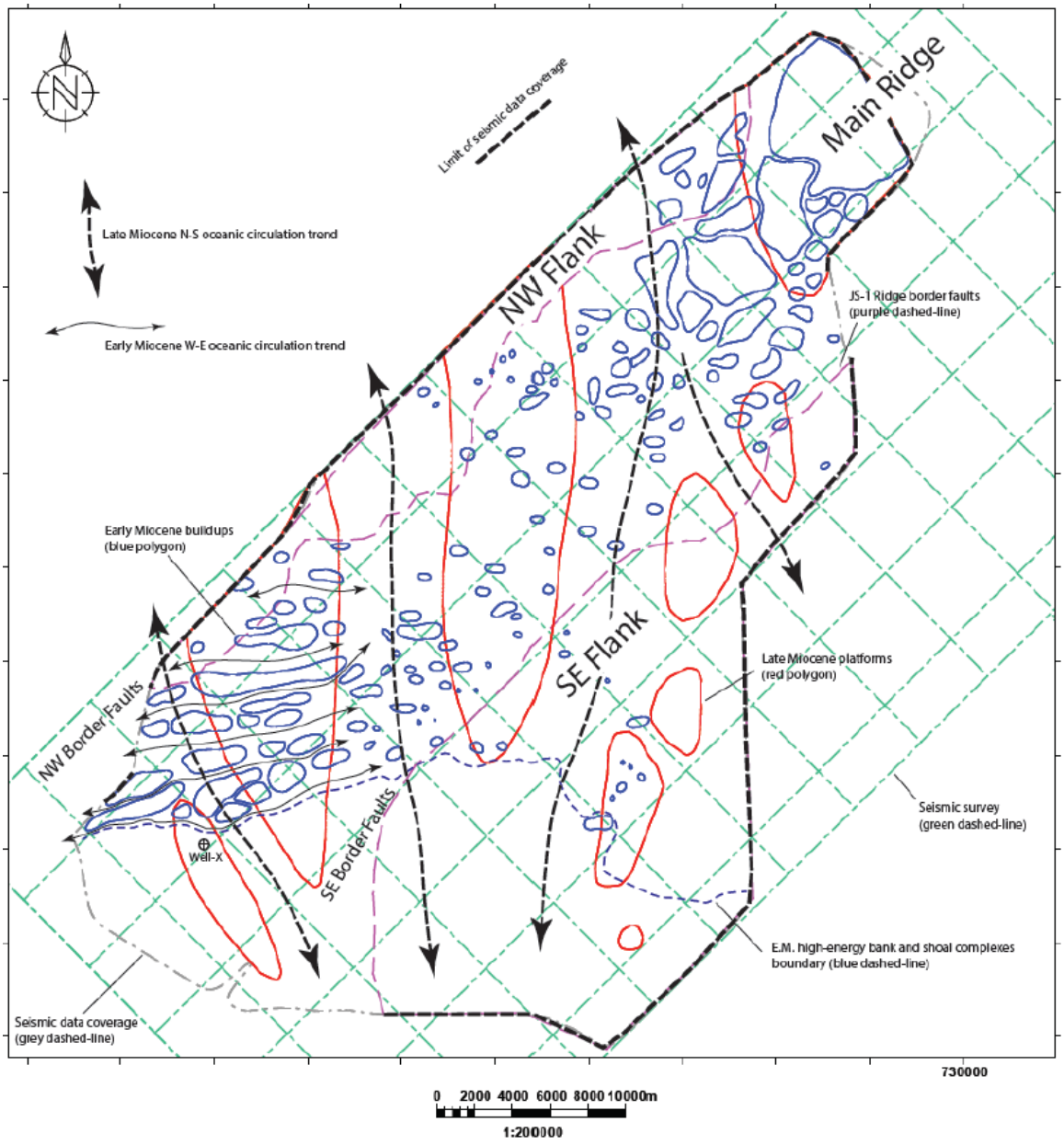

Figure 3.14. Outlines of the Early Miocene carbonate buildups (blue) and the Late Miocene carbonate platforms (red) were overlain. Interpretation of the oceanic circulation patterns in the Early and Late Miocene carbonate shelf was based on carbonate buildups and platforms orientation. In the Early Miocene, the carbonate buildups in the southern area were elongated west-east. In the Late Miocene most of the larger carbonate platforms were oriented north-south.

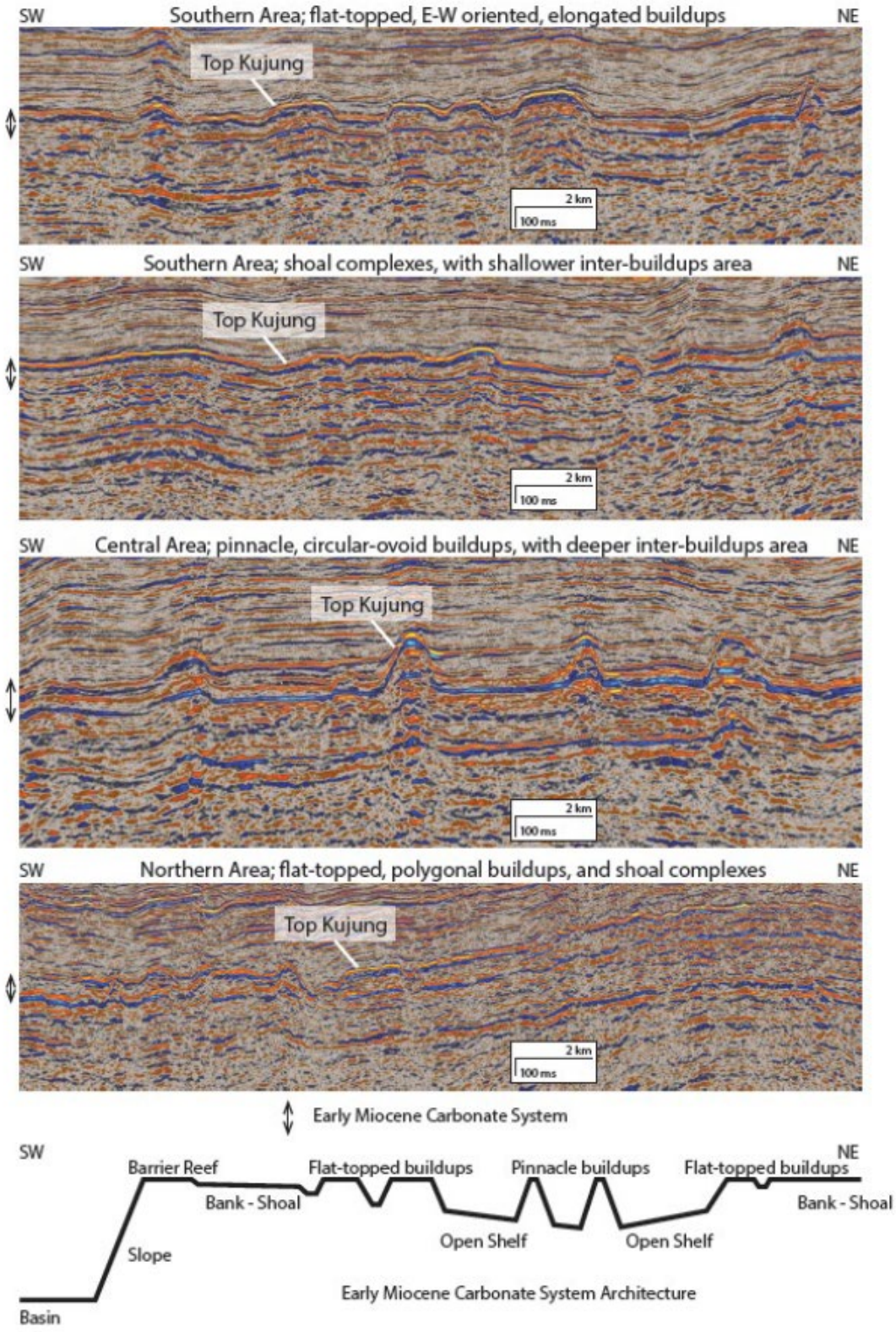
SW
Southern Area; flat-topped, E-W oriented, elongated buildups
NE
Top Kujung
2 km
100 ms
SW
Southern Area; shoal complexes, with shallower inter-buildups area
NE
Top Kujung
2 km
100 ms
SW
Central Area; pinnacle, circular-ovoid buildups, with deeper inter-buildups area
NE
Top Kujung
2 km
100 ms
SW
Northern Area; flat-topped, polygonal buildups, and shoal complexes
NE
Top Kujung
2 km
100 ms
Early Miocene Carbonate System
SW
NE
Barrier Reef
Flat-topped buildups
Pinnacle buildups
Flat-topped buildups
Bank - Shoal
Bank - Shoal
Slope
Open Shelf
Open Shelf
Basin
Early Miocene Carbonate System Architecture

Figure 3.15.

Figure 3.15. Architecture of the Early Miocene carbonate shelf over the JS-1 Ridge. Elongated and polygonal flat-topped carbonate buildups with shoal complexes developed in the southern and northern areas. Circular-ovoid pinnacle carbonate buildups are distributed in the central area. Simplified architecture in the lower figure is not to scale. The deepest part of the shelf is interpreted to be around 30–50 m.

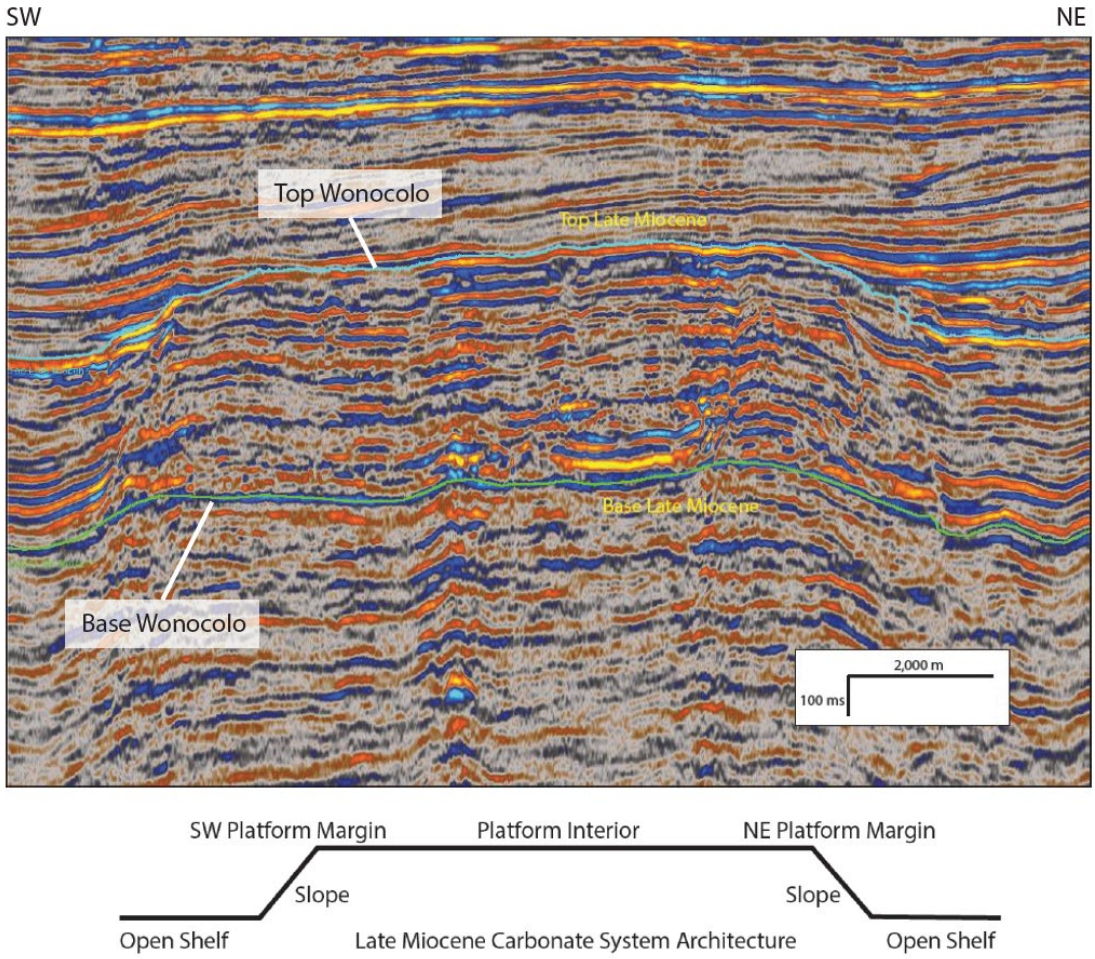

Figure 3.16. Architecture of the Late Miocene carbonate shelf characterized by flat-topped carbonate platform more than 5 kilometers wide. Platform interior, platform margin, slope, and open shelf to basin characterized the architecture of this carbonate shelf from shallower to deeper depositional environments. Simplified architecture in the lower figure is not to scale. The deepest part of the open shelf is interpreted to be approximately 30 m.

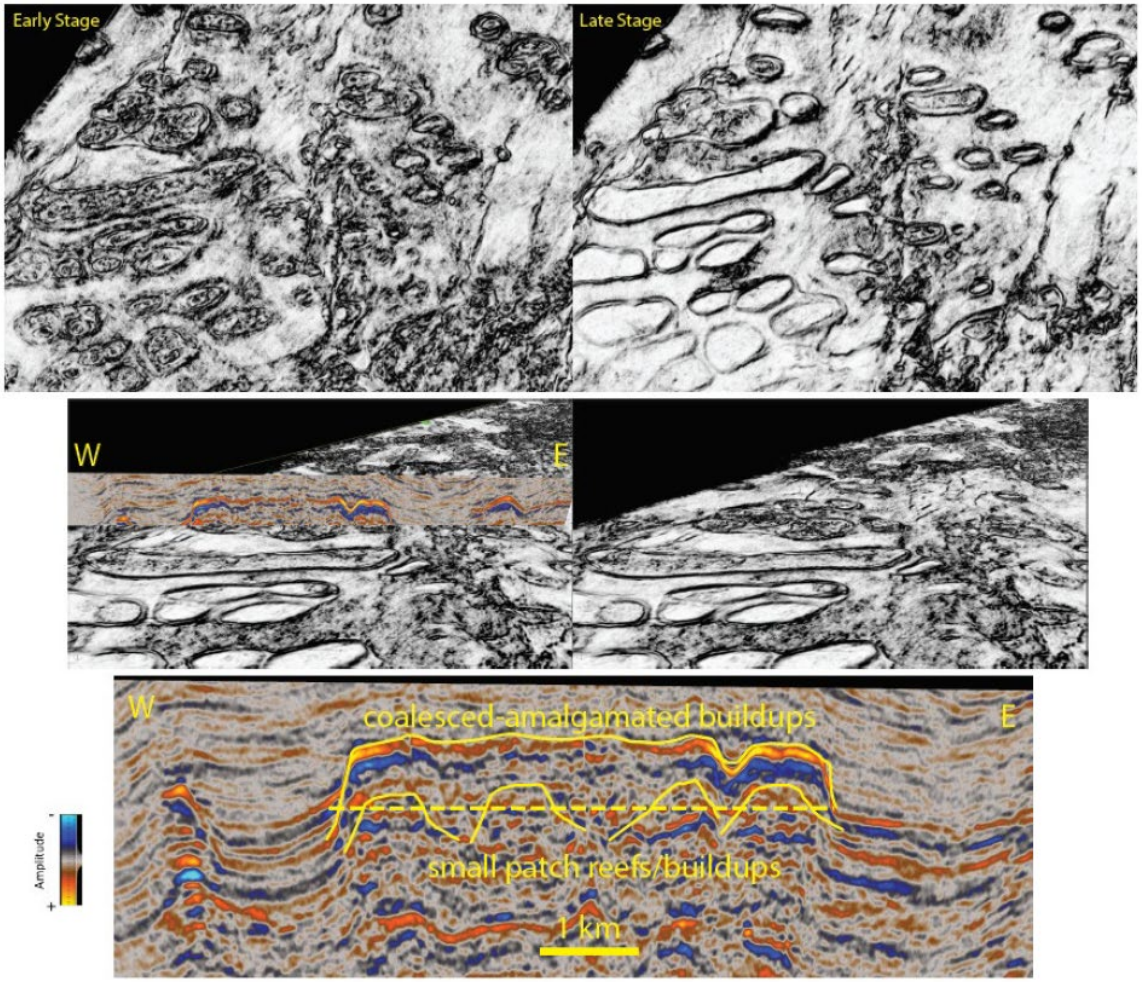

Figure 3.17. Growth pattern of the Early Miocene carbonate buildups shown by the three stages of development, 1) initiation of patch reefs, 2) coalescence of patch reefs, and 3) amalgamation into larger buildup. Hudreds-of-meters-scale circular-ovoid patch reefs coalesced and subsequently amalgamated to form a larger, ≥ 5 km long, west-east elongated carbonate buildup.

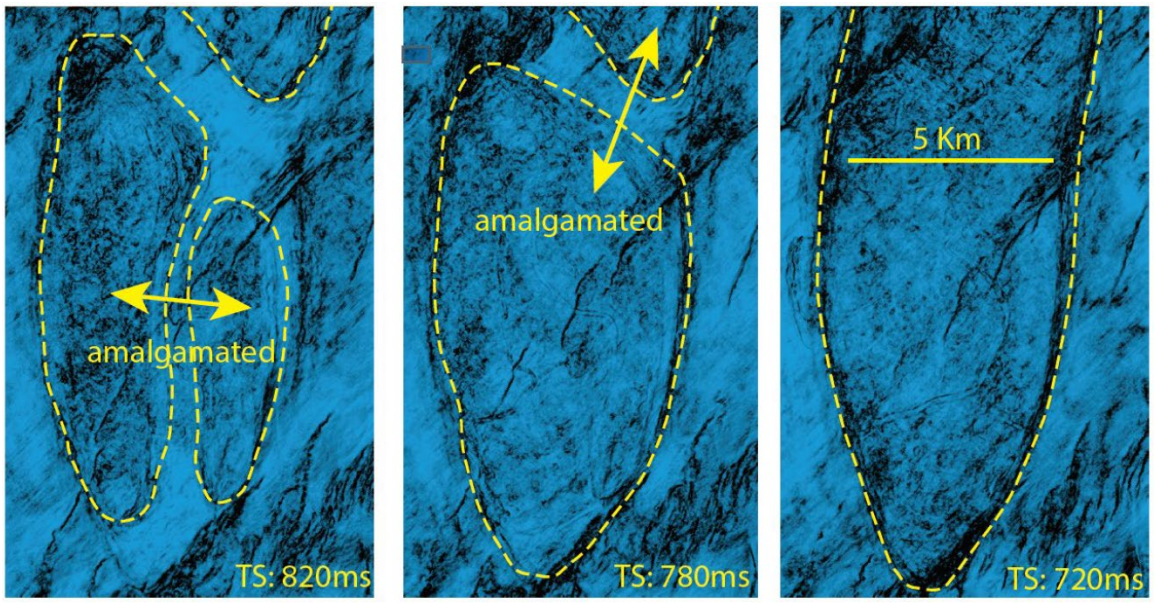

Figure 3.18. Amalgamation of smaller carbonate platforms in the Late Miocene carbonate shelf. Smaller carbonate platforms (few kilometers wide and long) formed by coalesced patch reefs over an area of initiation. These smaller carbonate platforms then amalgamated to form a larger scale (≥ 5 km wide, ≥ 20 km long), north-south elongated carbonate platform.

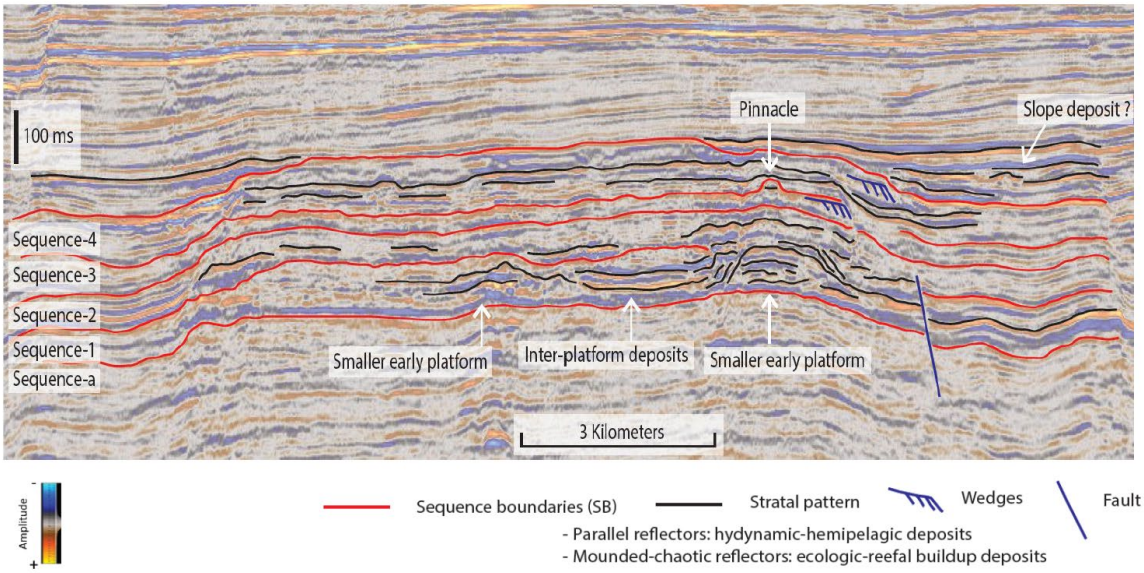

Figure 3.19. Interpretation of depositional sequences of a carbonate platform in the Late Miocene. At least four depositional sequences can be identified within the interval. Sequence-1 is characterized by smaller early platforms with narrow inter-platforms area that later amalgamated into larger platforms starting in Sequence-2. Wedges-shaped and slope deposits were observed at the later stages of the platform development, in Sequence-3 and Sequence-4.

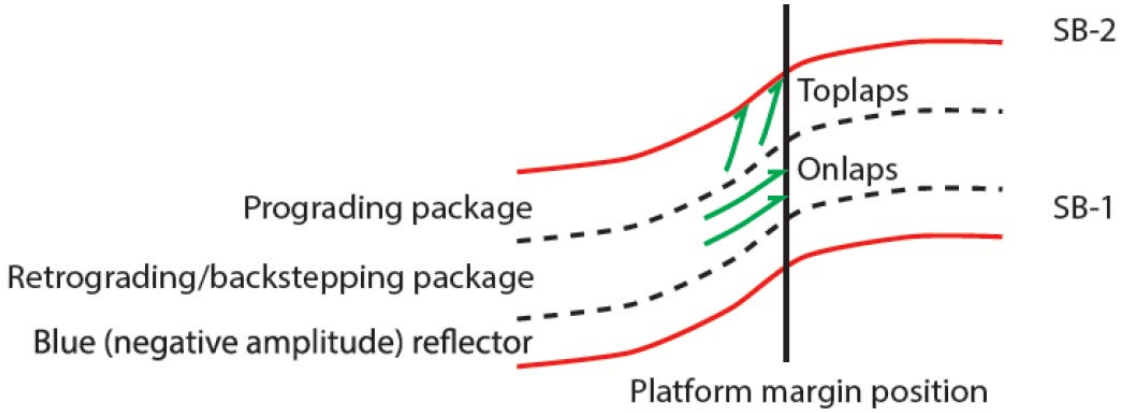

Figure 3.20. Idealized platform margin characteristics in Late Miocene carbonate platforms that represent a single depositional sequence, interpreted based on seismic stratal configuration. A depositional sequence is bounded by sequence boundaries (SB-1 & SB-2) on both its top and bottom. The sequence generally started and marked by negative-amplitude seismic reflector, followed by retrograding or back-stepping package that shows onlaps to the platform margin, and subsequently overlain by prograding package that sometimes shows toplaps to the bounding upper sequence boundary.

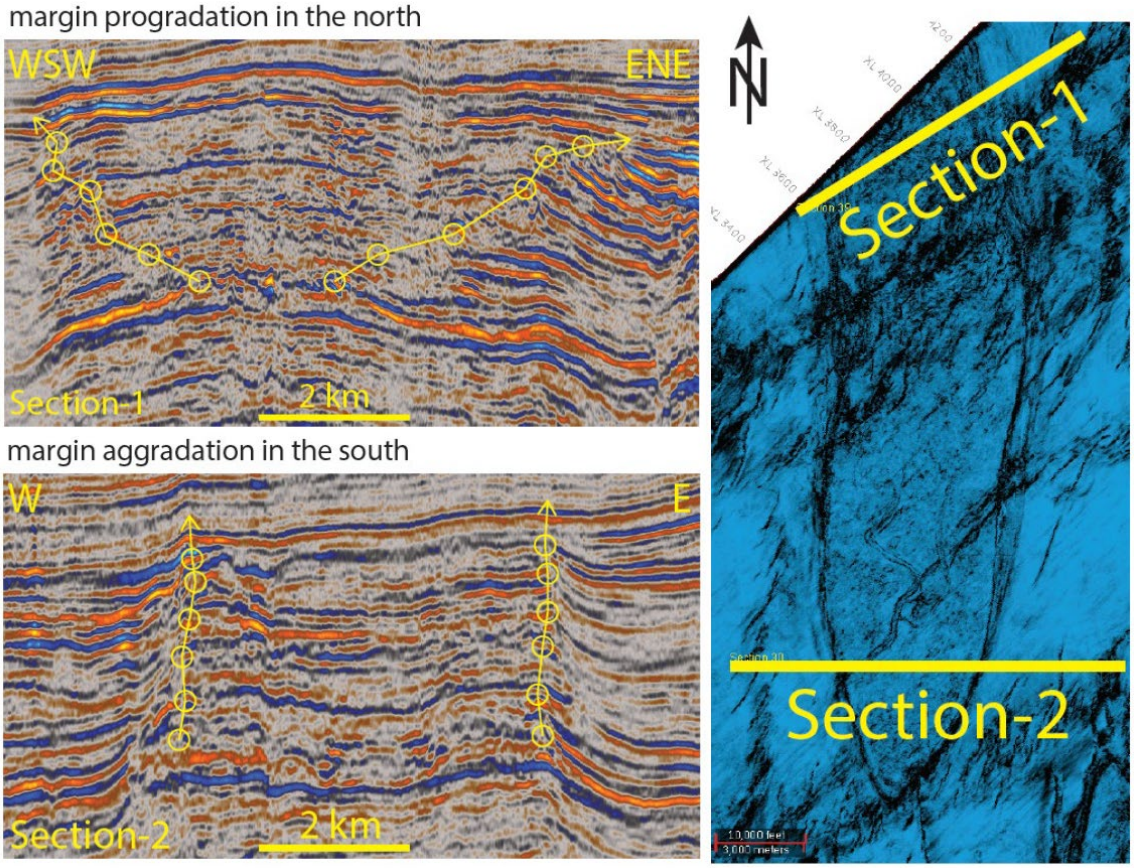

Figure 3.21. Contemporaneous yet totally different platform margin styles within a single Late Miocene north-south elongated carbonate platform. Highly progradational margins (Section-1), to both direction—east and west, in the northern part and highly-aggradational margins (Section-2) in the southern part.

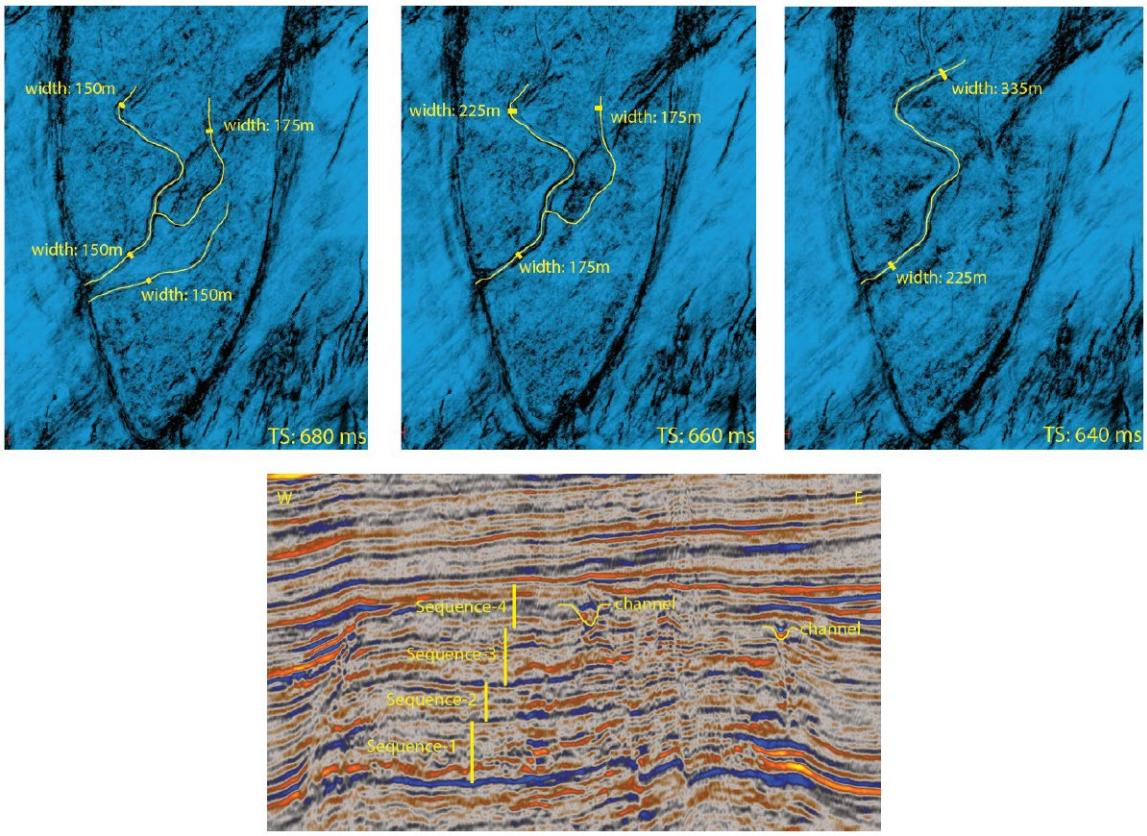

Figure 3.22. Sinuous channels developed in later stage of the carbonate platform development (Sequence-4). These channels are only observed on the larger carbonate platforms in the Late Miocene. Channels shown in this figure have width is few hundreds of meters and have an enlarged mouth to the western side of the platform.

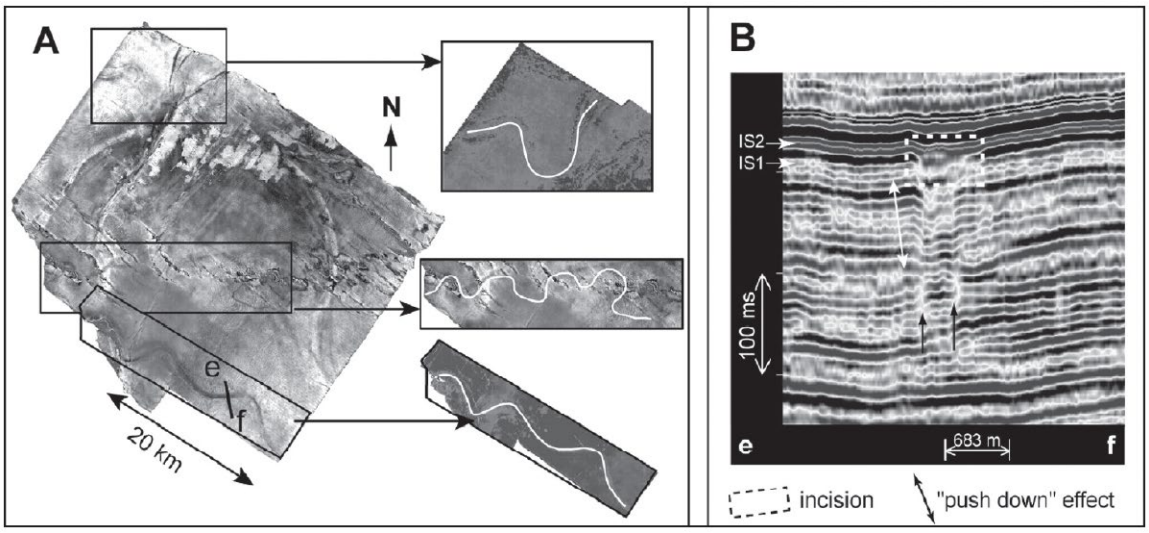

Figure 3.23. Analogue for sinuous channels development, the Cretaceous Top Natih Formation, Oman (Grélaud et al., 2010). Tidal channels were interpreted to be developed as a result of a periodically emergent shelf. These channels show relatively similar dimension to those of the study area.

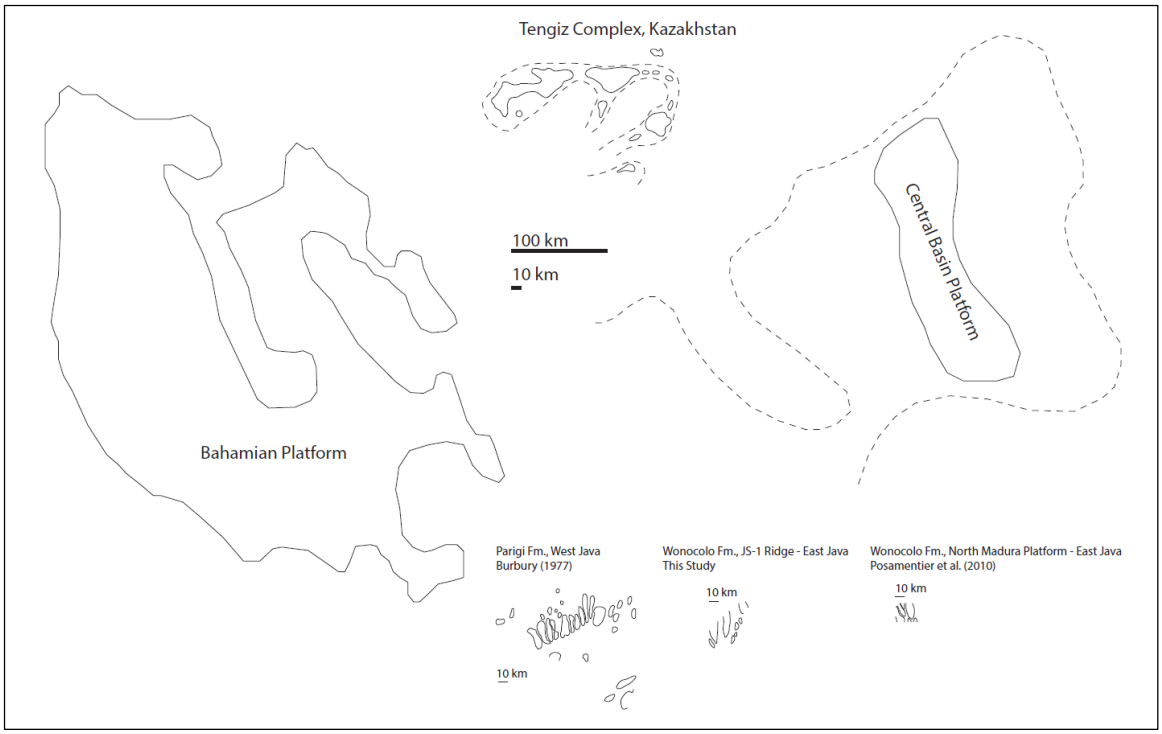

Figure 3.24. Miocene platform morphology and dimension compared to three well-known carbonate platforms—Bahamian Platform (Modern), Central Basin Platform (Permian), and Tengiz Complex (Devonian–Carboniferous).

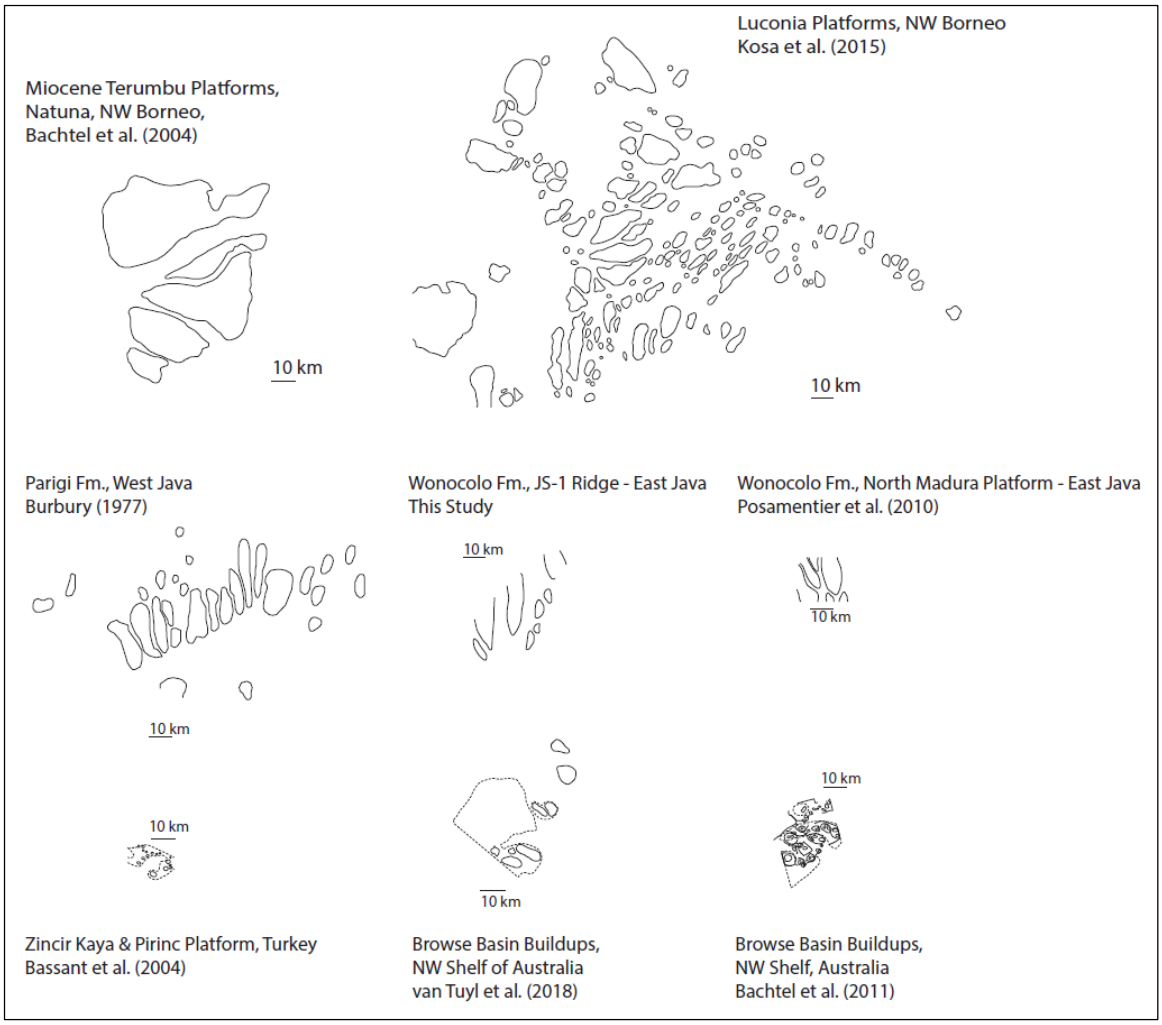

Figure 3.25. Miocene platform morphology and dimension compared to other Miocene buildups and platforms, regionally and globally—Terumbu Platform (Natuna, NW Borneo), Luconia Platforms (NW Borneo), Zincir Kaya & Pirinc Platforms (Turkey), and Browse Basin Buildups (NW Shelf of Australia).

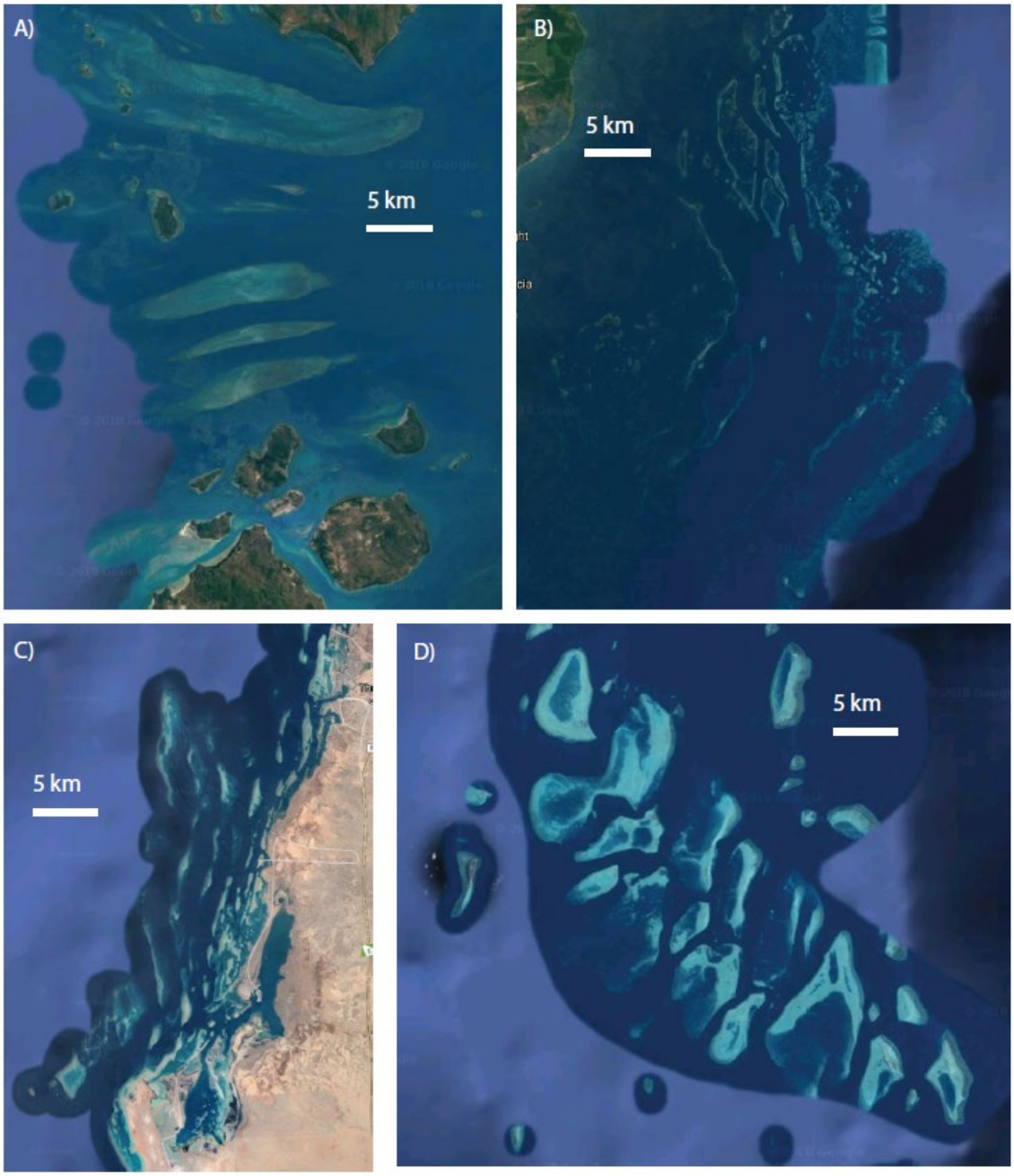

Figure 3.26. Modern example of various carbonate platform morphology influenced by A) tidal flows (Torres Reefs, Selayar Islands), B) paleo-fluvial systems (Belize), C) fault trends (Red Sea), and D) oceanic circulations, both tidal and oceanic currents (east of Selayar Islands, northeast Flores Sea). These figures are plotted in the same scale (5 km scale bar). Imagery ©2018 Landsat / Copernicus, Data SIO, NOAA, U.S. Navy, NGA, GEBCO, TerraMetrics, CNES / Airbus, DigitalGlobe, Map Data ©2018 GBRMPA, Google.

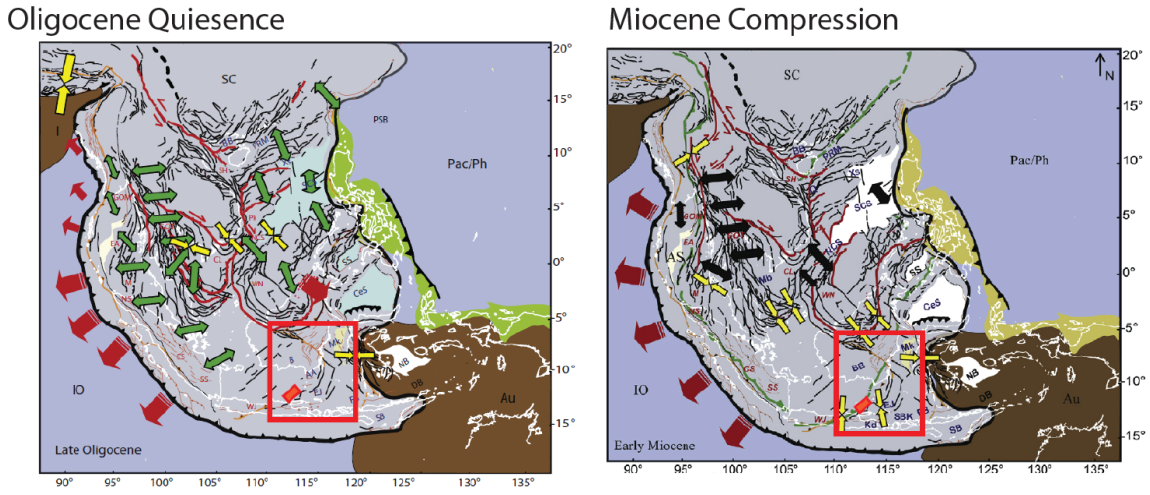

Figure 3.27. Regional compressional tectonic in the southeast Sundaland region in the Miocene (Pubellier & Morley, 2014). Study area indicated by red box.

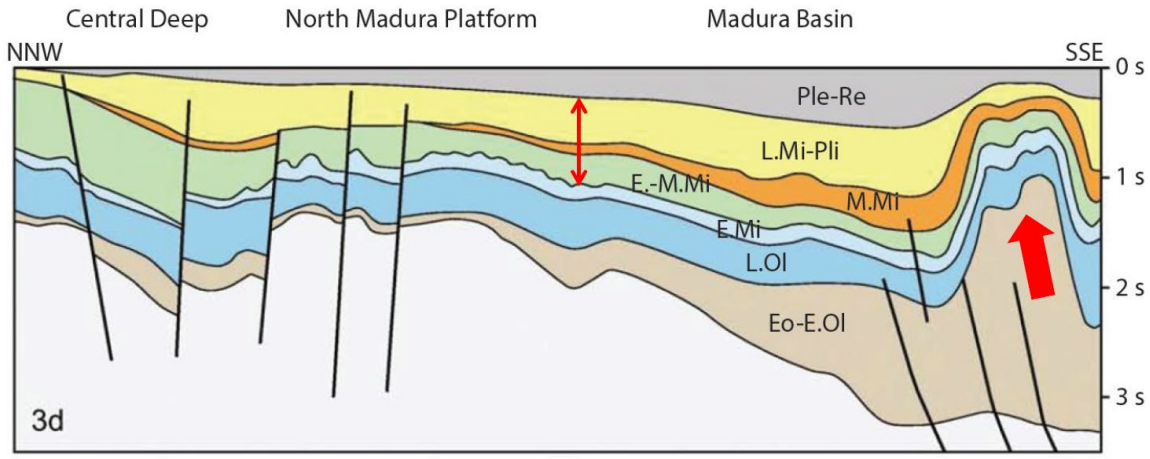

Figure 3.28. Basin inversion shown in simplified seismic section interpretation of the Cenozoic interval (Johansen, 2003). Initial inversion, inverted strata; Early Miocene to Late Miocene–Pliocene (thin red double-arrowed line). Later inversion, further uplift through intense compression in the East (thick red arrow). Some of the Middle Miocene interval is missing over the North Madura Platform, showing uplift and hiatus during this time.

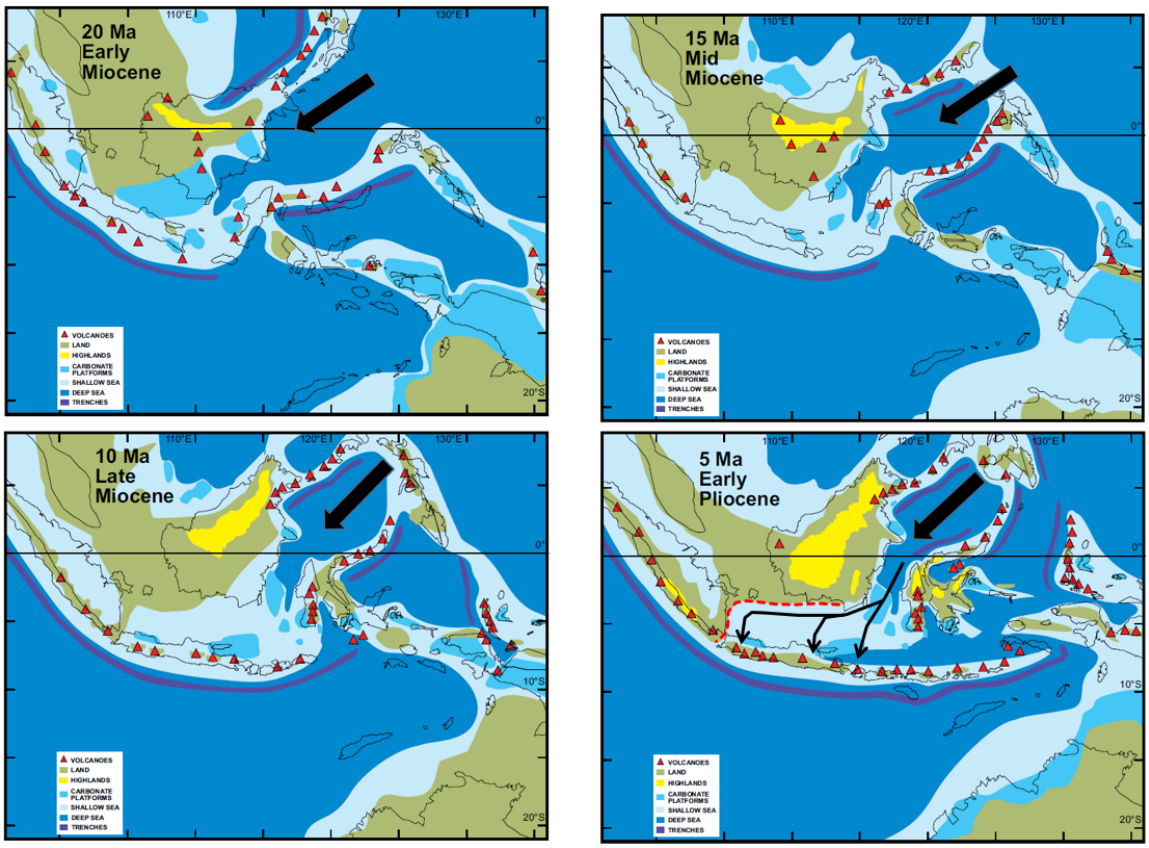

Figure 3.29. Regional oceanic circulation control, flowing relatively from north–south, in the Miocene (20–5 Ma) in the southeastern southeast Asia region, as shown by thick black-arrow. Distribution of land and sea (Hall, 2009) shows the development of Indonesian through-flow (ITF) circulating water from Pacific Water in the northeast, around the Philippines, to the Indian Ocean in the south-southwest through choking point as the Makassar Strait was forming (Kuhnt et al., 2004). Lands between southwestern part of Borneo and southeastern part of Sumatran Arc became connected starting 10 Ma. This paleo-geographic change may have influenced and enhanced the north-south oceanic circulation pattern of the shelf area of the southeastern Sundaland toward the end of the Miocene–Early Pliocene (lower right figure).

Chapter 4: Investigating the Potential of an Early Miocene Off-buildup Carbonate-dominated Strata, Offshore East Java, Indonesia: Insights from Static Reservoir Modeling

ABSTRACT

Cenozoic carbonates are proven prolific hydrocarbons reservoir in the Southeast Asia region. In the East Java Basin, Indonesia, significant amounts of hydrocarbon have been produced from the Oligocene–Miocene Kujung Formation, especially from the Early Miocene Kujung-1 carbonate buildup complexes. This study investigates the potential of the off-buildup carbonates utilizing a static reservoir modeling workflow incorporating well and 3D seismic data.

From seismic and well data, the Kujung-1 interval is interpreted as isolated carbonate buildup complex that can be subdivided into three areas: buildup-core, buildup-flank, and inter-buildups. Hydrocarbon has been mainly produced from the buildup-core that is characterized by massive reefal-carbonates with less than 5% shale content. Distinctively, wells from the X3, X4, and X8 fields, which penetrated buildup-flank and inter-buildups, show interbeddings of carbonate and shale. This alternation is interpreted as results of episodic carbonate sedimentation and possible resedimentation in response to sea-level fluctuations.

A carbonate-dominated interval, approximately 100 ft thick, near the top of this carbonate-shale alternation, is considered as an upside potential in X8 field because of indications of gas accumulation. Petrophysical calculation results in this interval, namely the Kujung-UP, show promising reservoir quality. The calculated porosity ranges from 15–22 %, and the highest permeability is measured at 42.6 mD, according to core analysis.

Subsequently, static reservoir modeling was performed to map the carbonate reservoir distribution. Volumetric calculation of gas resources and reserves yielded encouraging results for this interval to be developed as part of an integrated field development strategy.

INTRODUCTION

Oligocene–Miocene carbonates of the East Java Basin are prolific carbonate reservoirs. Estimated hydrocarbon reserves are as much as several billion barrels of oil equivalent (Bboe) (Doust & Noble, 2008; Wilson & Hall, 2010). These Oligocene–Miocene carbonates were deposited under various and complex Southeast Asia region tectonic settings (Fulthorpe & Schlanger, 1989; Hall, 2002; Wilson, 2002). Activities related to hydrocarbon exploration and production in the region have resulted in extensive availability of valuable subsurface data sets, such as well and seismic data for studying the Oligocene–Miocene carbonates (Kenyon, 1977; Mudjiono & Pireno, 2002; Welker-Haddock et al., 2002; Maynard & Morgan, 2005; Carter et al., 2005).

The study area is located offshore of East Java, northwest of present-day Madura Island, Indonesia. It is situated in a present-day back-arc setting of the east-west trending Java subduction (Figure 1.2 and Figure 1.3). By utilizing a set of interpretation methods of the 3D seismic data acquired in 1999, the exploration well success rate was more than 60% within 5-year period, from 2000-2005, when targeting the Kujung-1 carbonate buildups in this area (Carter et al., 2005). Lately, the production has been declining and this situation incentivizes the investigation of the under-explored and under-developed off-buildup carbonates.

This study demonstrates a volumetric assessment of the off-buildup carbonates in the X8 field utilizing static reservoir modeling workflow using integration of well and seismic data. Well data indicate possible hydrocarbon accumulations within an interval in the upper part of the Kujung Formation, namely the Kujung-UP. Depth-converted 3D seismic data was used to interpret and map the distribution of the reservoir. Volumetric calculation results from this study include the original gas in-place (OGIP) and estimated gas reserves from the Kujung-UP. These numbers can be used as analogues to other areas or interval with regard to the potentiality of the Miocene off-buildup carbonates.

This study aims to assess the potential of the Miocene off-buildup carbonates by integrating well and seismic data into a static reservoir model. A depositional model for the Kujung Formation from the previous chapter was utilized. Well-tops were correlated, seismic horizons were interpreted, and reservoir properties were taken from petrophysical calculation results. Seismic geobodies from inverted acoustic impedance (AI) depth-converted volume were extracted in which the top and base of the upside potential interval of the off-buildup carbonates (Kujung-UP) were mapped. Structural and property modeling were performed as inputs for volumetric calculations of the OGIP and the gas reserves. Facies and depositional geometries analogues from X3 field and three selected ancient and modern outcrops were described and presented.

DATA AND METHODS

This study utilized a subsurface data set that consists of well and seismic data from an existing field in an active block operated by Pertamina Hulu Energi - West Madura Offshore (PHE-WMO). The 3D seismic data for the entire block were acquired in 1999

and cover an approximately 1,300 km^2 area and has a dominant frequency content of 25–35 Hz around the top of the Kujung Formation level (Carter et al., 2005). This study utilized a part of the main seismic volume that covers approximately 70 km^2 in the X8 field area that has been depth-converted. Six wells were used, five wells (Well-1, Well-2, Well-3, Well-4, and Well-6) that penetrated off-buildup area were used in subsurface analysis and static reservoir modeling conducted in this study, and one exploration well (Well-5) was used as a reference well to show distinct buildup-core characteristics in well correlation (Figure 4.1 and Figure 4.2). Secondary data include depth-converted seismic volumes, petrophysical logs, and production-related data.

By using the depositional and lithofacies distribution model of the Kujung Formation (Figure 4.3), seismic horizons interpretation, well correlation, and subsurface mapping were performed. The upside potential interval was then defined, and reservoir properties such as porosity, permeability, and water saturation were generated from petrophysical calculations. Seismic geobody extraction from acoustic impedance depth-converted volume was performed in order to map the top and base of the Kujung-UP interval. Static reservoir modeling was then performed in order to generate geo-cellular structural model that was subsequently populated by upscaled reservoir properties. Volumetric calculations for gas resources and reserves were then performed using two scenarios of fluid contacts for the upside potential interval.

RESULTS

This study utilizes the depositional model of the Kujung Formation based on its facies and architecture (as discussed in a previous chapter of this dissertation) in which the

Kujung Formation carbonate buildups were subdivided into buildup-core, buildup-flank, and inter-buildups (Figure 4.3). By using this depositional model, the uppermost layer of carbonates in the buildup-flank and inter-buildups area can be described in several ways: 1) highstand resedimented carbonates from the buildup-core, 2) in-situ lowstand accumulation of foraminifer packstone facies, or 3) a combination of both scenarios.

Seismic Interpretation

Based on seismic facies, buildup-core is characterized by mounded-chaotic to sub-parallel, semi-continuous to discontinuous, low to moderate frequency and amplitude seismic reflectors. Buildup-flank and inter-buildups are characterized by sub-parallel to sometimes chaotic, semi-continuous to discontinuous, moderate to high frequency and amplitude seismic reflectors (Figure 4.4). Two main seismic horizons were picked and interpreted. They are the Top Kujung horizon and Top Buildup Envelope (TBE) horizon (Figure 4.5). The Top Kujung Horizon includes the off-buildup strata in the buildup-flank and inter-buildups. In contrast, the TBE horizon excludes most of the off-buildup strata and also known as Kujung "Reef" horizon (Carter et al., 2005). Structure maps of these horizons were used as input in the static reservoir modeling workflow.

Well Correlation

Three well tops were correlated between wells in the study area in Sub Sea True Vertical Depth (SSTVD) domain in present-day structural configuration (Figure 4.6). This approach normalizes the apparent thickness recorded in Measured Depth (MD), and hence it represents the stratigraphic thickness. The three well-tops are Top Kujung, Base Kujung-

UP, and Top Buildup Envelope (TBE). Based on lithologic data from cuttings in the Kujung Formation, low gamma-ray log values correspond to carbonates, whereas high gamma-ray log values correspond to shale. Well-5 shows a distinct massive carbonate without a shale-dominated interval of the buildup-core represented by low gamma-ray log values in cylindrical shape. In contrast, five other wells, Well-1, Well-2, Well-3, Well-4, and Well-6, which penetrated buildup-flank and inter-buildups, show a shale-dominated interval before the uppermost carbonate strata of Kujung-UP. The thickness of this shale-dominated interval between Base of Kujung-UP and Top Buildup Envelope varies from 92 feet in Well-1 to 464 feet in Well-6.

Reservoir Properties of the Off-buildup Carbonates

Reservoir properties of the Kujung-UP, including porosity, permeability, and water saturation, were obtained from petrophysical calculations performed in-house with current industry standards as secondary data for this study. Petrophysical calculations were performed in all wells except Well-5, which is located in the buildup-core. Calculated porosity values range from 15.1–22.1%. Permeability can be as much as 42.6 mD. Water saturation ranges from 28.9–58.9%. The Kujung-UP interval in Well-1 is saturated with brine, and thus the water saturation is 100%. Figure 4.7 shows an example of petrophysical logs in Well-6, and Table 4.1 summarizes the reservoir properties of the Kujung-UP interval in five wells used in modeling.

Static Reservoir Modeling

Static reservoir modeling was performed using Petrel™ software from Schlumberger in two main steps, 1) structural modeling and 2) property modeling. The structural modeling was done in order to generate the Kujung-UP geo-cellular model. Cells within the structural model were then assigned reservoir properties value distributed using particular geostatistics methods. The static reservoir model was then used to calculate gas resources and reserves of the Kujung-UP (Figure 4.8).

Structural Modeling

Structural modeling was done in order to map the geometrical distribution of the Kujung-UP. Seismic inversion was completed in the Kujung-1 interval in order to generate an acoustic impedance (AI) depth-converted seismic volume that can distinguish rock layers better than conventional seismic data. AI is used to interpret and map the distribution of the Kujung-UP interval due to its enhanced seismic impression of rock layer instead of the boundary between two rock layers as represented by conventional seismic amplitude. By utilizing the AI volume, the seismic geobody was extracted using a pre-determined opacity threshold to generate additional horizons input for structural modeling, namely the top and base of the Kujung-UP. Figure 4.9 shows the Kujung-UP layer whose top and base were inferred from the AI volume. Figure 4.10 shows the isopach map of the Kujung-UP generated using the top and base of the Kujung-UP that resulted from seismic geobody extraction, and Figure 4.11 shows a southwest-northeast section view of the Kujung-UP interval around Buildup-D, Buildup-C, and Buildup-A of the X8 field. These structural

horizons were utilized and tied with well tops in order to generate the Kujung-UP geo-cellular model with pre-determined dimensions.

Property Modeling

Property modeling was done in order to populate continuous reservoir properties such as porosity and water saturation into the previously built geo-cellular model of the Kujung-UP. Petrophysical logs were previously upscaled into the cells within the geo-cellular model. Two discrete properties, facies and net-to-gross, were also generated. Facies, for the property modeling purpose, were subdivided into Kujung Buildup, Kujung-UP, and shale facies. The Kujung Buildup facies represents the main buildup that, despite having good reservoir properties, was excluded in volumetric calculations. The Kujung-UP facies represents strata that are considered to be a reservoir, and shale facies represents strata that are considered non-reservoir. Net-to-gross values were calculated by simply applying the cutoff parameters (net reservoir; porosity > 7% and water saturation < 70%). Figure 4.12 shows intersecting northwest-southeast and northeast-southwest fence diagrams, on which are posted the assigned facies from the static reservoir model. Figure 4.13 shows intersecting northwest-southeast and northeast-southwest fence diagrams, on which are posted the porosity values from the static reservoir model.

Volumetric Calculation

Volumetric calculations were done using the geo-cellular model in order to estimate the quantities of original gas in-place and gas reserves within the Kujung-UP. These calculations were conducted using two scenarios of fluid contacts. First, lowest-known

water (LKW) from Well-1 was used as the volumetric calculation boundary in the low estimate. Second, the structural spill point of the Top Kujung structure was used as the volumetric calculation boundary in the high estimate (Figure 4.14). In order to perform the volumetric calculations, the following formula was used:

$$OGIP = GRV \times NTG \times Por \times (1 - Sw) / Bg \quad \ldots\ldots\ldots\ldots (1)$$

$$Gas\ Reserves = OGIP \times RF \quad \ldots\ldots\ldots\ldots (2)$$

Where:

OGIP = Original Gas in Place (BCF – Billion Cubic Feet)

GRV = Gross Rock Volume (Acre-feet)

NTG = Net-to-gross ratio after property cutoffs (fraction or percentage)

Por = Calculated porosity (fraction or percentage)

Sw = Calculated water saturation (fraction or percentage)

Bg = Formation volume factor for gas (RB/MSCF)

RF = Gas recovery factor taken from nearby fields (fraction/percentage)

Structural parameter (GRV) and reservoir property parameters (NTG, Por, and Sw) were intrinsic values of the reservoir model. Other calculation parameters such as Bg and RF were taken from nearby gas fields with relatively similar reservoir depths. The results of volumetric calculations for the Kujung-UP are, from the low estimate to the high estimate: OGIP numbers are approximately 17–50 BCF, and Gas Reserves are approximately 12–35 BCF (Table 4.1 and Table 4.2).

DISCUSSION

Off-Buildup Carbonates Upside Potential

In term of architecture, these off buildup carbonates are situated in the buildup-flank to inter-buildups of the Miocene Kujung Formation carbonate buildup complex. They are characterized by interbedded carbonate-shale, that are biostromal, inclined, draped to the margin, or deposited following the buildup-flank topography. In well correlation, variation in the thickness of the shale-dominated interval between the Kujung-UP and the Top Buildup Envelope is due to the well's proximity to the buildup-core (Figure 4.6). The closer to the buildup-core, the thinner the shale-dominated interval is. This study shows that the off-buildup carbonates are characterized by good reservoir quality, according to well logs, petrophysical calculation, and sidewall core data. Parameters related to reservoir quality include porosity and permeability. Porosity ranges from 15–22% and permeability can be as much as 42.6 mD according to core analysis. Off-platform carbonates elsewhere were also recognized in previous studies to act as potential reservoirs for large hydrocarbon accumulations (Zampetti et al., 2010; Janson et al., 2011). Off-buildup carbonates showed onlaps and were interpreted as part of a drowned platform (Kusumastuti et al., 2003). However, the depositional timeline from the buildups/platforms to their adjacent off-buildups carbonate can also be continuous (Koša et al., 2015). Results from this study suggest that the latter is most likely the case, in which the Top Kujung seismic horizon and well-top were picked instead of the Top Buildup Envelope to include the off-buildup carbonates as the contemporaneous deposits of buildup-core.

Analogues from Nearby Fields and Outcrops

In order to better understand the architecture of the carbonate buildups, core samples from the nearby X3 field and outcrops from several locations were chosen to serve as analogues for the Early Miocene Kujung Formation carbonate buildup. These Miocene and present-day analogues include 1) Core samples from X3 field, 2) the Miocene isolated carbonate buildup, Pirinc outcrop, Turkey (Bassant et al., 2004); 3) the Miocene Wonosari Platform, onshore southern East Java (Janson, 2012 – *unpublished*); and 4) the Seribu Islands, offshore Jakarta (Jordan Jr., 1998; Park et al., 2010).

All of these field and outcrop analogues show depositional geometries, architecture, and facies relatively similar to that of the study area (Figure 4.15, Figure 4.16, Figure 4.17, Figure 4.18, and Figure 4.19). Carbonate buildups are hundreds of meters to several kilometers wide, and circular to elongate in plan view, and they have vertical relief up to 150 m from the buildup-core to the basinal inter-buildups area. The facies within the buildups is dominated by *coralgal boundstone* to *floatstone – rudstone*, and the facies of the off-buildup carbonates is dominated by *foraminifer packstones*. These *packstones* can be grainy, possibly influenced by shallower water-depth and higher depositional energy closer to the buildup-core (Jordan Jr., 1998; Bassant et al., 2004; Park et al., 2010; Janson, 2012 – *unpublished*).

Insights from Volumetric Analysis

Fluid contacts based on well data of the X8 field are observed on different levels for each buildup (Figure 4.2). This suggests that the X8 field carbonate buildups complex is not a single hydrocarbon tank system. However, all of the fluid contacts in the main

buildups are significantly lower/deeper than the two fluid contact scenarios used for volumetric calculations of the Kujung-UP.

Volumetric calculation results of the Kujung-UP give insight as to how the off-buildup carbonates could have a significant volumetric contribution to support the cumulative production of the main buildup. Production data from the other nearby field, the X9 field, which has solution gas and gas cap driving mechanism, show that the cumulative production can be as high as 10 times the initial estimate of the hydrocarbon in-place of the main buildup (Setiawan, 2018). Unfortunately, no wells penetrate the off-buildup carbonates of the X9 field. Volumetric contributions from the off-buildup carbonates would be necessary and highly likely in order to explain such a case.

Implications to Regional and Global Oligocene–Miocene Carbonate Reservoir Exploration

The off-buildup carbonates in the study area are situated in buildup-flanks to inter-buildups, constituting almost more than 85% of the under-explored and under-developed area of the JS-1 Ridge shelf as an active block for hydrocarbon exploration and production. This study shows that within this area, carbonate beds of *packstone* facies can be potential reservoirs with good reservoir quality (porosity and permeability) and considerable storage capacity.

Connectivity of the off-buildup carbonates to the main buildups remains the main concern. If they are connected, the off-buildup carbonates can contribute volumetrically to the original hydrocarbon in-place and production. If they are disconnected, the off-buildup

carbonates can be a potential reservoir which is stand-alone and stratigraphically trapped. This study suggests that both cases are possible.

If these off-buildup carbonates are connected to the main buildups, they should be included in volumetric assessment of the main buildups in order to avoid underestimation of the hydrocarbon in-place numbers. Gas produced from off-buildup carbonates can be used for further field development, such as to increase the existing hydrocarbon lifting capacity.

CONCLUSIONS

Cenozoic carbonates, especially the Oligocene–Miocene carbonate reservoirs, are proven and prolific in southeast Asia and other regions. These carbonate reservoirs are usually targeted for their 4-way closure, carbonate buildup geometry. Despite constituting as much as 85% of areal coverage, the associated off-buildup carbonates in buildup-flank and inter-buildups area are often overlooked, underexplored, and underdeveloped. This study shows that these off-buildup carbonates may have a good reservoir quality and storage capacity. The connectivity of the off-buildup carbonates to their adjacent buildup-core is critical to the development strategy of a field. This study demonstrates the possible explanation of unaccounted-for hydrocarbon volumes from the off-buildup carbonates that may explain the problem regarding cumulative production numbers exceeding the volumetrically possible, original hydrocarbons in-place, stored in the main carbonate buildups (buildup-core). Results from this study will give insights to other regions with Oligocene–Miocene carbonate reservoirs in terms of improving the strategy of new exploration, current, and future field development.

Table 4.1. Reservoir parameters of five wells that penetrated off-buildup carbonates in X8 field

	A7	A8	A17	A22	A9
Gross Pay (ft TVD)	27.0	83.0	55.0	110.0	32.0
Net Pay (ft TVD)	16.5	31.8	20.0	36.2	0.0
Net-to-Gross (%)	61.1	38.3	36.4	32.9	0.0
Porosity (%)	22.1	16.4	15.1	20.5	17.5
Permeability (mD)	42.6	8.6	2.0	39.2	8.0
Water Saturation (%)	28.9	43.2	58.9	37.0	100.0

Table 4.2. Results of volumetric calculation using two cases, 1) upper table; GWC at -#,560 ft, 10 ft above Top Kujung-1 in A-9 Well, where lowest-known water (LKW) is observed, and 2) lower table; GWC at -#,800 ft as structural spill point, 240 ft lower than LKW. Potential gas reserves resulting from these calculations range from 12–35 BCF

Volumetric Calculation Parameters	Results
Gross Rock Volume (Acre-feet)	47,443.00
Average Net-to-Gross (%)	55.00
Average Porosity (%)	16.00
Average Water Saturation (%)	52.00
Formation Volume Factor - Bg (RB/MSCF)	0.90
Original Gas In Place (BCF)	17.28
Recovery Factor (%)	70.00
Gas Reserves (BCF)	12.10

Volumetric Calculation Parameters	Results
Gross Rock Volume (Acre-feet)	125,441.00
Average Net-to-Gross (%)	62.00
Average Porosity (%)	15.00
Average Water Saturation (%)	50.00
Formation Volume Factor - Bg (RB/MSCF)	0.90
Original Gas In Place (BCF)	50.28
Recovery Factor (%)	70.00
Gas Reserves (BCF)	35.20

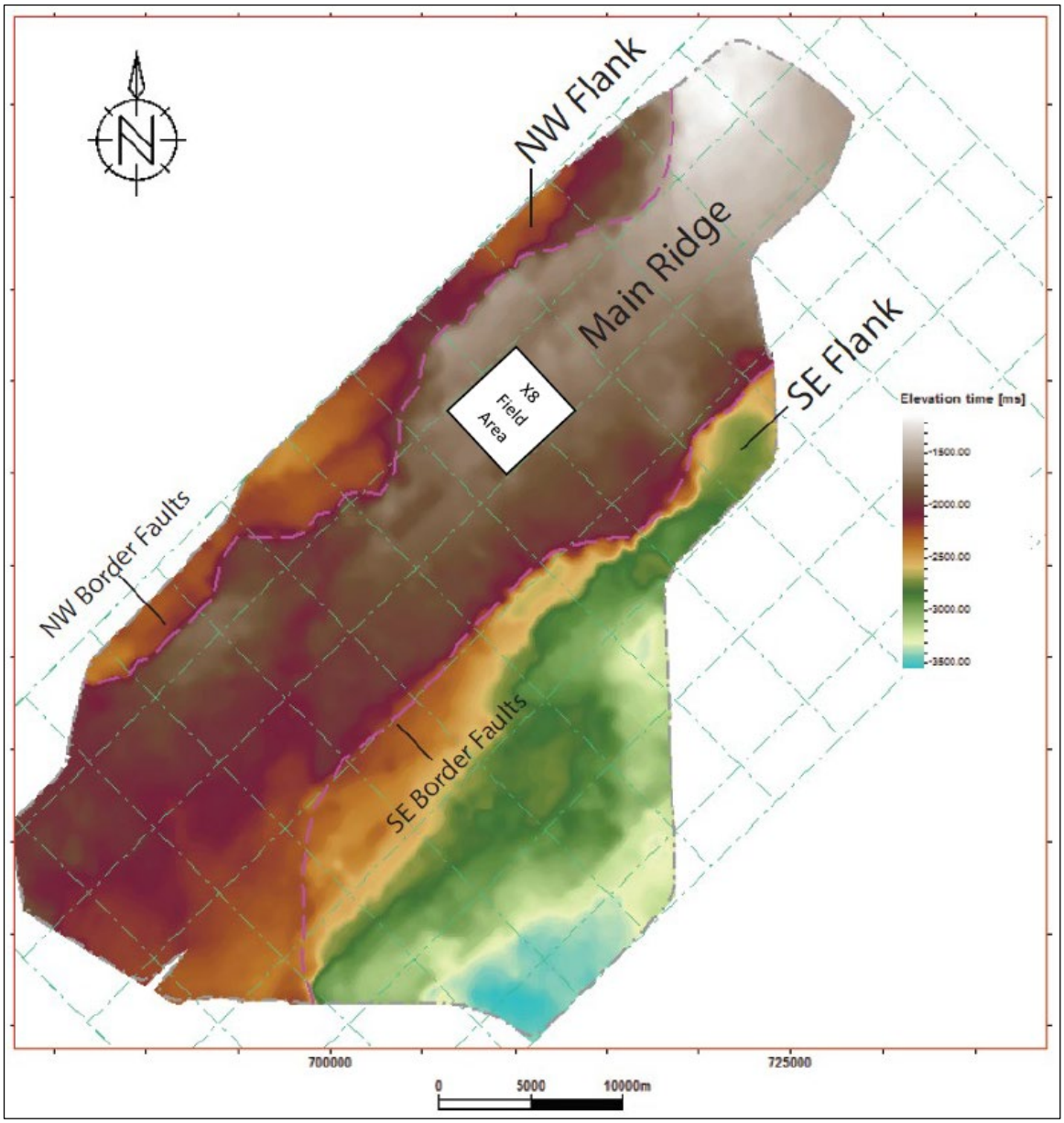

Figure 4.1. Basement structural configuration of the study area shown in a time structure map of the Top Basement. The JS-1 Ridge is subdivided into three main areas, the northwest-southeast trending main ridge, and the northwest and southeast flanks on both sides. Border faults system (normal faults) separate the main ridge and the flanks. The X8 Field area is located near the NW border faults system.

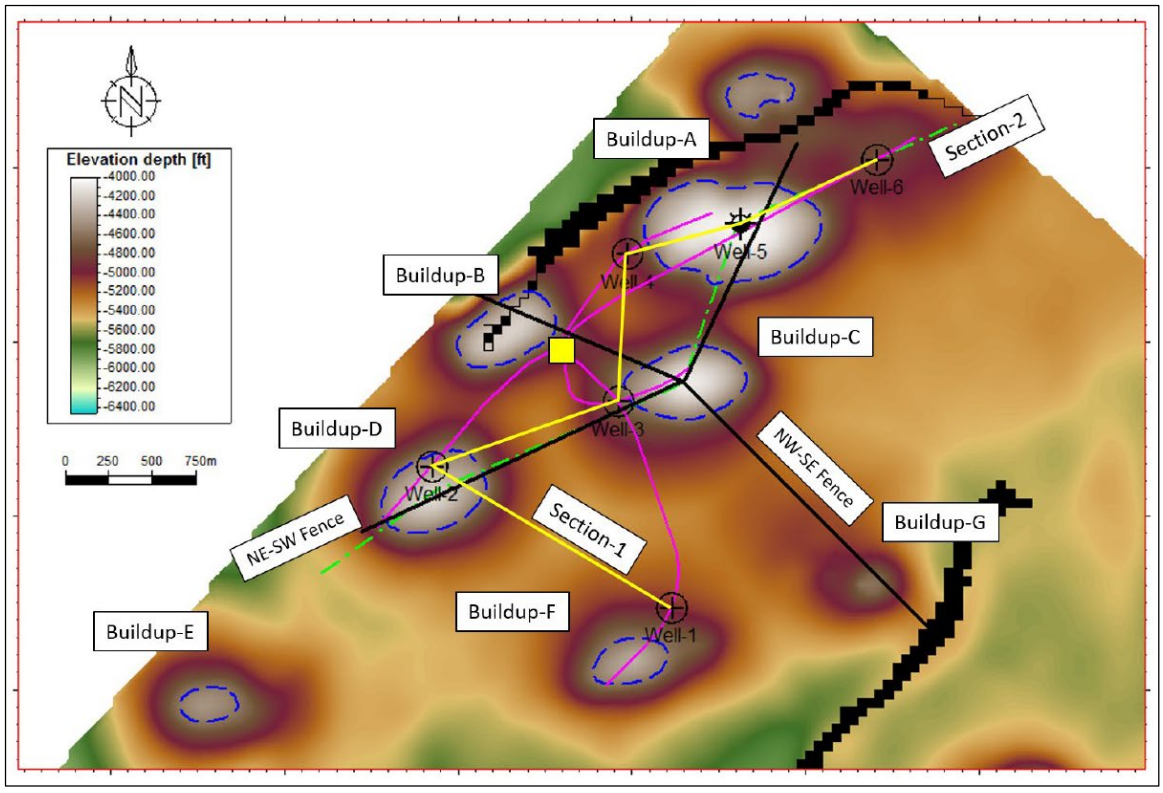

Figure 4.2. Base map of the X8 field area. Six wells were used in this study, 1 vertical exploration and 5 deviated. Well paths are shown in purple lines. Yellow box is the location of the drilling platform. Seven buildups were analyzed in this study. Buildup-A includes smaller buildups northeastward of the main buildup. Well correlation section is shown by yellow line. Fence diagrams for Figure 4.12 and Figure 4.13 are shown by black lines.

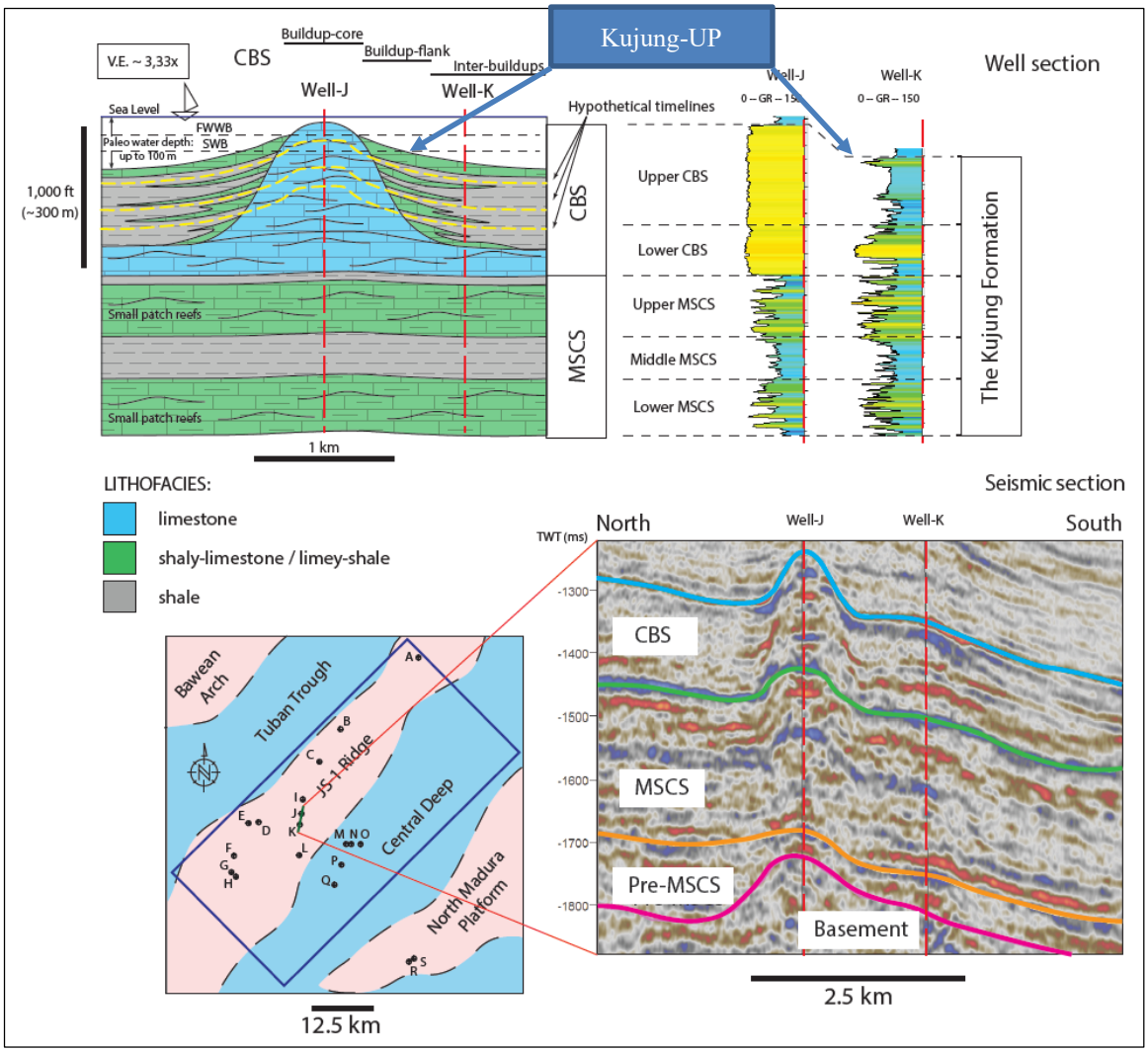

Figure 4.3. Conceptual lithofacies distribution based on well and seismic data. Well data include gamma-ray log and cuttings lithology. Off-buildup carbonates were deposited in the buildup-flank and inter-buildups area (Figure 2.5, Chapter 2). The Kujung-UP (upside potential) discussed in this study is located outside of the buildup-core and is distributed in the buildup-flank and inter-buildups. Hypothetical timelines following the buildup topography in the Upper CBS interval are shown in yellow-dashed line.

Seismic Facies	Amplitude	Frequency	Continuity	Geometry	Interpretation	Lithology
1	High (positive)	Low	Mostly continuous	Parallel to mounded	Top CBS	Carbonates
2	Moderate	Moderate	Semi-continuous to discontinuous	Mounded-chaotic to sub-parallel	CBS interval (Buildup core)	Carbonates
3	Moderate to low	Moderate	Semi-continuous to discontinuous	Sub-parallel to chaotic	CBS interval (Buildup flank & Inter-buildups)	Carbonates-shales interbedding
4	High (negative)	Low	Mostly continuous	Parallel to sub-parallel (mounded due to	Top MSCS	Mostly shales

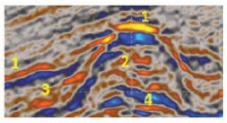

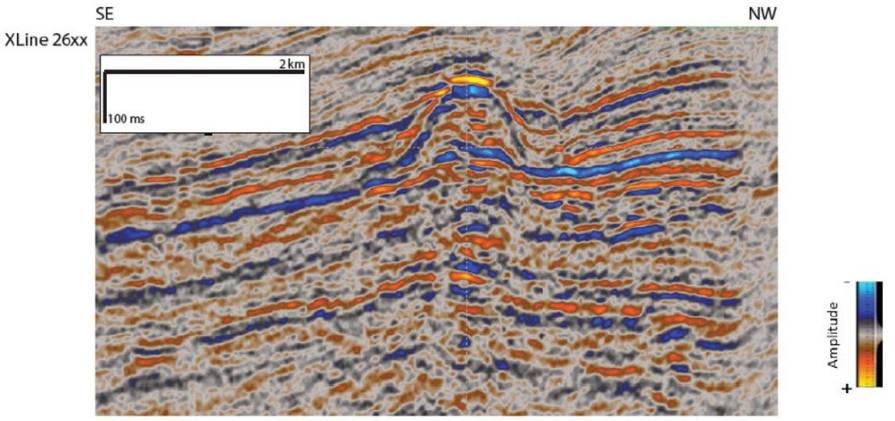

Figure 4.4. Seismic facies of the upper Kujung Formation (Kujung-1, CBS interval in Chapter 2) carbonate buildups that are subdivided into buildup-core, buildup-flank, and inter-buildups. The Kujung-UP strata show converging reflectors to the buildup-core.

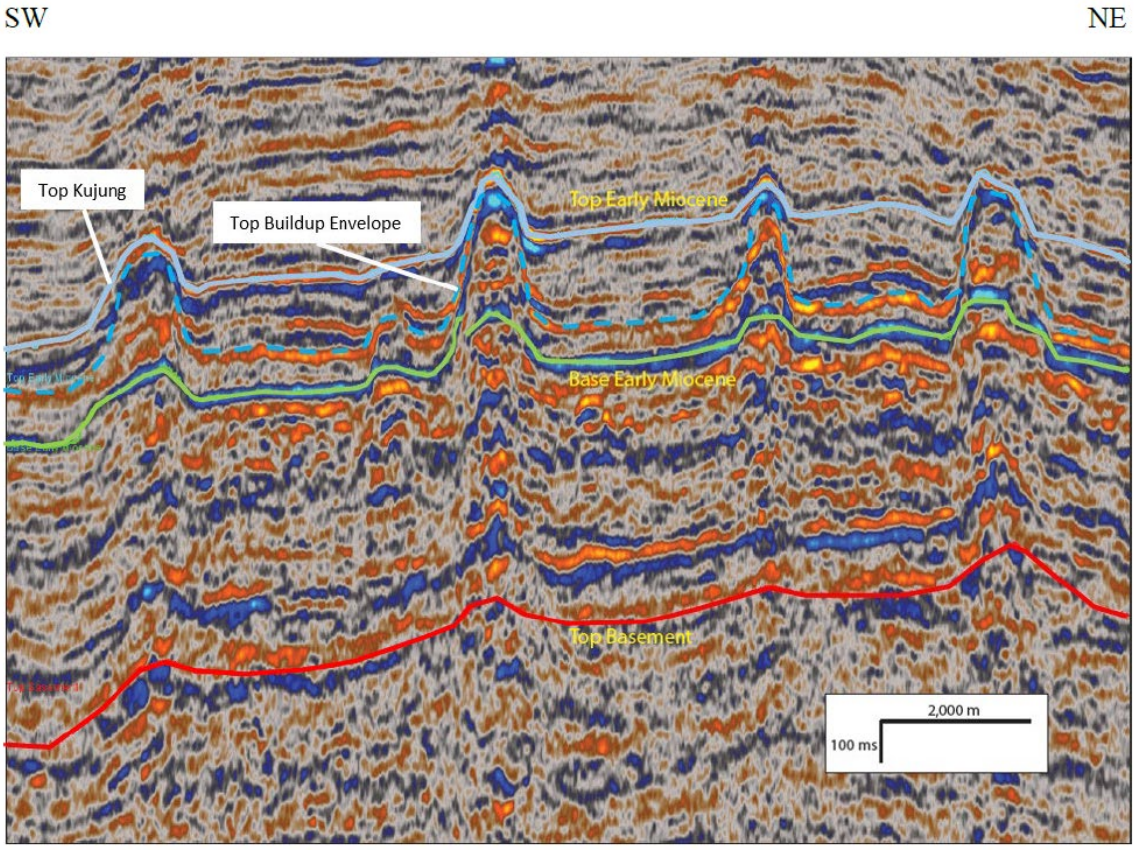

Figure 4.5. Seismic interpretation of seismic horizons shown in southwest-to-northeast seismic section outside of the X8 field area. These two main seismic horizons are commonly used in-house; 1) Top Kujung Horizon (pale blue) that includes the off-buildups strata in the buildups flank and inter-buildups area, and 2) Top Buildup Envelope or Kujung "Reef" Horizon (Carter et al., 2005) that excludes most of the off-buildups strata. Four pinnacle carbonate buildups, more than a kilometer wide, are laterally distributed somewhat evenly within the Early Miocene interval across the seismic section.

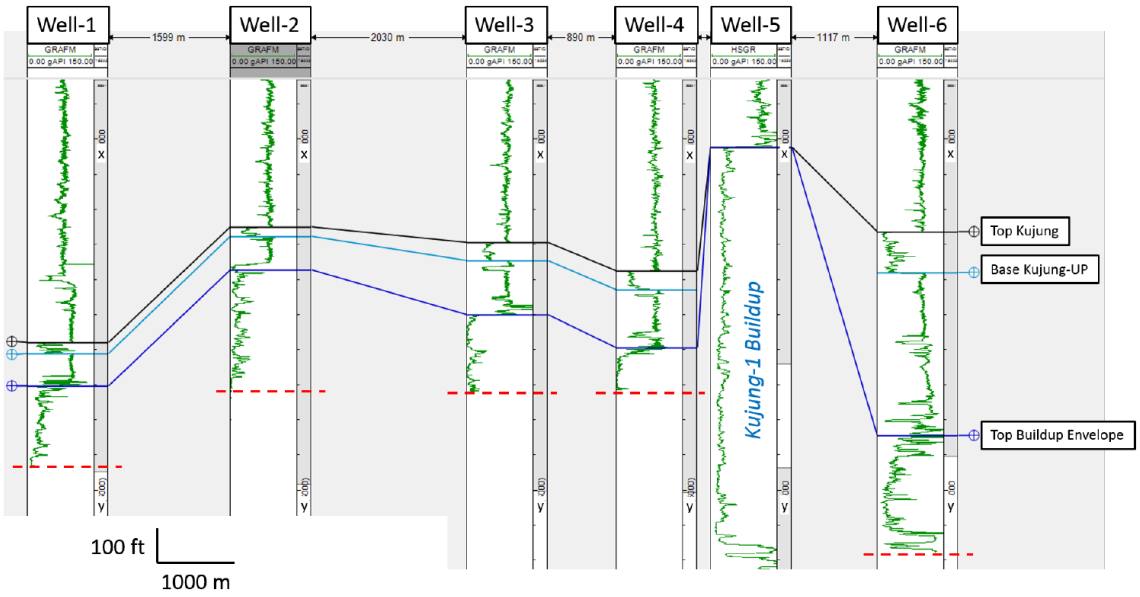

Figure 4.6. Present-day structural correlation (unflattened) between buildups structure within the X8 field. Wells are separated as much as 2 km away from the closest well in this section. Well-1 is part of Buildup-F, Well-2 is part of Buildup-D, Well-3 is part of Buildup-C, and Well-4, -5, and -6 are part of Buildup-A (Figure 4.2). Well-5 shows the distinctive gamma-ray log (green curve) characteristics of the buildup-core, low gamma-ray values in cylindrical shape. Approximate levels of total depth (TD) of the deviated wells are shown by red dashed lines. The thickness of the shale-dominated interval between Base of Kujung UP and Top Buildup Envelope ranges from 92 ft in Well-1 to 464 ft in Well-6.

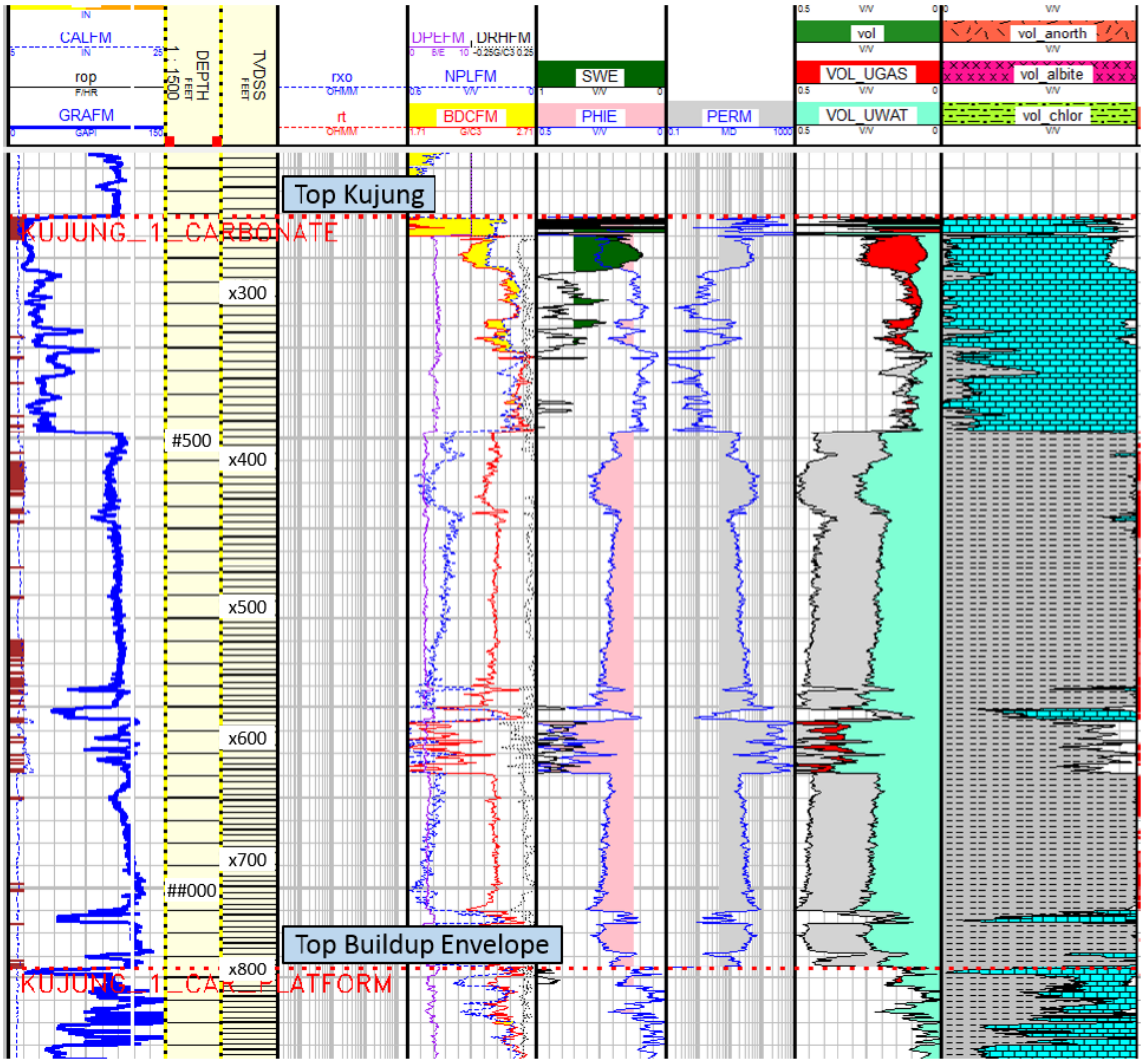

Figure 4.7. Example of type logs (gamma-ray, resistivity, neutron, and density) and reservoir parameters (porosity, water saturation, and permeability) resulting from petrophysical calculation of the off-buildup carbonate strata (Kujung-UP) in Well-6.

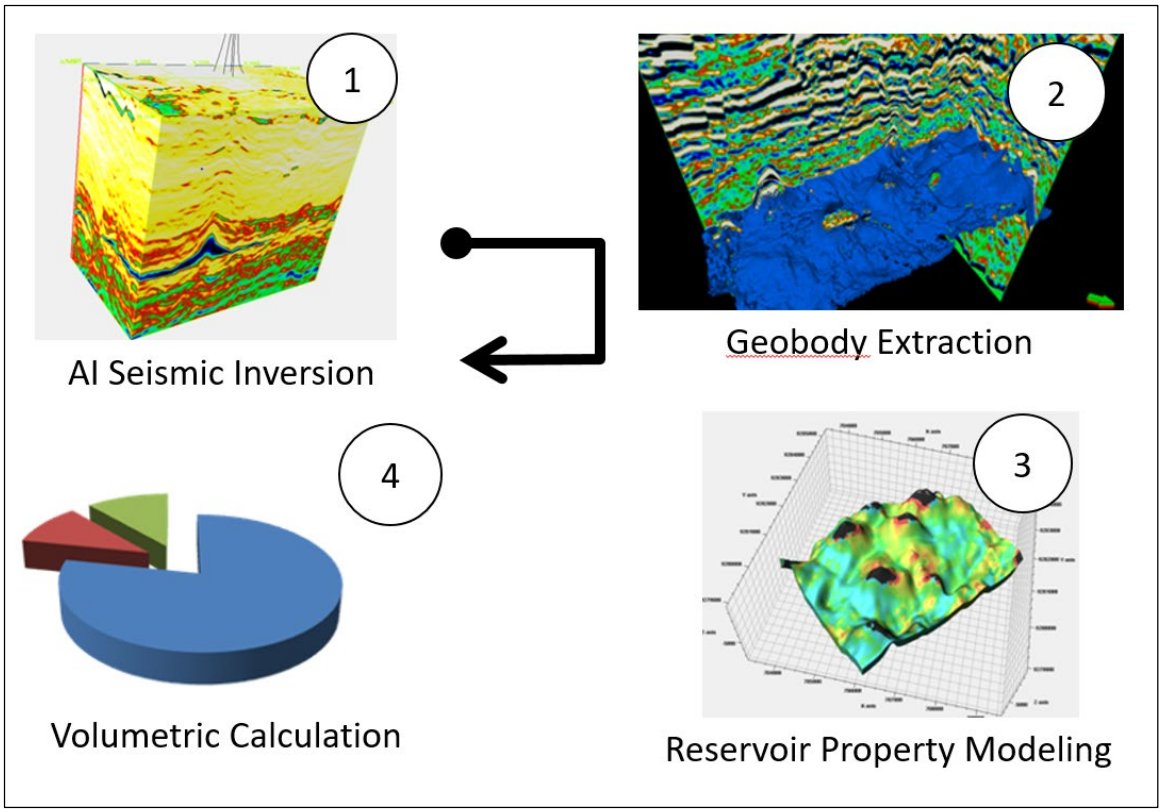

Figure 4.8. Work flow of subsurface data analysis done in this study. Seismic geobody extraction from acoustic impedance (AI) volume was done in order to generate the top and base of the Kujung-UP that were then used as inputs for sturctural modeling. Petrophysical logs were upscaled to the geo-cellular model and subsequently populated in property modeling. The Kujung-UP reservoir model was used in volumetric calculations of the off-buildup carbonates strata as the upside potential.

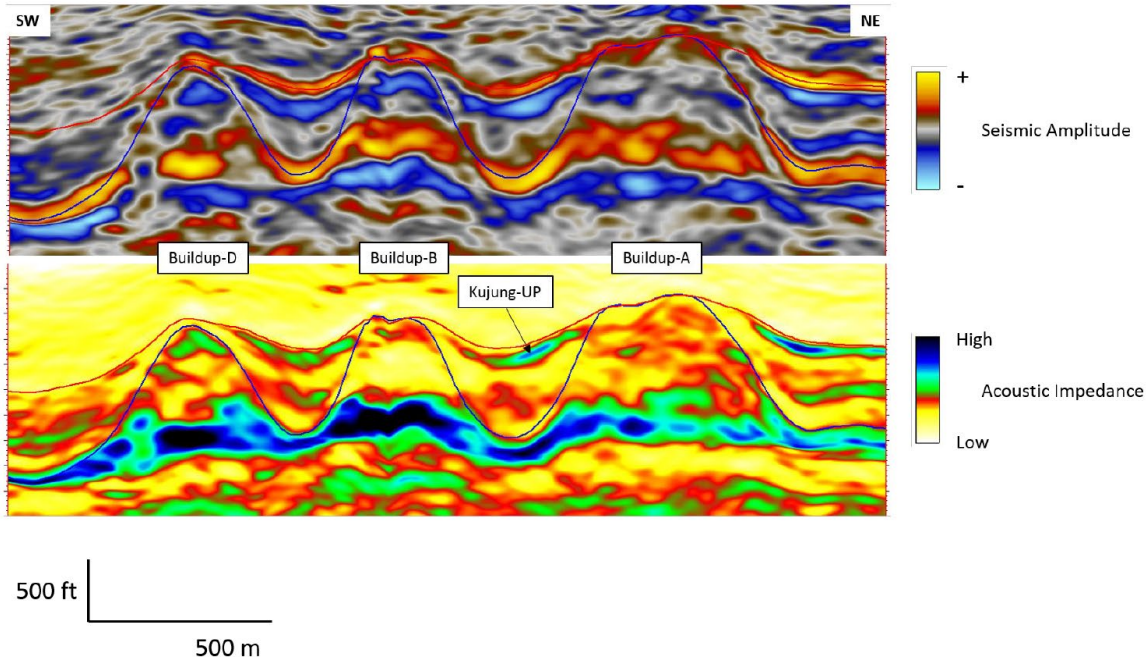

Figure 4.9. Acoustic inversion (AI) volume was used in the seismic geobody extraction. Extracted seismic geobodies were then used to provide the top and bottom of the Kujung-UP as an upside potential interval that subsequently were used as the framework for the static reservoir model.

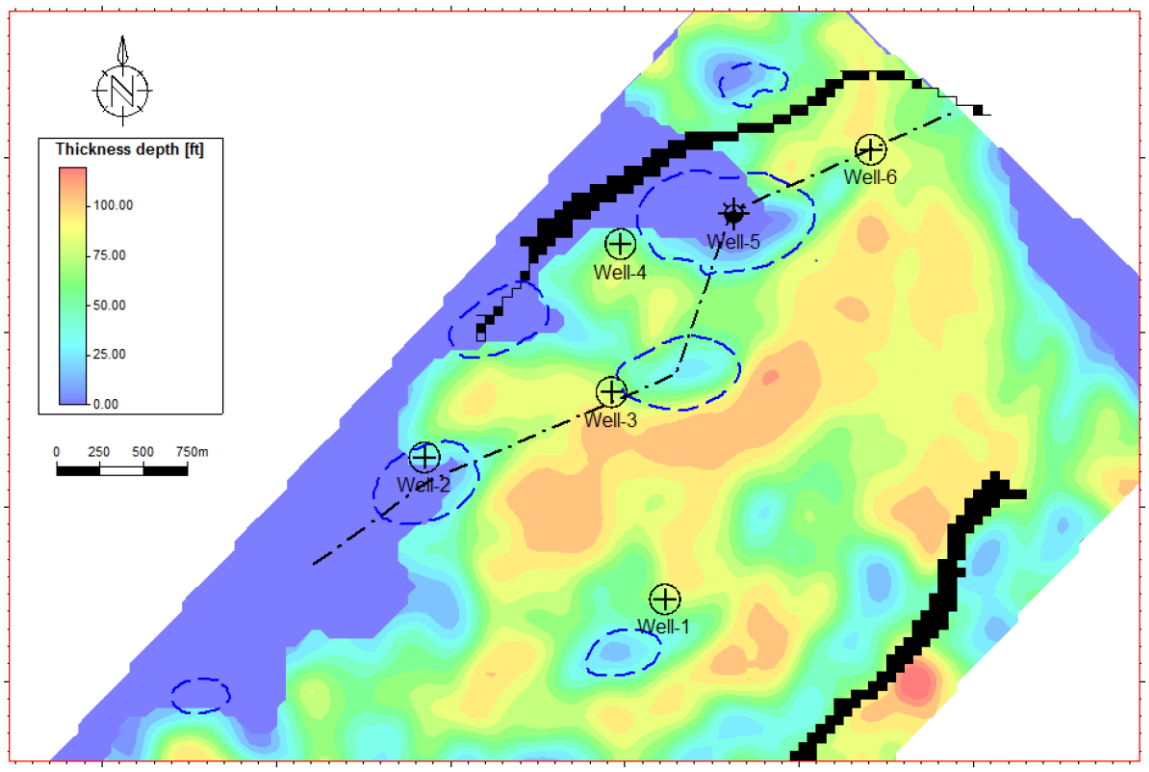

Figure 4.10. Plan view of isopach map of the Kujung-UP within the study area showing thickening in the inter-buildups area and a thinner interval of buildup-flank, draping toward the buildups.

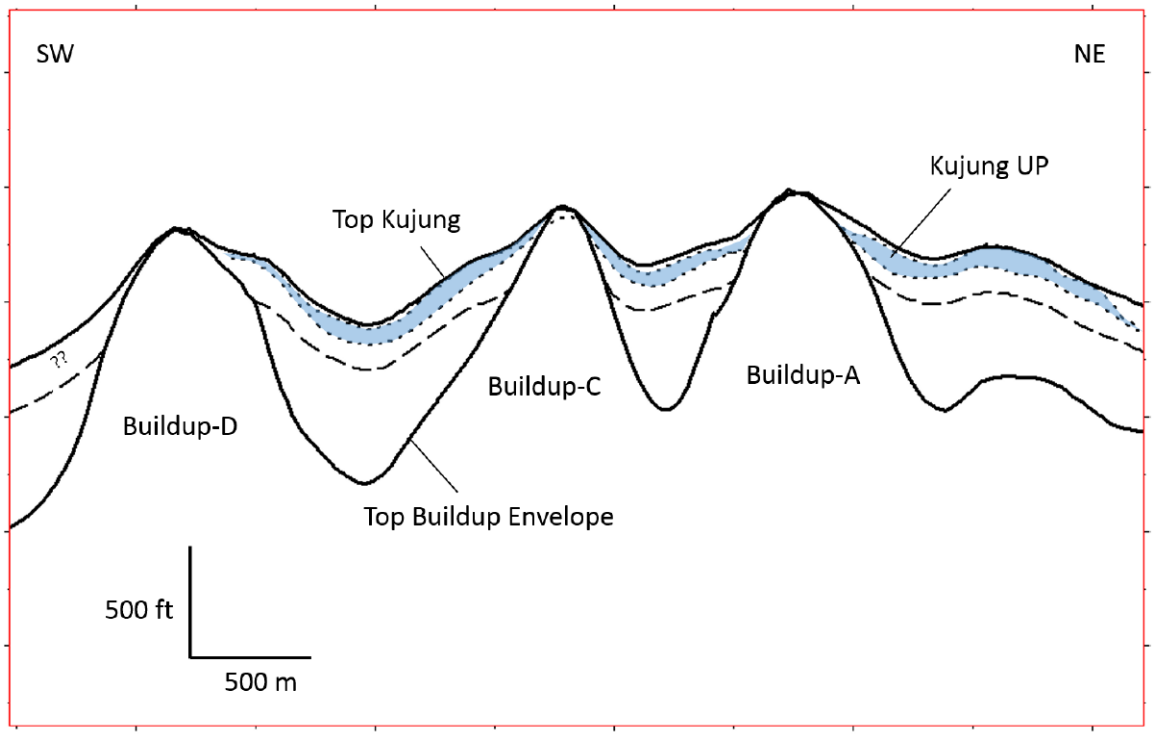

Figure 4.11. Section view of the Kujung-UP distribution around the main buildups of the X8 field. No distribution of the Kujung-UP exists southwest of the Buildup-D, probably due to limitations regarding the acoustic impedance volume. Interpretation of timelines across buildup-core, buildup-flank, and inter-buildups area referring to Figure 2.5 and Figure 4.3.

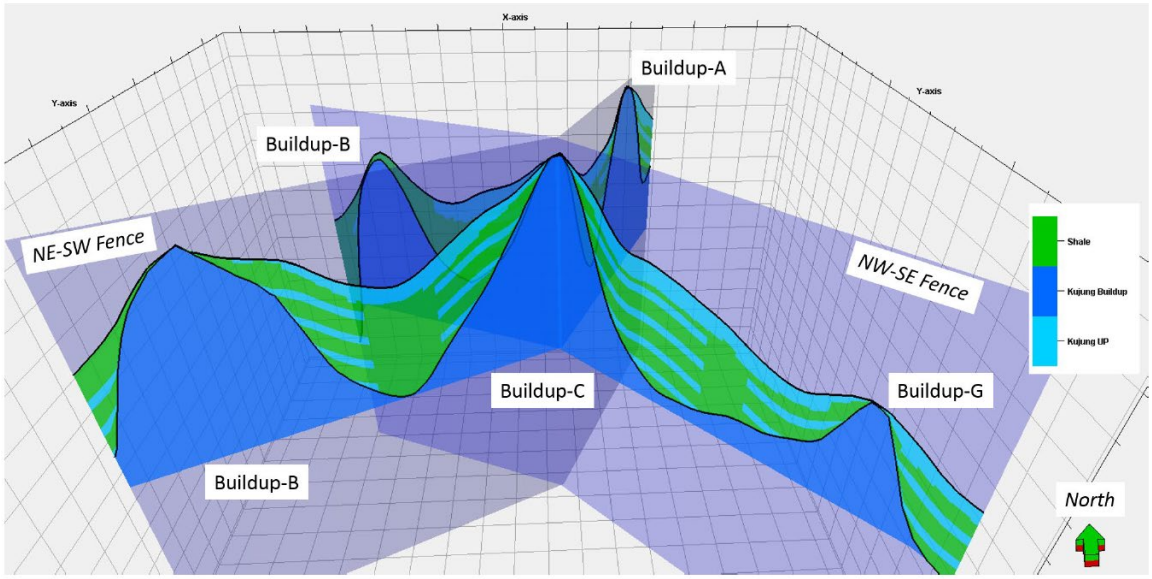

Figure 4.12. Intersecting fence diagrams with reservoir facies model plotted on the sections. Facies consist of Kujung Buildup (buildup-core), Kujung-UP (buildup-flank and inter-buildups), and shale-dominated layers. Interpretation of timelines across buildup-core, buildup-flank, and inter-buildups area referring to Figure 2.5 and Figure 4.3.

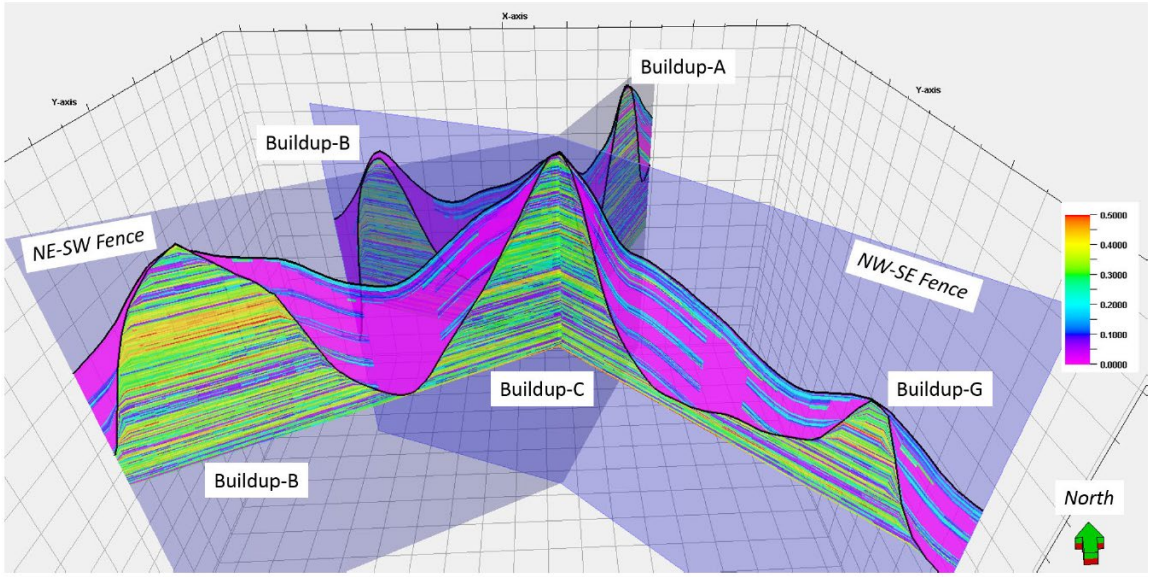

Figure 4.13. Intersecting fence diagrams with the reservoir porosity model plotted on the sections show porosity development in the Kujung-UP interval and other carbonate beds in the buildup-flank and inter-buildups area. Shale-dominated layers were considered non-reservoir and were assigned zero-porosity. Interpretation of timelines across buildup-core, buildup-flank, and inter-buildups area referring to Figure 2.5 and Figure 4.3.

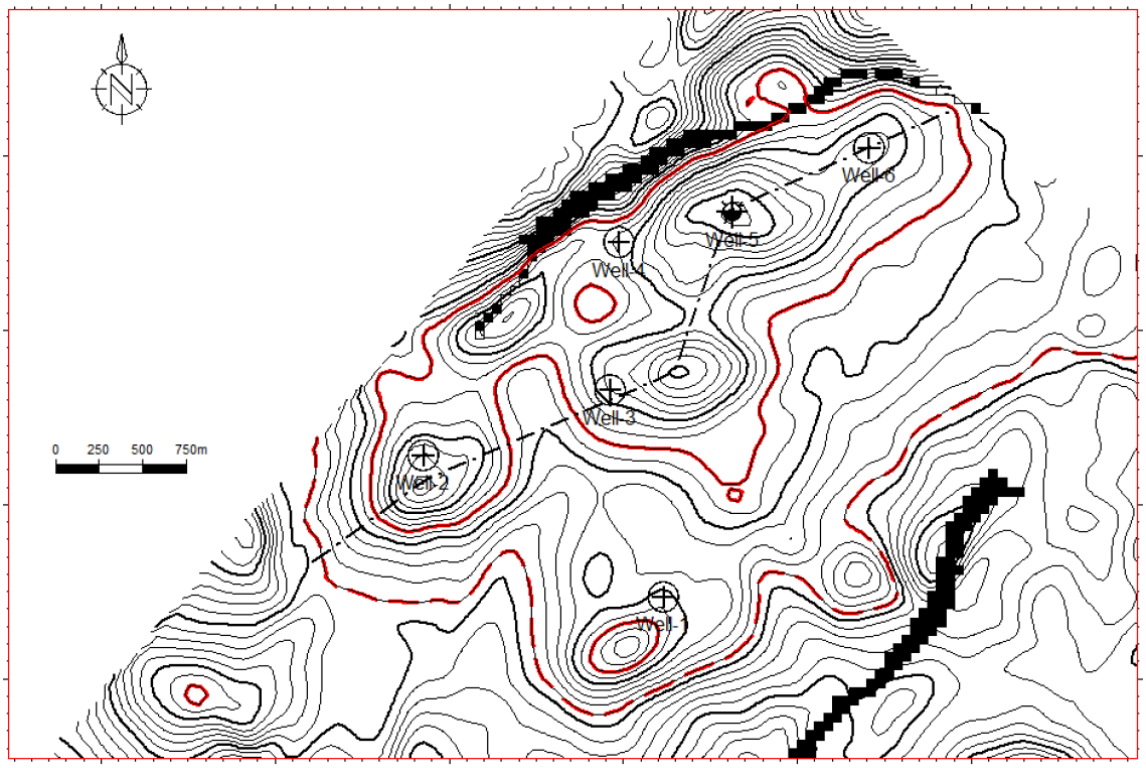

Figure 4.14. Fluid contacts plotted on the depth structure map of the Top Kujung horizon that includes off-buildups strata (refer to Figure 4.5 and 4.6). Two cases were performed: 1) lowest-known water (LKW) based on Well-1 (red solid line) and 2) structural spill point limited by northwestern to northeastern boundary of the reservoir model (red dashed line). The difference in TVD level between the two fluid contacts is approximately 240 ft.

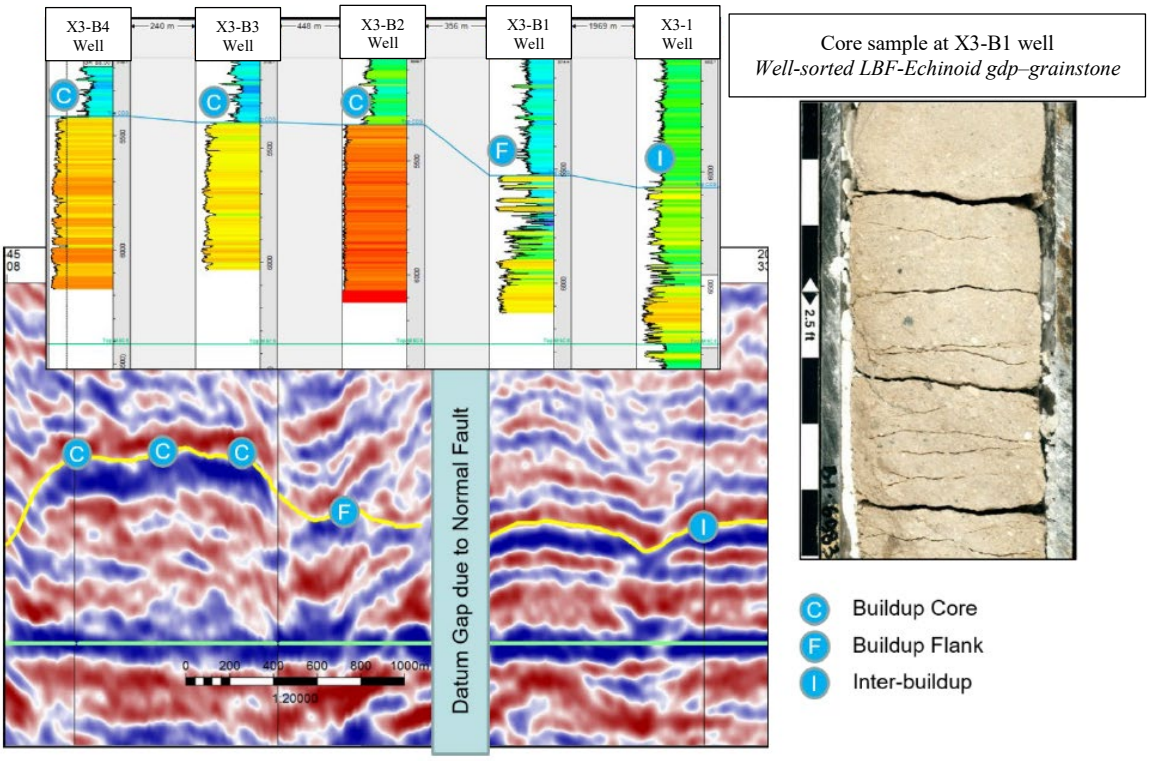

Figure 4.15. Facies analogue for the off-buildups strata from the nearby X3 field located approximately 15 kilometers south of the study area. Gamma-ray log patterns show similar characteristics of interbedded carbonate-shale in the buildup-flanks. Facies of one of these carbonate beds based on core sample is well-sorted LBF-Echinoid *grain-dominated packstone* to *grainstone*.

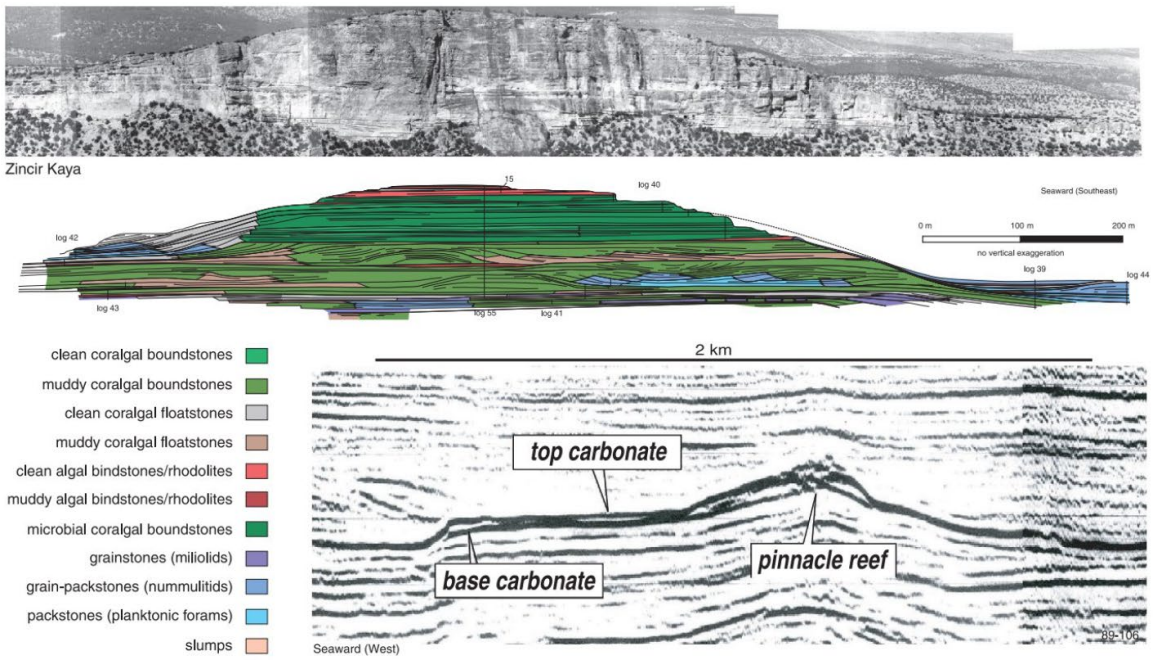

Figure 4.16. Outcrop analogue from the Miocene isolated carbonate buildup from the Pirinc outcrop, Turkey (Bassant et al., 2004). This carbonate buildup shows geometry similar to that of the Kujung Formation carbonate buildups. Vertical relief is approximately 150 meters from the core of the buildup to the basinal inter-buildups area. Carbonate buildup size is hundreds of meters to a few kilometers in width. *Packstones*, sometimes grainy, characterized the off buildups area, in contrast to the *coralgal boundstones* that dominated buildup-core.

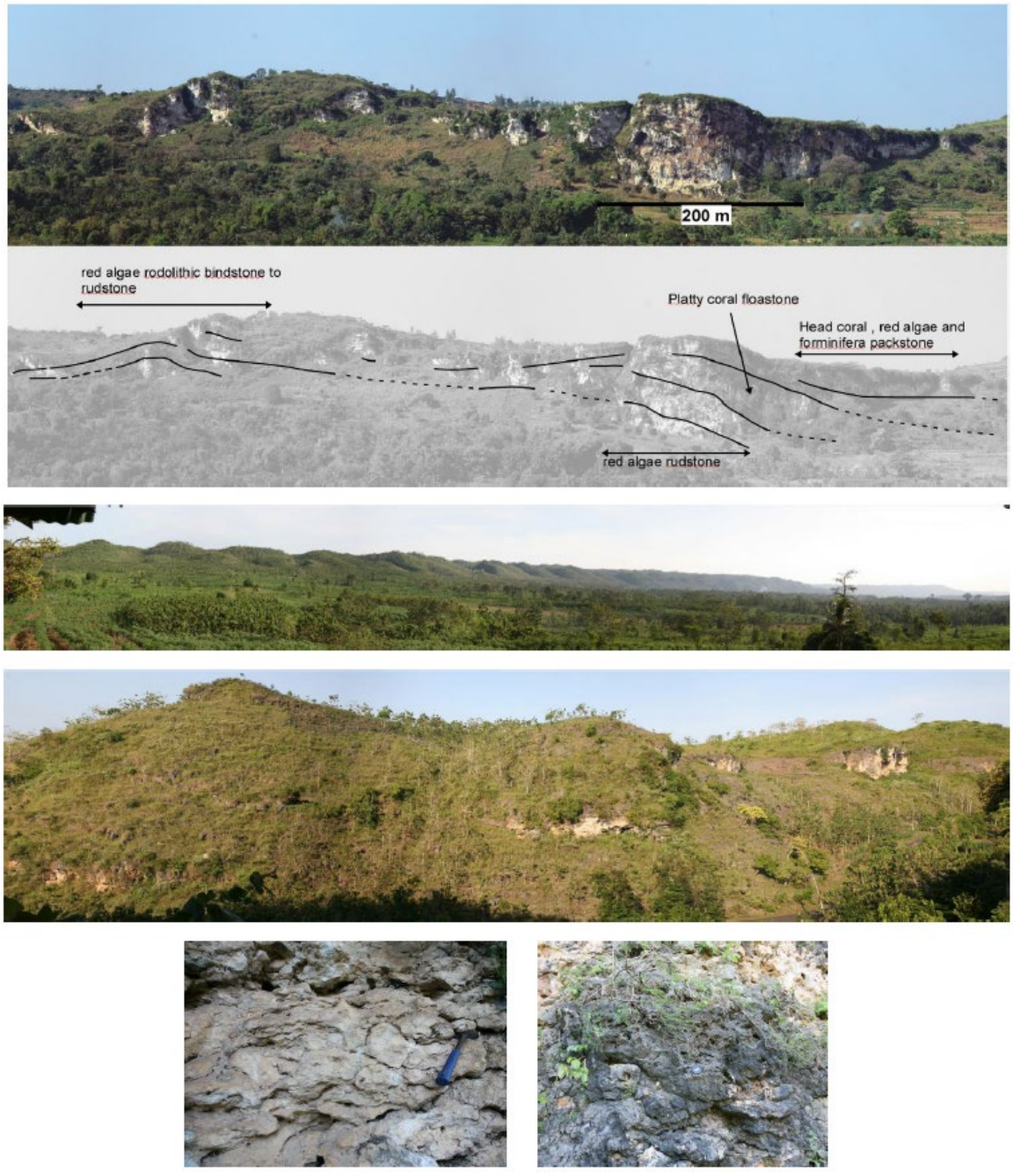

Figure 4.17. Outcrop analogue from Wonosari Platforms, onshore, southern East Java area (Photo and interpretation by Janson, 2012 – *unpublished*). Buildups are in similar scale of hundreds of meters to several kilometers wide, dominated by red-algae, rhodolith, coral *bindstone*, to *floatstone – rudstone*. Off the buildups, along the flank to the inter-buildups area, coral-red algae-foraminifer *packstones* were found.

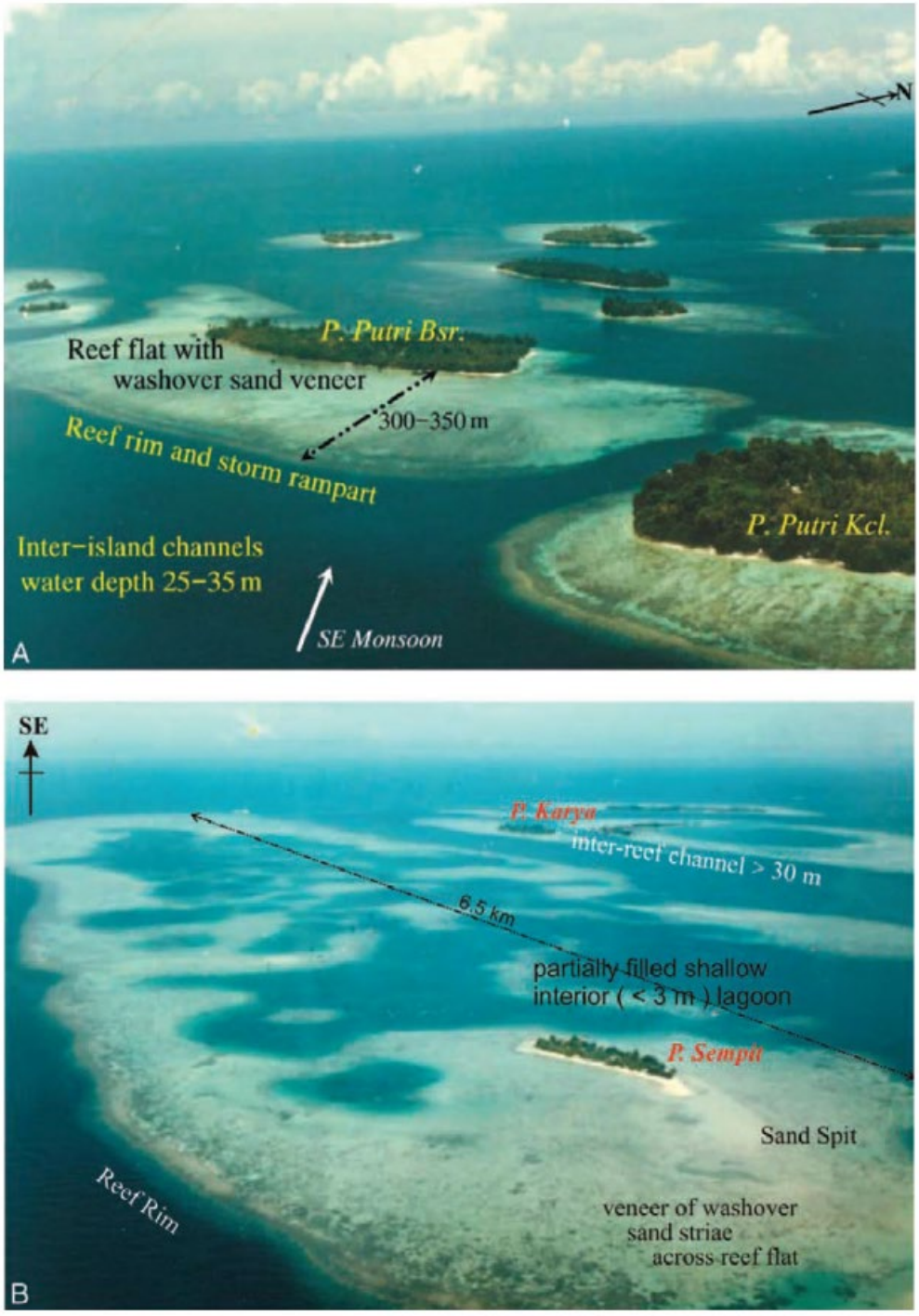

Figure 4.18. Present-day analogue from Seribu Islands, offshore Jakarta, Indonesia. Both figures show architectural elements of the carbonate buildups islands that include reef rim, grainy interior, and inter-reef channel more than 30 m deep (Park et al., 2010).

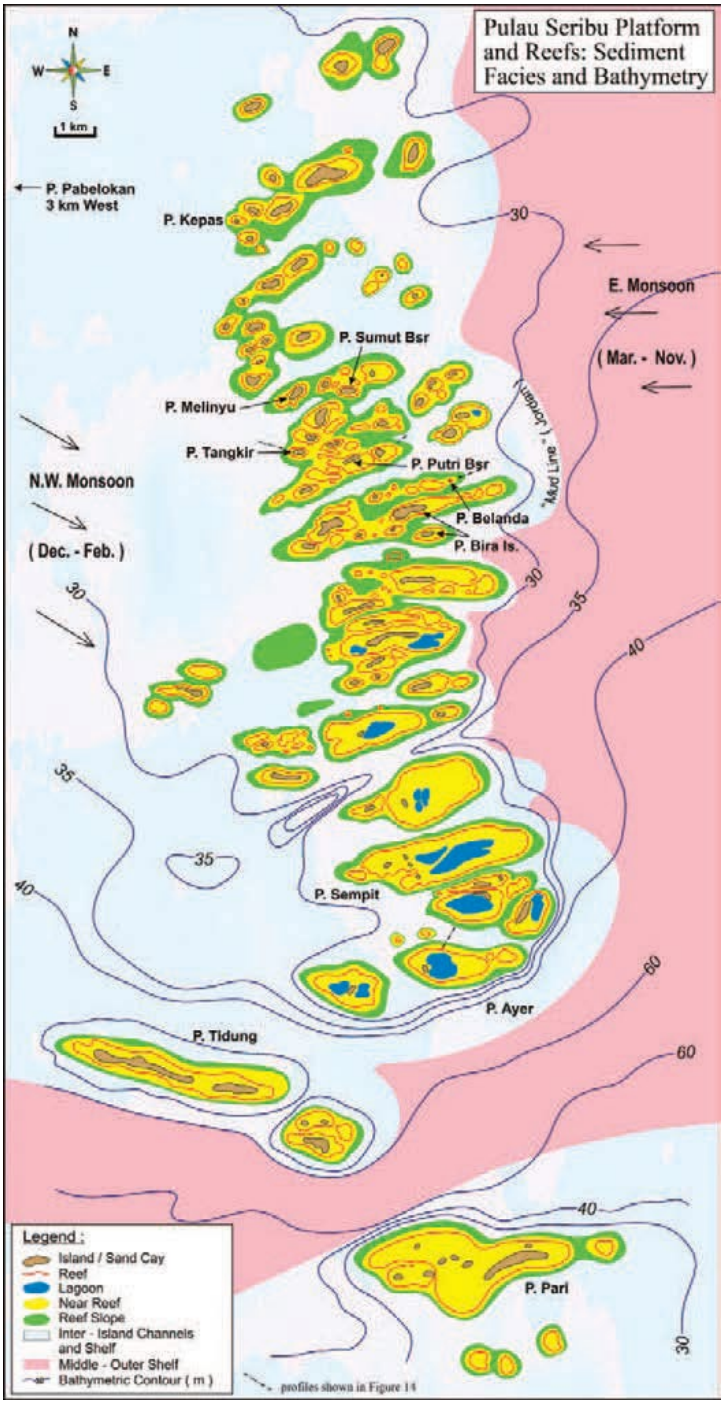

Figure 4.19. Plan view of the Seribu Islands facies distribution map plotted together with bathymetric contour (Park et al, 2010). Strikingly similar geometry to that of the Early Miocene carbonate buildups in the study area (Carter et al., 2005) that were situated in a relatively similar setting (back-arc, detached, and isolated).

Chapter 5: Conclusions

Depositional setting of the Kujung Formation in the study area changed from a mixed-siliciclastic-carbonate shelf (MSCS) in the Rupelian–Chattian to a carbonate-buildups shelf (CBS) in the Aquitanian, during a total duration of 13.5 million years. The accumulation rate within the CBS interval is up to three times higher than that of the MSCS, suggesting higher accommodation and sedimentation/production rates. Spatial variations and temporal trends in tectonically inherited antecedent topography, age range of the carbonate formations, underlying as well as overlying formations, architecture, and facies were observed when comparing the Kujung Formation to other Oligocene-Miocene carbonate formations in the southeastern Sundaland region. This study demonstrates that these trends and variations can be observed across almost all geographic scales; intra- and inter-platform, basin, and regional scale.

By utilizing 3D seismic geomorphology techniques, spectacular three-dimensional images of the Miocene carbonate buildups and platforms were generated. The Early Miocene carbonate shelf is characterized by circular, east-west elongated, and polygonal buildups. These buildups are 0.5–2 km wide and as much as 8 km long. The Late Miocene carbonate shelf is characterized by north-south elongated to oval-shaped, flat-topped-like carbonate platforms, which are 5–8 km wide and up to 20 km long. Both intervals can reach thickness as much as 1,100–1,200 ft and demonstrated development in stages: 1) initiation, 2) coalescence, and 3) amalgamation. Early Miocene carbonate buildups distribution follows the basement structure whereas the Late Miocene carbonate platform distribution does not. Sinuous tidal channels developed over the larger platforms near the end of

Miocene, not observed in the smaller ones. Variation in margin style within a single north-south elongated platform, highly progradational in the north and highly aggradational in the south, may suggest higher subsidence southward. This indicates syn-depositional influence from tectonic events to the shelf during the Late Miocene intense compressional regime. Growth faults were also observed on the inter-platform area.

By utilizing static reservoir modeling workflow, this study suggests that off-buildup carbonates may have a good reservoir quality and storage capacity. The connectivity of the off-buildup carbonates to their adjacent buildup-core remains critical to development strategy for existing fields. This study offers a possible explanation for some volumetric problems. Additional volumes of hydrocarbon from the off-buildup carbonates may help explain problems regarding cumulative production numbers that exceed volumetrically possible, original hydrocarbons in-place, stored in the buildup-core.

This study advances the understanding of the interplay between controls on the Oligocene–Early Miocene carbonate shelf evolution within a complex tectonic setting. This study suggests that tectonically inherited antecedent topography and siliciclastic sediment routing are the most dominant controls for the spatial variations in architecture and facies of the carbonate shelves. Regional and global controls such as sea-level fluctuation patterns, and subsidence due to tectonic activity and volcanism might have partly contributed to the temporal change observed in the region, such as the extensive development of carbonate buildups in the Early Miocene. The influence of regional climatic change observed in the mainland Borneo, from seasonal to everwet–superwet condition, throughout Oligocene–Miocene appeared to be overrode by previously-

mentioned controls. The details observed in the Late Miocene carbonate platforms suggest that, toward the end of Miocene time, accommodation on the shelf had been decreasing, marked by development of sinuous tidal channels and wedge-shaped deposits off the margin. This condition is interpreted to be mainly caused by the regional tectonic inversion during the Miocene compressional tectonic regime. Regional trends in north-south elongated platforms also suggest a strong influence from regional oceanic circulation strongly influenced by the development of the Indonesian through-flow.

Results from this study will give insight into other regions with Oligocene–Miocene carbonate reservoirs, specifically for improving new exploration concepts and existing field development strategies.

References

Adhyaksawan, R., 2003, Seismic facies and growth history of Miocene carbonate platforms, Wonocolo Formation, North Madura area, East Java Basin, Indonesia: Proceedings of the Indonesian Petroleum Association, Twenty-Ninth Annual Convention, v. 1, p. 1-22.

Ardhana, W., 1993, A depositional model for the early Middle Miocene Ngrayong Formation and implications for exploration in the East Java basin: Proceedings of the Indonesian Petroleum Association, Twenty-Second Annual Convention, v. 1, p. 395-443.

Bachtel, S. L., Kissling, R. D., Martono, D., Rahardjanto, S. P., Dunn, P. A., and MacDonald, B. A., 2004, Seismic stratigraphic evolution of the Miocene-Pliocene Segitiga Platform, East Natuna Sea, Indonesia: The origin, growth, and demise of an isolated carbonate platform, *in* Seismic imaging of carbonate reservoirs and systems: AAPG Memoir 81, p. 309-328.

Bachtel, S. L., Posamentier, H. W., Gerber, T. P., Wood, L. J., Simo, T. T., and Rosen, N. C., 2011, Seismic geomorphology and stratigraphic evolution of a Tertiary-aged isolated carbonate platform system, Browse Basin, North West Shelf of Australia, Part II, *in* Seismic imaging of depositional and geomorphic systems: 30th Annual Gulf Coast Section, SEPM Foundation, Bob F. Perkins Research Conference, p. 115-135.

Bassant, P., 1999, The high-resolution stratigraphic architecture and evolution of the Burdigalian carbonate-siliciclastic sedimentary systems of the Mut Basin, Turkey [Ph.D. Dissertation]: Université de Fribourg, 277 p.

Bassant, P., F. Van Buchem, A. Strasser, and A. Lomando, 2004, A comparison of two early Miocene carbonate margins: The Zhujiang carbonate platform (subsurface, South China Sea) and the Pirinc¸ Platform (outcrop, southern Turkey), *in* Integration of outcrop and modern analogs in reservoir modeling: AAPG Memoir 80, p. 153–170.

Bassant, P., Van Buchem, F. S. P., Strasser, A., and Görür, N., 2005, The stratigraphic architecture and evolution of the Burdigalian carbonate—siliciclastic sedimentary systems of the Mut Basin, Turkey: Sedimentary Geology, v. 173(1), p. 187-232.

Burbury, J. E., 1977, Seismic expression of carbonate build-ups, Northwest Java Basin: Proceedings of the Indonesian Petroleum Association, Sixth Annual Convention, v. 2, p. 239-268.

Cahyono, A. B. and Burgess, C. F., 2007, Cepu 3D seismic-variations in Oligo-Miocene carbonate buildup morphology: Proceedings of the Indonesian Petroleum Association, Thirty-First Annual Convention, p. 122-128.

Carter, D. C. and Hutabarat, M., 1994, The geometry and seismic character of Mid-Late Miocene carbonate sequences, SS area, offshore northwest Java : Proceedings of the Indonesian Petroleum Association, Twenty-Third Annual Convention, v. 1, p. 323-338.

Carter, D. C., Mandhiri, D., Park, R. K., Asjhari, I., Basyuni, S., Birdus, S., ..., and Nugroho, M. A., 2005, Interpretation methods in the exploration of Oligocene-Miocene carbonate reservoirs, offshore Northwest Madura, Indonesia: Proceedings of the Indonesian Petroleum Association, Thirtieth Annual Convention, v. 1, p. 3-39.

Cohen, K. M., Finney, S. C., Gibbard, P. L., and Fan, J. X., 2013, The ICS international chronostratigraphic chart: Episodes, v. 36(3), p. 199-204.

Collins, J. F., Kenter, J. A. M., Harris, P. M., Kuanysheva, G., Fischer, D. J., and Steffen, K. L., 2006, Facies and reservoir-quality variations in the late Visean to Bashkirian outer platform, rim, and flank of the Tengiz buildup, Precaspian Basin, Kazakhstan, in Giant hydrocarbon reservoirs of the world: From rocks to reservoir characterization and modelling: AAPG Memoir 88/SEPM Special Publication, p. 55-95.

Courel, R., Hollomon, G., Kim, M., Richert, D., Tiranda, C., and Tognini, P., 2011, A re-evaluation of the South Makassar Basin using an integrated multi-discipline approach: Proceedings of the South East Asia Petroleum Exploration Society (SEAPEX) Conference, p. 1-11.

Doust, H. and Noble, R. A., 2008, Petroleum systems of Indonesia: Marine and Petroleum Geology, v. 25(2), p. 103-129.

Dunham, R. J., 1962, Classification of carbonate rocks according to depositional textures: AAPG Memoir 1, p. 108-121.

Embry III, A. F. and Klovan, J. E., 1971, A late Devonian reef tract on northeastern Banks Island, NWT: Bulletin of Canadian Petroleum Geology, v. 19(4), p. 730-781.

Esker, D., Eberli, G. P., and McNeill, D.F., 1998, The structural and sedimentological controls on the reoccupation of Quarternary incised valleys, Belize southern lagoon: AAPG Bulletin, v. 82(11), p. 2075-2109

Fifariz, R., Setiawan, M., Janson, X., Kerans, C., & Thoha, S., 2017, The Upside Potential of the Early Miocene Kujung-1 Carbonate, Offshore East Java, Indonesia. AAPG Annual Convention and Exhibition, Houston, Texas.

Fifariz, R., Janson, X., & Kerans, C., 2018, Seismic Geomorphology of the Early and Late Miocene Carbonate Systems in an Active Tectonic Margin, Offshore East Java, Indonesia. AAPG Annual Convention and Exhibition, Salt Lake City, Utah.

Fontaine, J. M., Cussey, R., Lacaze, J., Lanaud, R., and Yapaudjian, L., 1987, Seismic interpretation of carbonate depositional environments: AAPG Bulletin, v. 71(3), p. 281-297.

Fulthorpe, C. S. and Schlanger, S. O., 1989, Paleo-oceanographic and tectonic settings of early Miocene reefs and associated carbonates of offshore Southeast Asia: AAPG Bulletin, v. 73(6), p. 729-756.

Gao, S. and Collins, M. B., 2014, Holocene sedimentary systems on continental shelves: Marine Geology, v. 352, p. 268-294.

Gradstein, F. M., 2012, Introduction, *in* The geologic time scale 2012: Elsevier, p. 1-29.

Grélaud, C., Razin, P., and Homewood, P., 2010, Channelized systems in an inner carbonate platform setting: differentiation between incisions and tidal channels

(Natih Formation, Late Cretaceous, Oman): Geological Society, London, Special Publications, v. 329(1), p. 163-186.

Hakiki, F., Sekti, R. P., Simo, T., Fullmer, S. M., and Musgrove, F., 2012, Oligo-Miocene carbonate reservoir quality controls–deposition and diagenesis study of Banyu Urip Field, onshore East Java: Proceedings of the Indonesian Petroleum Association, Thirty-Sixth Annual Convention, p. 37-49.

Hall, R., 1997, Cenozoic plate tectonic reconstructions of SE Asia: Geological Society, London, Special Publications, v. 126(1), p. 11-23.

Hall, R., 1998, The plate tectonics of Cenozoic SE Asia and the distribution of land and sea: Biogeography and geological evolution of SE Asia, p. 99-131.

Hall, R. and Nichols, G., 2002, Cenozoic sedimentation and tectonics in Borneo: climatic influences on orogenesis: Geological Society, London, Special Publications, v. 191(1), p. 5-22.

Hall, R., 2002, Cenozoic geological and plate tectonic evolution of SE Asia and the SW Pacific: computer-based reconstructions, model and animations: Journal of Asian Earth Sciences, v. 20(4), p. 353-431.

Hall, R., van Hattum, M. W., and Spakman, W., 2008, Impact of India–Asia collision on SE Asia: The record in Borneo: Tectonophysics, v. 451(1), p. 366-389.

Hall, R., 2009, Southeast Asia's changing palaeogeography: Blumea-Biodiversity, Evolution and Biogeography of Plants, v. 54(1-2), p. 148-161.

Hall, R., 2012, Late Jurassic–Cenozoic reconstructions of the Indonesian region and the Indian Ocean: Tectonophysics, v. 570, p. 1-41.

Hallock, P. and Glenn, E. C., 1986, Larger foraminifera: A tool for paleoenvironmental analysis of Cenozoic carbonate depositional facies: Palaios, v. 1(1), p. 55-64.

Handford, C. R. and Loucks, R. G., 1993, Carbonate depositional sequences and systems tracts--responses of carbonate platforms to relative sea-level changes: Chapter 1, *in* Carbonate sequence stratigraphy: Recent developments and applications: AAPG Memoir 57, p. 3-41.

Haq, B. U., Hardenbol, J., and Vail, P. R., 1987, Chronology of fluctuating sea levels since the Triassic: Science, v. 235(4793), p. 1156-1167.

Janson, X., Kerans, C., Loucks, R., Marhx, M. A., Reyes, C., and Murguia, F., 2011, Seismic architecture of a Lower Cretaceous platform-to-slope system, Santa Agueda and Poza Rica fields, Mexico: AAPG Bulletin, v. 95(1), p. 105-146.

Johansen, K. B., 2003, Depositional geometries and hydrocarbon potential within Kujung carbonates along the North Madura Platform, as revealed by 3D and 2D seismic data: Proceedings of the Indonesian Petroleum Association, Twenty-Ninth Annual Convention, v. 1, p. 1-26.

Jones, M. R., 1995, The Torres Reefs, North Queensland, Australia—strong tidal flows a modern control on their growth: Coral Reefs, v. 14(2), p.63-69.

Jones, B. and Desrochers, A., 1992, Shallow platform carbonates, *in* Facies models: Response to sea level change: Geological Association of Canada. Dep. Earth Sci., Memorial Univ., St. John's, Newfoundland, p. 277-301.

Jordan Jr., C. F., 1998, The sedimentology of Kepulauan Seribu: A modern patch reef complex in the west Java Sea, Indonesia: Indonesian Petroleum Association Field Guide, 81 p.

Jordan Jr., C. F., 1998, Kepulauan Seribu, West Java Sea, Indonesia: A modern reef analog for Miocene oil and gas fields in Southeast Asia: Proceedings of the Indonesian Petroleum Association, Twenty-Sixth Annual Convention, v. 1, p. 71-83.

Kenyon, C. S., 1977, Distribution and morphology of early Miocene reefs, East Java Sea: Proceedings of the Indonesian Petroleum Association, Sixth Annual Convention, v. 2, p. 215-238.

Koša, E., Warrlich, G. M., and Loftus, G., 2015, Wings, mushrooms, and Christmas trees: The carbonate seismic geomorphology of Central Luconia, Miocene–present, offshore Sarawak, northwest Borneo: AAPG Bulletin, v. 99(11), p. 2043-2075.

Kuhnt, W., Holbourn, A., Hall, R., Zuvela, M., and Käse, R., 2004, Neogene history of the Indonesian throughflow, in Continent-ocean interactions within East Asian marginal seas: Geophysical Monograph, v. 149, p. 299-320.

Kupecz, J., Sayers, I., Tognini, P., Hilman, A., Tanos, C., and Ariyono, D., 2013, New insights into the tectono-stratigraphic evolution of the South Makassar Basin: Proceedings of the Indonesian Petroleum Association, Thirty-Seventh Annual Convention, p. 158-198.

Kusumastuti, A., Van Rensbergen, P., and Warren, J. K., 2002, Seismic sequence analysis and reservoir potential of drowned Miocene carbonate platforms in the Madura Strait, East Java, Indonesia: AAPG Bulletin, v. 86(2), p. 213-232.

Longman, M. L., Siemers, C. T., and Siwindono, T., 1992, Characteristics of low-relief carbonate mudbank reservoir rocks, Baturaja Formation (lower Miocene), Air Serdang and Mandala fields, South Sumatra Basin, Indonesia, *in* Carbonate rocks and reservoirs of Indonesia: A core workshop: Indonesian Petroleum Association, p. 9-1–9-29.

Lukasik, J. and Simo, J. A., 2008, Controls on development of Phanerozoic carbonate platforms and reefs: Introduction and synthesis, *in* Controls on carbonate platform and reef development: SEPM Special Publications, v. 89, p. 5-12.

Manur, H. and Barraclough, R., 1994, Structural control on hydrocarbon habitat in the Bawean area, East Java Sea: Proceedings of the Indonesian Petroleum Association, Twenty-Third Annual Convention, v. 1, p. 129-144.

Matthews, S. J. and Bransden, P. J., 1995, Late cretaceous and cenozoic tectono-stratigraphic development of the East Java Sea Basin, Indonesia: Marine and Petroleum Geology, v. 12(5), p. 499-510.

Maulin, H. B., Nugraha, A., Sutisna, C., Prasetya, A., Harun, I., Rubyanto, D., and Wibowo, B., 2016, JS-1 Ridge: Exploration in ancient mélange basement high: GEOSEA XIV Congress and 45th IAGI Annual Convention.

Maynard, K. and Morgan, W. A., 2005, Appraisal of a complex, platform carbonate, Bukit Tua discovery, Ketapang PSC, East Java Basin, Indonesia: Proceedings of the Indonesian Petroleum Association, Thirtieth Annual Convention, v. 1, p. 317-330.

McArthur, J. M., Howarth, R. J., and Bailey, T. R., 2001, Strontium isotope stratigraphy: LOWESS version 3: Best fit to the marine Sr-isotope curve for 0–509 Ma and accompanying look-up table for deriving numerical age: The Journal of Geology, v. 109(2), p. 155-170.

Miller, K. G., Kominz, M. A., Browning, J. V., Wright, J. D., Mountain, G. S., Katz, M. E., Sugarman, P. J., Cramer, B. S., Christie-Blick, N., and Pekar, S. F., 2005, The Phanerozoic record of global sea-level change: Science, v. 310(5752), p. 1293-1298.

Morley, R. J., 2012, A review of the Cenozoic palaeoclimate history of Southeast Asia, *in* Biotic evolution and environmental change in Southeast Asia: The Systematics Association Special, v. 82, p. 79-114.

Mudjiono, R. and Pireno, G. E., 2002, Exploration of the North Madura Platform, offshore East Java, Indonesia: Proceedings of the Indonesian Petroleum Association, Twenty-Eighth Annual Convention, v. 1, p. 707-726.

Mutti, M., Piller, W. E., and Betzler, C., 2010, Miocene carbonate systems: An introduction, *in* Carbonate Systems During the Olicocene-Miocene Climatic Transition: International Association of Sedimentologists Special Publications 42, p. vii-xii.

Park, R. K., Crevello, P. D., and Hantoro, W., 2010, Equatorial carbonate depositional systems of Indonesia, *in* Cenozoic Carbonate Systems of Australasia: SEPM Special Publications 95, p. 41-77.

Pelton, P. J., 1974, Exploration of the south Barito Basin reef tract, Kalimantan, Indonesia: Proceedings of the Indonesian Petroleum Association, Third Annual Convention, p. 153-169.

Posamentier, H. W., 2004, Seismic geomorphology: Imaging elements of depositional systems from shelf to deep basin using 3D seismic data: Implications for exploration and development: Geological Society, London, Memoirs, v. 29(1), p. 11-24.

Posamentier, H. W., Laurin, P., Warmath, A., Purnama, M., and Drajat, D., 2010, Seismic stratigraphy and geomorphology of Oligocene to Miocene carbonate buildups offshore Madura, Indonesia, *in* Cenozoic carbonate systems of Australasia: SEPM Special Publication 95, p. 175-194.

Pubellier, M. and Morley, C. K., 2014, The basins of Sundaland (SE Asia): Evolution and boundary conditions: Marine and Petroleum Geology, v. 58, p. 555-578.

Rider, M. H., 1990, Gamma-ray log shape used as a facies indicator: Critical analysis of an oversimplified methodology: Geological Society, London, Special Publications, v. 48(1), p. 27-37.

Rosleff-Soerensen, B., Reuning, L., Back, S., and Kukla, P., 2012, Seismic geomorphology and growth architecture of a Miocene barrier reef, Browse Basin, NW-Australia: Marine and Petroleum Geology, v. 29(1), p. 233-254.

Ruf, A. S., Simo, J. T., and Hughes, T. M., 2008, Insights on Oligocene-Miocene carbonate mound morphology and evolution from 3D seismic data, East Java Basin,

Indonesia: Proceedings of the Indonesian Petroleum Association, Thirty-Second Annual Convention, 10 p.

Satyana, A. H., 2005, Oligo-Miocene carbonates of Java, Indonesia: tectonic-volcanic setting and petroleum implications: Proceedings of the Indonesian Petroleum Association, Thirtieth Annual Convention, p. 217-249.

Sekti, R. P., Hakiki, F., Derewetzky, A. N., Strohmenger, C. J., Fullmer, S. M., Simo, T., Sapiie, B., and Nugroho, D., 2011, Facies analysis and sequence stratigraphy of Tertiary subsurface (Cepu Block) and surface (Rajamandala Limestone) carbonates of Java, Indonesia: Proceedings of the Indonesian Petroleum Association, Thirty-Fifth Annual Convention, 15 p.

Serra, O. T. and Abbott, H. T., 1982, The contribution of logging data to sedimentology and stratigraphy: Society of Petroleum Engineers Journal, v. 22(1), p. 117-131.

Setiawan, M., 2018, X9 Field cumulative production and initial hydrocarbon in place numbers, *in* Personal Communication with Fifariz, R., ed.: Austin - Jakarta

Sharaf, E., Simo, J. T., Carroll, A. R., and Shields, M., 2005, Stratigraphic evolution of Oligocene–Miocene carbonates and siliciclastics, East Java basin, Indonesia: AAPG Bulletin, v. 89(6), p. 799-819.

Sharaf, E., Boudagher-Fadel, M. K., and Carroll, A. R., 2014, A revision of the biostratigraphy and strontium isotope dating of Oligocene-Miocene outcrops in East Java, Indonesia: Berita Sedimentologi, v. 30, p. 44-81.

Shimazu, T., Janson, X., Yagi, M., and Ichimaru, Y., 2017, インドネシア東ジャワ・カンゲアン島における上部漸新統～ 下部中新統 Kujung 層炭酸塩岩の岩相

と貯留岩性状: Journal of the Japanese Association for Petroleum Technology, v. 82(1), p. 34-43.

Siemers, C. T., Deckelman, J. A., Brown, A. A., and West, E. R., 1992, Characteristics of the fractured Ngimbang carbonate (Eocene), West Kangean-2 well, Kangean PSC, East Java Sea, Indonesia, *in* Carbonate rocks and reservoirs of Indonesia: A core workshop: Indonesian Petroleum Association, p. 9-1–9-29.

Simo, T., Weidmer, M., Van Simaeys, S., Sekti, R., van Gorsel, H., Strohmenger, C., and Derewetsky, A., 2011, Sequence stratigraphic correlation and sedimentological implications, East Java Basin: Comparisons and lessons learned from outcrop and subsurface studies: Proceedings of the Indonesian Petroleum Association, Thirty-Fifth Annual Convention, 9 p.

Simo, T., Sekti, R. P., Hakiki, F., Sun, M., Myers, R. D., Fullmer, S. (2012). Reservoir characterization and simulation of an Oligocene-Miocene carbonate platform: Banyu Urip Field, East Java, Indonesia.

Smyth, H. R., Hall, R., and Nichols, G. J., 2008, Significant volcanic contribution to some quartz-rich sandstones, East Java, Indonesia: Journal of Sedimentary Research, v. 78(5), p. 335-356.

Soeria-Atmadja, R., Maury, R. C., Bellon, H., Pringgoprawiro, H., Polve, M., and Priadi, B., 1994, Tertiary magmatic belts in Java: Journal of Southeast Asian Earth Sciences, v. 9(1-2), p. 13-27.

van Simaeys, S., Musgrove, F., Stephens, N., Weidmer, A., Zeiza, A., Sekti, R., Derewetzky, A., and Simo, T., 2011, Early carbonate growth in the East Java

Basin, Indonesia: A case study from the Jambaran Field: Proceedings of the Indonesian Petroleum Association, Thirty-Fifth Annual Convention, 13 p.

van Tuyl, J., Alves, T. M., and Cherns, L., 2018, Pinnacle features at the base of isolated carbonate buildups marking point sources of fluid offshore Northwest Australia: Geological Society of America Bulletin, v. 130 (9-10), p. 1596-1614.

Waltham, D., Hall, R., Smyth, H. R., and Ebinger, C. J., 2008, Basin formation by volcanic arc loading: Special Papers-Geological Society of America, v. 436, p. 11-26.

Welker-Haddock, M., Park, R., Asjhari, I., Bradfield, J., and Nguyen, B., 2002, The transformation of Poleng Field: Proceedings of the Indonesian Petroleum Association, Twenty-Eighth Annual Convention, v. 1, p. 681-698.

Werdaya, A. A., Wulansari, M., and Billing, I., 2013, Gross depositional environment model of the Berai Carbonate Formation and its implication for reservoir prospectivity, Barito Basin, South Kalimantan, Indonesia: Proceedings of the Indonesian Petroleum Association, Thirty-Seventh Annual Convention, 21 p.

Wilson, J. L., 1975, Carbonate facies in geologic history: Springer-Verlag.

Wilson, M. E. J., Bosence, D. W., & Limbong, A., 2000, Tertiary syntectonic carbonate platform development in Indonesia: Sedimentology, v. 47(2), p. 395-419.

Wilson, M. E. J., 2000, Tectonic and volcanic influences on the development and diachronous termination of a Tertiary tropical carbonate platform: Journal of Sedimentary Research, v. 70(2), p. 310-324.

Wilson, M. E. J., 2002, Cenozoic carbonates in Southeast Asia: implications for equatorial carbonate development: Sedimentary Geology, v. 147(3), p. 295-428.

Wilson, M. E. J. and Vecsei, A., 2005, The apparent paradox of abundant foramol facies in low latitudes: Their environmental significance and effect on platform development: Earth-Science Reviews, v. 69(1), p. 133-168.

Wilson, M. E. J., 2008, Global and regional influences on equatorial shallow-marine carbonates during the Cenozoic: Palaeogeography, Palaeoclimatology, Palaeoecology, v. 265(3), p. 262-274.

Wilson, M. E. J. and Hall, R., 2010, Tectonic influences on SE Asian carbonate systems and their reservoir development, *in* Cenozoic carbonate systems of Australasia: SEPM Special Publication 95, p. 13-40.

Witts, D., Hall, R., Morley, R. J., and BouDagher-Fadel, M. K., 2011, Stratigraphy and sediment provenance, Barito basin, Southeast Kalimantan: Proceedings of the Indonesian Petroleum Association, Thirty-Fifth Annual Convention, 18 p.

Zachos, J., Pagani, M., Sloan, L., Thomas, E., and Billups, K., 2001, Trends, rhythms, and aberrations in global climate 65 Ma to present: Science, v. 292(5517), p. 686-693.

Zampetti, V., Morgan, W. A., George, A. D., Harris, P. M., Kupecz, J. A., and Sarg, J. F., 2010, Controlling factors of a Miocene carbonate platform: implications for platform architecture and off-platform reservoirs (Luconia Province, Malaysia), *in* Cenozoic Carbonate Systems of Australasia: SEPM Special Publication 95, p. 129-145.

Vita

Reynaldy Fifariz was born in Dumai, Riau, Indonesia on September 18th, 1984, the eldest son, the first of three siblings, of Afifah and Basrizal. After completing his high school at SMAN 3 Bandung, West Java, he entered Institut Teknologi Bandung in 2002, and earned a Bachelor of Science degree in Geological Engineering in September 2008. He then continued seeking his Master of Science degree in Geological Engineering at the same university and graduated cum laude in September 2010. He married Desi Maulani Rosadi in October 2010. In the following year of 2011, his daughter—Syalabiyyah Naura Fifariz (Sasya) was born, and he was awarded a Fulbright Presidential Ph.D. Scholarship. In the fall of 2012, he continued his graduate school career to pursue a Doctor of Philosophy degree in Geological Sciences at the Jackson School of Geosciences, The University of Texas at Austin. He was part of the Reservoir Characterization Research Laboratory (RCRL) and his dissertation research about Oligocene–Miocene carbonates was co-supervised by Dr. Xavier Janson and Dr. Charles Kerans.

Permanent address: rfifariz@utexas.edu

This dissertation was typed by Reynaldy Fifariz.